WRDC-TR-89-3076
VOLUME I

ADVANCED ACTUATION SYSTEMS DEVELOPMENT

Gavin D. Jenney
Harry W. Schreadley
John A. Anderson
William G. Talley
Carl A. Allbright

DYNAMIC CONTROLS, INC.
DAYTON, OHIO 45424-2929

August 1989

Final Report for Period May 1983 - January 1987

FLIGHT DYNAMICS LABORATORY
WRIGHT RESEARCH DEVELOPMENT CENTER
AIR FORCE SYSTEMS COMMAND
WRIGHT-PATTERSON AIR FORCE BASE, OHIO 45433-6553

NOTICE

When Government drawings, specifications, or other data are used for any purpose other than in connection with a definitely related Government procurement operation, the United States Government thereby incurs no responsibility nor any obligation whatsoever; and the fact that the Government may have formulated, furnished, or in any way supplied the said drawings, specifications, or other data, is not to be regarded by implication or otherwise as in any manner licensing the holder or any other person or corporation, or conveying any rights or permission to manufacture, use, or sell any patented invention that may in any way be related thereto.

This report has been reviewed by the Office of Public Affairs (ASD/PA) and is releasable to the Nation Technical Information Service (NTIS). At NTIS, it will be available to the general public, including foreign nations.

This technical report has been reviewed and is approved for ratification.

GREGORY J. CECERE, Program Manager
Control Systems Development Branch
Flight Control Division

FRANK R. SWORTZEL, Chief
Control Systems Development Branch
Flight Control Division

FOR THE COMMANDER

JAMES E. HUNTER, Acting Chief
Flight Control Division
Flight Dynamics Laboratory

"If your address has changed, if you wish to be removed from our mailing list, or if the addressee is no longer employed by your organization, please notify WRDC/FIGL, Wright-Patterson AFB, OH 45433-6553 to help us maintain a current mailing list."

Copies of this report should not be returned unless return is required by security considerations, contractual obligations, or notice on a specific document.

REPORT DOCUMENTATION PAGE

Form Approved OMB No. 0704-0188

1a. REPORT SECURITY CLASSIFICATION: UNCLASSIFIED	1b. RESTRICTIVE MARKINGS: NONE
2a. SECURITY CLASSIFICATION AUTHORITY: N/A	3. DISTRIBUTION/AVAILABILITY OF REPORT: Approved for Public Release: distribution unlimited.
2b. DECLASSIFICATION/DOWNGRADING SCHEDULE: N/A	
4. PERFORMING ORGANIZATION REPORT NUMBER(S)	5. MONITORING ORGANIZATION REPORT NUMBER(S): WRDC-TR-89-3076, Volume I
6a. NAME OF PERFORMING ORGANIZATION: Dynamic Controls, Inc. / 6b. OFFICE SYMBOL (If applicable)	7a. NAME OF MONITORING ORGANIZATION: Flight Dynamics Laboratory (WRDC/FIGL) Wright Research and Development Center
6c. ADDRESS (City, State, and ZIP Code): 7060 Cliffwood Place Dayton, OH 45424-2929	7b. ADDRESS (City, State, and ZIP Code): Wright-Patterson AFB, OH 45433-6553
8a. NAME OF FUNDING/SPONSORING ORGANIZATION / 8b. OFFICE SYMBOL (If applicable)	9. PROCUREMENT INSTRUMENT IDENTIFICATION NUMBER: F33615-S3-C-3600
8c. ADDRESS (City, State, and ZIP Code)	10. SOURCE OF FUNDING NUMBERS

PROGRAM ELEMENT NO.	PROJECT NO.	TASK NO	WORK UNIT ACCESSION NO.
62210F	2403	02	91

11. TITLE (Include Security Classification): ADVANCED ACTUATION SYSTEMS DEVELOPMENT - Volume I

12. PERSONAL AUTHOR(S): John A. Anderson, Carl A. Allbright, Gavin D. Jenney, Harry W. Schreadley, William G. Talley

13a. TYPE OF REPORT	13b. TIME COVERED	14. DATE OF REPORT (Year, Month, Day)	15. PAGE COUNT
Final	FROM 5/83 TO 1/87	1989 August	338

16. SUPPLEMENTARY NOTATION: None

17. COSATI CODES			18. SUBJECT TERMS (Continue on reverse if necessary and identify by block number)
FIELD	GROUP	SUB-GROUP	Sealing Systems, Digital Servovalve, Direct Drive F16, Flutter Suppression, Flight Control Actuator
01	03		

19. ABSTRACT (Continue on reverse if necessary and identify by block number)

1. This report describes six different research and development activities in flight control actuation. The activities are: (1) the development and test of a unique linear actuator sealing system for high-pressure systems, (2) the development and test of a digital servovalve using piezo-controlled high-speed solenoid valves, (3) the performance evaluation of an F-15 rudder actuator under applied loads, (4) the performance evaluation of a Mission Adaptive Wing section under different load conditions, (5) the evaluation of output impedance modification of an electrohydraulic actuator for flutter suppression, and (6) the development and test of a direct drive valve and electronics (analog and digital) for an F-16 Horizontal Tail/Flaperon actuator. This Volume ~~I of the report~~ presents activities 1, 2, and 3. Volume II presents activities 4, 5 and 6. (KR) ←

2. The sealing system was based upon using two-stage sealing for the piston rod seals and a pressure-activated backup ring configuration for the piston seals. The system eliminated the use of elastomeric dynamic seals. The piston rod first-stage seal was a laminar pressure-drop design which also served as a rod-support bearing. The piston rod seal used commercial non-elastomeric seals. The design was tested in actuators with thin wall cylinders at 8000 psi. Both MIL-H-83282 and CTFE hydraulic fluid systems were used for the testing. The system was tested with 500,000 impulse-loading cycles without any seal degradation.

20. DISTRIBUTION/AVAILABILITY OF ABSTRACT	21. ABSTRACT SECURITY CLASSIFICATION
☒ UNCLASSIFIED/UNLIMITED ☐ SAME AS RPT ☐ DTIC USERS	UNCLASSIFIED

22a. NAME OF RESPONSIBLE INDIVIDUAL	22b TELEPHONE (Include Area Code)	22c. OFFICE SYMBOL
Mr. Gregory Cecere	513-255-2831	AFWAL/FIGL

DD Form 1473, JUN 86 — Previous editions are obsolete. — SECURITY CLASSIFICATION OF THIS PAGE

3. The digital servovalve was constructed with discrete high-speed solenoid valves to control the flow to a control actuator. The solenoid valves were a poppet design using a piezoelectric stack and a hydraulic motion amplifier. The valves activated in less than one millisecond. A microprocessor was used to control the valve and close the control loop. The servovalve worked successfully. Since the output flow of the solenoid valves is low, the approach is suitable primarily for small actuators.

4. The performance of an F-15 rudder actuator was evaluated in a loading test stand. The evaluation was limited to the electrical command mode with the manual input grounded. The input/output performance characteristics in both unloaded and loaded operation were documented and analyzed. The actuator is a rotary vane actuator. The performance characteristics were similar to those of a linear actuator with the exception of characteristics directly affected by the vane sealing method.

5. The Mission Adaptive Wing evaluation was a measurement of the loaded and unloaded performance characteristics of a test specimen produced by General Dynamics Corporation as a feasibility model. The actuation system for changing the camber of the test specimen is unique and was evaluated with a series of input/output measurements. The testing verified the general concept and revealed two design areas requiring additional development effort before flight test evaluation.

6. The impedance modification investigation used electronic load pressure sensing to change the output impedance of an actuator over a selected frequency band. Changing the output impedance of an actuator potentially can be used to suppress classical slab-surface flutter. A demonstration actuator was sized to evaluate the impedance change capability. The test results indicated that the output impedance of an electrohydraulic actuator can be modified over a useful but limited frequency range using electronic pressure sensing and the control servovalve for the actuator. The limitation in the range of the impedance modification is primarily determined by the frequency response characteristics of the servovalve used to control the actuator.

7. The F-16 Direct Drive Actuator development effort produced a direct drive control valve package which replaces the normal control valve and secondary actuator mounted on the actuator body of an F-16 Horizontal Tail/Flaperon ISA. The design maintains the failure-mode characteristics of the normal F-16 ISA including the centering mode as the final failure mode. The measured performance was equivalent to or better than that of the normal F-16 ISA. As part of the evaluation, a microprocessor-controlled initial checkout, failure monitor, and failure switching unit was evaluated with the test actuator.

FOREWORD

The effort described in this document was performed by Dynamic Controls, Inc., (DCI) of Dayton, Ohio, under Air Force Contract F33615-83-C-3600. The contract was performed under Project Number 2403, Task 02. The work under the contract was carried out in the Air Force Flight Dynamics Laboratory, Wright-Patterson Air Force Base, Ohio. The work was administered by Mr. Gregory Cecere, AFFDL/FIGL Program Manager.

This report covers work performed between May 1983 and January 1987. The technical report was submitted in September 1988.

The authors wish to express their appreciation to DCI technicians Steve Murphy, Connie Graham, and Julie Minch for their contributions in implementing designs, testing, and engineering support for the efforts described in the report. Appreciation is also expressed to Linda Pytosh and Lynda Gopinath for their efforts in preparation of the data and text which make up the report.

TABLE OF CONTENTS

VOLUME I

Section II - Page No.

SECTION III - F-15 RUDDER ACTUATOR EVALUATION — Section III - Page No.

VOLUME I

Section III - Page No.

VOLUME I

LIST OF FIGURES

SECTION I - HIGH-PRESSURE SEAL INVESTIGATION — Section I - Page No.

SECTION II - DIGITAL SERVOVALE INVESTIGATION — Section II - Page No.

Section II - Page No.

SECTION III - F-15 RUDDER ACTUATOR EVALUATION Section III - Page No.

VOLUME I

LIST OF TABLES

SECTION I - HIGH-PRESSURE SEAL INVESTIGATION — Section I - Page No.

SECTION II - DIGITAL SERVOVALVE INVESTIGATION — Section II - Page No.

SECTION III - F-15 RUDDER ACTUATOR EVALUATION — Section III - Page No.

SUMMARY

This report describes six different research and development activities in flight control actuation. The activities are: (1) the development and test of a unique linear actuator sealing system for high-pressure systems, (2) the development and test of a digital servovalve using piezo-controlled high-peed solenoid valves, (3) the performance evaluation of an F-15 rudder actuator under applied loads, (4) the performance evaluation of a Mission Adaptive Wing section under different load conditions, (5) the evaluation of output impedance modification of an electrohydraulic actuator for flutter suppression, and (6) the development and test of a direct drive valve and electronics (analog and digital) for an F-16 Horizontal Tail/Flaperon actuator. Volume I of the report presents activities 1, 2, and 3. Volume II presents activities 4, 5, and 6.

The sealing system was based upon using two-stage sealing for the piston rod seals and a pressure-activated backup ring configuration for the piston seals. The system eliminated the use of elastomeric dynamic seals. The piston rod first-stage seal was a laminar pressure-drop design which also served as a rod-support bearing. The piston rod seal used commercial non-elastomeric seals. The design was tested in actuators with thin wall cylinders at 8000 psi. Both MIL-H-83282 and CTFE hydraulic fluid systems were used for the testing. The system was tested with 500,000 impulse-loading cycles without any seal degradation.

The digital servovalve was constructed with discrete high-speed solenoid valves to control the flow to a control actuator. The solenoid valves were a poppet design using a piezoelectric stack and a hydraulic motion amplifier. The valves activated in less than one millisecond. A microprocessor was used to control the valve and close the control loop. The servovalve worked successfully. Since the output flow of the solenoid valves is low, the approach is suitable primarily for small actuators.

The performance of an F-15 rudder actuator was evaluated in a loading test stand. The evaluation was limited to the electrical command mode with the manual input grounded. The input/output performance characteristics in both unloaded and loaded operation were documented and analyzed. The actuator is a rotary vane actuator. The performance characteristics were similar to those of a linear actuator with the exception of characteristics directly affected by the vane sealing method.

The Mission Adaptive Wing evaluation was a measurement of the loaded and unloaded performance characteristics of a test specimen produced by General Dynamics Corporation as a feasibility model. The actuation system for changing the camber of the test specimen is unique and was evaluated with a series of input/output measurements. The testing verified the general concept and revealed two design areas requiring additional development effort before flight test evaluation.

The impedance modification investigation used electronic load pressure sensing to change the output impedance of an actuator over a selected frequency band. Changing the output impedance of an actuator potentially can be used to suppress classical slab-surface flutter. A demonstration actuator was sized to evaluate the impedance change capability. The test results indicated that the output impedance of an electrohydraulic actuator can be modified over a useful but limited frequency range using electronic pressure sensing and the control servovalve for the actuator. The limitation in the range of the impedance modification is primarily determined by the frequency response characteristics of the servovalve used to control the actuator.

The F-16 Direct Drive Actuator development effort produced a direct drive control valve package which replaces the normal control valve and secondary actuator mounted on the actuator body of an F-16 Horizontal Tail/Flaperon ISA. The design maintains the failure-mode characteristics of the normal F-16 ISA including the centering mode as the final failure mode. The measured performance was equivalent to or better than that of the normal F-16 ISA. As part of the evaluation, a microprocessor-controlled initial checkout, failure monitor, and failure switching unit was evaluated with the test actuator.

SECTION I

HIGH-PRESSURE SEAL INVESTIGATION

I. INTRODUCTION AND SUMMARY

This section describes the design and testing of a sealing system for a servovalve-controlled hydraulic actuator operating at 8000 psi. Also included in this section is a description of the actuators and pumping systems installed to perform the 8000 psi testing. Two actuators and pumping systems were built, one for testing with MIL-H-83282 hydraulic fluid, and one for testing with chlorotrifluoroethelene (CTFE) fluid.

The seals the investigation was concerned with are the actuator dynamic seals, i.e., the rod seals and the piston seals. The rod-sealing system investigated is a two-stage system consisting of a laminar pressure drop (provided by a close-fitting aluminum-bronze bushing) and a standard Teflon rod seal. The laminar flow past the bushing is fed back to the return so the final stage rod seal sees only return pressure and a standard graphite-filled, spring-energized Teflon seal can be used. The piston-sealing system consists of two heavy-duty Teflon seals that are unidirectional, carbon-graphite-filled, and spring-energized. These two seals are supported by solid aluminum-bronze backup rings. These Teflon seals are rated for 8000 psi but require a smaller clearance between the piston and the cylinder wall than can practically be maintained in a flight-control actuator. The aluminum-bronze backup rings overcome this problem by fitting closely to the cylinder wall and are pressure-energized to follow the *breathing* of the cylinder as pressure changes. The high friction usually associated with metal backup rings is a result of mechanically compressing the backup rings so their own spring rate causes them to follow the cylinder's *breathing*. The mechanical compression causes the rings to be forced against the cylinder wall, creating friction. Pressure energizing allows the rings to move freely in the cylinder unless a large load is applied (thus minimizing the friction problem).

The pumping systems for the investigation used fixed-displacement pumps with the output pressure controlled by adjustable relief valves. Accumulators, filters, and heat exchangers were mounted on pump stands to provide complete pumping systems which continuously supplied 2.0 gpm at 8000 psi.

The actuators were tested for 500,000 full-pressure cycles with a fluid temperature of 130-150° F. A full-pressure cycle consisted of stroking the actuator about .08 inches (from near mid-stroke) against a hard external stop to bring the pressure across the piston to 8000 psi as quickly as possible. The actuator was then backed-off .08 inches and the cycle repeated. The seals worked properly with no noticeable change in seal performance although a visual inspection showed the piston seals to be somewhat extruded. A slight change in appearance was also noticed in the Teflon surface which was

in contact with the cylinder wall. On the seals used with the MIL-H-83282 fluid, this surface had a shiny, polished appearance while the same surface on the seals used with the CTFE fluid appeared slightly dulled. This could be due to the lower lubricity of the CTFE fluid which allowed the seal to scuff. Although test results appear promising, more testing of the seals is required to determine their suitability for long-term use in high-pressure actuators.

II. TECHNICAL APPROACH

Sealing System Description

General

Dynamic seals are seals between parts which have motion relative to one another. The dynamic seals of a linear hydraulic actuator are the rod seals and the piston seals. The rod seals are located in the cylinder end-caps and seal between the cylinder end-cap and piston rod. The rod seals prevent fluid loss from the cylinder. The piston seals are located on the piston, between the piston and cylinder wall. They prevent fluid from leaking across a piston so a pressure difference (and load) can be maintained. For the investigation, the commercial seals used in the system were made from Teflon (PTFE). This material was selected because of PTFE's apparent compatibility with CTFE fluid. Figure I-1 is a cross-section of the test actuator and illustrates the sealing system.

Rod Seals

The rod seals prevent fluid loss from the hydraulic system, so they must provide a positive (non-leaking or nearly non-leaking) seal over the entire pressure and temperature range. In an 8000 psi system, the pressure on the rod seal will vary from near-zero psi to a nominal pressure of 8000 psi with pulses (due to system dynamics) above 8000 psi. The temperature range for a class I seal is from a -65°F to 275°F. This requires a seal with enough compliance and mechanical preload to conform to the rod and prevent leaking at -65°F and near-zero cylinder pressure but strong enough to withstand 8000 psi at 275° F. Such seals tend to be thick and tough, requiring a large mechanical preload. The preload is generally provided by a metal spring or an elastomeric material loaded against the seal. Under a no-load condition, a rod seal will have 4000 psi (half of system pressure) plus the large mechanical preload forcing it against the rod. This results in high seal-friction. High seal-friction leads to seal wear. The friction is also seen as dead band in the control of a flight-control actuator.

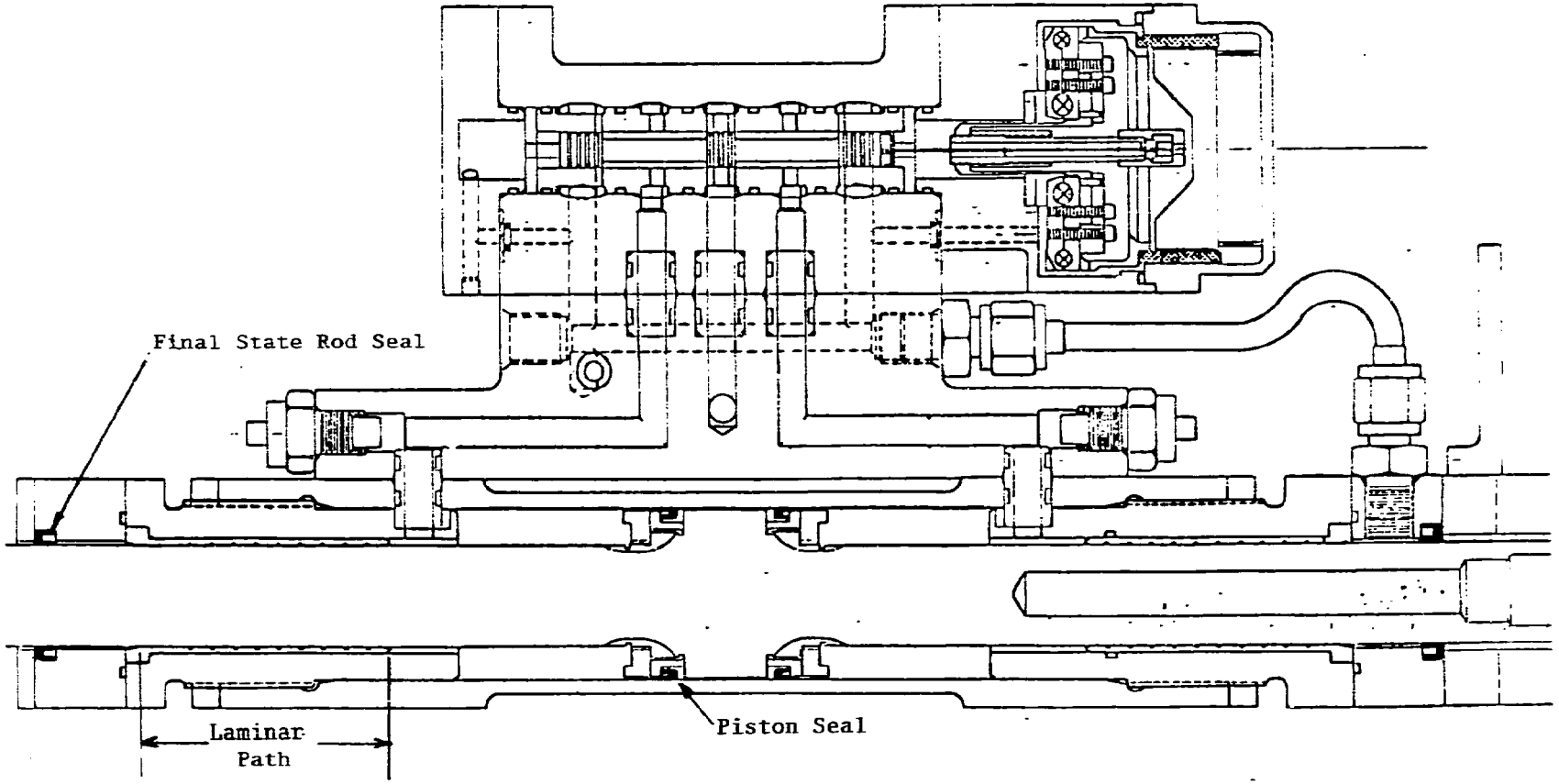

Figure I-1. Test actuator cross-section.

To avoid the friction problems associated with high-pressure rod seals, the approach used on this sealing system was to substitute a two-stage rod seal for the conventional high-pressure seal. The first stage is a laminar path seal created by closely fitting the bushing to the rod. The laminar flow past the bushing is fed back to return and the final-stage seal is a conventional low-pressure rod seal. The low-pressure rod seal sees only return pressure so it can be made of a lower-strength, more-pliable material which requires less mechanical preload to maintain a positive seal. Because there is little hydraulic pressure loading the seal against the rod, the friction is decreased, increasing seal life and decreasing actuator control dead band. This system has been employed successfully in 3000 psi systems where low friction and long seal life were the primary concerns.

The principal design problem with this approach is maintaining the close fit between the rod and bushing throughout the required temperature range. The close fit must be maintained because laminar flow past the bushing represents a power loss. The larger the clearance between rod and bushing, the greater the flow. Figure I-2 illustrates the parameters involved in laminar flow and the power loss due to this laminar flow. The power loss is represented by the equation:

Eq. 1

$$\text{Power Loss} = \frac{\pi r c^3}{6 L \mu} \left(1 + 1.5 (e/c)^2 \right) P^2$$

where:

c = radial clearance between the bushing and rod
e = eccentricity between bushing and rod
L = bushing length
P = pressure drop across the bushing
r = bushing internal radius
π = constant, approximately 3.14
μ = fluid absolute viscosity

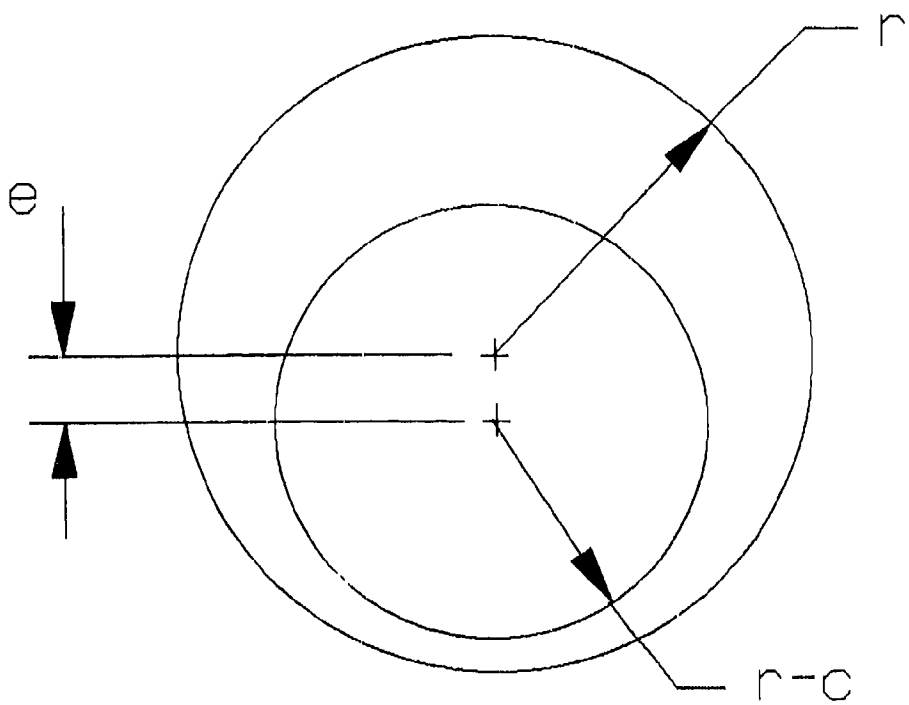

Figure I-2. Laminar flow parameters.

As seen from Equation 1, maximum leakage occurs when the eccentricity is maximum and equal to the clearance. The minimum leakage will occur when the rod is centered in the bushing and the eccentricity is zero. In both cases, the power loss is proportional to the clearance cubed and demonstrates that radial clearance is the dominate variable in controlling power loss. This clearance should be kept to a minimum. However, there are practical limits to the minimum clearance that can be achieved due to the straightness of the rod and the alignment of the bushings. If the clearance is too small, the misalignment will cause the rod to bind, making the actuator difficult to control and wearing the rod end bushings. Due to thermal expansion of the rod, bushing, and end cap, the clearance will change with temperature. The parts should be designed to allow adequate clearance at all temperatures (but not so great a clearance that the power loss becomes significant). The clearance as a function of temperature is given by the following equations:

Eq. 2 $$c(T) = [D_h(T) - 2\,t(T) - D_r(T)] / 2$$

Eq. 3 $$t(T) = [D_h(T) - [D_h^2(T) - (D_{b_o}^2(T) - D_{b_i}^2(T))]^{\frac{1}{2}}] /2$$

Eq. 4 $$D_h(T) = D_h(T_o)\,[\,1 + \alpha_h\,(T - T_o)\,]$$

Eq. 5 $$D_{bi}(T) = D_{bi}(T_o)\,[\,1 + \alpha_b\,(T - T_o)]$$

Eq. 6 $$D_{bo}(4T) = D_{bi}(T_o)\,[\,1 + \alpha_b\,(T - T_o)]$$

Eq. 7 $$D_r(T) = D_r(T_o)\,[\,1 + \alpha_r\,(T - T_o)$$

where:

$c(T)$ = radial clearance between bushing and rod as a function of temperature
$D_{bi}(T)$ = bushing internal diameter (if not pressed into end cap) as a function of temperature
$D_{bo}(T)$ = bushing outer diameter (if not pressed into end cap) as a function of temperature
$D_h(T)$ = end cap internal diameter as a function of temperature
$D_r(T)$ = rod outer diameter as a function of temperature
T = temperature
T_o = constant, reference temperature
$t(T)$ = bushing wall thickness as a function of temperature
α_b = coefficient of thermal expansion for bushing material
α_h = coefficient of thermal expansion for end cap material
α_r = coefficient of thermal expansion for rod material.

These equations assume that the end cap's wall thickness is considerably greater than the bushing's wall thickness, the bushing is pressed into the end cap, and that the volume and length of the bushing is a function of temperature only (i.e., it does not change with the press fit). Figure I-3 illustrates the physical relationship of the parameters involved in the above equations. The press fit must be heavy enough to be maintained over the temperature range in order to keep the bushing aligned. $D_{bi}(T)$ and $D_{bo}(T)$ are the diameters of the bushing if it were not pressed into the end cap. Because the end cap has a much heavier wall than the bushing, it is assumed $D_h(T)$ remains constant when the bushing is pressed into the end cap and the bushing outer diameter is compressed to $D_h(T)$. The change in the bushing inner diameter will be greater than the amount of the press, $D_h(T) - D_{bo}(T)$, because the volume of the bushing remains constant at a given temperature. The equations indicate that if the bushing material expands much more rapidly than the end-cap material, the increased bushing volume will reduce the clearance between the rod and bushing as temperature increases. If the expansions of the materials are equal or the bushing expands less rapidly, the clearance will increase with increasing temperature. Whether the clearance increases or decreases with temperature and the rate the clearance changes with temperature depends upon the relative coefficients of thermal expansion of the materials and the nominal thickness of the bushing wall. Several materials were

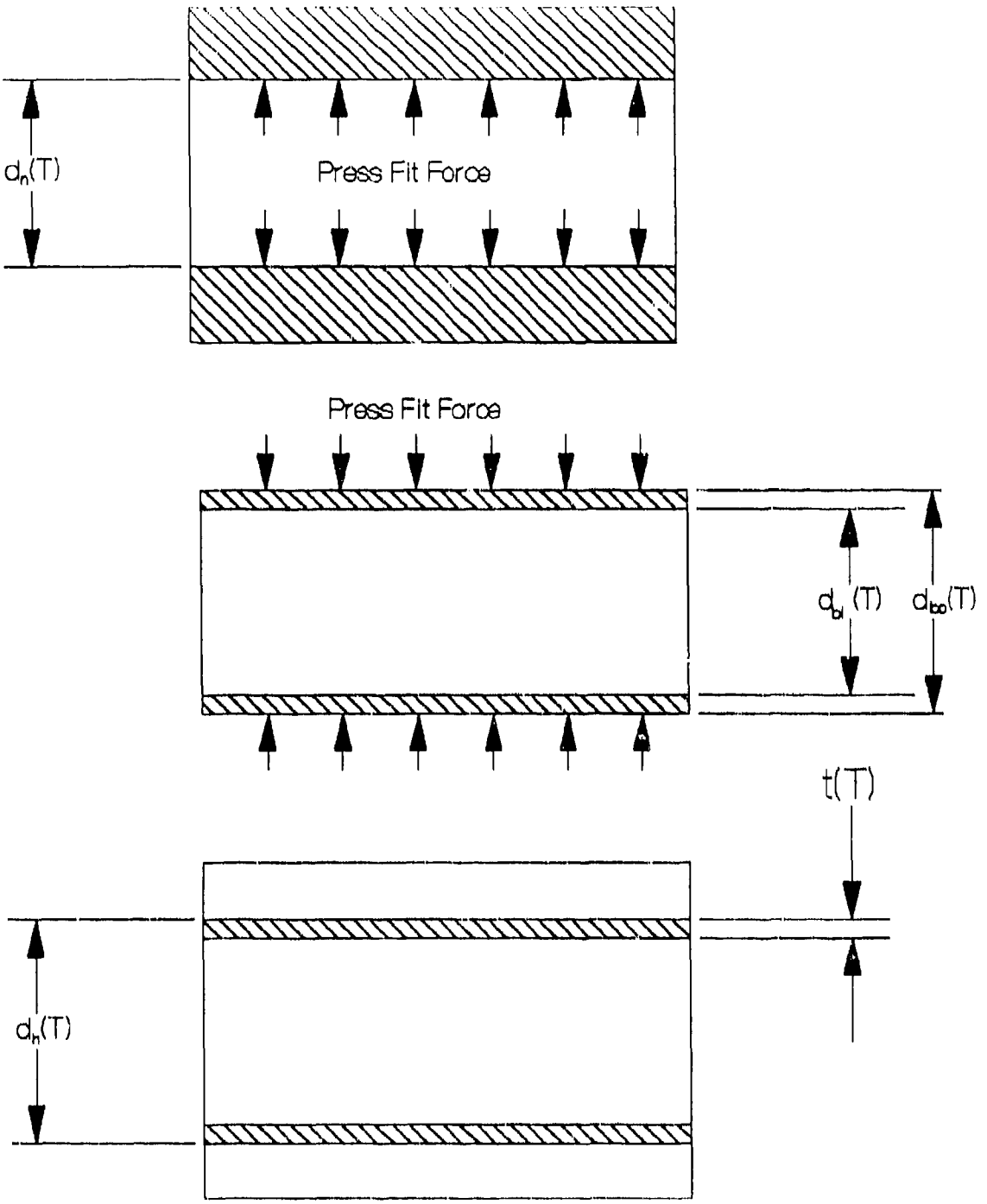

Figure I-3. Bushing dimensions.

considered for use in fabricating the rod, bushing and end cap. Some of these materials, along with their coefficients of thermal expansion, are shown in Table I-1.

For the actuators used for the seal system verification tests, the rod was made of stainless steel type *303*, the bushings of aluminum-bronze *Ampco 18*, and the end caps of stainless steel type *304*. These materials allowed nearly the same clearance to be maintained throughout the required temperature range. The rod was nominally 0.875 inches in diameter and the end-cap internal diameter nominally 1.000 inches. This left a nominal bushing-wall thickness of .0625 inches. The bushing was 3.00 inches long. Minimizing the thickness of the bushing wall minimizes the effects caused by the difference in the coefficients of thermal expansion between the stainless steel and aluminum bronze. The parts were machined to nominal size and trial assembled. The rod was then removed and lapped to a 22-micro finish until the rod moved freely in the assembled cylinder. Figure I-4 is a picture of a bushing pressed into an end cap.

Table I-1. Coefficients of thermal expansion for the materials used for dynamic seals.

MATERIAL	COEFFICIENT	SOURCE
Bushing Materials		
Aluminum-Bronze	9.0×10^{-6}	Sales office
Phosphor Bronze	9.0×10^{-6}	Sales office
Rod & End Cap Materials		
Stainless Steel (type *3XX* series)	8.7 to 9.6×10^{-6}	[1]
Stainless Steel (type *4XX* series)	5.5 to 6.5×10^{-6}	[1]
Stainless Steel *17-4 PH*	5.5 to 6.4×10^{-6}	[1]
Steel *4130*	6.3 to 8.6×10^{-6}	[1]
Nickel Steel	5.6 to 6.3×10^{-6}	Sales office

[1] Aerospace Fluid Component Designer's Handbook, Volume II, Report FDL-TDR-64-25, TRW Systems Group, Redondo Beach, California, November 1968.

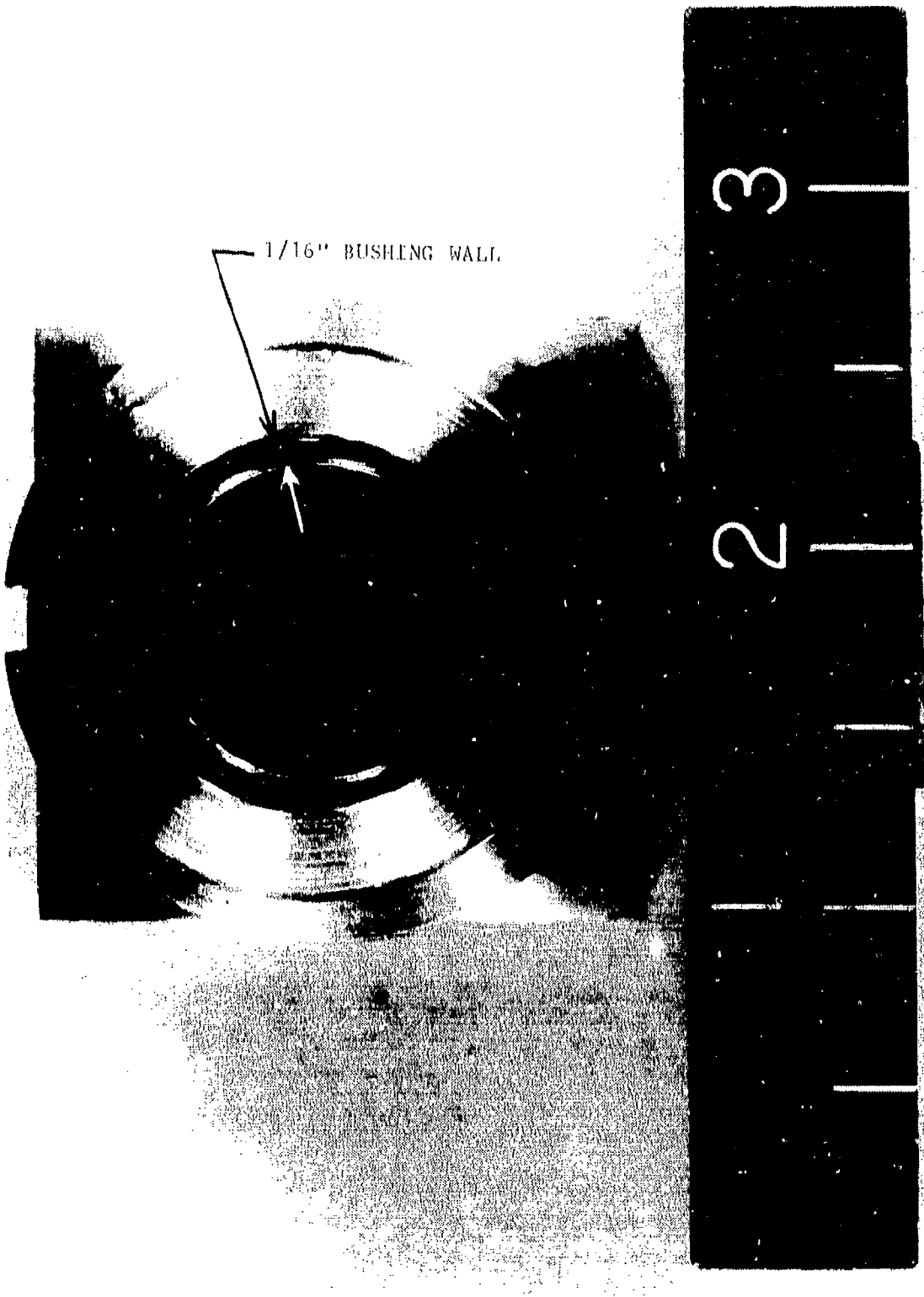

Figure I-4. Bushing pressed into end cap.

Piston Seals

A review of manufacturers' literature on commercially available piston seals showed the existence of several seals rated for 8000 psi and 275° F. However, these seals require maintaining an extremely small clearance between the piston and cylinder to prevent the seal from extruding. To maintain a close clearance with a conventional actuator design when the cylinder is pressurized (causing the cylinder to *breathe*), requires a very thick cylinder wall. This adds weight to the actuator and makes use of the actuator for flight controls undesirable.

The approach used for the piston seals was to use commercially available piston seals and a solid aluminum-bronze backup ring, thus eliminating the gap between the piston and cylinder wall at high differential pressures. To be effective, the backup ring must follow the cylinder wall as the cylinder *breathes* radially without pressing against the cylinder wall with such a force as to cause high friction. High friction is undesirable because it causes dead band in the control of the actuator as well as wear of the cylinder wall and backup ring.

Two methods of forcing the backup ring out against the cylinder wall were considered. The first method was to make the outer diameter of the ring larger than the bore of the cylinder by the amount the cylinder is expected to breathe. At assembly, the ring would be mechanically compressed to fit into the cylinder. In this way, as the cylinder expands radially, the spring rate of the ring keeps the ring pressed against the cylinder wall. This method was not used because the force to compress the ring would be high enough to cause substantial friction between the cylinder and the ring.

The method chosen to keep the backup ring against the cylinder wall was to pressure-energize the backup ring. This configuration is illustrated in Figure I-5. In this way, the ring is not forced out against the cylinder wall unless there is sufficient pressure to expand the ring. Because the ring is solid, most of the pressure is spent in expanding the ring. This results in less force between the ring and cylinder than the configuration where the ring is mechanically compressed. A soft seal ring of Teflon is placed under the backup ring to prevent fluid from leaking behind the backup ring. A soft Teflon ring can be used to seal beneath the backup ring because hydraulic pressure keeps the backup ring against the piston and there is no space in which to extrude the soft seal. This configuration seals only in one direction so two seals are needed if the duration of pressure is reversed. As seen in Figure I-5, the commercial seal prevents leakage over the backup ring and the soft Teflon seal prevents leakage beneath and behind the backup ring. In this way, the rings are forced back against the piston and out against the cylinder wall. The aluminum-bronze backup ring has sufficient strength to allow using considerable clearance between the piston and cylinder wall, thus reducing the requirement for concentricity of the bushings, cylinder, and piston. The backup ring in the configuration is free-floating so it remains concentric to the cylinder even if the piston is not.

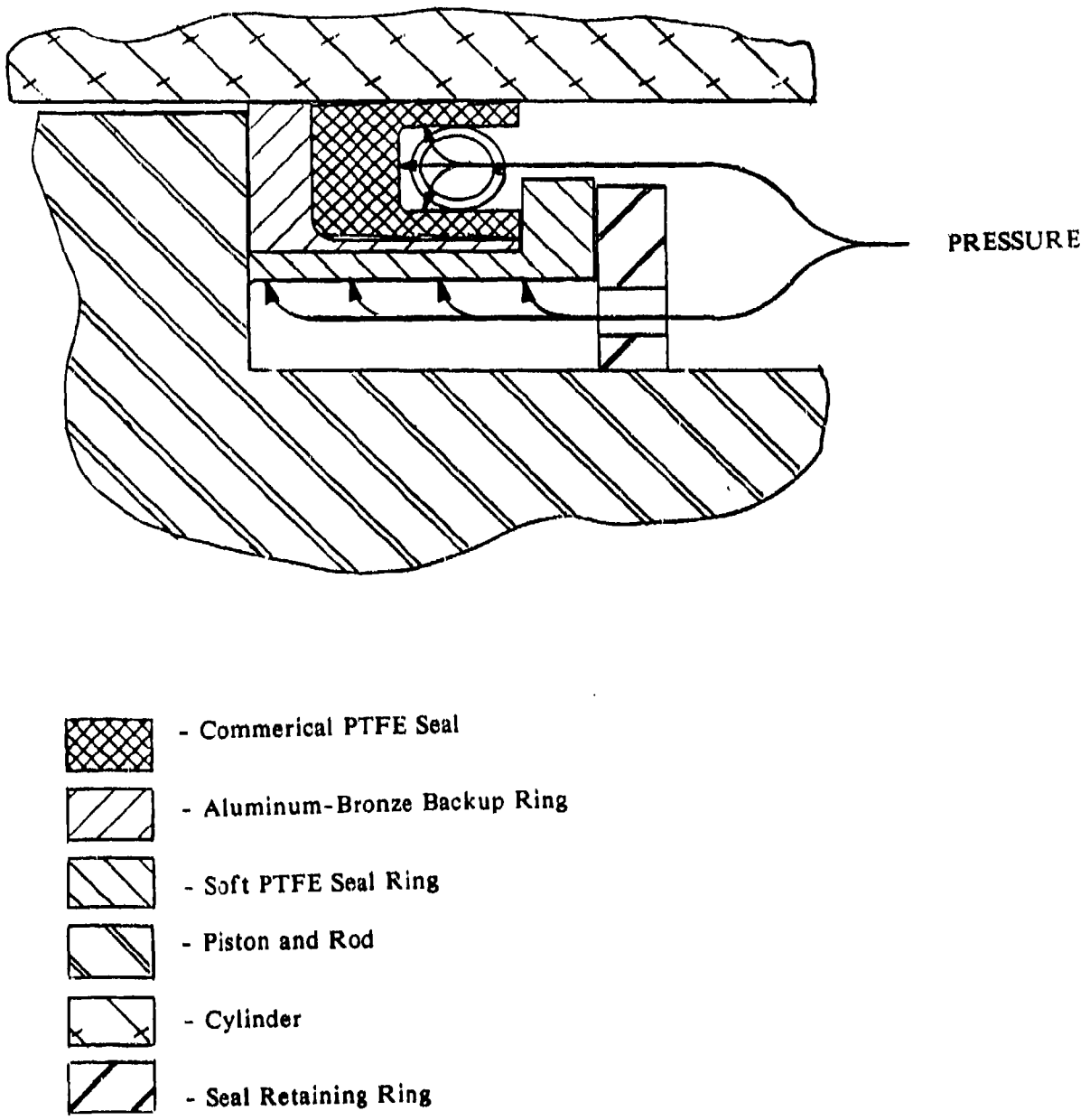

Figure I-5. Piston seal cross section.

A design consideration of this approach is selecting the thickness of the backup ring so that pressure expands the ring to follow the cylinder wall without locking it against the wall. When the actuator is unloaded, the cylinder will have an internal pressure of 4000 psi expanding it radially while the backup rings will have zero differential pressure across them. As the actuator is loaded, the differential pressure across the piston will increase from near zero to 8000 psi. The pressure inside the cylinder will increase from 4000 to 8000 psi at one end and decrease from 4000 to 0 psi at the other end. The pressure distribution makes predicting the diameter of the cylinder directly above the backup rings difficult. For this design, it was therefore conservatively assumed the cylinder diameter directly above the backup ring remained the same as when the internal pressure is 4000 psi. The basis for this assumption is that when pressure increases above 4000 psi on one side of the backup ring, the pressure decreases below 4000 psi by an equal amount on the other side. With this assumption, the backup ring expands with load while the cylinder diameter at the backup ring does not change. The backup ring is designed to have clearance under no-load (when the cylinder has 4000 psi at both ends) and expand radially to close the gap as the actuator is loaded. The backup ring must keep the radial seal gap within the limits of seal strength at any pressure differential. The backup ring is sized for a particular cylinder-wall thickness. At assembly there will be some drag between the backup ring and the cylinder wall because the cylinder is not expanded (by the 4000 psi). The backup ring was made somewhat large and then fitted to the cylinder to obtain the proper amount of drag.

Figure I-6 is a picture of the three separate rings which make up the piston seal. The commercial seal is upper left, the aluminum-bronze backup ring is upper right, and the soft Teflon seal ring is at the lower part of the figure. Figure I-7 is a picture of the piston seal assembled as a single cartridge along with the seal retainer.

The seal retainer threads onto the rod and keeps the backup ring against the piston. Figure I-8 is a picture of the seals assembled on the rod and piston, showing that there are two piston seals with the backup ring of each seal being positioned against the piston.

Static Seals

Viton O-rings were used in all static seal applications in the CTFE unit and in the static high-pressure applications on the MIL-H-83282 unit. Buna-N O-rings were used for the static low-pressure applications on the MIL-H-83282 unit. Polyurethane backup rings were used on the high-pressure applications in which the backup ring was not in direct contact with the fluid. Polyurethane rings were not used in applications where they would soak in CTFE fluid because the material is not rated as being compatible with CTFE.

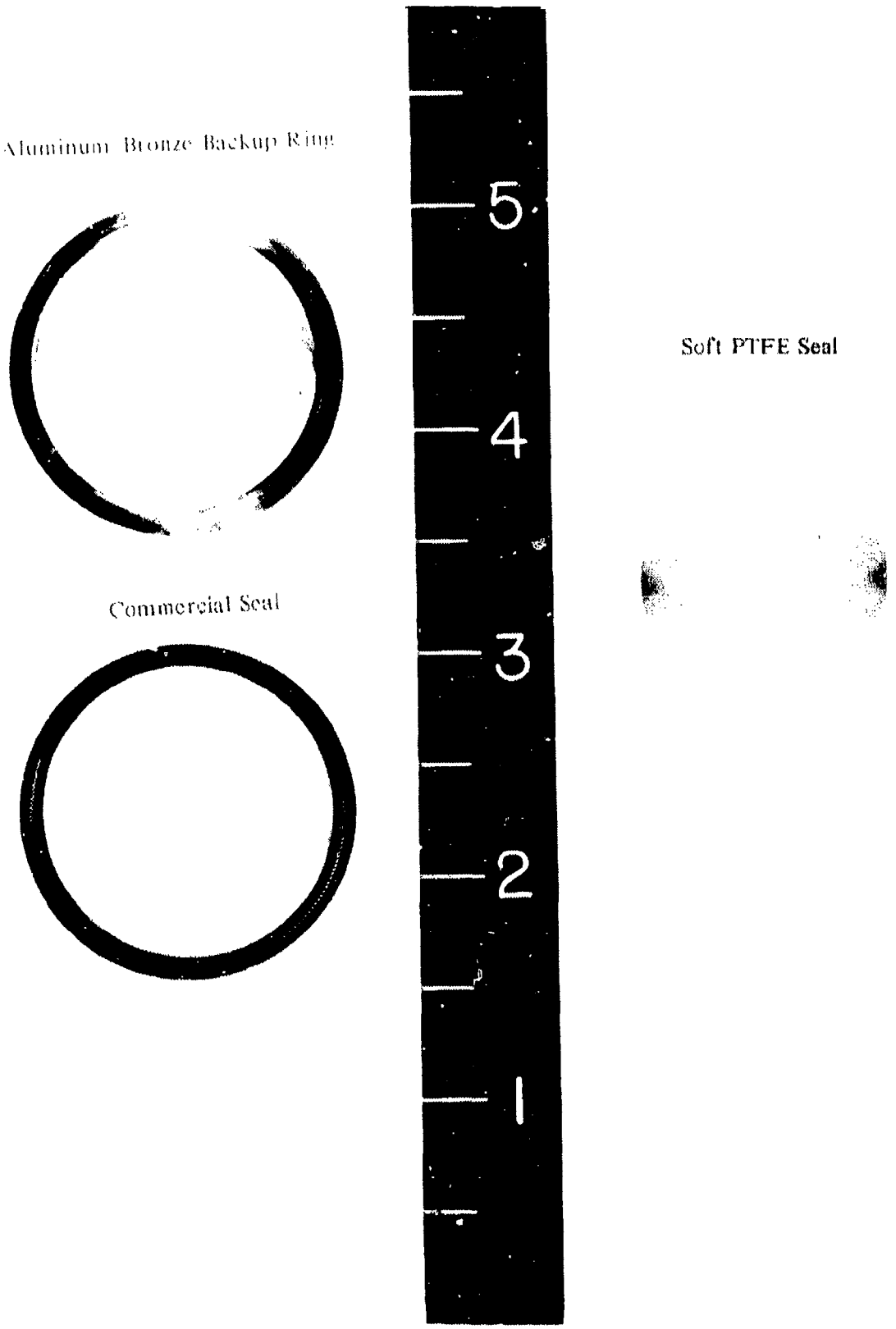

Figure 1-6. Piston seal made of three separate rings.

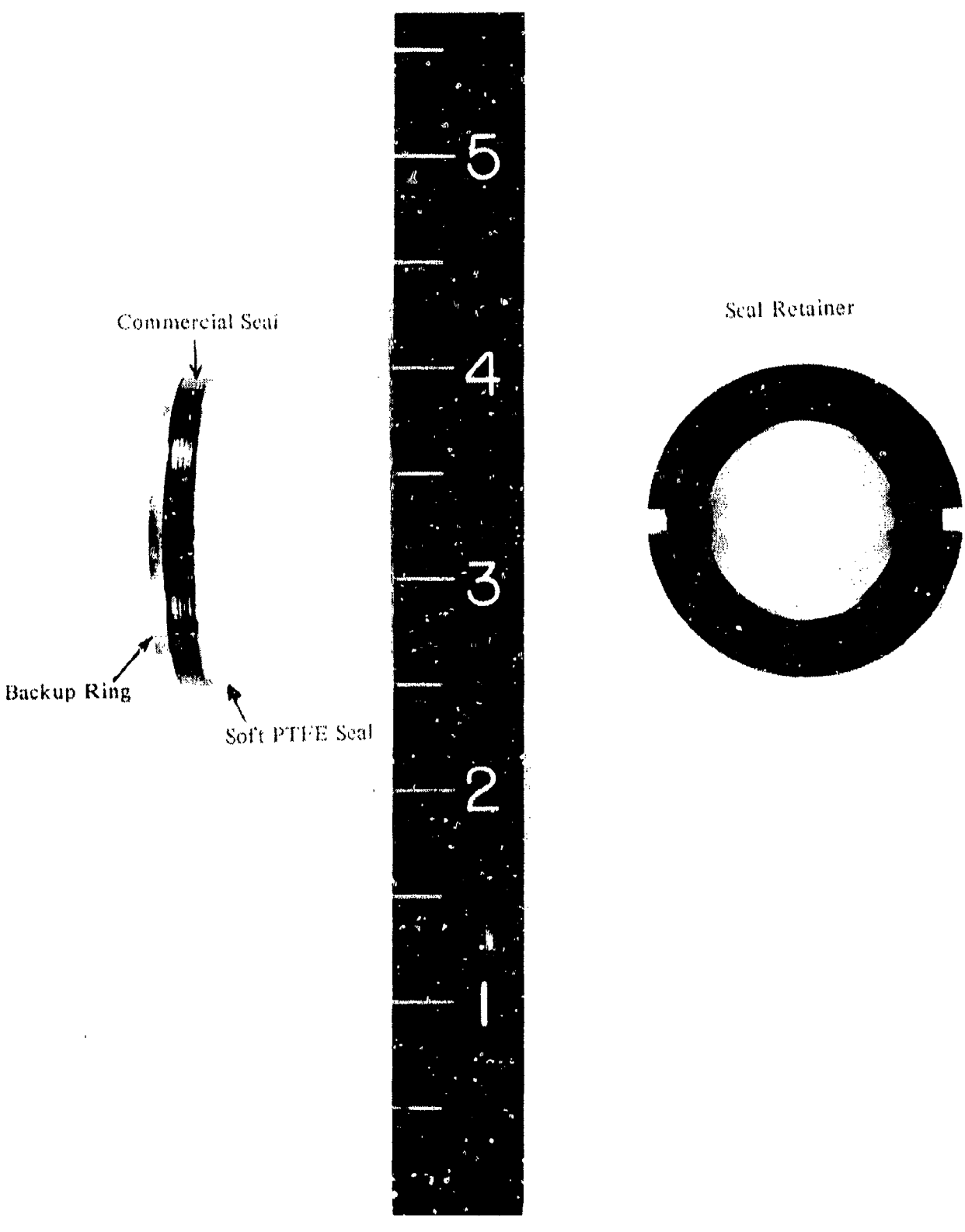

Figure I-7. Piston seal cartridge.

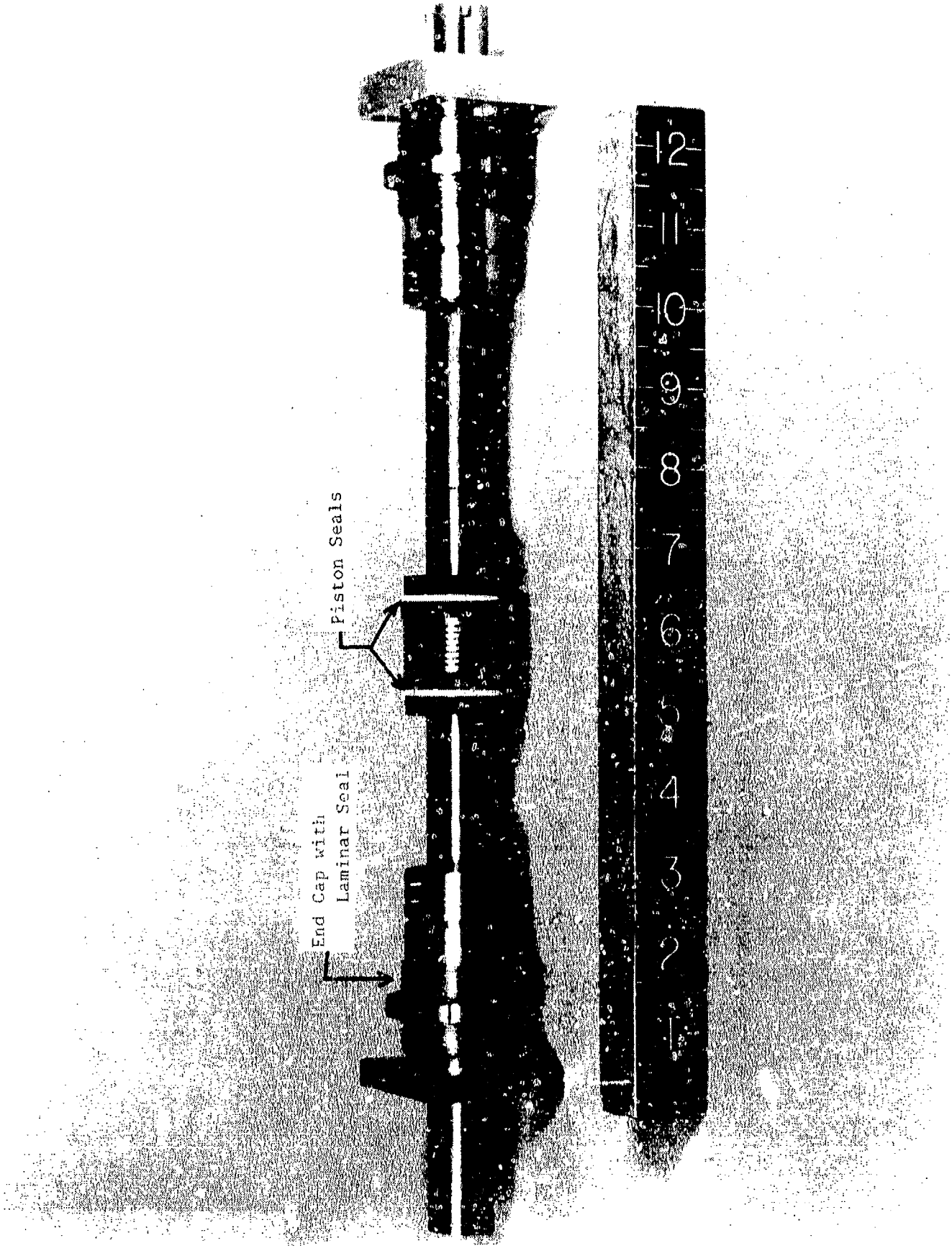

Figure I-8. Seals on rod.

Test Actuator Description

To test this sealing system, two actuators were designed and built. One actuator was tested using CTFE fluid and the other was tested using Mil-H-83282 hydraulic fluid. This approach was used to differentiate between the effects of the 8000 psi pressure and the effects of the CTFE alone. Figures I-9 and I-10 are pictures of the assembled actuator. The actuator and valve fit in a package 23.75 inches long (at null) and 2.5 inches square. The dry weight of the actuator and valve was nominally 26 lbs.

Cylinder

The test cylinder had a 1.500-inch internal diameter with a 1/8-inch-thick wall and was made from a high-strength nickel steel, *Vasco Max 300*, a Teledyne product. An 1/8-inch cylinder wall was used. The cylinder had (theoretically) as much as .0013-inch diameteral expansion on the internal diameter when pressurized to 4000 psi. If the actuator was assembled with zero clearance between the piston and cylinder, the .0013-inch diameteral expansion would be enough to cause the commercial piston seal to fail when pressurized to 8000 psi if the solid aluminum-bronze backup ring were not functioning as designed. The high-strength Vasco material provided a safety factor of 2.0 for fatigue with pressure cycling from 0 to 8000 psi. The piston drive area was 1.16 square inches which provided 9280-lb output force at 8000 psi. The actuator stroke was ± 1.5 inches. The cylinder used with CTFE fluid was machined to the same dimensions and tolerances as the cylinder used with MIL-H-83282 fluid.

Direct Drive Valve

The control valves were single-ended direct-drive spool valves using the same design as the direct-drive valves developed by DCI under Air Force contracts F-33615-75-C-3077 and F-33615-77-C-3608. The valve spool had a 0.3125-inch diameter and a ± .006-inch stroke. The port width of the two valves differed to compensate for the difference in fluid densities. A total port width of 0.387 inches was used for the denser CTFE fluid and 0.274 inches used for the MIL-H-83282 fluid. The linear force motors used to drive the valves were able to produce 35-lb force on the spool when driven with 4 amps and 32 volts. The valve bodies were made of stainless steel type 416 and fit a package 2.5 inches square and 7.75 inches long. Figure I-11 is a picture of the direct drive motor and Figure I-12 an exploded picture of the end cap, valve body, spool, and direct-drive motor. The valve body and magnetic structure were made of stainless steel type 416. The force motor coil housing was made of non-magnetic stainless steel type 316.

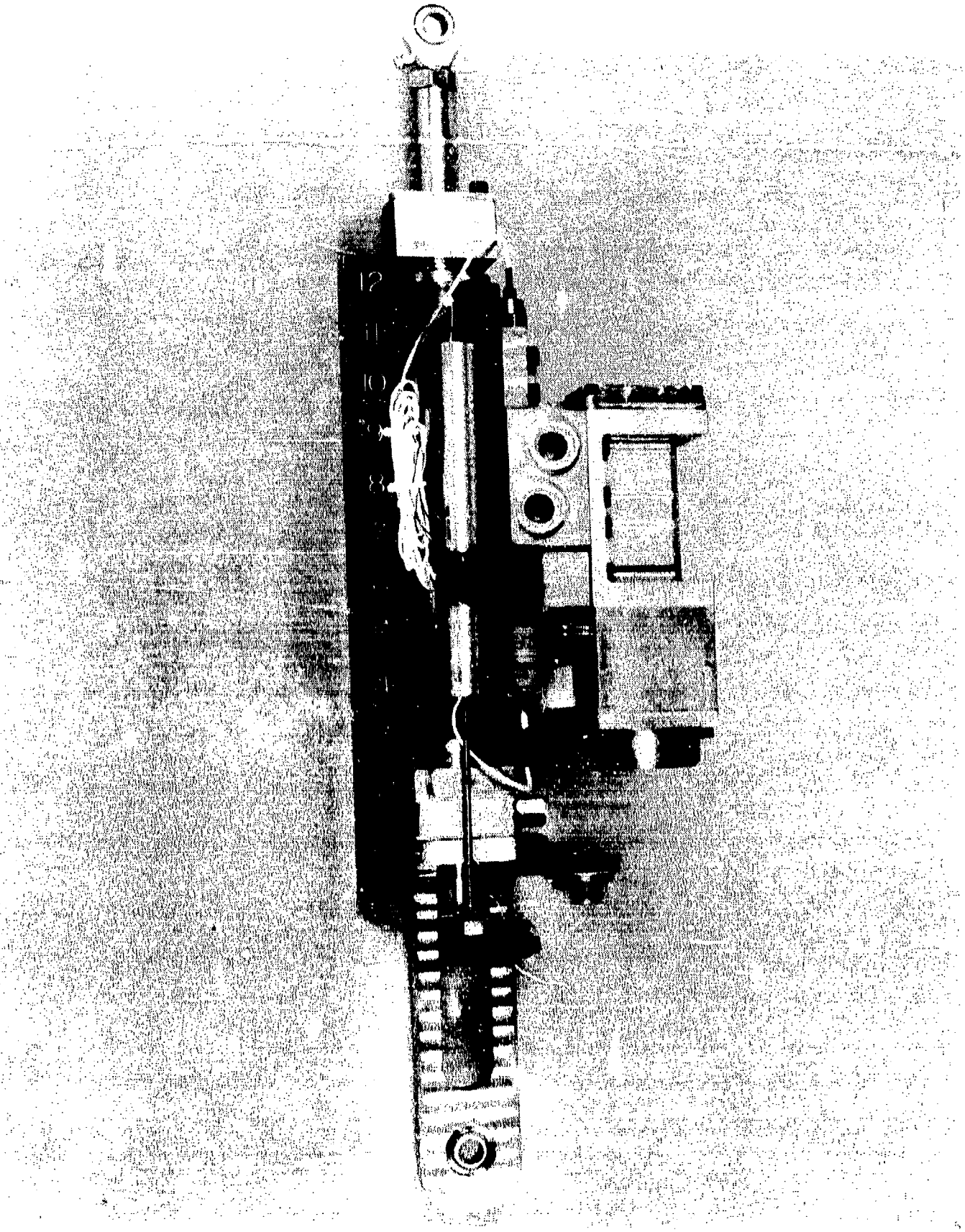

Figure I-9. Side view of test actuator.

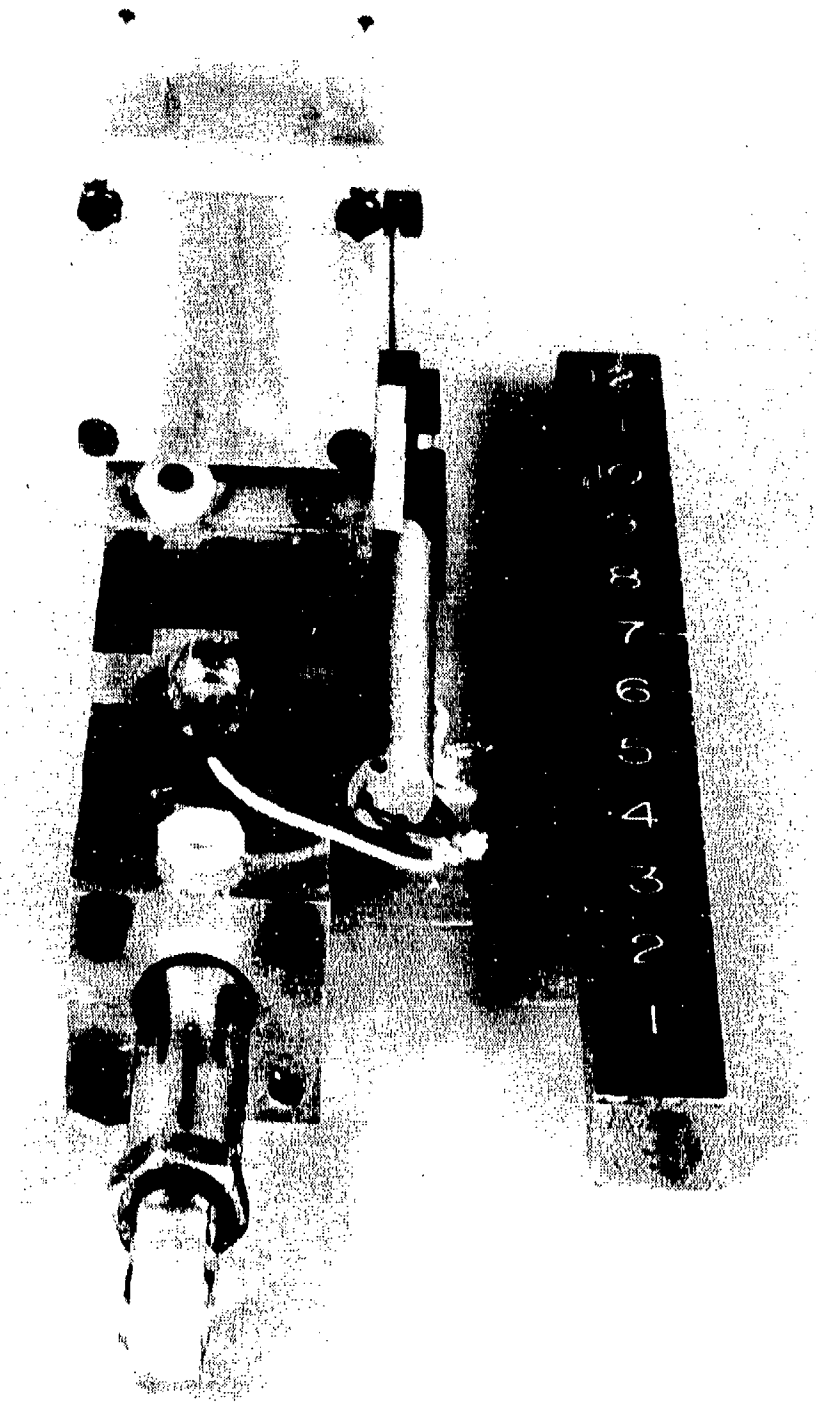

Figure I-10. Front view of test actuator.

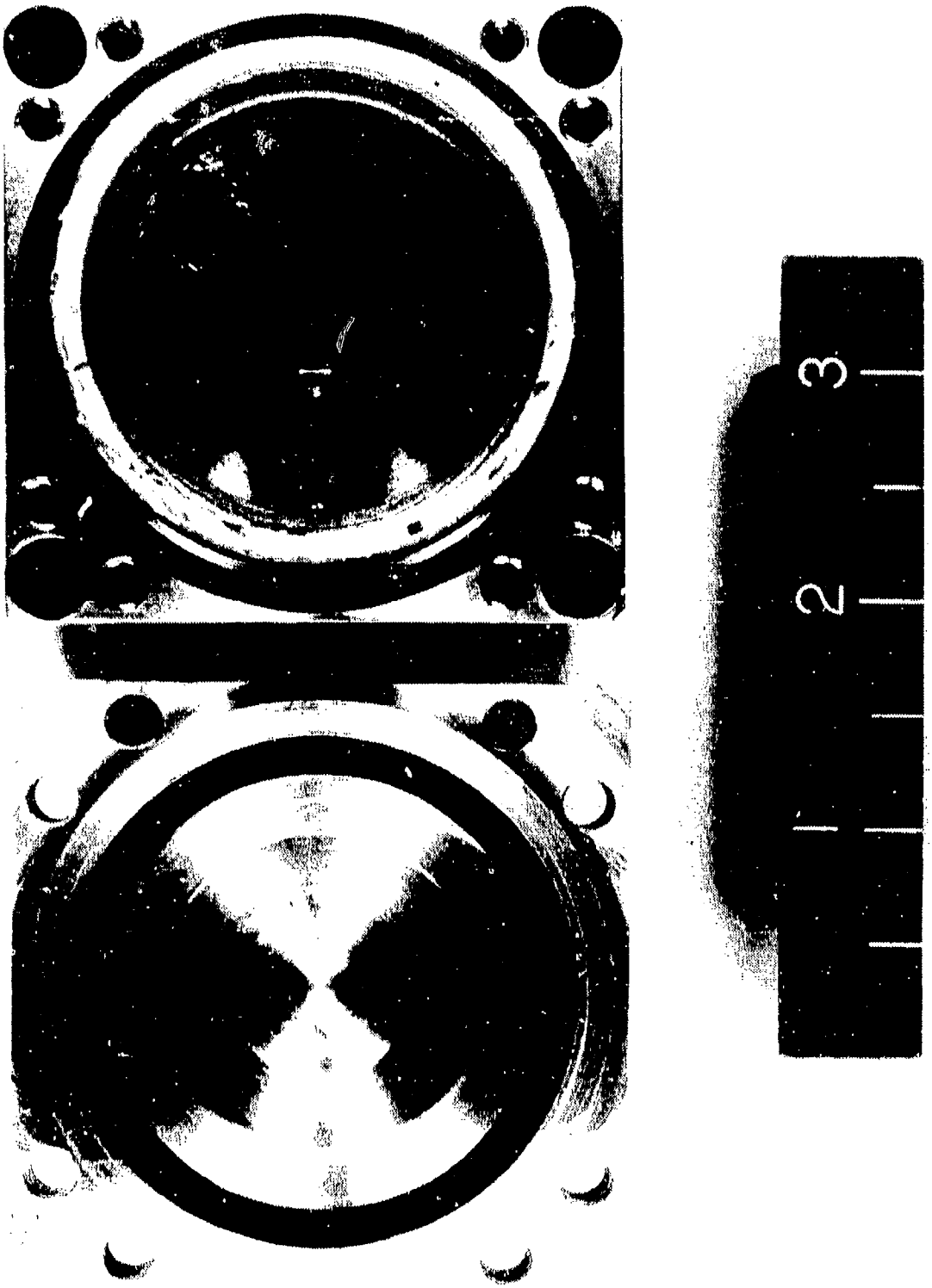

Figure I-11. Direct drive motor.

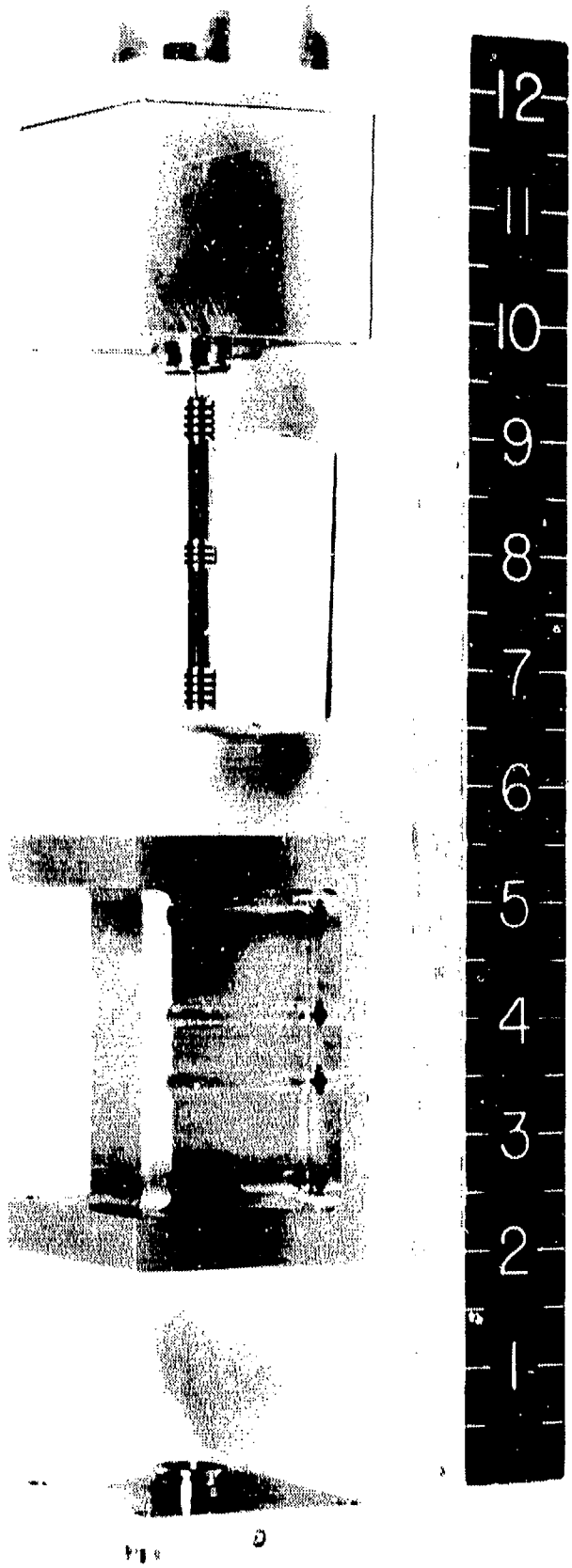

Figure I-12. Disassembled valve.

Manifold

The manifold connected the actuator to the hydraulic supply and return lines and acted as an interface between the valve and cylinder. The manifold was constructed of stainless steel type 416 (because aluminum does not have sufficient strength for 275°F and 8000 psi). Figure I-13 is a picture of the manifold. The manifold had ports at each end for pressure transducers. This located the transducers directly above the quills feeding the cylinder. The high-pressure connections between the manifold and valve were 7/16-inch diameter quills with 1/4-inch diameter flow areas. The manifold package measures 1¼ by 2¼ by 7¼ inches.

Pumping System Description

The pumping system used an Enerpac hydraulic power supply. Several filters, an accumulator, a heat exchanger, and other hardware were selected and assembled to form a complete pumping system for continuous high-pressure operation. A framework was designed to mount the pumping system components. The framework mounted on the hydraulic power supply to make a semiportable pumping system. Two such units were assembled, one using Mil-H-83282 as the working fluid and the other using CTFE. These units were self-contained and needed only to be connected to cooling water and an electric power supply. For use in the lab, these units were connected to the emergency hydraulic shutoff switches found throughout the lab. The switches de-energized the electric motors but did not release the energy stored in the accumulators. A schematic of the pumping system is shown in Figure I-14. Figure I-15 is a picture of the system.

Hydraulic Power Supply

The hydraulic power supply used in the pumping system was an Enerpac model *PEM-8418-1*. This unit consists of a fixed-displacement axial-piston pump driven by a constant-speed, 440-volt, 60-hertz, 12.5 horsepower AC motor. The pump output is divided between two ports with each port supplied by half the pistons. The two outputs are fed into a bypass valve. The pressures are summed at low pressures. At high pressures, the bypass valve is activated to dump one output back to the reservoir. In this way, the pump has about a 4-gpm output at low pressures and a 2-gpm output at high pressures. The transition occurs at about 3000 psi. The bypass valve also contains a safety relief valve which is factory set at 10,000 psi.

The output from the bypass valve goes into a manual valve and an adjustable relief valve connected in parallel. The manual valve is a 4-way, 3-position valve with one position supplying flow to the test stand, one position blocking the ports, and the third position dumping the flow back to the reservoir. The adjustable relief valve was used to set the pressure to the test stand.

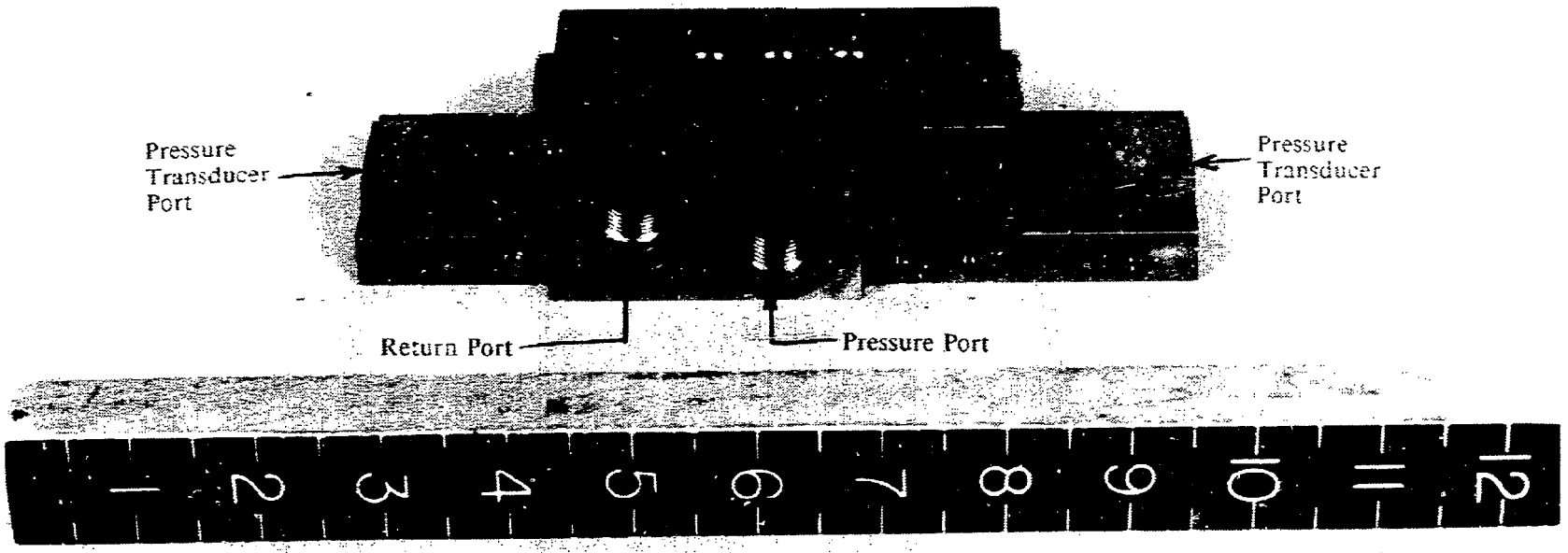

Figure I-13. Manifold.

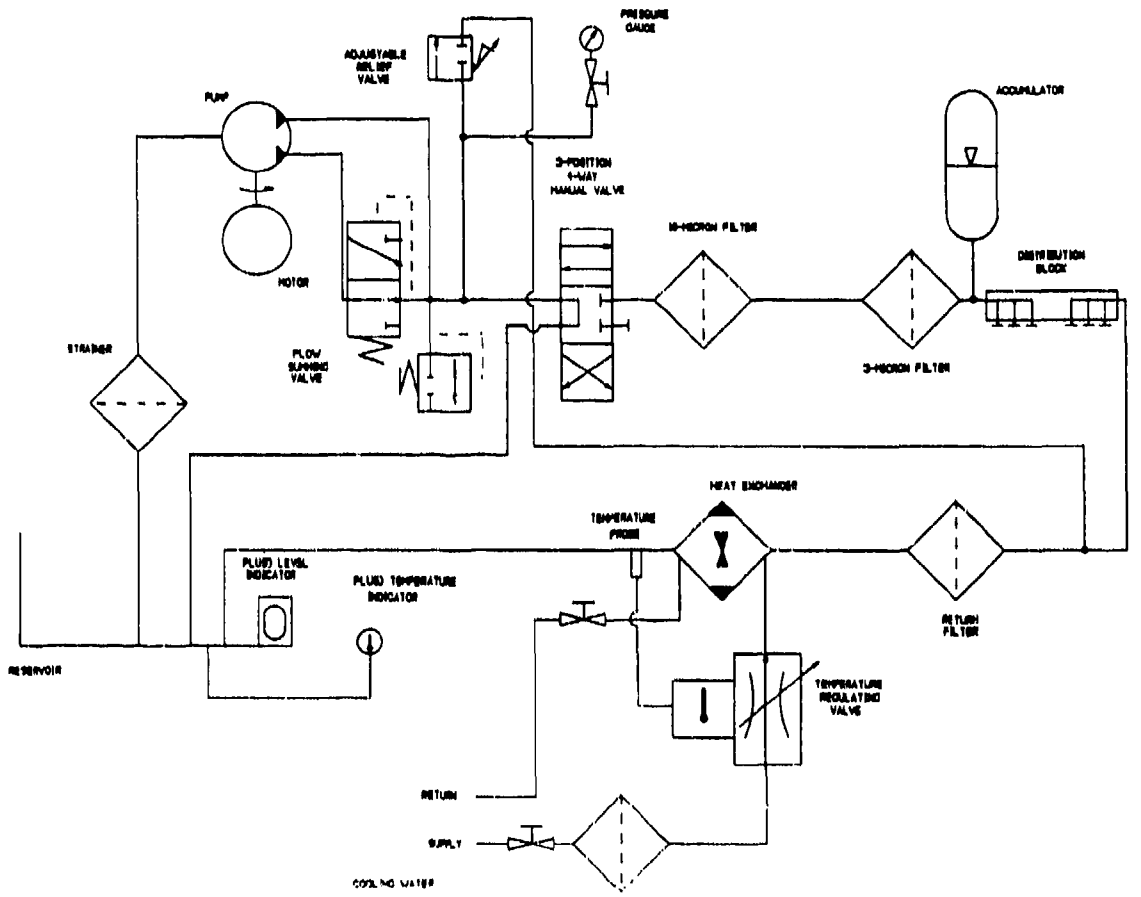

Figure I-14. Pumping system schematic.

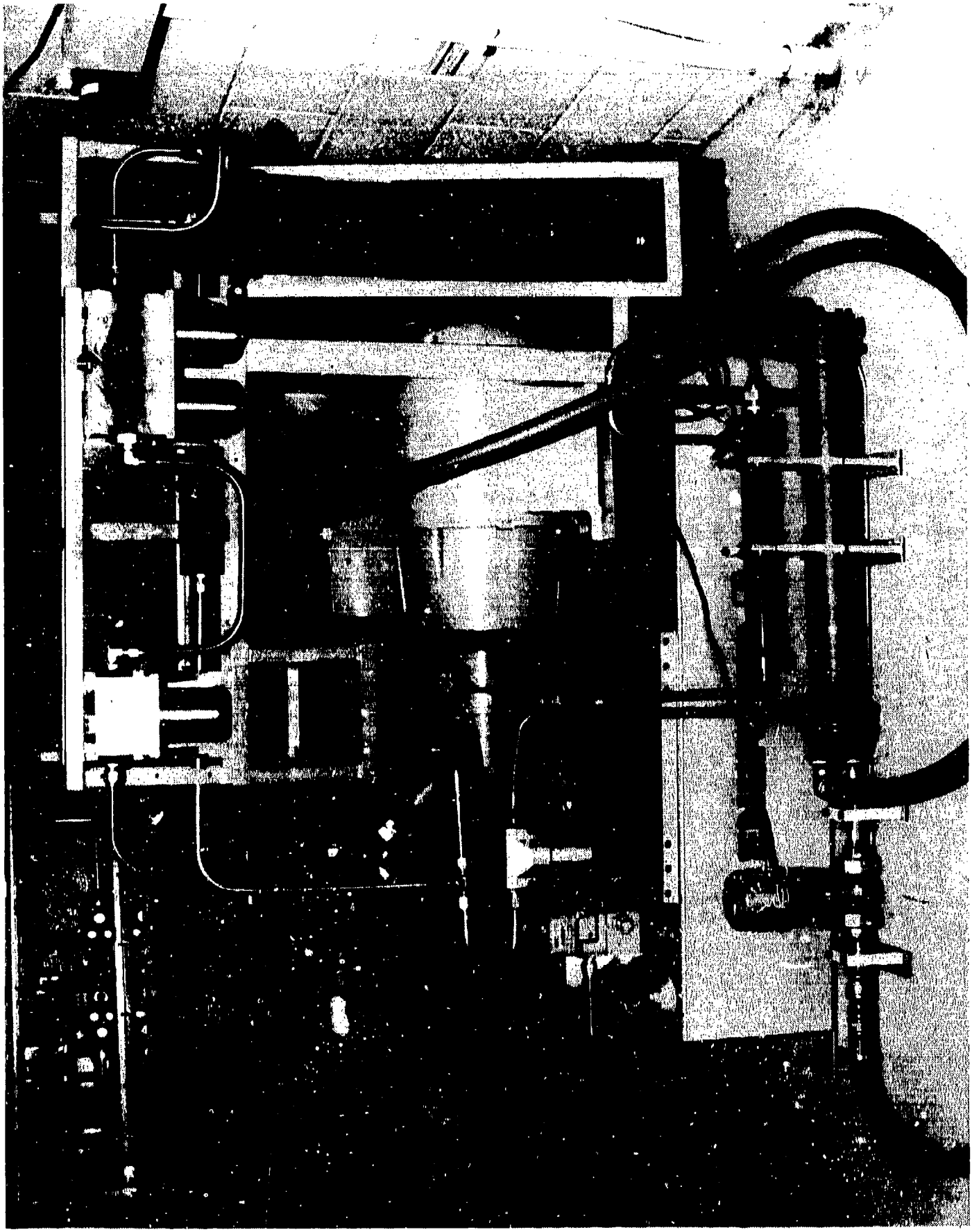

Figure 1-15. Pumping system.

Filtration

The flow supplied to the test stand passed through a two-stage filter. The first stage was a 10-micron absolute filter and the second stage was a 3-micron absolute filter. The return side had a single 10-micron absolute filter which filtered the flow from the test stand and the bypass flow from the adjustable relief valve. All filter elements on the CTFE unit were metal because CTFE is reported to break down the bonding of paper elements. Except for the 3-micron final-stage supply pressure filters, paper elements were used on the Mil-H-83282 unit. Metal element filters were used for the 3-micron filters so both units had identical final stage filtration on the supply lines.

Accumulator

A one-gallon, nitrogen-charged piston accumulator was located on the supply line between the final-stage filter and the distribution block. The purpose of this accumulator was to filter the pump ripple, filter the spikes caused by the opening and closing of the adjustable relief valve, and to maintain a constant pressure to the distribution block as the test actuators drew flow. The accumulator was sized to allow a pre-charge pressure of 1800 psi (which is readily available) to be used while maintaining an adequate gas volume at 8000 psi to perform the required functions. The accumulator piston was fitted with a poppet on the oil side which closes off the oil port when the piston bottoms out. The poppet traps oil inside the accumulator, thereby balancing the gas pressure and preventing the gas from leaking into the hydraulic system when the system is shut down. Accumulators in both systems used Viton seals and were supplied by Chicago Fluid Power.

Distribution Block

The distribution block provided standard SAE straight-thread O-ring pressure and return ports to the test stand. The pressure and return ports were two each of size SAE-8 and one each of size SAE-3. The block was machined from cold-worked medium-carbon steel and the SAE-8 port fittings were torqued to 100 ft-lbs. The SAE-3 port fittings were torqued to 50 ft-lbs. There was no internal bypass valve in this block so the pressure and return sides of the block were completely isolated.

Hydraulic Lines

The hydraulic lines connecting the components were sized to handle 4.0-gpm flow and 8000 psi pressure with a safety factor of 5.75. The fittings installed were Imperial-Eastman Hi-Seal tube fittings with *17-4 PH* stainless steel sleeves. The tubing chosen had a 1/2-inch outer diameter with a .083 thick wall and was made of type *304* stainless steel (1/8 hard). The fittings adapted to standard SAE straight thread ports.

Cooling System

The cooling system was designed to allow continuous operation of the hydraulic power supply. The cooling system was sized to remove the heat generated by a flow of 2.0 gpm across a 8000 psi pressure drop (because the pump has a fixed displacement and is working against a relief valve). This required a minimum cooling capacity of 400 Btu/min and an oil-to-water, multi-pass heat exchanger was chosen to handle the loading. The cooling water inlet was throttled by a temperature control valve with its temperature probe in the oil outlet port. The system used external cooling water and had 3/4-14 NPT ports for water inlet and outlet.

III. TEST PROCEDURE AND RESULTS

General

The testing had two purposes. One purpose was to establish that the seals did prevent leaking. The second was to determine if the seals had friction and wear characteristics suitable for use in a flight-control actuator. The fluid temperature during testing was from 130°F to 150°F. The tests and their results are described in the following section.

Laminar Flow Past Bushings

This test consisted of stroking the actuator to one end and maintaining an error signal to the valve to keep the valve open. In this manner the cylinder pressure in the bushing being tested would be equal to supply pressure. The supply pressure was then varied and laminar flow past the bushing was recorded as a function of pressure drop across the bushing. The results are plotted in Figure I-16. The average leakage at the no-load pressure of 4000 psi was about .025 cis per bushing. This represents about .03 horsepower lost in leakage for the two bushings of the actuator. The relationship is not linear (as predicted by laminar flow equations). This is probably due to the expansion of the bushing and end cap when pressurized (the clearance between the rod and bushing increased as pressure increased). The front bushing of the MIL-H-83282 actuator closed down at high pressures. This anomaly was probably due to pressurized fluid leaking between the end cap and bushing, forcing the bushing in against the rod.

Piston Seal Leakage

To check the leakage across the piston seal, the manifold and valve were removed from the cylinder and a new manifold was mounted on the cylinder. This approach was necessary to differentiate between the piston seal leakage and the leakages of the bushings and direct drive valve. Figure I-17 is a schematic of the test set up used to measure piston seal leakage. Table I-2 summarizes the results of this test.

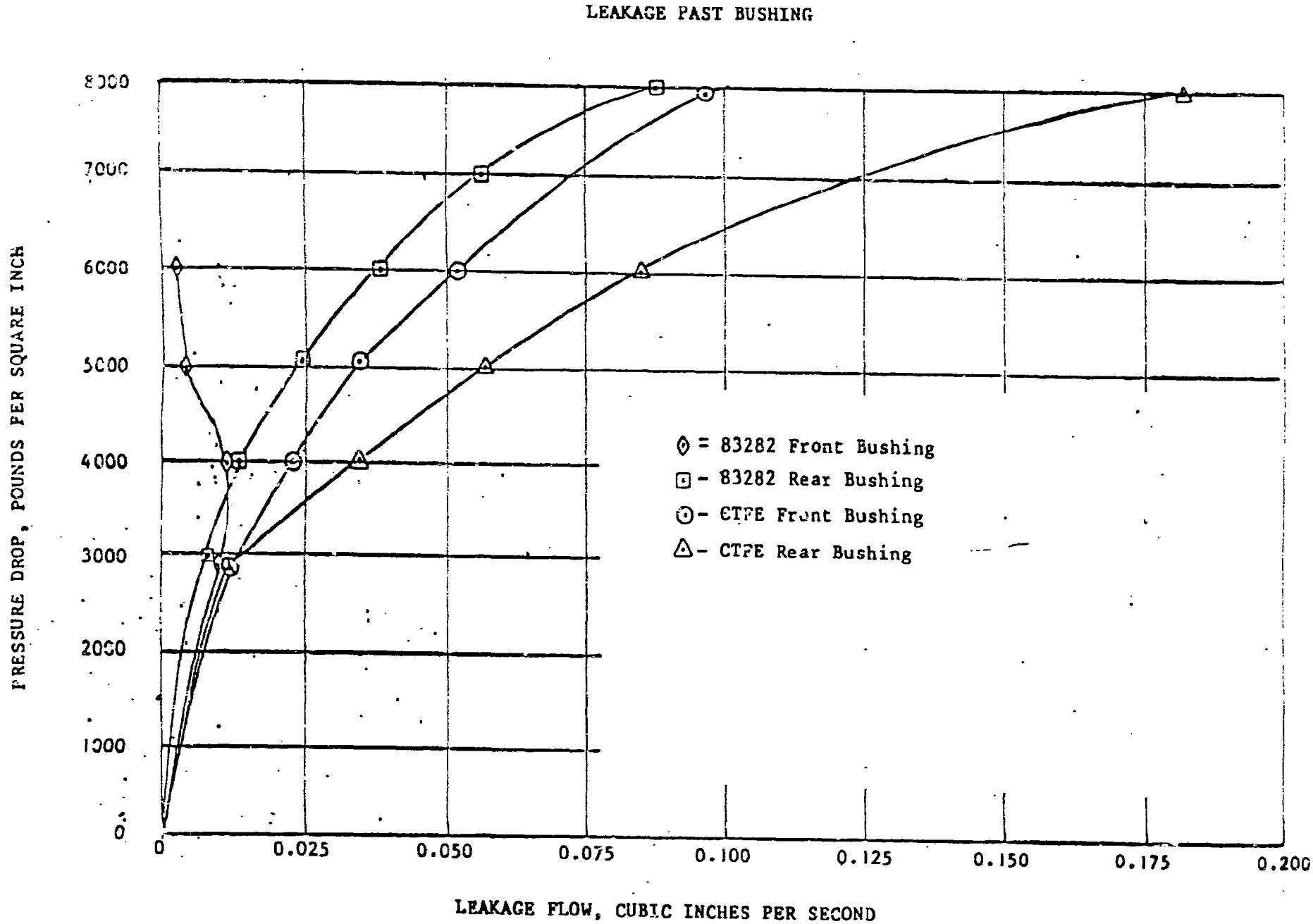

Figure I-16. Laminar flow plots.

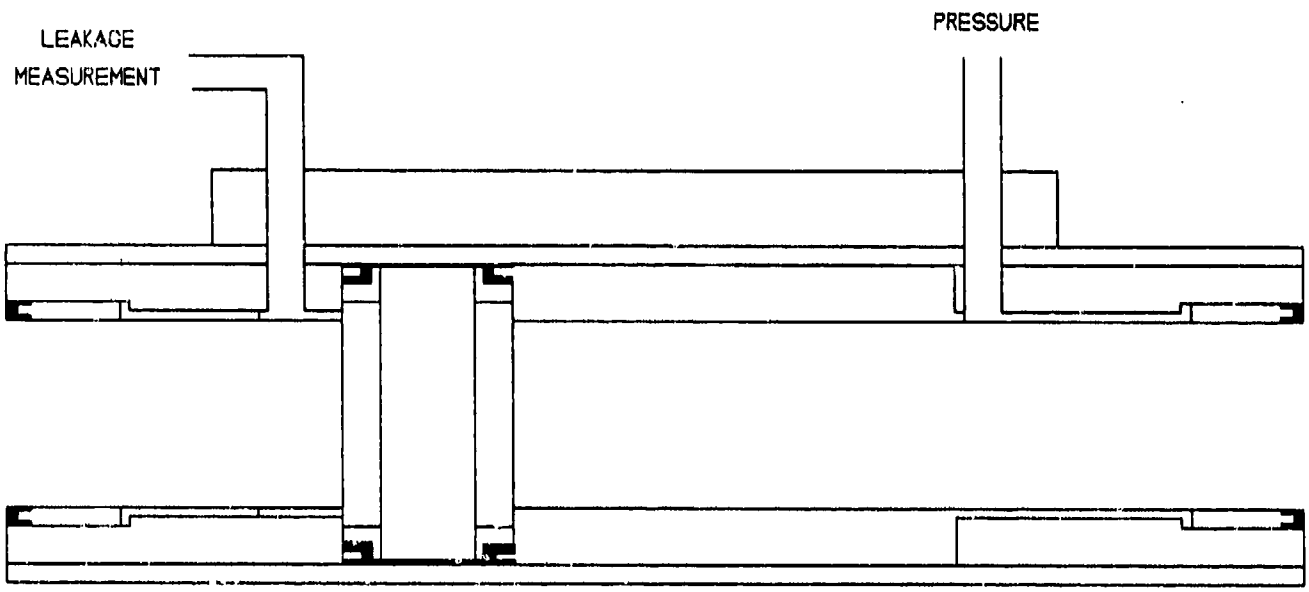

Figure I-17. Piston seal test setup.

Table I-2. Leakage past piston seal.

	leakage drops per minute	
PSI	MIL-H-83282	CTFE
1000	9.0	7.0
2000	9.5	6.8
3000	9.0	6.8
4000	6.2	6.8
5000	7.3	6.4
6000	6.7	6.5
7000	6.1	6.0
8000	5.6	6.0

Seal Friction

The actuator was tested for running friction by applying a .05 Hz triangular wave and measuring the pressure required to move the actuator at 0.1 inches per second. Figure I-18 is the plots of these results. These plots show the running friction for both actuators to be less than 25 psi (which is about 0.3 percent of the system pressure). It is also noted from these plots that the static gain of the CTFE actuator is 0.21 inches per volt and 0.24 inches per volt for the MIL-H-83282 actuator. At the time the data was recorded, the MIL-H-83282 actuator showed an uneven slew rate. The problem was in the valve -- the seals showed no extra friction or leakage.

Frequency Response

The loop gain was established arbitrarily to give a nominal 4 Hz response from the test actuator. The frequency response of the actuators was checked by driving the actuators at 4.0 Hz. Figure I-19 is the plot of the results. The figure shows the CTFE response at 0.15 inch per volt to be - 2.92 dB relative to the response at 0.1 Hz. The response of the MIL-H-83282 actuator was - 1.58 dB (at 0.20 inches per volt) relative to the response at 0.1 Hz. The sealing system had no apparent adverse effect on actuator response.

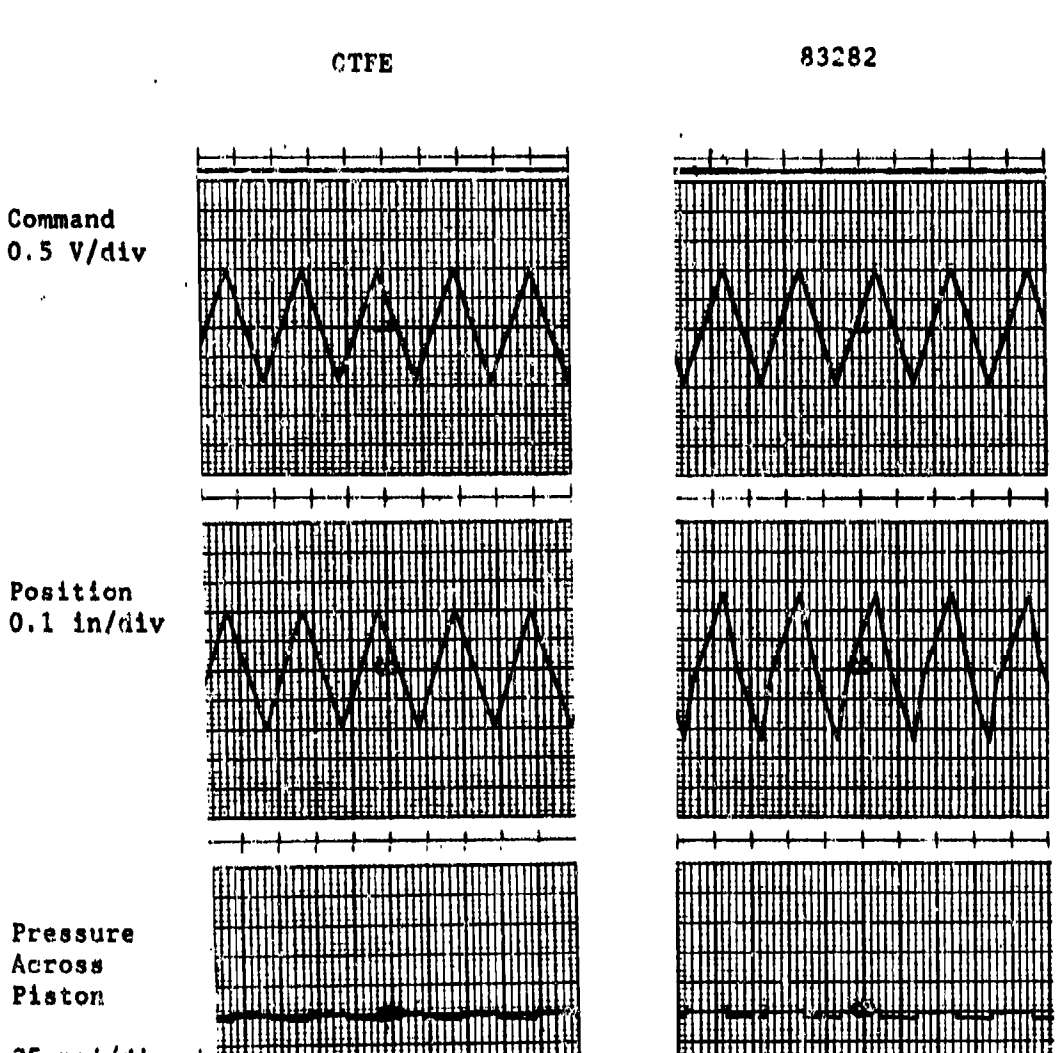

Figure I-18. Seal friction.

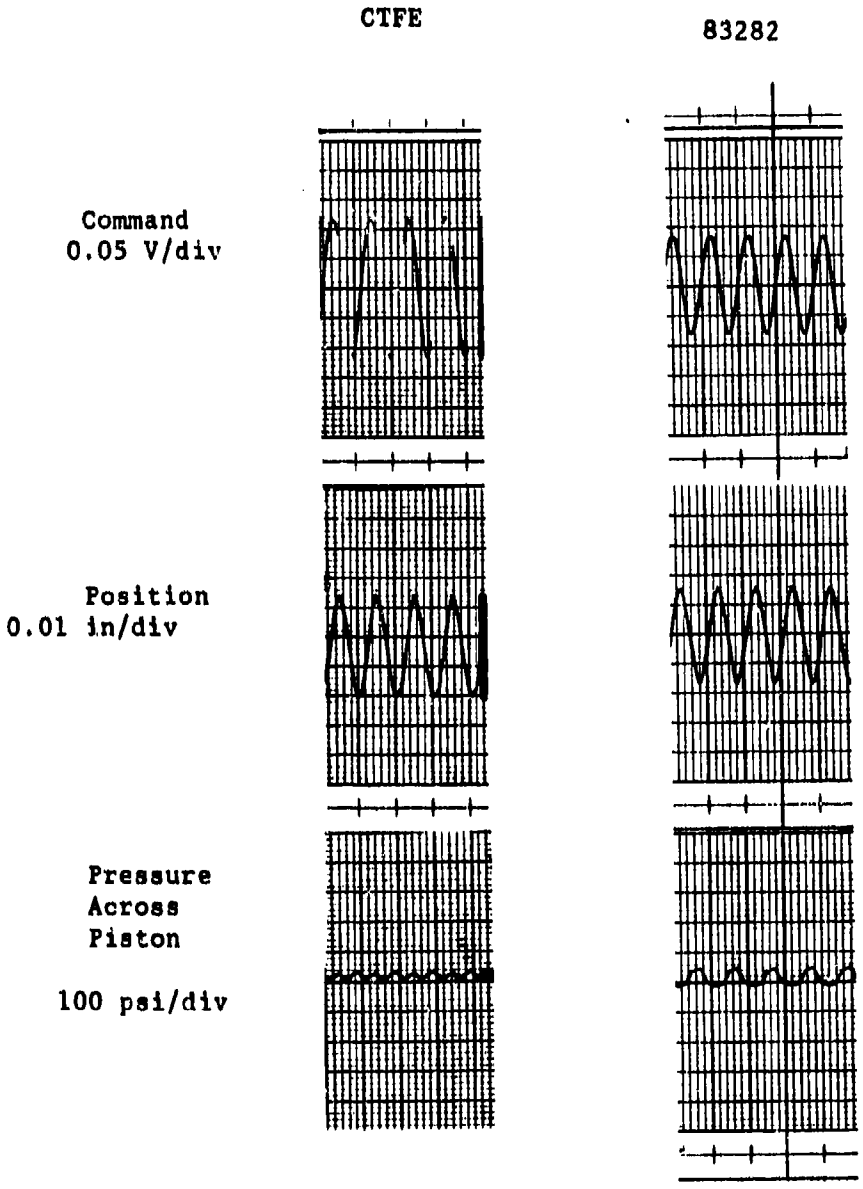

Figure I-19. Response -- 4.0 Hz.

Life Cycle Test

A limited amount of life-cycle testing was performed. The test cycles consisted of driving the actuator against an external hard stop (with the piston seal near the center of the cylinder where maximum breathing occurs) to cause the pressure across the piston rapidly to rise to 8000 psi. The actuator was brought off the stop by about .08 inches to bring the pressure across the piston back to 0 psi, completing the cycle. In this way, only one of the piston seals experienced the pressure cycles so the effects of pressure could be differentiated from other wear factors. The input command for the cycling was a 10.0 Hz sinusoid. Figure I-20 is a typical test cycle and a total of 500,000 full-pressure cycles were performed. There was no significant change is actuator performance during the cycling so the actuators were disassembled and the seals were visually inspected. Figure I-21 is a picture of the CTFE piston seal and Figure I-22 is a picture of the MIL-H-83282 piston seal after 500,000 cycles. The seals are slightly extruded and show only moderate wear on the surface which runs on the cylinder wall.

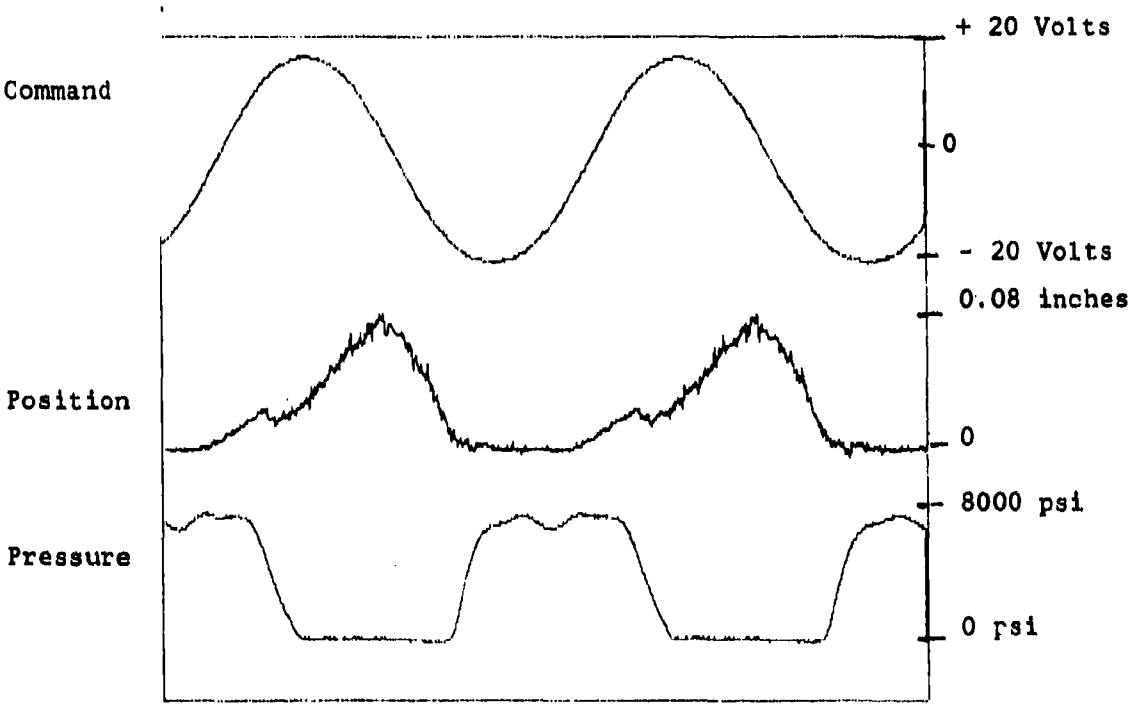

Figure I-20. Typical endurance test cycle.

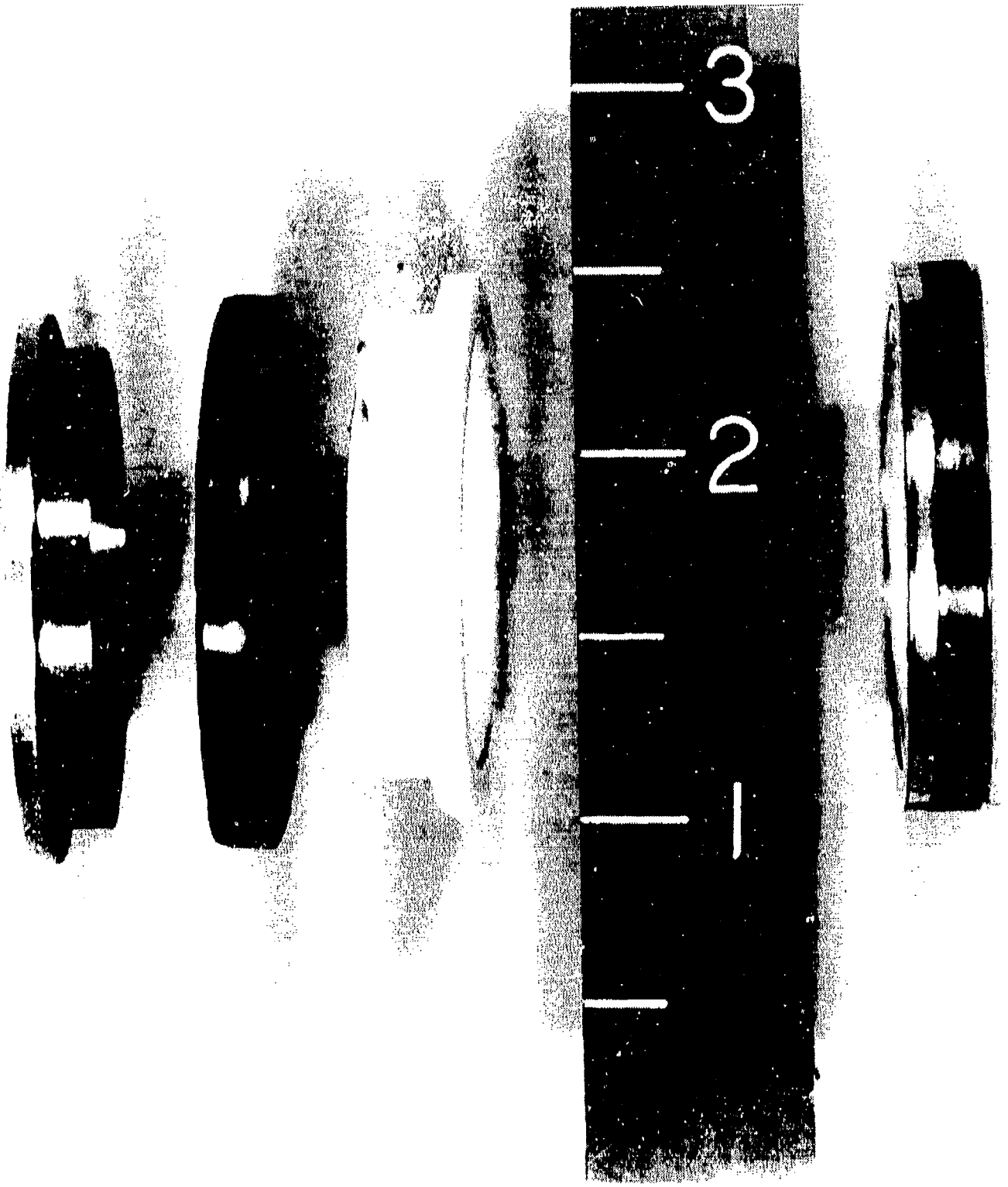

Figure I-21. CTFE piston seals after testing.

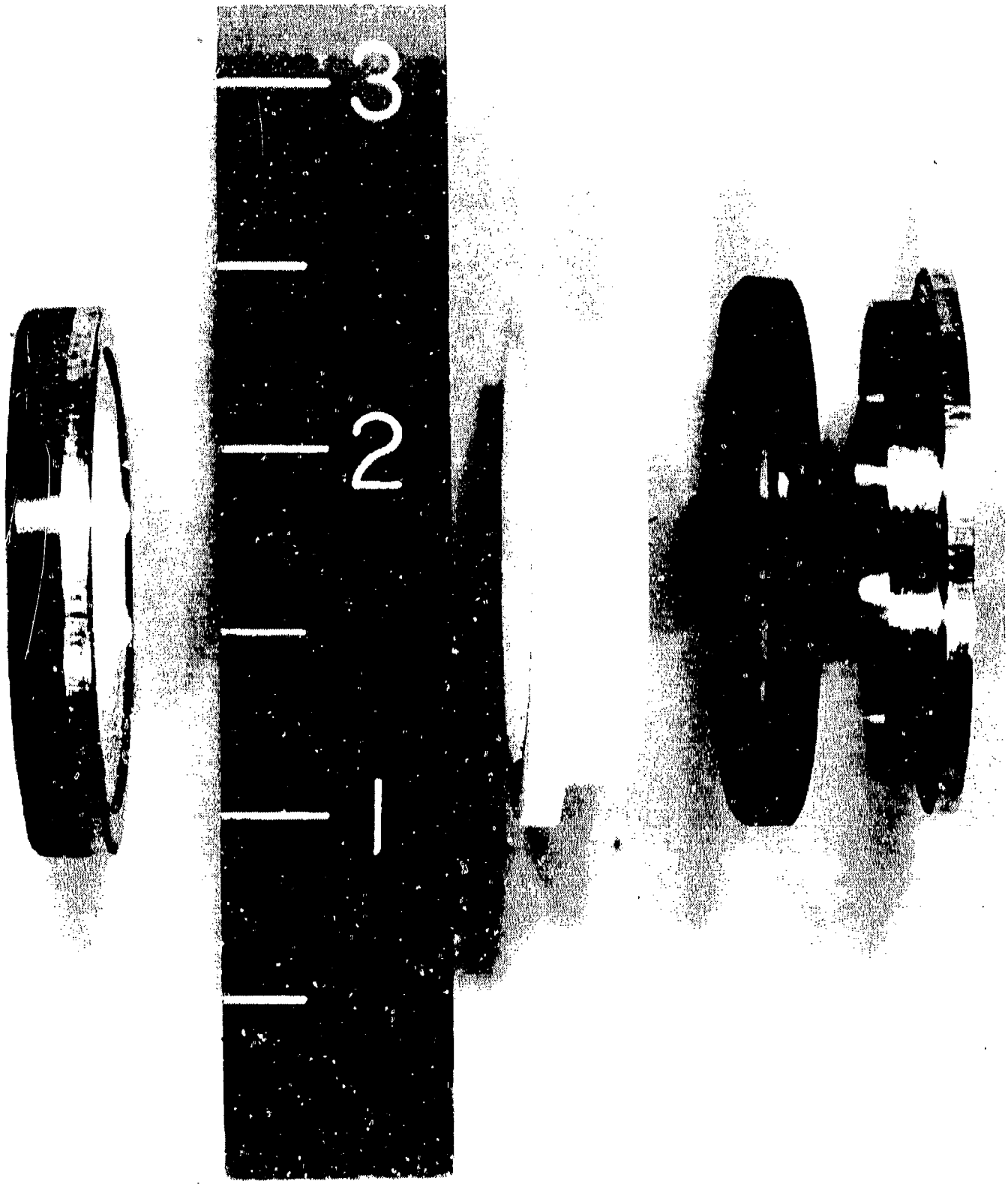

Figure 1-22. MIL-H-83282 piston seals after testing.

IV. CONCLUSIONS AND RECOMMENDATIONS

Even though the *303* and *304* stainless steels have a coefficient of thermal expansion similar to that of aluminum bronze, it is not a good material for piston rods and end caps. Materials usually used for these parts have a higher yield strength. In addition, seals do not wear well running on *303* and *304* stainless steel. Hard chrome plating would increase rod seal life. However, better results can be obtained if the rod base material is a high-strength steel and then hard-chrome plated. High-strength steels have a lower coefficient of thermal expansion than most bushing materials. With proper design, high-strength steels can be used for the rod and end cap. The thin-wall aluminum-bronze bushing, expanding faster than the end cap, will reduce the rod clearance as temperature increases. The bushings will need to be designed and fitted so the least clearance occurs at the highest temperature. This has the advantage of having the least clearance when the viscosity of the fluid is lowest.

The sealing system performed well with both CTFE and MIL-H-83282 fluids and is a good candidate for further testing. More life-cycle testing and high-temperature testing are needed to verify the life and temperature capability. The rod sealing system will mainly be a problem of allowing adequate clearance between bushing and rod throughout the temperature range. The PTFE rod seal can work a temperature of up to 500°F at low pressures. For very severe environments or where zero external leakage is required, the PTFE rod seals could be replace with metal bellows. The high-temperature performance of the piston seals is more questionable. Even if the backup rings prevent extrusion at high temperatures, the PTFE material tends to lose its dimensional integrity when subjected to a combination of high loads and temperatures. However, this sealing system is unique and should be tested at high temperatures before final conclusions as to the suitability for temperatures about 275°F are made. If PTFE materials became unsatisfactory, alternative materials should be investigated. The pressure-operated backup rings are not temperature-limited and will minimize the radial real clearance for high-pressure piston seals.

The high-pressure sealing system investigated will have a higher cost of production, require more space, and allow more power loss through internal laminar flow. These factors may make the use of this sealing system in every high-pressure flight-control actuator undesirable. However, in applications requiring low friction, operation in a severe environment, and long seal-life, this sealing system appears to be a viable design.

SECTION II

DIGITAL SERVOVALVE INVESTIGATION

I. INTRODUCTION AND SUMMARY

The digital servovalve investigation was an expansion of research on a digital electrohydraulic servovalve concept previously conducted by Dynamic Controls, Inc. The initial investigation was performed under USAF Contract F33615-79-C-3605 and is described in the report AFWAL-TR-80-3074. Phase I of the expanded investigation used high-response poppet valves driven by piezoelectric (PZ) force motors in a configuration similar to the initial investigation. The piezoelectric drive poppet valves had a step response thirty times faster than the electromagnetic solenoid valves originally used. The high-response valves potentially allowed significant improvement of the test actuator's dynamic response. Phase II of the expanded investigation used a microprocessor to close the actuator's position control loop and to drive the digital servovalve. For both phases of the expanded investigation, the digital servovalve was evaluated in a control system which included a feedback transducer, control electronics and actuator.

The results from Phase I of the expanded investigation demonstrated that the digital servovalve operated as intended in terms of control and waveform. The 0.5 millisecond operating speed of the piezoelectric poppet valve was rapid enough to minimize time delay effects of the solenoids on the control of the actuator. However, because of the final flow obtained from the piezoelectric poppet valves was one third of the design goal, the dynamic performance of the actuator (slew rate and frequency response) failed to meet the original design goals.

The Phase II use of the microprocessor to control the digital servovalve system was quite successful. Using off-the-shelf Z80 hardware, the maximum frame time for the real-time program was 600 microseconds, primarily due to using efficient machine-code programming. The processor provided the flexibility necessary for varying the operating characteristics of the system.

The high-speed characteristics demonstrated by the piezoelectric drivers and on-off drive requirements provide excellent compatibility for interfacing a with a digital control system.

II. TECHNICAL APPROACH

General

Servovalve Description

Figure II-1 is a schematic of the operational elements of the digital servovalve connected to an actuator. The servovalve uses seven poppet valves and four orifices. Four of the poppet valves (1 through 4) are used for directional control. Valves 1 and 4 are connected from a cylinder port of the valve to hydraulic return. Valves 2 and 3 are each connected to one cylinder port. A gallery is connected to the combined output flow from the flow modulation poppet valves and orifices. As shown in Figure II-1, four orifices (0_1, 0_2, 0_3, and 0_4) are used for flow modulation. Orifice 0_1 is connected directly to hydraulic supply while orifices 0_2, 0_3, and 0_4 are connected through valves 5, 6, and 7, respectively. Valves 5, 6, and 7 are used in combination with the non-switched orifice 0_1 to provide the flow to the directional solenoid valves. Opening valves 2 and 4 causes the actuator to move to the right as shown on Figure II-1. The rate at which the actuator moves is determined by the operation of valves 5, 6, and 7.

Figure II-2 illustrates the flow modulation capability of the four fixed orifices and three-valve mechanization of Figure II-1. This figure shows the stepwise approximation of the flow characteristics of a conventional servovalve assuming the normalized values of 0_2, 0_3, and 0_4 are 1, 2, and 4 respectively. Eight flow-rate steps are available from the one fixed orifice and the three switched orifices. Table II-1 lists the eight combinations determining the flow steps.

Table II-1. Flow steps tabulation.

Flow Rate Orifice Combinations	Flow Rate Combination No.
0_1	1
$0_1 + 0_2$	2
$0_1 + 0_3$	3
$0_1 + 0_2 + 0_3$	4
$0_1 + 0_4$	5
$0_1 + 0_2 + 0_4$	6
$0_1 + 0_3 + 0_4$	7
$0_1 + 0_2 + 0_3 + 0_4$	8

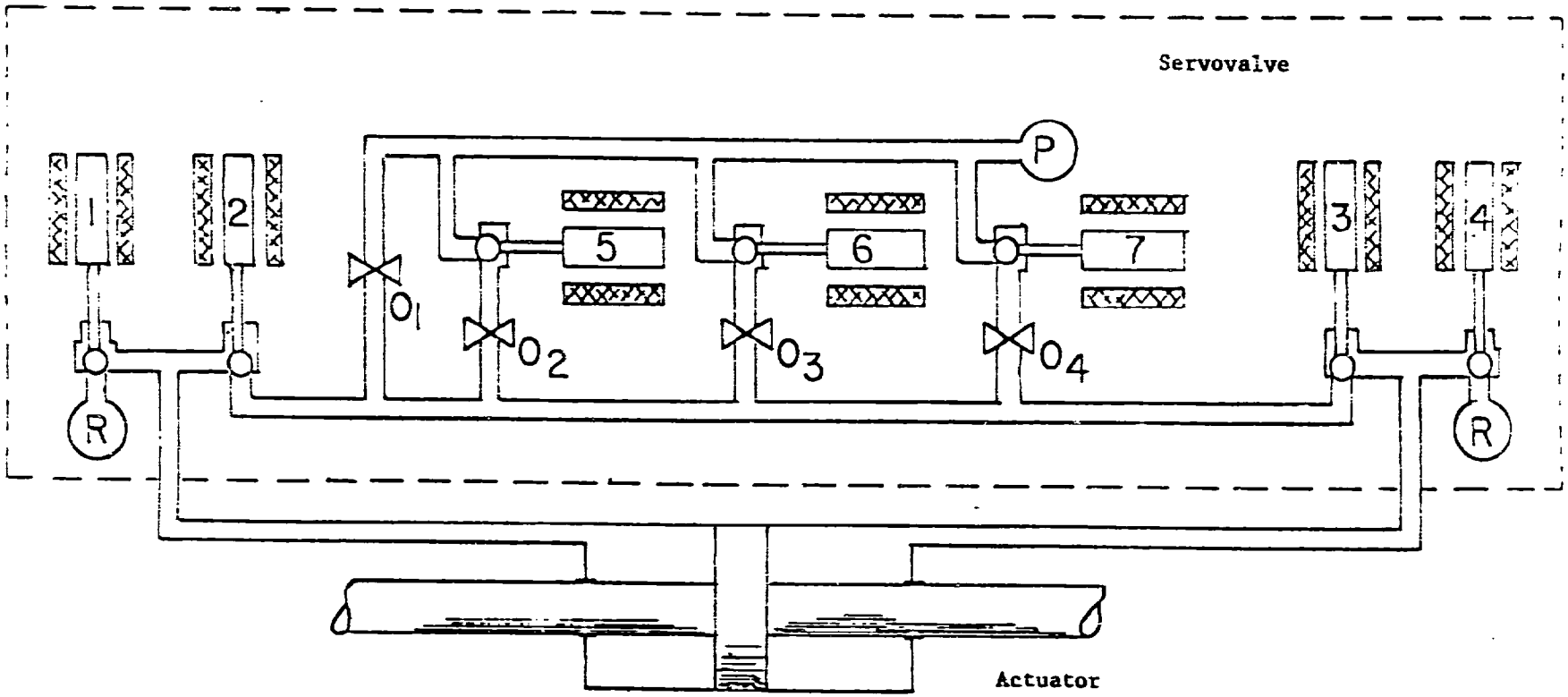

Figure II-1. Digital servovalve schematic.

As shown in Figure II-2, the flow at zero input is shown to be zero. This reflects the effect of the threshold built into the driving electronics for directional valves. With the actuator stopped, no flow is required from the control valve to the actuator. The *zero flow* at *zero input* when added to the eight flow combinations of Table II-1 gave a total of 9 different flow rates.

In general, the number of flow modulation steps available from a particular configuration of a fixed orifice and a given number of switched orifices is:

$$S = 2^n$$

where S is the number of flow steps and n is the number of poppet valves used for switching in the flow modulation orifices.

With eight flow steps, flow linearity is maintained within ± 6.25 percent of a linear output flow. This non-linearity would not normally cause a problem in a closed-loop-position system, although there will be some harmonic distortion in the actuator motion at high-frequency operation. If better linearity is desired, adding one more flow control poppet valve would provide a flow linearity of ± 3.1 percent (comparable to most analog aerospace servovalves).

To achieve the best approximation of the linear flow curve with the digital valve operation, the pressure drop across the directional solenoids at the maximum flow demand from the valve should be much smaller than the pressure drop across the feed orifices used for the flow modulation.

As shown on Figure II-1, the solenoid valves are normally closed, two-way ball poppets. Flat-disc and cone poppets are variations on the poppet design which offer similar seal-off and contamination-insensitivity characteristics. The flow available through a poppet valve at a given pressure drop is a function of the porting area. To open the valve against large differential pressures, the operator force (and size) increases with porting area.

Direct-operating poppet valves are limited in flow capacity unless large operators are used. For applications requiring flows above 2 gpm at pressure drops not exceeding 100 psi, pilot-operated poppet valves can be used. With pilot-operated solenoid valves, there is some increase in the response time of the valve and potentially some slight increase in contamination sensitivity as compared to direct-operating poppet valves.

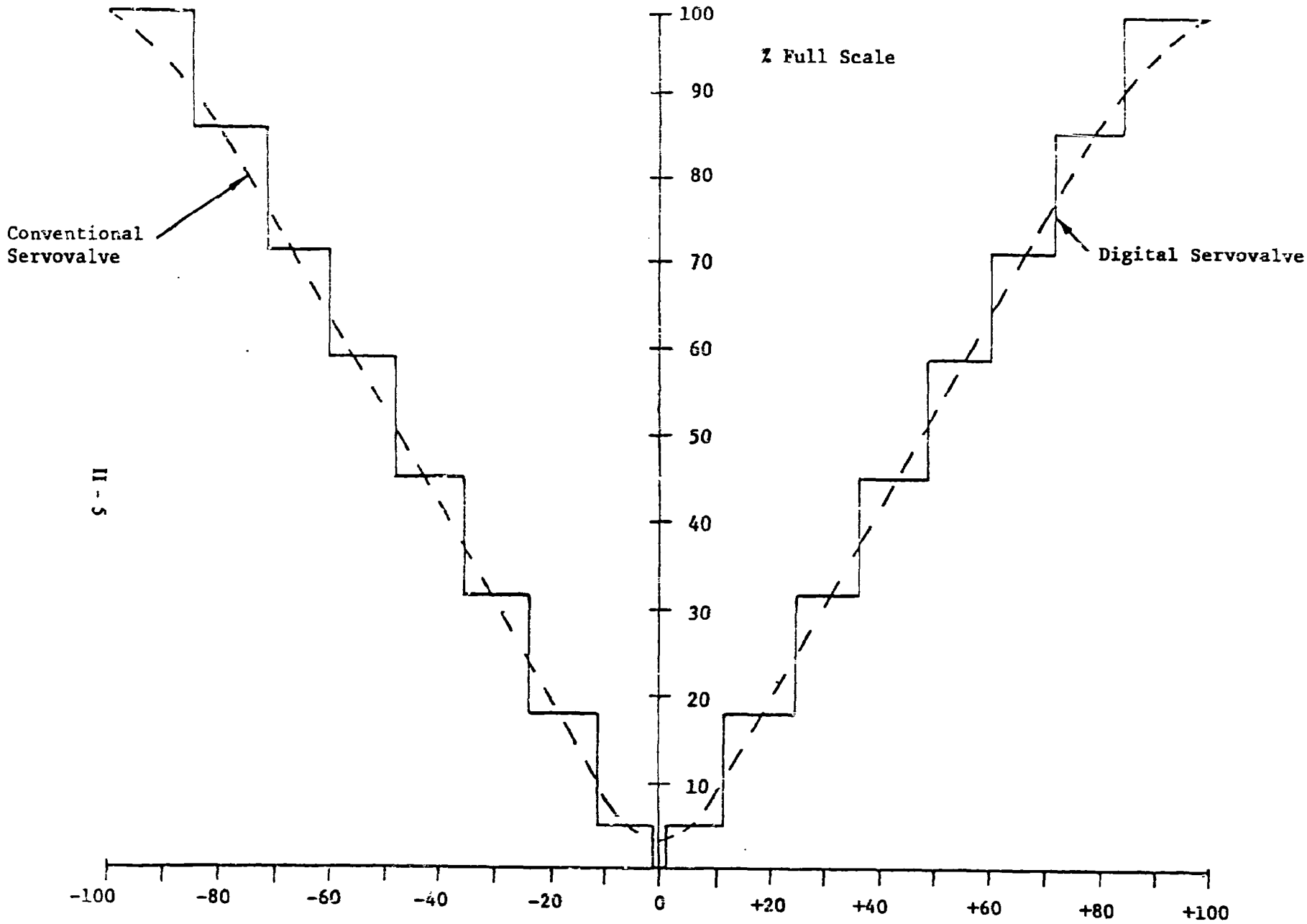

Figure II-2. Flow linearity of digital servovalve.

Control Loop Requirements

The performance requirements of the control actuator used with the digital servovalve defined the flow and time response characteristics of the servovalve's individual poppet valves. For the investigation, the actuator was the same as originally used with electromagnetic poppet valves. The actuator had a drive area of 0.77 in^2 and a total stroke of 4 inches. The drive area of the actuator and the required frequency response of the actuator at a particular stroke determine the maximum flow requirement from the servovalve. For an actuator requiring a response of 10 Hz (frequency at which amplitude response is attenuated by 3 dB) at a stroke of ± 5 percent of the maximum actuator stroke, the peak actuator velocity (from harmonic motion equations) is:

$$\dot{X} = \hat{X}\omega$$
$$= 4.44 \text{ inches/second}$$

Where: $\hat{X} = .05\ (.707)\ (2 \text{ inches}) = .0707 \text{ inches peak}$

$\omega = 2\pi f = 2\pi\ 10 = 62.8 \text{ radians/second}$

The maximum flow required from the servovalve is the product of the actuator drive area and peak velocity. For the test actuator, the maximum flow required from the digital servovalve was:

$$Q = A\dot{X}$$
$$= 3.41 \text{ inch}^3\text{/second}$$

Where: Q = maximum flow in inch^3/second

$A = 0.77 \text{ inch}^2$

$\dot{X} = 4.44$ inch/second

Figure II-3 is a block diagram (in transfer function form) for the actuator control loop.

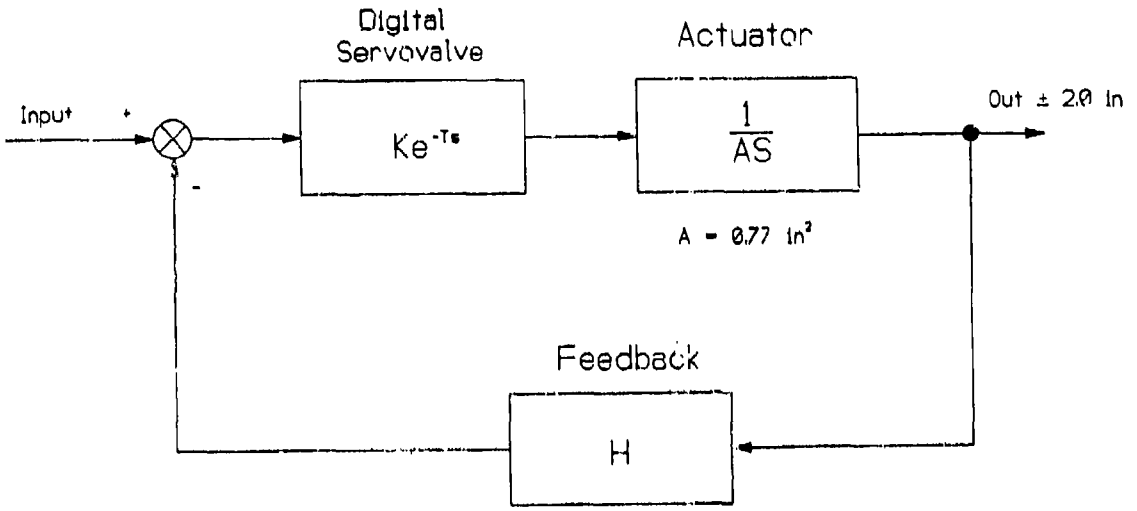

Figure II-3. Control loop with digital servo.

The transfer function term of the poppet valve configuration (Ke^{-Ts}) implies that the value is a gain with a time delay of T seconds. This time delay creates a phase lag in the control loop that is equal to:

$$\emptyset = T\ 360\ f$$

where f equals the frequency and $\emptyset$ is the phase lag in degrees. Previous analysis and evaluation of digital control systems[1] indicated that system stability is not significantly degraded by a time delay when the frequency equivalent (reciprocal) of the time delay is at least eight times the systems' frequency response. A frequency that is eight times the system response is generally beyond any frequency of interest because the amplitude response of the system at that frequency is very low. Applying the *eight times* criteria, a total time delay of less than .012 seconds is desirable for operation of a 10 Hz bandwidth system. This requires

[1] AFFDL-TR-77-30

that the on (and off) time of the poppet valve be no longer than .012 seconds. To provide for growth and push current technology, an operate time .001 seconds was established as a goal for the poppet valve performance. The flow of 3.41 inch^3/second (nominally 1 GPM) and a response time of nominally 1 millisecond were used as the basis of the poppet valve performance specification listed in Table II-2. This specification was used to conduct a market survey for off-the-shelf valves.

Table II-2. Poppet valve performance requirements.

Fluid Type	-	MIL-H-5606
System Pressure	-	3000 psi
Valve Type	-	Two Way Poppet
Fluid Flow	-	1 GPM @ 500 psid
Control Voltage	-	As required
Temperature Range	-	Laboratory Environment
Mounting	-	Cartridge
Operating Time	-	1 Millisecond (On and Off)

The flow requirement of the poppet valve was established at 1.0 gpm because the normal high-speed poppet designs are generally limited to 1.00 gpm (because of the operating forces required when the flow orifice diameter increases in size). An increase in operating force requires the poppet driver's physical size to increase to the point that the operating speed becomes limited by the mass of the valve operator.

Market Survey

The poppet valve specification was sent to hydraulic valve manufacturers using Thomas Register as a reference source. The request for information suggested that the poppet valve be an aerospace type. The request also identified the specifications as ideal and suggested that the manufacturer should respond with a product that would qualify as a high-response poppet valve. Four poppet valves designs were received. General Controls P.N. AV11D1235 and Consolidated Controls P.N. 13271 were aerospace-qualified designs, although not in current production. Table II-3 lists the results of the survey. None of the valves met the goals of the poppet valve specification.

Manufacturer	Part Number	Flow & ΔP	System Pressure psi	Response On msec	Response Off msec	Cost/Unit
ITT, General Controls	AVIID1235	0.6 gpm @ 1000 psi	1500 psi	3.5	3.5	$1500.00** (aerospace)
BKM, Inc. Orshausky Division	N/A	1.0 gpm @ 300 psi	500 psi	2.5	2.5	$400.00 (commercial)
Brunswick Technetics Circle Seal Controls Div.	649T--2PP -0A	1.3 gpm @ 500 psi	750 psi	14	3.2	$675.00 (commercial)
Consolidated Controls, Corp.	13271	1.0 gpm @ 500 psi	3600 psi	>10	>10	$4014.00 (aerospace)

**Telephone estimate

Table II-3. Poppet valve market survey comparison.

Alternative Approach

All of the poppet valves reviewed in the market survey were driven with electromagnetic solenoid-type operators. All of the poppet valves reviewed in the market survey also failed to meet the performance specifications. The difficulty in designing high-response poppet valves is described in the following material. Figure II-4 represents the normal design configuration of an electromagnetic poppet valve.

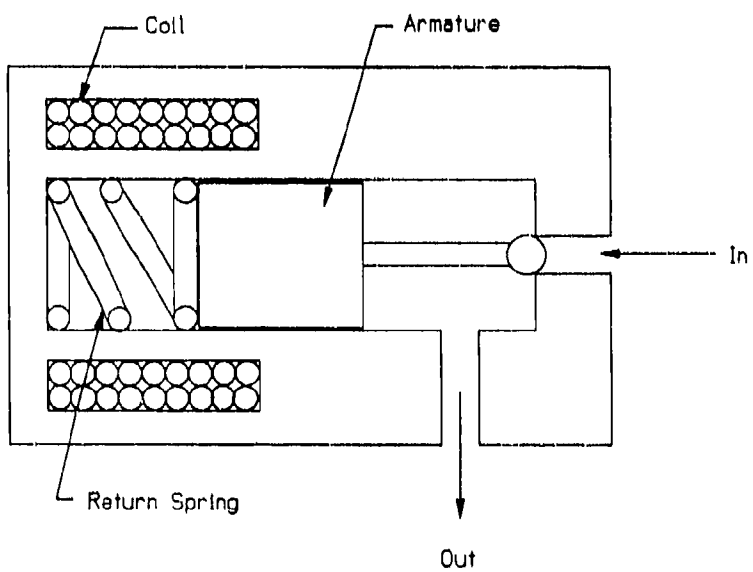

Figure II-4. Solenoid poppet valve.

The electromagnetically created force induced by current flow in the solenoid coil must overcome the difference between the spring preload force and the force from the differential pressure operating on the poppet ball. The induced force must also be large enough to quickly accelerate the armature to open the poppet within the desired opening time. For example, an armature weighing .022 lbs and traveling .020 inches in .001 seconds from rest will require a driving force of 2.27 lbs. The spring preload force required to close a 0.30 inch diameter orifice with 3000 psi differential pressure is 2.12 lbs.

Although the spring preload force and differential-pressure force can be balanced against each other for one operating condition, with lower differential pressures (as occur in applications where the discharge pressure varies) the solenoid must overcome a large portion the spring preload force to open the valve.

To both open the valve and to quickly accelerate the armature, the force to operate the valve is nominally double the force to slowly open the valve. Doubling the force requires doubling the number of turns of the coil (for constant coil current). Increasing the number of turns of the solenoid coil increases the inductance-resistance or LR time constant. The LR time constant is a measurement of the time to establish the current flow in the coil and therefore the force to accelerate the armature and/or open the valve. The LR effect on the coil current is defined by:

$$I_{out} = I_{hold}\,(1 - e^{-tR/L})$$

Where:
- I_{out} = coil current at time t
- I_{hold} = final value coil current
- R = coil resistance
- L = coil inductance
- t = time

The LR time delay can be reduced by using a variable supply voltage to drive the solenoid in a current feedback mode. This technique does not require more turns on the coil but does require a higher supply voltage. However, even with a current driver for the coil, one of the principal difficulties with high-speed operation with an electromagnetic driver is the time required to establish the coil current.

Because of the response difficulties with the magnetic driver, alternative approaches to drive the poppet valves were reviewed. One approach reviewed was uses of a moving permanent magnet in place of the armature of a solenoid. The moving magnet approach has been applied by DCI to other R&D projects and has similar response limitations as conventional solenoid valves. A second approach, using a piezoelectric element as the valve operator, was also reviewed. A piezoelectric actuator has a high force-to-mass ratio, which results in excellent dynamic response. A PZ actuator also has a high total-output force capability. The alternate approach review indicated excellent potential for building a PZ poppet valve with a response time of less than 1 millisecond. The PZ driver was therefore selected for use in the Phase I digital servovalve development.

Piezoelectric Characteristics

The word *piezoelectric* refers to pressure electricity, a property of certain crystalline materials. A body of piezoelectric material will distort when an electrical charge is applied to it. Conversely, an electric field will be generated when a force is applied to the piezoelectric body. The quantitative values for the relationship between mechanical deformation and field depend upon the type of material, the poled axis and the physical configuration. PZ materials are well established and the current state of the art permits accurate prediction of the material's performance under various field conditions.

The output force capability of PZ materials are typically very high (on the order of 3000 lb/in^2), although the strain (output motion) is very small (on the order of 0.1 percent of the thickness). The electrical input characteristic of PZ material is the same as a capacitor. Because of the high force-to-mass ratio for the PZ material, the strain can be obtained within a few microseconds. For PZ materials, the relationship between strain and applied field is generally designated "d" in units of meters/volt. Strain is defined as the *ratio of change-in-length to length* and field as the *ratio of voltage to distance between the electrodes*. Two subscripts are used with d, making the general form d_{ij}. The first subscript indicates the direction of the field and the second the direction of the resulting strain. Typically, fields of 25,000 volts/inch are required to produce a strain of .001 inches. To reduce the driving voltage, the PZ drivers are produced in thin layers, bonded together and connected electrically in parallel. For a field of 25,000 volts/inch, a layer thickness of .020 inches requires applying a voltage of only 500 volts across the layer. Figure II-5 shows a representative PZ stack and the electrical driving arrangement.

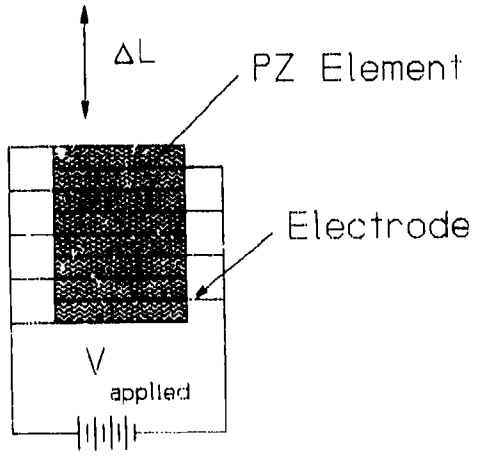

Figure II-5. PZ stack construction.

The strain predicted by d_{ij} is *free strain* with the PZ element not being loaded or restrained. If the element is restrained, a stress is created in the element with the stress-strain relationship being defined by Young's Modulus or modulus of elasticity for the material. A typical value for PZ material is 7×10^6 psi (about 25 percent the modulus of elasticity for steel). Figure II-6 is a plot of the stress/strain relationship at a field of 40,000 volts/inch. The maximum potential energy stored in the material occurs at the operating point defined by (maximum stress/2, maximum strain/2).

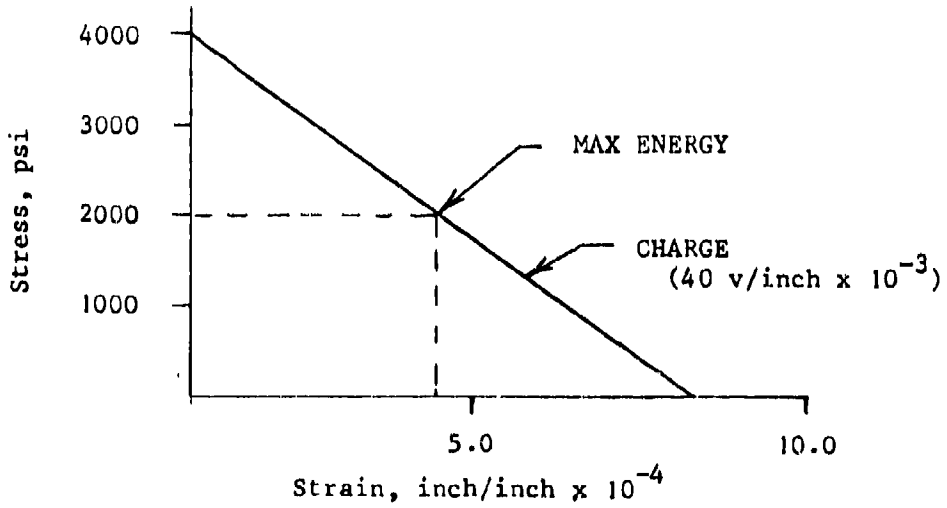

Figure II-6. Stress/strain characteristics of Physics International PZWT 100 material.

A feature of a PZ actuator is that a preload of several thousand psi may be applied to a stack without affecting the performance, providing that the preload remains constant. Once the stored energy corresponding to the charge (or field) applied has been used in performing work, no further motion or force output can be obtained. When a stack is discharged, the strain is relieved and the stack will return to its initial position. The charge and discharge signature as shown in Figure II-7 is the hysteresis loop, typically with a 20 to 30 percent hysteresis value. The large hysteresis value limits using PZ motors for linear proportional control. However, if only the end positions are used (with on-off control), repeatability is good and the hysteresis loop becomes unimportant for the control application.

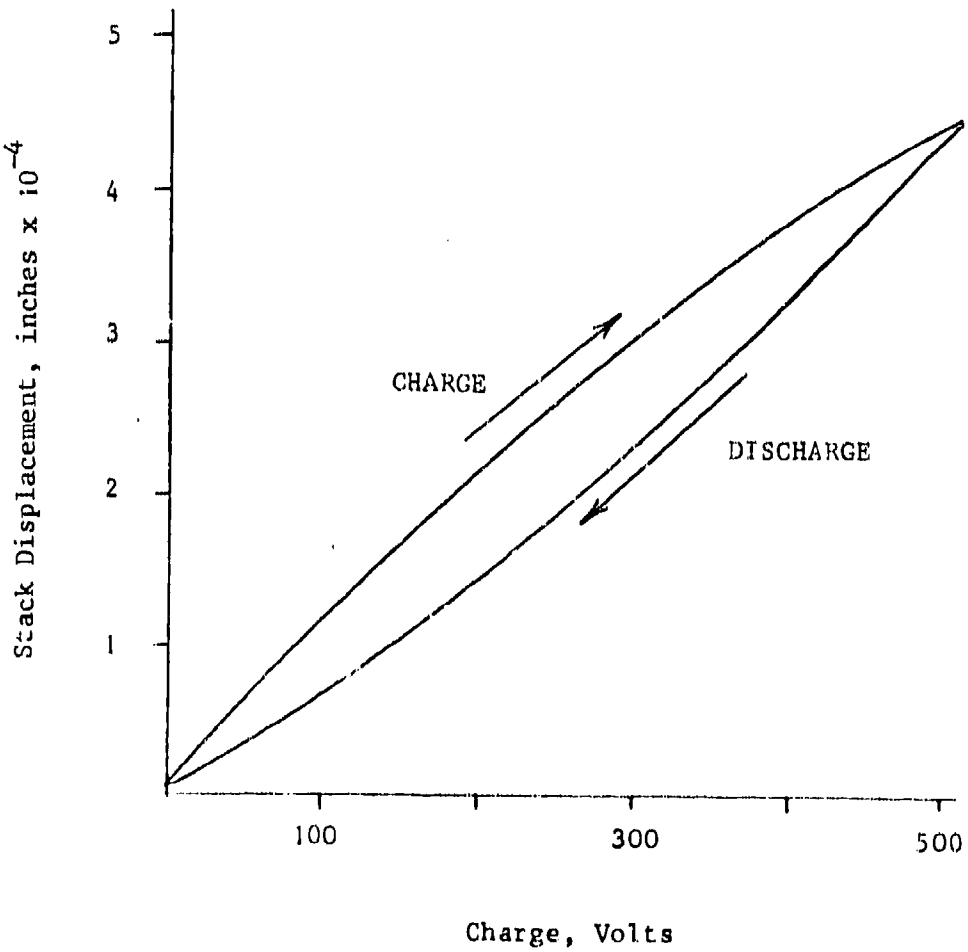

Figure II-7. PZ stack charge/discharge hysteresis.

Hardware Design

Piezoelectric Poppet-Valve Design and Development

Piezoelectric actuators were selected as the drivers for operating the poppet valves. Although PZ actuators presented the highest technical risk, they also presented the greatest potential for meeting the speed and force requirements for high-speed poppet valves. Physics International Co. (Physics International) was selected as the piezoelectric motor supplier and as a valve design consultant, based upon that company's experience with similar development projects. Hardware detail design and fabrication of the poppet valve was accomplished by DCI. The PZ actuators (stacks) were designed, fabricated and installed into PZ housings by Physics International. The joint working relationship allowed pursuing the PZ poppet design within the resources available.

The PZ poppet valve design in layout form was purchased from Physics International. The poppet valve is a cartridge design, allowing convenient installation in a single manifold package. Physics International sized the poppet valve, hydraulic amplifier and the PZ stack. The PZ actuator consisted of a stack of forty elements, each with a .020 inch thickness and a 0.50 inch diameter. The stack was designed to have a free strain of 500 microinches when charged with 500 volts. A charge value of 270 VDC was initially requested, since that voltage is the rectified AC voltage from current aircraft generating systems. At 270 VDC the free strain would have been approximately half that at the design drive voltage of 500 VDC. The reduced value of strain which would have been marginal for the application. A voltage doubler circuit was used to convert the 270 volts to a nominal 500 VDC to charge the stack.

As shown in Figure II-8 (the original design received from Physics International) the PZ actuator stack is coupled through a 0.75-inch diameter hydraulic piston to an amplifying chamber. The chamber is pressurized by system hydraulic pressure through a check valve. A bleed valve is provided to remove air from the amplifying chamber. The poppet piston (with a diameter of 0.20 inches and a length of 0.45 inches) couples the PZ motion to open the cone-type poppet valve. Amplification of the PZ stack motion is defined by the ratio of the coupling piston area to the poppet piston area (a nominal ratio of 14). The return spring has a design preload of 2.2 pounds. The poppet stop controls the valve's stroke. The design stroke was .004 inches. For the design displacement of the PZ stack, an amplification of 8 was required to achieve the valve stroke of .004 inches.

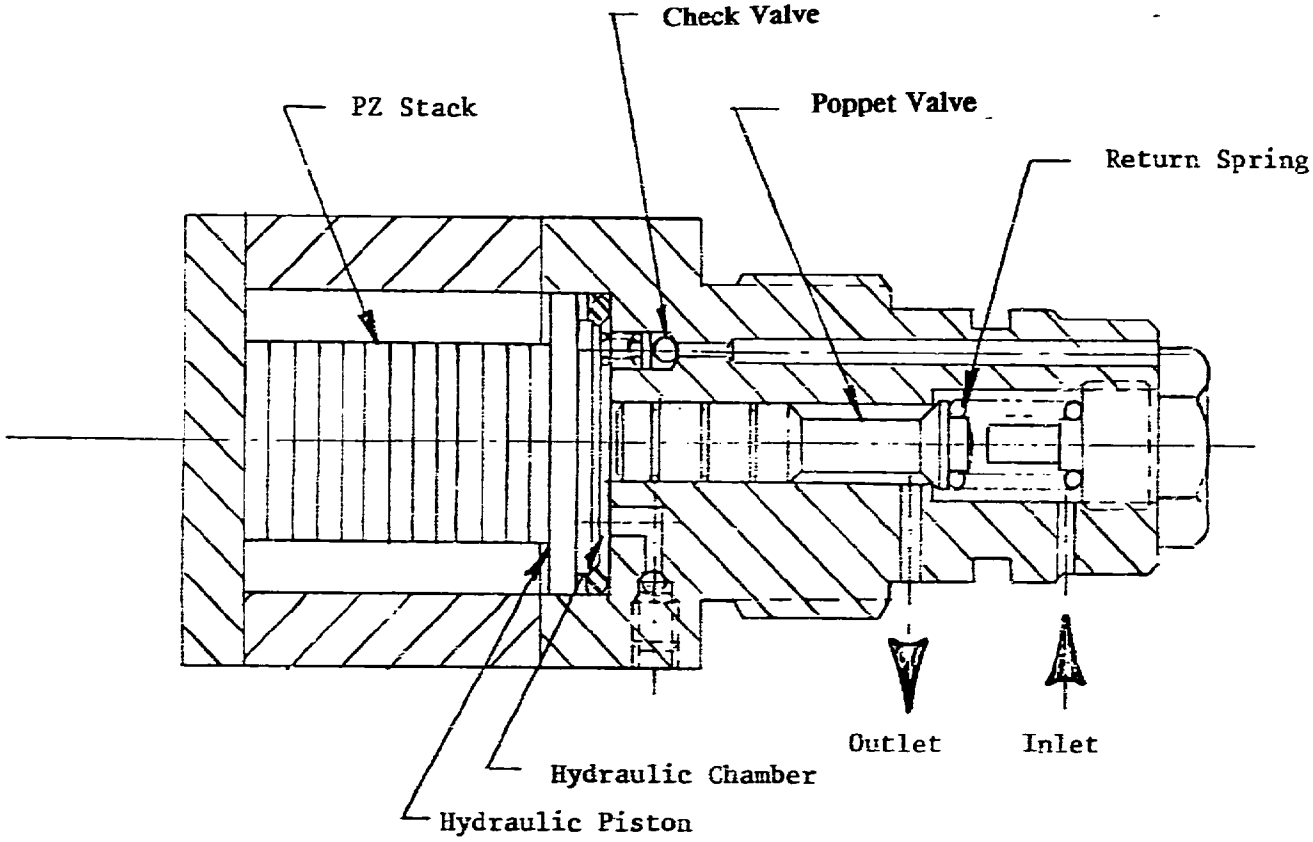

Figure II-8. Original poppet valve design.

An evaluation of the original PZ valve designs indicated a problem with using the design for the downstream directional-control valves. The inlet pressure to the downstream valves of the digital servovalve may have variations in pressure from 300 to 2000 psi, depending upon the flow rate and the actuator load condition. Since the hydraulic amplifier chamber's pressure is supplied through a check valve from the flow inlet port, inlet-port peak pressure will be trapped in the chamber. The 2.2-lb preload of the poppet return spring will be overcome by the pressure imbalance when the inlet pressure drops 71 psi below the peak chamber pressure. The valve will then self-energize until the inlet drops below the chamber pressure by 71 psi. The three flow-control valves would not be affected by this problem because supply pressure would be applied directly to the flow inlet port and the amplifier chamber. To solve the problem, an isolation piston of the same 0.20-inch diameter was added to the valve as shown in Figure II-9. Supply pressure was applied to both ends of the configuration, maintaining a pressure balance which was independent of inlet pressure. Figure II-10 is a photograph of the poppet valve components and an assembled poppet valve with an isolation piston.

Electronic PZ Driver

The electronic driver for the PZ stack was designed to convert the 270 VDC supply to 500 VDC. The circuit is basically a *flyback* design for charging and discharging the PZ stacks. The rate of charge and discharge is controlled by the PZ driver. Referring to Figure II-11, SC_1 is the charging switch and SC_2 is the discharging switch. The charging RLC circuit is L_1, $C_2 + C_{pz}$, RL_1, D_1, and SC_1 where RL_1 is the resistance of L_1. C_1 stores the instantaneous stack-charging energy provided by the unregulated 270 volt supply. R_1 is sized to prevent pulling down the power supply when C_1 is charged. The circuit is basically an underdamped second-order system. Figure II-12 is the predicted charge voltage for the components selected. The charge time can be increased by adding series resistance and decreased by reducing the total effective capacitance (C_2). When the voltage reaches its peak charge, the current is zero and SC_1 turns off, allowing the PZ element to maintain its charge. D_1 and D_1 must have very low reverse-current ratings to prevent bleeding of the PZ charge and relaxing the stack. The discharge rate of the PZ stack is controlled with components L_1, $C_2 + C_{pz}$, RL_1, R_4 and R_8. Figure II-13 is the predicted current when $RL_1 + R_4 + R_8 = 232$ ohm, $L_1 = 5$ millihenry and $C_2 + C_{pz} = 0.85$ microfarads. SC_2 turns off when the current is zero.

The SCRs are transformer-triggered to allow direct TTL control. Q_1 and Q_3 control the charge and discharge transformers. Q_2 and Q_4 provide charge and discharge lock-out protection when the opposite function takes place. U_1 is an RS latch in the switch-operated breadboard circuit.

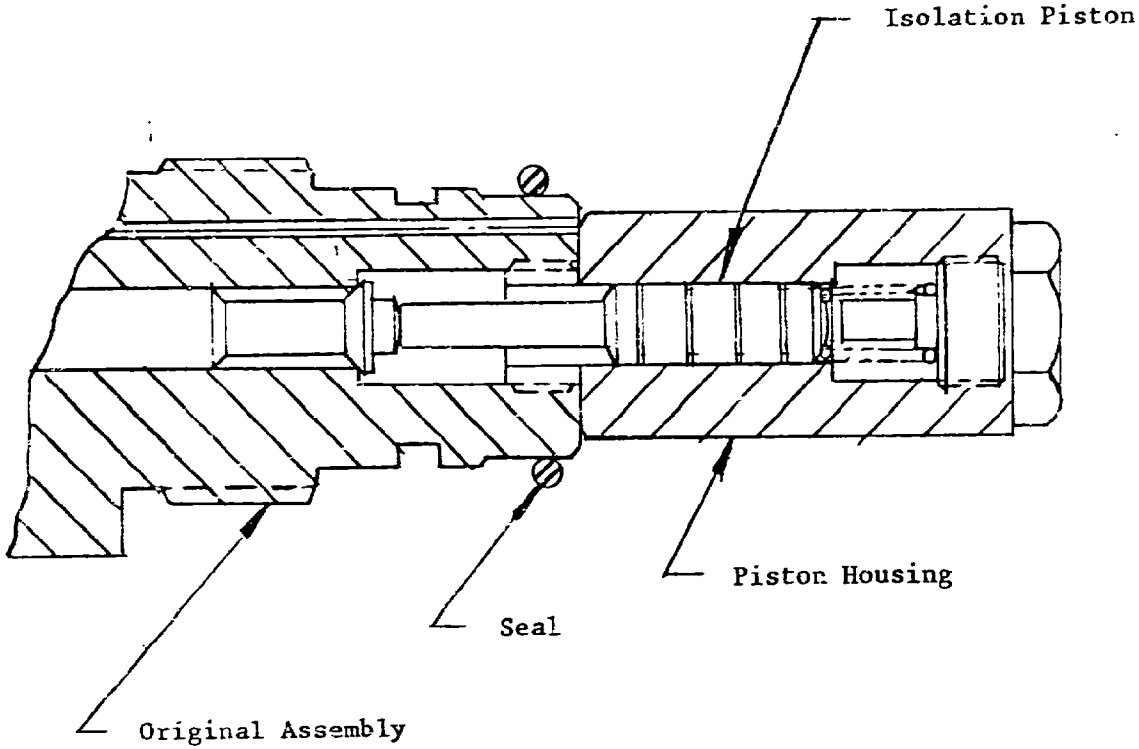

Figure II-9. Isolation piston-housing modification.

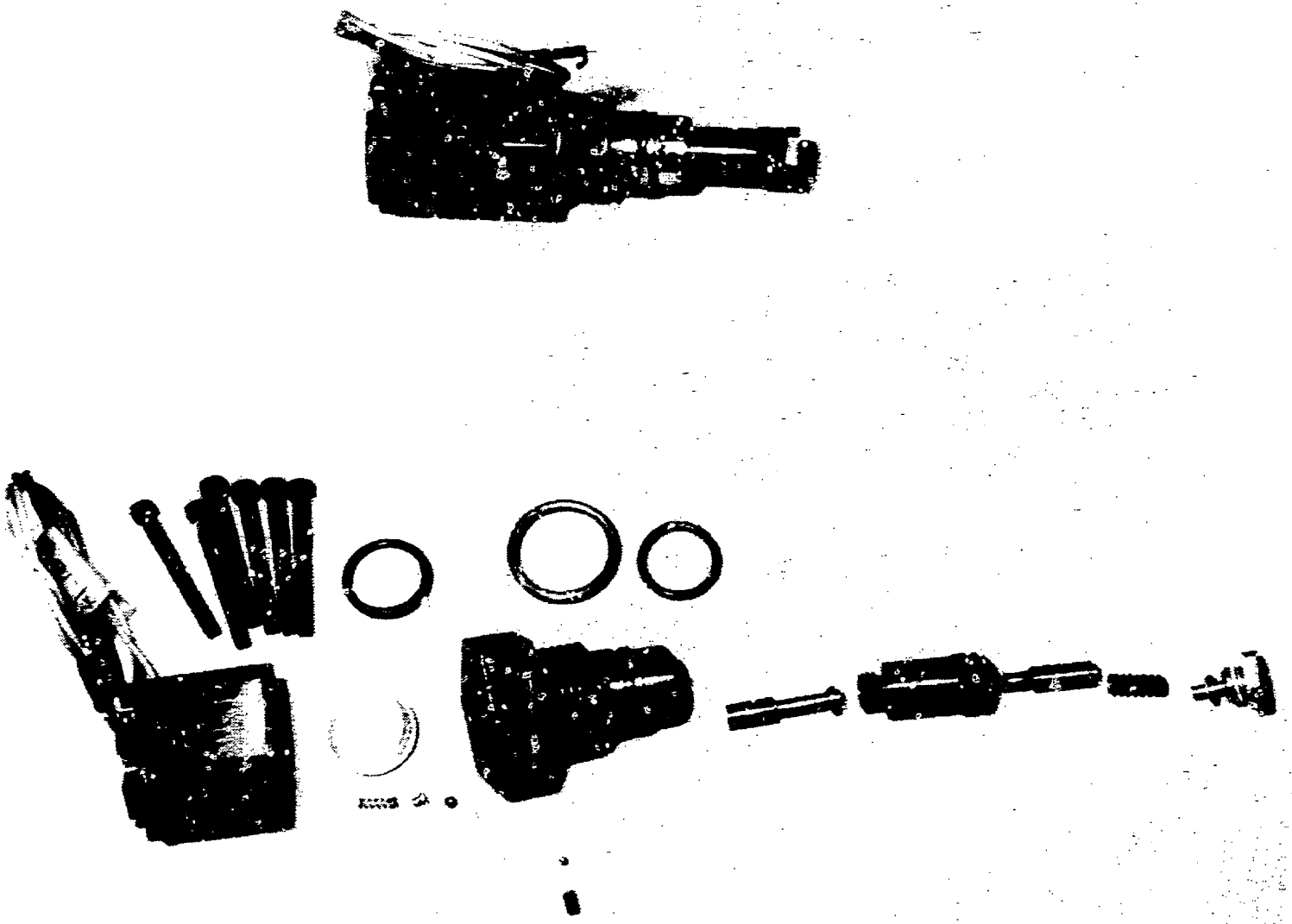

Figure II-10. Piezoelectric poppet valve components.

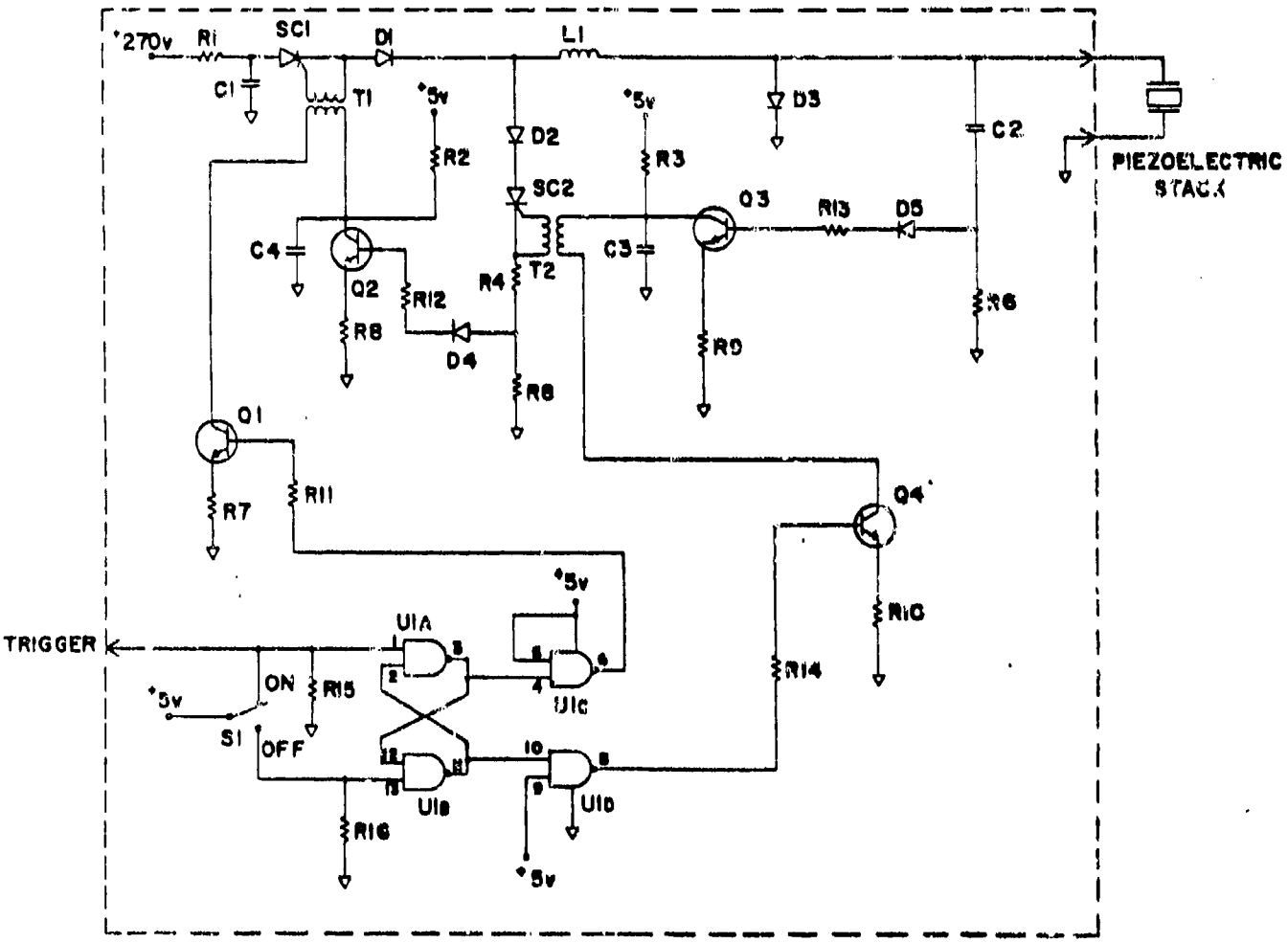

Figure II-11. High-voltage driver schematic.

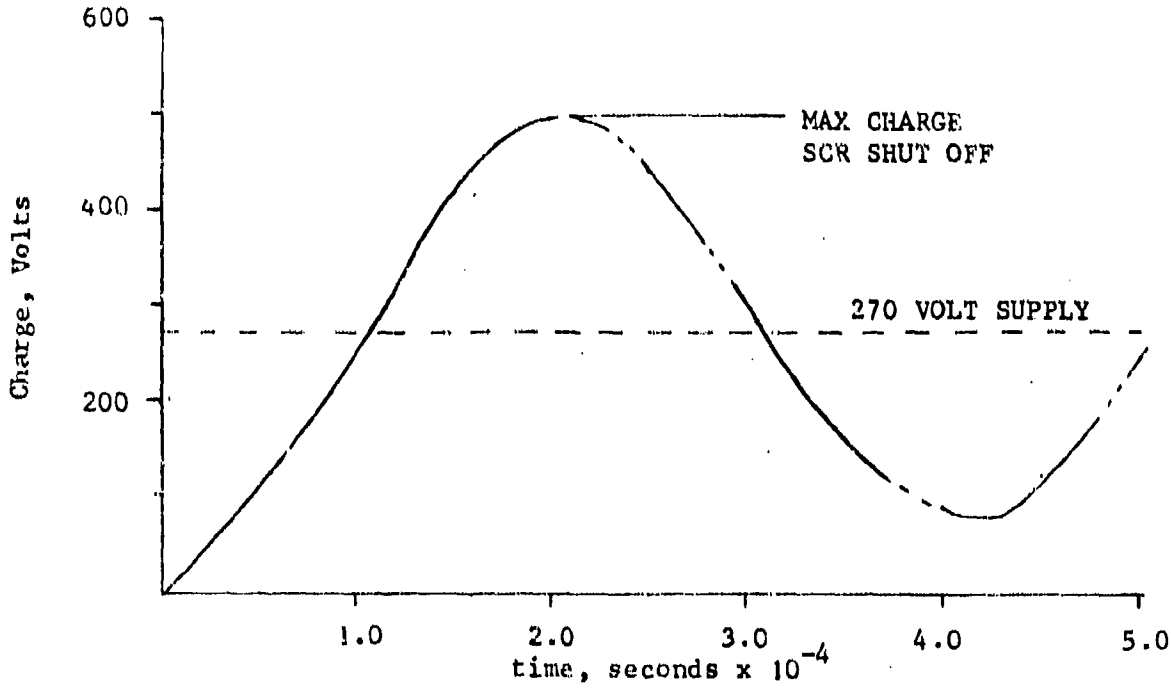

Figure II-12. High-voltage driver charge current.

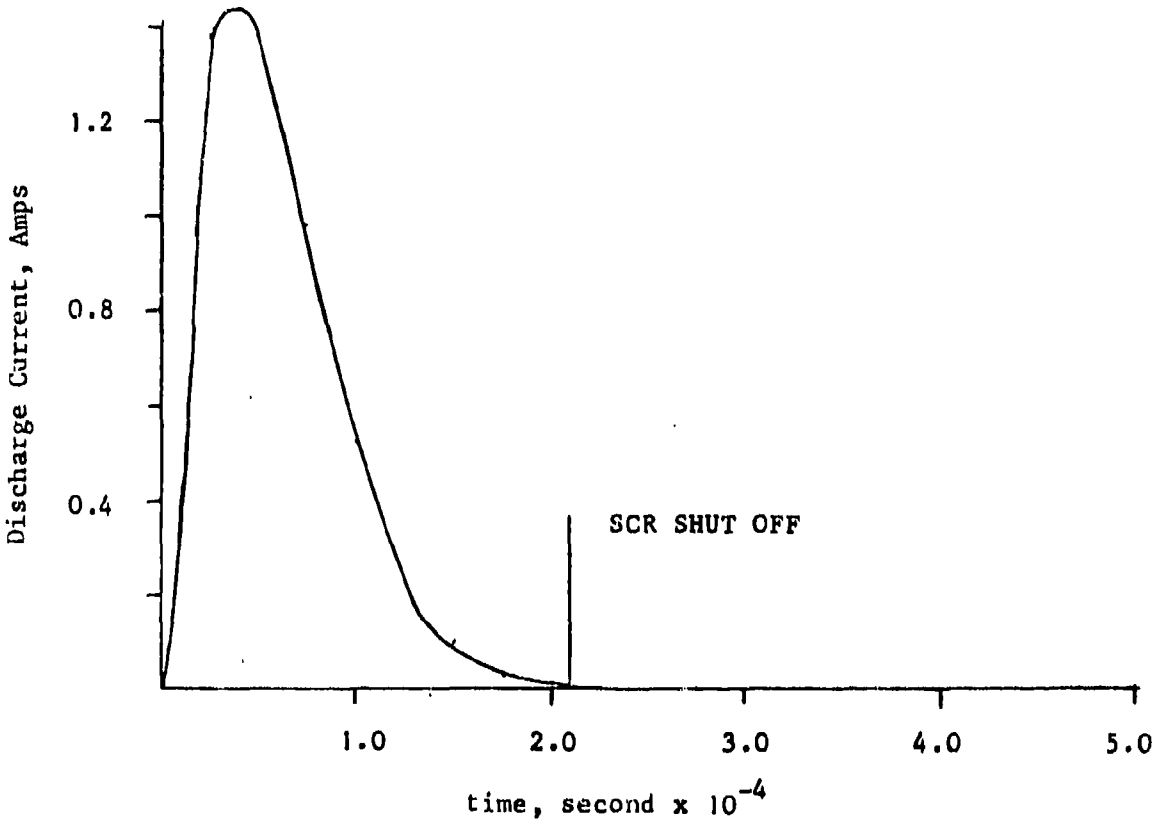

Figure II-13. High-voltage driver discharge current.

Flow Orifice Sizing

Figure II-14 is a schematic of the hydraulic flow path through the digital valve from supply to return (including flow through the actuator) when the actuator is moving.

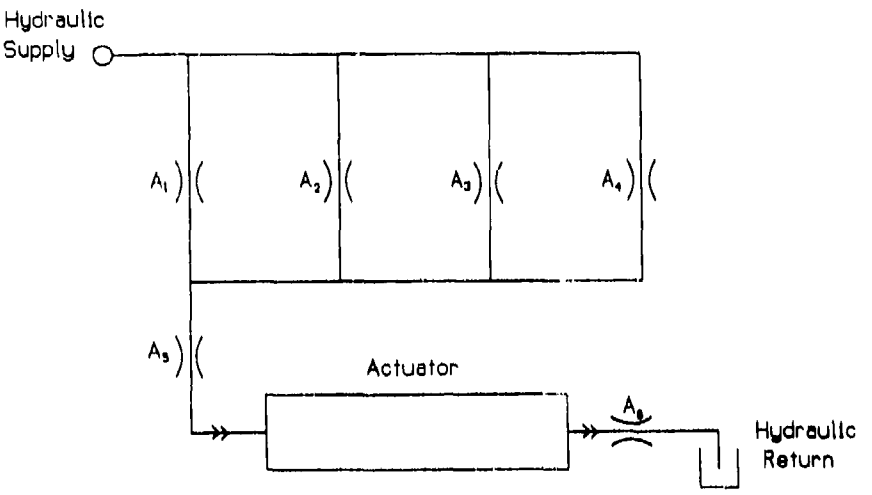

Figure II-14. Digital servovalve flow path.

A_1 represents the fixed orifice area that provides the first flow step when the directional valves port to the actuator. This orifice is not switched in and out, but provides a flow contribution anytime the actuator moves. A_2, A_3 and A_4 are the step flow control orifices used in binary combinations to provide the flow modulation. A_5 and A_6 represent the orifice areas of the directional control poppet valves that port fluid into and out of the actuator. Either separate orifices for A_2, A_3 and A_4 can be used or the poppet valves can be used for the orifices (by adjusting the stroke of the poppet piston to achieve the required orifice area). The flow through an orifice for MIL-H-5606 fluid at 100 °F is determined by the following equation:

$$Q = 103\ A\ (\Delta P)^{1/2}$$

Where: Q = flow in cis
A = porting area in in^2
ΔP = differential pressure in psi

Where the orifices are operated in parallel, the flow calculation uses the sum of the orifice areas for A in the previous equation. Where orifices are in series, the calculation is more involved, since the ΔP for each orifice is different. For the flow representation of Figure II-14, the total flow from the valve is:

$$Qt = \frac{103\ (\Delta P)^{\frac{1}{2}}}{\left(\frac{1}{(A_1 + A_2 + A_3 + A_4)^2} + \frac{1}{A_5^2} + \frac{1}{A_6^2} \right)^{\frac{1}{2}}}$$

A computer program was written to allow convenient calculation of the orifice sizes and the flow linearity. The maximum flow through the directional control orifices (with .0031 in^2 area) was 13.4 cis at 3000 psi differential pressure. To achieve reasonable output flow linearity, the total flow from the servovalve should be much less than the maximum flow through the directional control orifices. The flow modulation valves should dominate the flow characteristics, not the directional control valves. The best theoretical flow linearity would be obtained with 13.5 percent (of maximum flow) steps, using a fixed orifice flow of 5.0 percent. The reason for the low flow selected for the fixed orifice was to provide null stability (minimizing hunting by limiting the actuator velocity around *zero* command inputs). The program used the total system flow to calculate the pressure drop across A_5 and A_6 for 5-percent fixed-orifice flow. By subtracting the pressure drop for A_5 and A_6 from the supply to return pressure differential, the area of A_1 was then calculated. A_2, A_3, and A_4 were calculated in the same way. Finally, the percent flow for each step was calculated.

For total servovalve output flows of less than 10 cis, the diameter of the A_1 area would be less than .010 inches. The A_1 diameter was fixed at .010 inches because manufacturing difficulty in obtaining smaller diameter orifices. The computer program was modified to fix A_1 at an area corresponding to an orifice diameter of .010 inches. With that variable fixed, a maximum servovalve flow of 8.0 cis was determined to give the best flow linearity while maintaining the desired performance of the actuator. Table II-4 lists the flow percentages, orifice area and poppet stroke for the flow modulation orifices. Figure II-15 is a plot of the output flow for the servovalve with the final sizing. The curve shows the servovalve flow linearity for the 8 flow combinations of the flow control orifices. The curve is a least squares fit to the flow data points and shows the effect of low flow for the first step and flow saturation due to the directional poppet valves.

Table II-4. Flow areas and percent flow.

SYMBOL	TOTAL % FLOW	AREA, in2	STROKE, in
A_1	6.2%	7.85X10-5	---------
A_2	25.8%	2.54X10-4	.0004
A_3	40.1%	4.52X10-4	.0007
A_4	56.0%	1.02X10-3	.0016

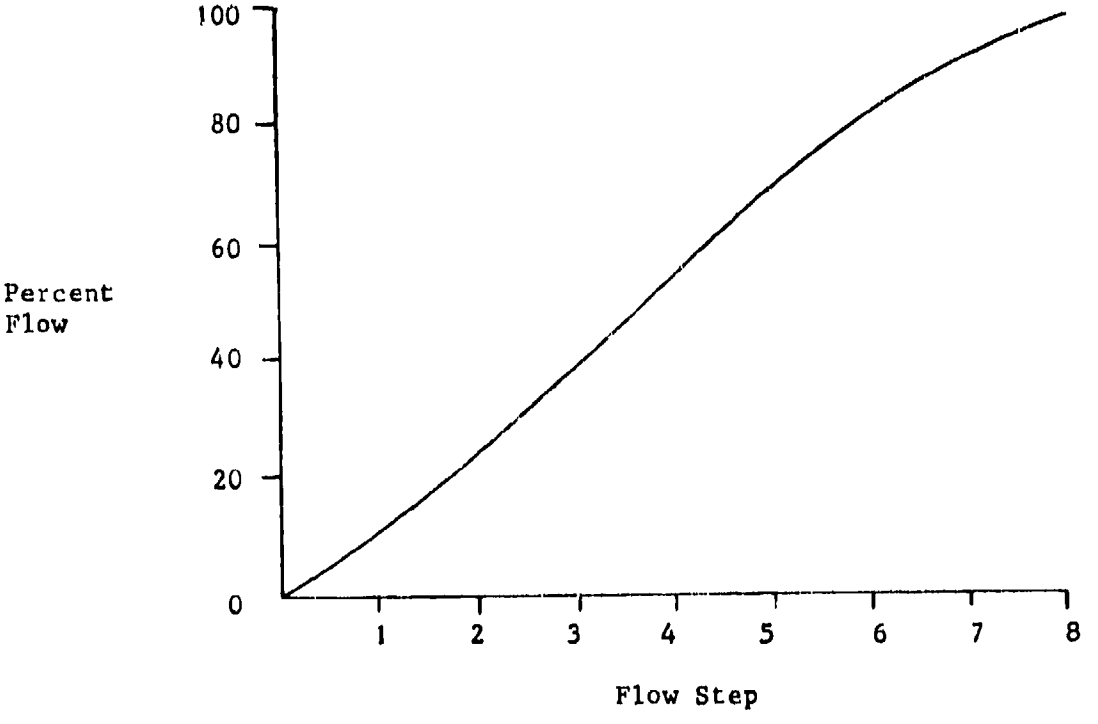

Figure II-15. Flow linearity for 8 cis and .010 orifice.

PZ Poppet Valve Development Testing

To evaluate and adjust individual poppet valve operating characteristics, a test configuration with a test manifold was constructed. Figure II-16 is a schematic of the setup, showing the instrumentation used to measure the flow and time response characteristics. The parameters evaluated for each valve were the maximum flow, operating time, poppet seat leakage, poppet piston leakage, check-ball leakage, and bleed valve leakage. A breadboard driver was fabricated for the development testing.

High Voltage Driver Testing

Figure II-17 shows the breadboard circuit built for the development testing of the PZ poppet valve and driver. Several problems with the driver were encountered and solved during the development testing of the poppet valve. One problem was the self-concatenating of the SCRs, a problem that is common in using SCRs to drive inductive circuits. The snubber circuit shown in Figure II-18 was added to prevent the dv/dt limit specified for the SCR from being exceeded. The original circuit allowed the dv/dt limit for the SCR to be exceeded, causing the self-concatenation of the SCRs. The snubber circuit's time constant of 5.6 microseconds had an insignificant effect of the PZ drivers's charge timing.

Another problem encountered with the breadboard circuit was the EMI field generated by inductor during the charging and discharging cycles. The field was large enough to couple to the trigger transformers, activating both SC_1 and SC_2. The effect of the problem was to pull down the 270 volt power supply and overheat the circuit components R_1, R_4 and R_8. The solution for the EMI coupling problem was the installation of a shielding around the trigger transformers.

PZ Poppet Valve Testing

The valves' poppet piston and check-ball seat were individually hand-lapped for fit for each valve. Leakage was verified by using an adapter to pressurize the hydraulic amplifier chamber to 500 psi (see Figure II-19). Leakage was then collected from the appropriate ports. The piston leakages were all less than one drop in 2.5 minutes and the check-ball leakage was less than one drop in 10 minutes.

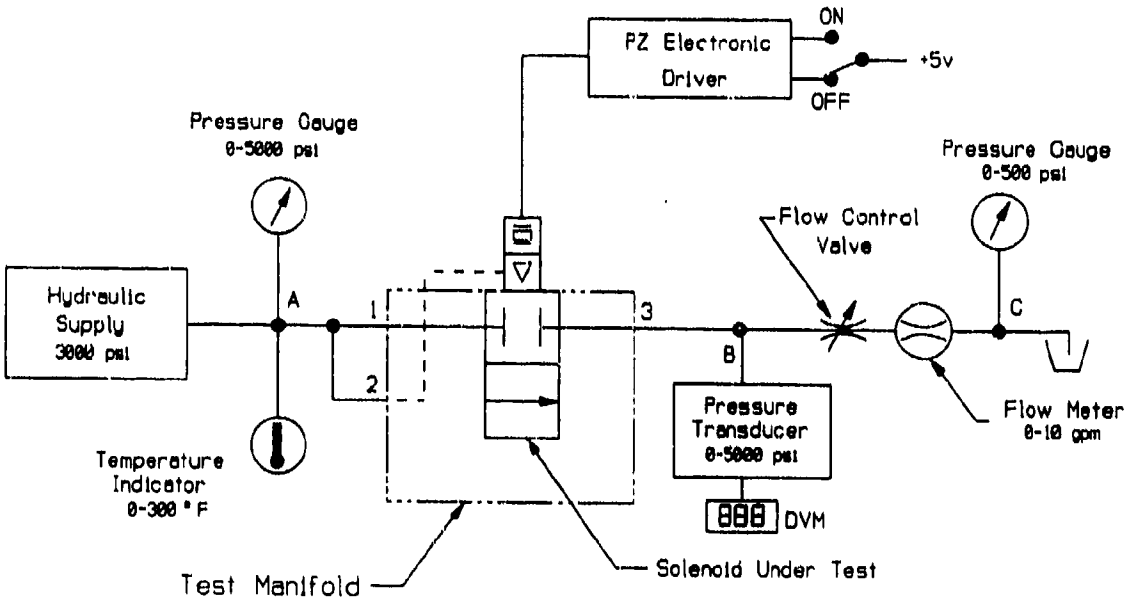

Figure II-16. Individual poppet test setup.

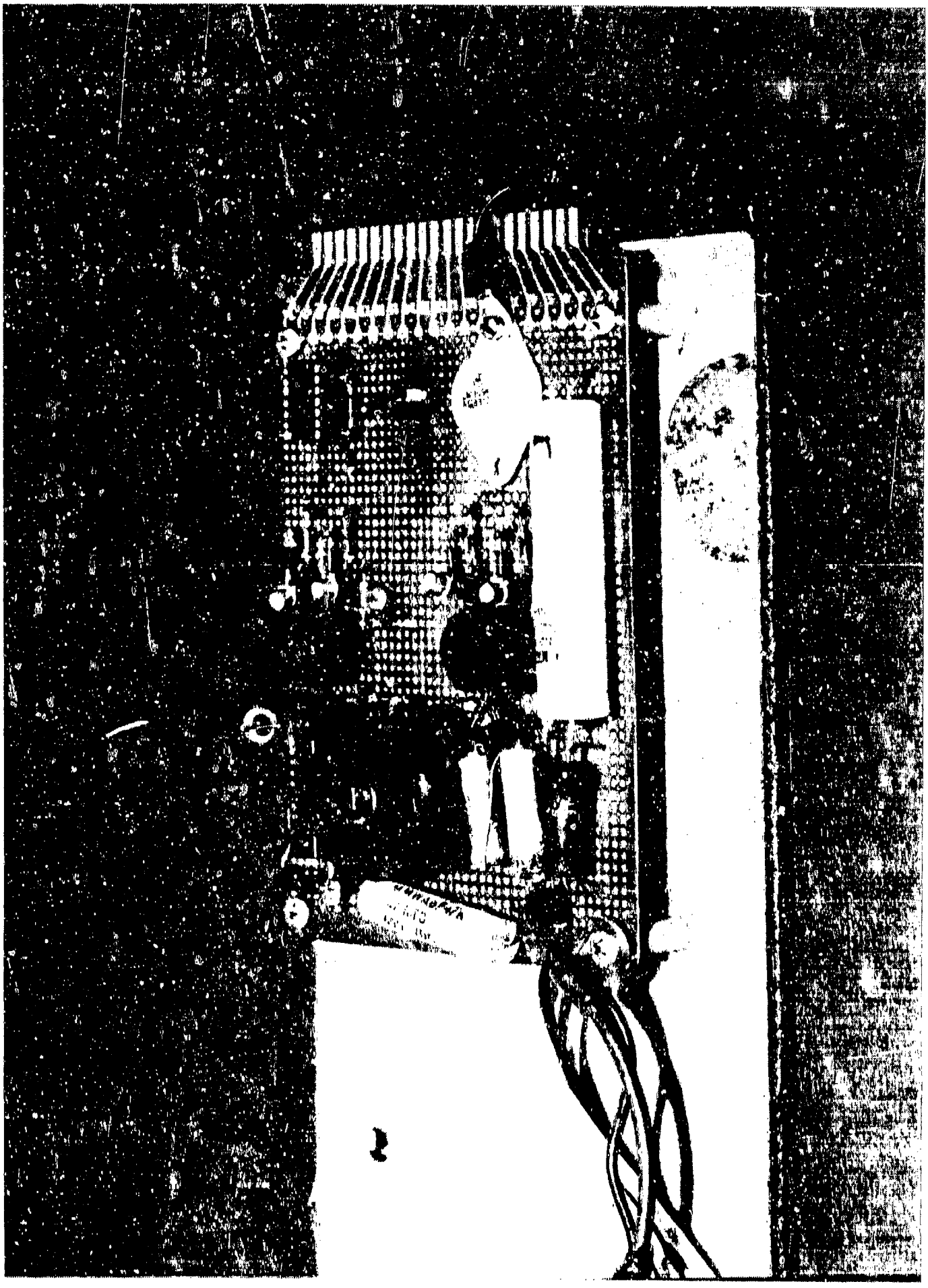

Figure II-17. High-voltage driver breadboard.

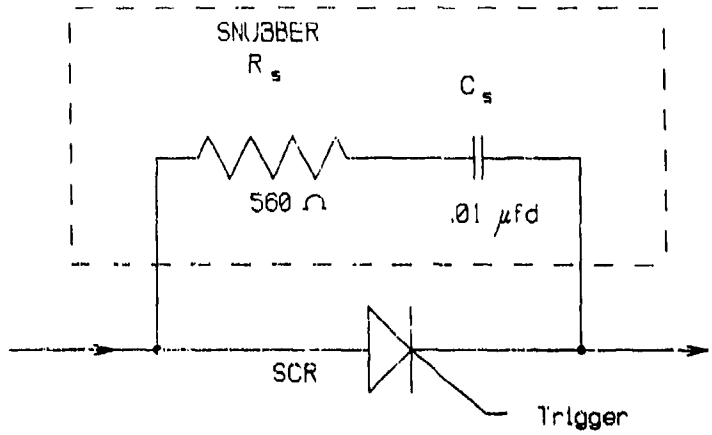

Figure II-18. SCR snubber circuit.

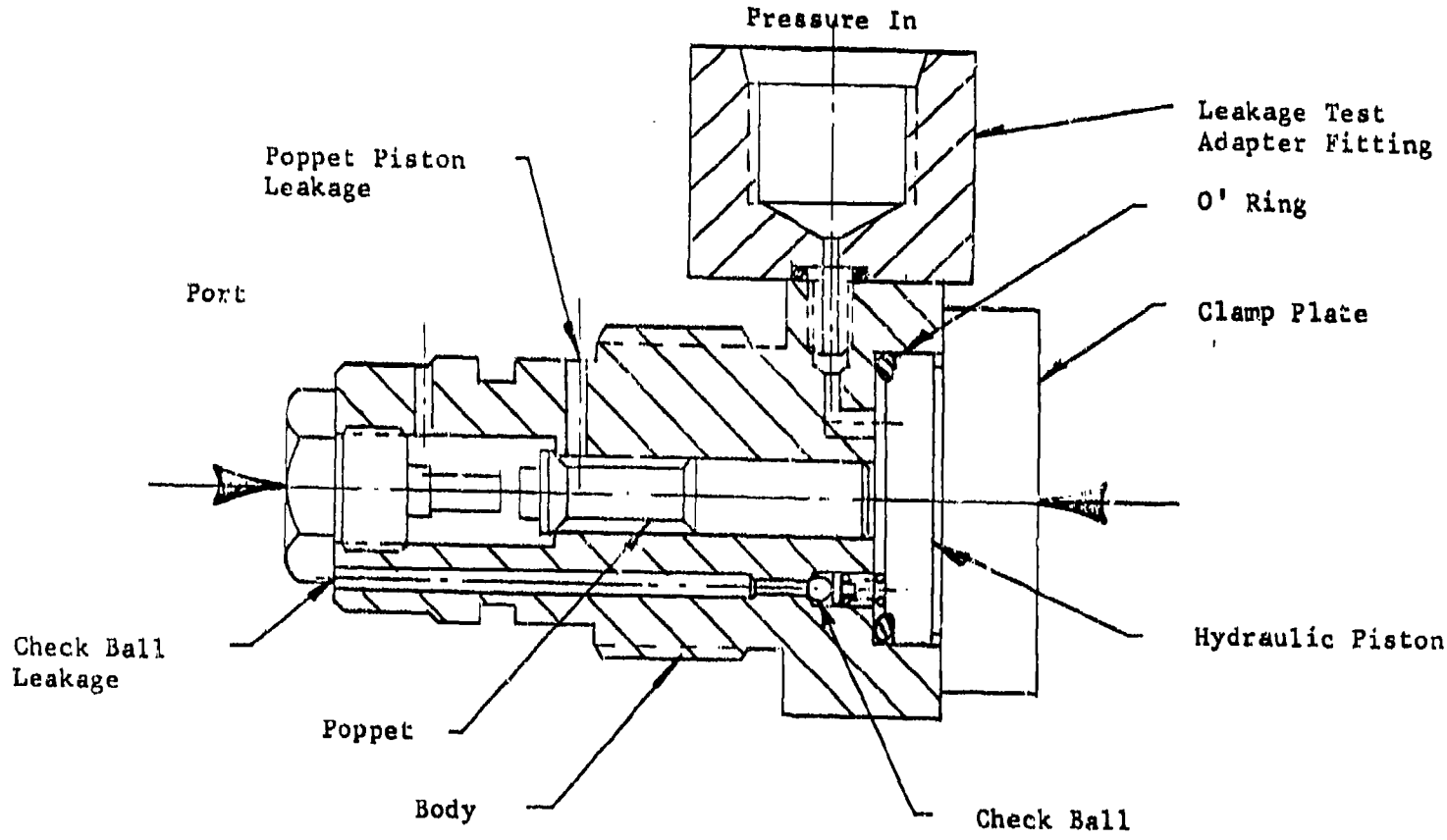

Figure II-19. Poppet valve leakage test adaptor.

The cone-poppet-seat leakage measured less than one drop in 5 minutes for all valves. This leakage was measured by installing each valve in the test manifold and pressurizing the inlet port to 500 psi. The seats were lapped much deeper than desireable because of problems with the manufacturing process and initial design dimensioning. The counterbore flat-seating area was not perpendicular to the bore within the .001 inch desired and the concentricity of the poppet-cone-seat and piston was net held within the desired .0001 inch. To obtain a seal, the lapping produced grooves on the poppet sealing face as deep as .005 inches. The result of the grooves was to make the seat area slightly larger than the poppet piston area and to create undesirable flow turbulence when open. The net effect of the grooving of the poppet cone was to require a higher driving force for operation of the poppet valve.

The initial operating test of the PZ poppet identified several problems. The valve would either would not open and instead emit a *click* sound (indicating that the PZ was energized) or the valve would open and sustain an oscillation in the range of 180 to 240 Hz (then stop and not operate when charged a second time).

Disassembly of the valve indicated a problem with the O-ring seal at the large driver piston of the hydraulic amplifier. The O-ring jammed the piston tight in the bore and when examined, deep cuts about the O-ring's circumference were observed. The cuts indicated that the O-ring was being extruded into the .002-inch diameter clearance between the piston and bore. To solve this problem, the piston was modified to accept a Parker scarf-cut teflon backup ring. This solved the extrusion problem and also helped the instability problem (although repeatable operation was still not achieved).

Analysis indicated that the oscillation frequency was very near the resonant frequency of the poppet mass with the return spring and the spring rate of the hydraulic chamber. The oscillation would not occur if the poppet were driven to the valve stop. The poppet stroke was temporarily reduced to .001 inch using the valve stop and the instability problem was eliminated.

An area that also contributed to the poor operation of the poppet is the effect of the flow direction through a poppet valve design. The graph shown in Figure II-20 indicates flow forces with respect to flow direction (for a flat poppet).

The cone-poppet flow force would be similar to the flat poppet. When flow is from the direction that the poppet opens, the force goes to 100 percent upon cracking, then quickly falls to less than 50 percent. In addition, the flow forces tend to be higher when small downstream chambers are used because higher fluid velocities are required. For the preceding reasons, the flow path used through the poppet valve was reversed. This produced a stabilizing effect on the valve and permitted the

stroke to be increased. With the flow path reversed, flow testing indicated that the valve stroke could not be greater than .003 inch and have reliable operation. Since this stroke was less than the original design, the development testing was expanded to identify the source of the anomaly.

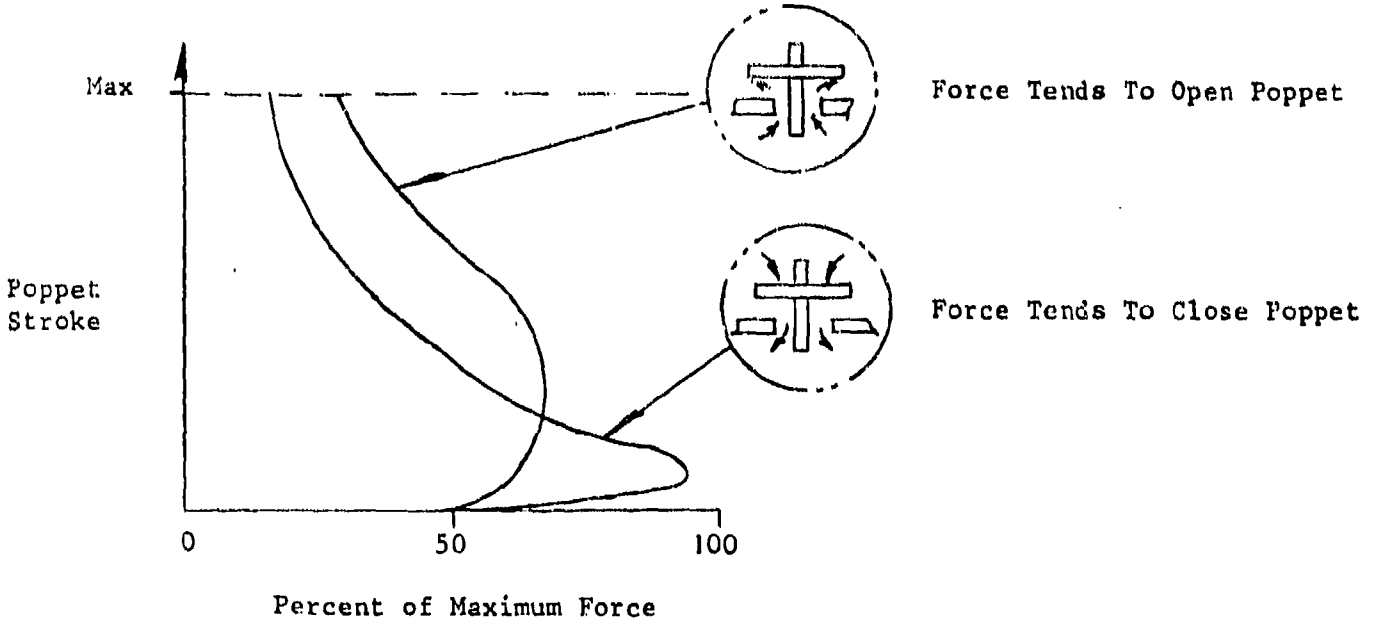

Figure II-20. Flat poppet flow force.

PZ Actuator Test

The test fixture shown in Figure II-21 was fabricated to evaluate the stroke versus preload characteristics of the PZ actuator.

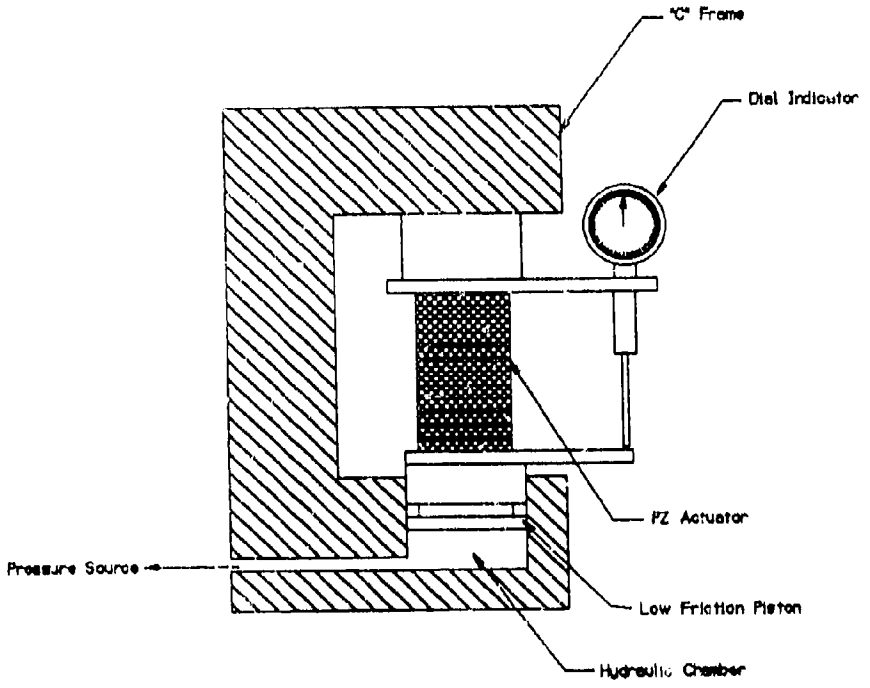

Figure II-21. PZ stroke-versus-preload test fixture.

The fixture consisted of a rigid C-frame containing a hydraulic piston with low-friction filled-teflon cap seals and connected to a dead-weight tester as a pressure source. The hydraulic chamber was drained of all fluid for each test to trap air, providing a compliant load that would appear as a constant force through the PZ actuator's short stroke. Using the normal bulk modulus of MIL-H-5606 as 150,000 psi, the change in pressure (without the trapped air) when the PZ actuator is charged would be:

$$\Delta P = \beta(\Delta V/V)$$

Where: β = bulk modulus = 150,000 psi

V = chamber volume = 2 in^3

ΔP = differential pressure (psi)

ΔV = change in volume when charged
= 1.0 x .0004 = $4x10^{-4}$ in^3

ΔP = 30 psi

The dead-weight tester was used to calibrate the pressure transducer to an accuracy of 1.0 percent. No change in the position of the floating weights or pressure transducer output was noticed when the PZ was charged. Therefore, the bulk modulus was assumed to be considerably less than the 150,000 psi specified (because of the intentionally trapped air) and the *constant force* load was realized.

For the PZ stroke measurements, a very sensitive mechanical dial indicator was attached to the inactive portion of the frame to avoid including the frame compliance in the measurements. Table II-5 is the recorded stroke versus preload data.

Table II-5. PZ stroke-versus-preload data at 520-volt charge.

ACTUATOR PRELOAD	Measured Stroke, inchesx10-4		
	S/N-01	S/N-05	S/N-113
250 LB	4.0	3.0	3.9
500 LB	4.0	3.0	3.9
1000 LB	3.5	2.8	3.2
2000 LB	3.0	2.3	2.5

The lower preload values of S/N-113 agree with the manufacturer's data sheet (which was recorded at a 20-lb preload). The recorded data did not agree with the original concept that the PZ actuator stroke was unaffected by preloads. The actuators being evaluated were affected by preload once the stress was greater than 2500 psi. It is assumed that this was the result the Modulus of Elasticity being lower than predicted (probably because of the minor imperfections in disc flatness or the stack assembly).

Poppet Stroke Analysis

The poppet stroke can be predicted from a PZ stress/strain curve once the PZ stress or output force is calculated. The following is the analysis of the expected stress that the PZ actuator will encounter. Figure 11-21 is a cross-section schematic of the valve with the dynamic parts labeled.

A_1 = 0.196 inch
A_2 = 0.441 inch
A_3 = .031 inch
F_1 = 6.5 lb (preload)
W = weight of poppet and iso-piston, 6.7×10^{-3} lbs
F_2 = flow force, 1 lb (estimated)
X = poppet stroke, .004 inch
t = operate time, .003 second

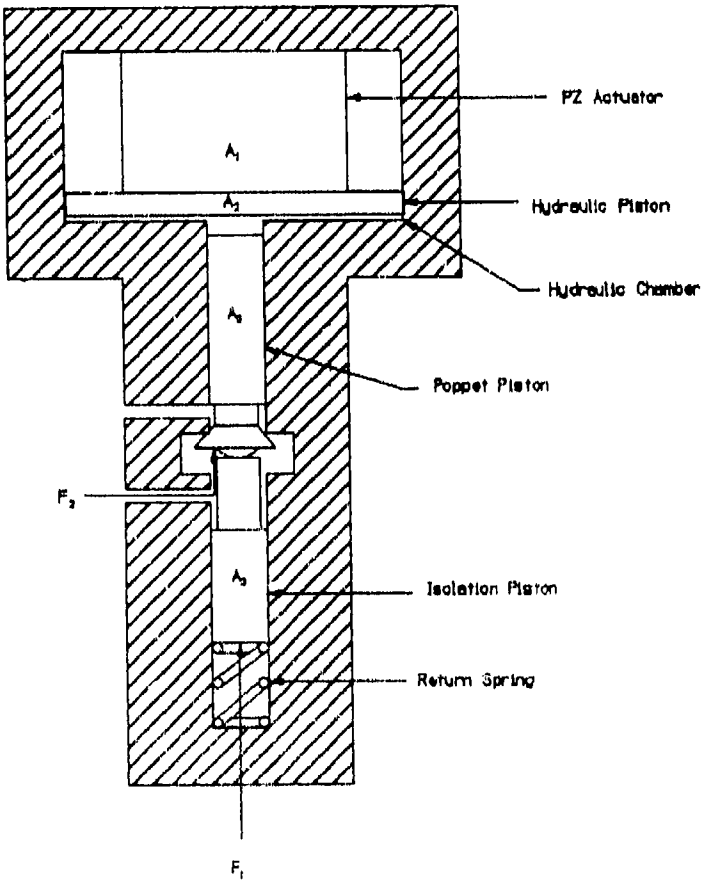

Figure II-22. PZ poppet valve area relationships.

PZ stress due to the return spring preload:

$$S_s = \frac{F_1}{A_3} \times \frac{A_2}{A_1} = \frac{6.5}{0.031} \times \frac{0.441}{0.196} = 471 \text{ psi}$$

PZ stress due to flow force:

$$S_f = \frac{F_2}{A_3} \times \frac{A_1}{A_2} = \frac{1.0}{0.031} \times \frac{0.441}{0.196} = 72.6 \text{ psi}$$

PZ stress due to acceleration:

$$F_a = \frac{W}{386} \times \frac{x}{2t^2} = \frac{6.7 \times 10^{-3}}{386} \times \frac{0.004}{0.196} = 0.38 \text{ psi}$$

$$S_a = \frac{F_a}{A_3} \times \frac{A_2}{A_1} = \frac{0.38}{0.31} \times \frac{0.441}{0.196} = 28 \text{ psi}$$

Therefore, the total PZ stress is defined as:

$$S_T = S_s + S_f + S_a = 471 + 72.6 + 28 = 571.6 \text{ psi}$$

The actual PZ stress/strain curve can be derived from the free or no-load strain current. The free or no-load strain was obtained from the stroke-versus-preload data. The amplifying chamber is normally pressurized to 3000 psi (presenting a preload force of 3000 psi times A2) or 1323 lbs plus the preload exerted by the O-ring. The O-ring force was measured to be 14 lbs at the normal operating point, making the total PZ preload force 1337 lbs. Table II-5 was used to establish the average PZ stroke at .0003 inches. The manufacture specified a PZ modulus of elasticity of 7×10^6 psi. Therefore the stress at zero strain would be 2100 psi. Figure II-23 is the stress/strain curve.

Since the total output stress in operating the poppet required was 571.6 psi, the stroke can be calculated from the slope form of $x/a + y/b = 1$ or interpreted from the stress curve to be 2.18×10^{-4} inches. The maximum-expected poppet stroke would be (from the motor's amplification, disregarding friction):

$$[A_2/A_3 \times (2.18 \times 10^{-4})] = 3.057 \times 10^{-3} \text{ inches}$$

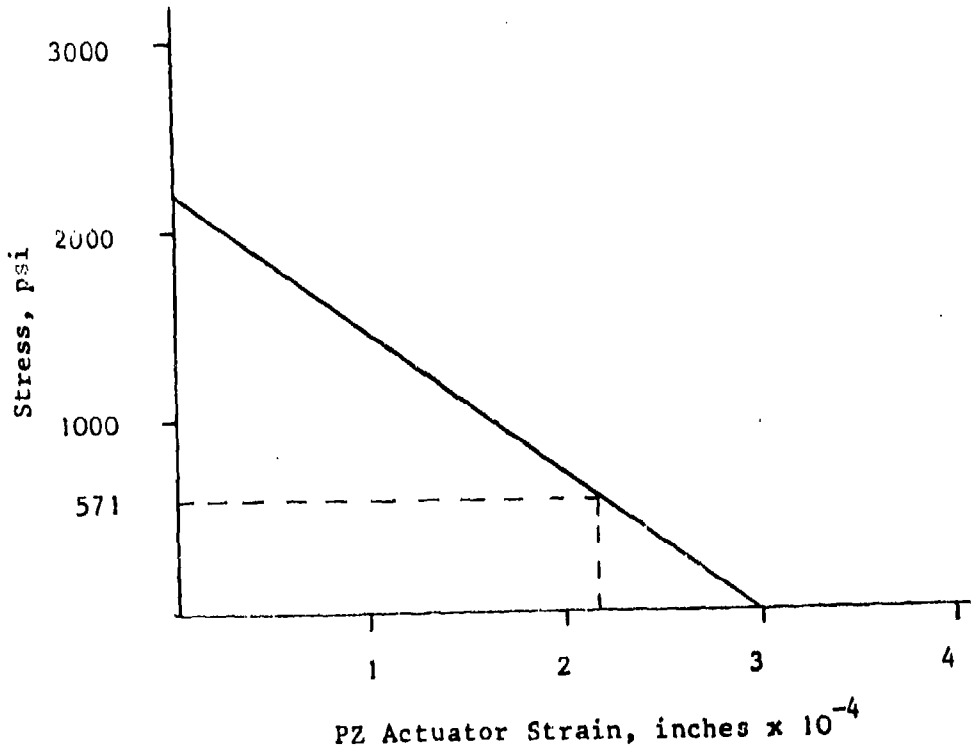

Figure II-23. Measurement PZ load curve.

An additional loss of stroke due to the bulk modulus of the oil in the amplifying chamber was calculated to be 2.5 x 10^{-4} inches (using $\Delta V = PV/\beta$). Subtracting the fluid compliance volume reduced the poppet stroke to 2.8 x 10^{-3} inches.

Final Poppet Configuration Testing

The range of poppet stroke was verified by increasing the valve's stroke by .0005-inch increments starting at .001 inches. When the total stroke was .003 inches, the valve would not close completely until the amplifying chamber was bled. When the poppet's driven stroke was less than its mechanical stop setting, the poppet's inertia would carry it a greater distance than the driven stroke. This action creates a larger volume in the amplifying chamber by drawing additional fluid through the supply check valve. When the PZ actuator was discharged, the greater volume would not allow the poppet to close. The volume was returned to normal by bleeding the excess fluid.

Experiment determined that a poppet stroke of .0027 inches produced reliable opening and closing with a 6.5-lb preload of the poppet return spring. The higher preload was required to maintain *off* time and poppet seat seal integrity. Although this shorter stroke produced less than original-flow goals, the flow levels were large enough to evaluate the application of PZ poppet valves.

Step response data was obtained from the test setup in Figure II-24. The adjustable orifice (flow control valve) was set to provide a pressure of 200 to 500 psi for the transducer pressures to measure when the valve was open. The response time data (Figures 25 and 26) was produced from photographic oscilloscope data.

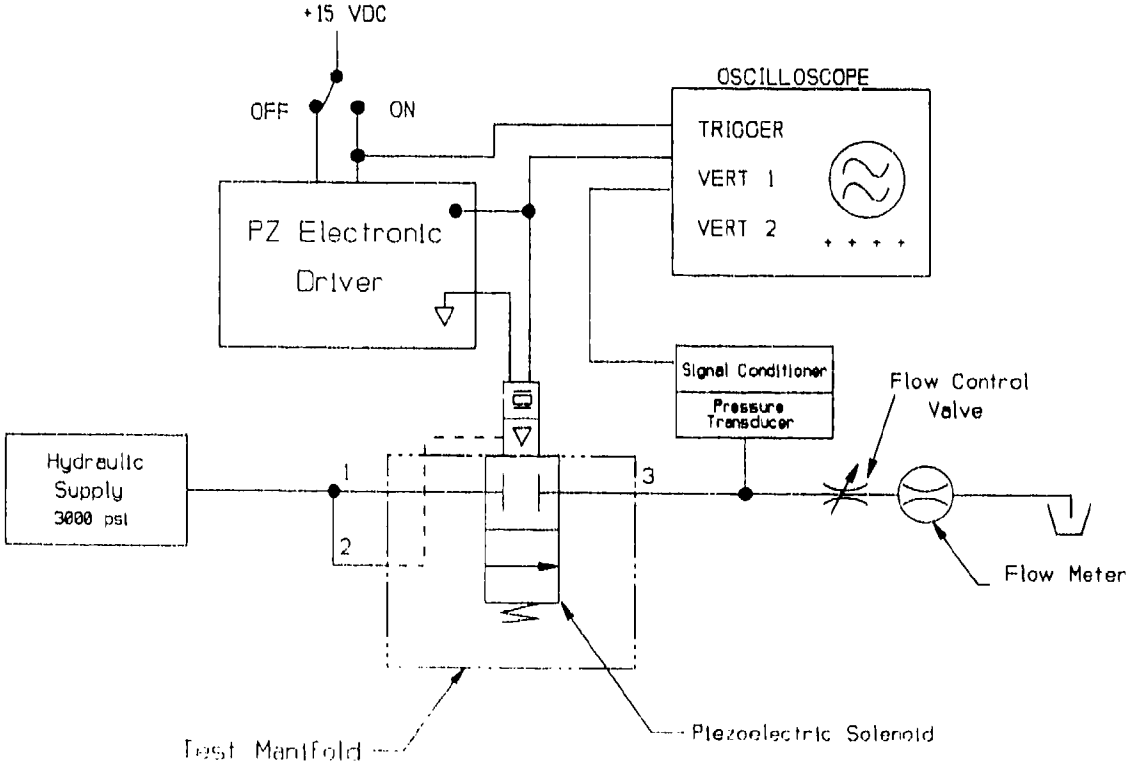

Figure II-24. Time response test setup.

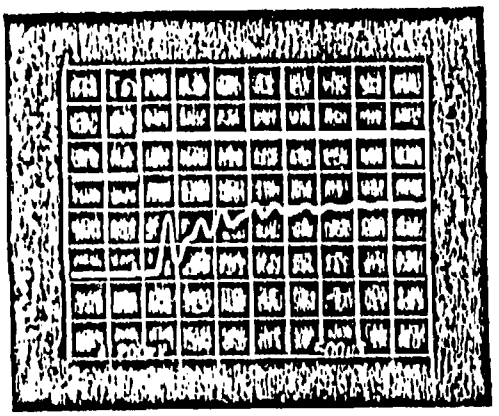

Input - 5 v/div

Pressure - 200 psi/div

t → 500×10^{-6} sec/div

Figure II-25. *On* valve response.

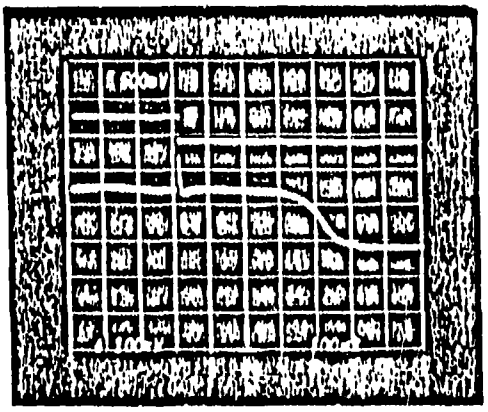

Input - 5 v/div

Pressure - 100 psi/div

t → 100×10^{-6} sec/div

Figure II-26. Poppet valve *off* response.

Figure II-25 (the *on* time response data) shows the pressure starting to rise 300 microseconds after command and reaching its peak value in a total of 400 microseconds. The oscillations were caused by the lightly dampened hydraulic resonant circuit of the test-setup plumbing.

The *off* response data (Figure II-26) indicates the pressure beginning to fall off after 250 microseconds and being at return pressure after 420 microseconds. The 300 and 250 microsecond delay times correspond respectively to the charge and discharge times of the high-voltage drivers. The small pulse on the pressure traces that coincide with the input are caused by the high-voltage driver's electromagnetic interference coupling to the pressure transducer electronics. Application of grounding and shielding design practices greatly reduced the coupling pulses.

Throughout the development testing, the output flow from the PZ poppet valves would tend to drop off 0.5 to 3 seconds after energizing. This anomaly was determined to be caused by the small amount of leakage past the poppet piston's lapped seal which would allow the valve to slowly close. To eliminate this effect, a pulse-modulation drive was applied to the poppet valve at a 120-Hz repetition rate (with an 80-percent *on* time and 20 percent *off* time provided for maximum flow from a valve). The data plot in Figure II-27 indicates the output flow verses the percent modulation for one of the PZ poppet valves. The flow indicates a sharp drop after the modulation exceeds 85 percent. This is because the *off* time is not sufficient to allow the full return of the poppet before the valve is recharged. A secondary advantage of the pulse modulation driving technique is that the individual poppet flow can be controlled electrically by changing the percent *on* modulation.

The four PZ poppet valves used for directional control and the high-flow control poppet were set equally for 0.60 gpm (2.31 cis) at a 2000 psi pressure drop. The remaining flow control valves were set near their predicted values and were electronically trimmed at final assembly.

Electronic Control Design

The electronic control of the digital servovalve program was set up in two phases. Phase I utilized the analog loop control previously used with an electromagnetic solenoid-type digital servovalve[2]. Phase II used a microprocessor for loop control.

---

[2]AFWAL-TR-80-3074

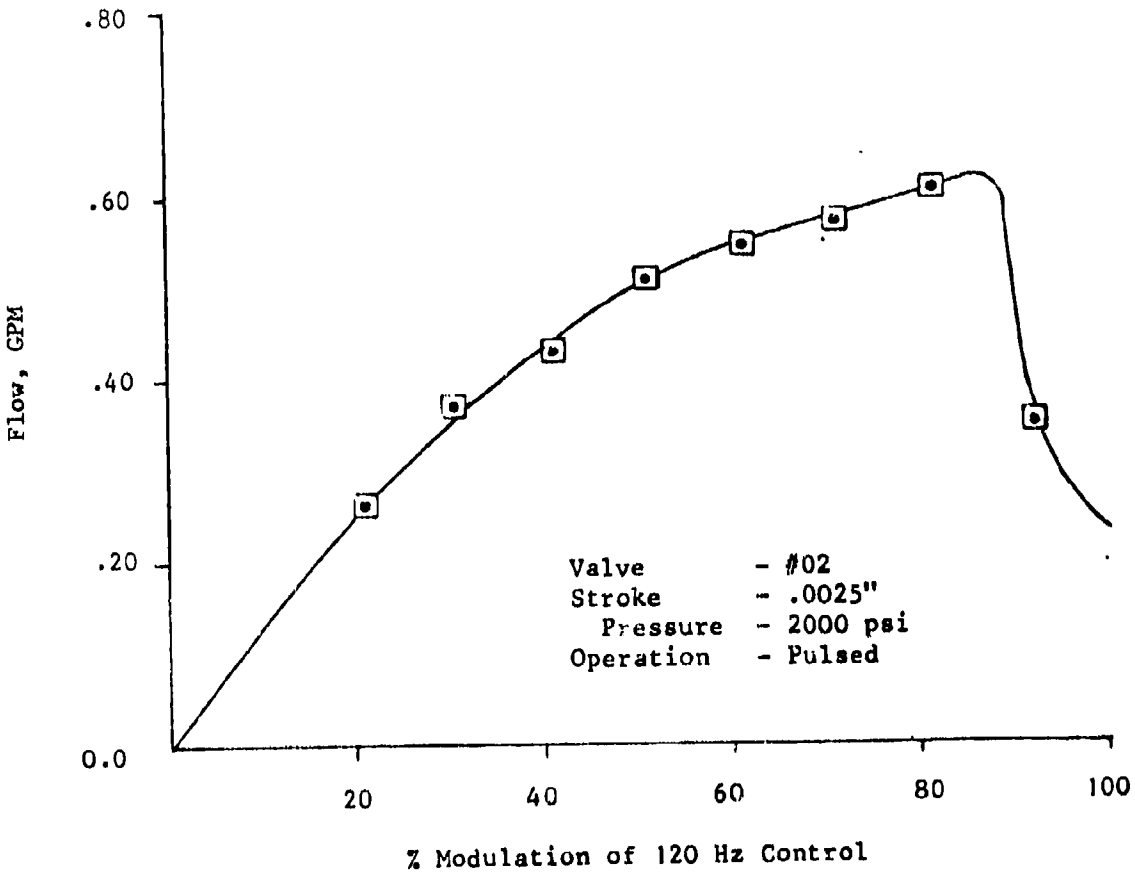

Figure II-27. PZ-pulsed drive.

Analog Electronic Controller

The controller package is shown in Figure II-28. The front panel provides an input jack for the system command. The front panel also contains monitor jacks for actuator position and control error, a dial pot for commanding a bias input, LEDs to indicate direction and percent flow amplitude (system error), power supply indicator LEDs, and a power switch.

The electronics were modified to drive the PZ actuators by adding the high-voltage drivers circuit cards and the required 270 VDC power supplies. The schematic of Figure II-29 is the complete analog control. Board 1 sums the command and bias with the actuator position at A_1. A_2 provides the adjustment for loop gain. A_3 was added to provide an absolute-value amplifier making the system error unidirectional, and thereby reducing the number of flow-level comparators on board 2. Board 2 is basically a ladder type analog-to-digital convertor made up of comparators that have incremented trip levels. Error signal polarity detectors with adjustable threshold levels are included on this board. Board 3 contains comparators to convert 15 VDC logic to 5 VDC logic and drivers for the panel mounted LEDs.

Board 4 converts the 7-bit decimal flow level code to a 3-bit coded decimal logic. U-28, U-29, and U-30 are *LM556* ICs that provide the 80-percent modulated 120-Hz pulse signal to drive the 74221, dual single-shot multivibrators. They provide the *on* and *off* pulses to the high-voltage driver's set-reset latch circuitry. The *off* output of the 74221 is connected to the *on* input and the *on* output to *off* output with a time constant of 1.0 millisecond to ensure that the high-voltage driver has ample time to charge or discharge. This is necessary because the *LM556* circuitry is immediately reset when control input changes state. The control input is dependent on the error amplitude or direction and is not synchronized to the pulse circuitry. The analog circuit cards were designed to permit Board 2 to be removed and replaced with the digital option interface/decoder. The use of Board 2 as the digital interface retains the use of the panel-mounted indicators and the same PZ high-voltage electronics and allowed connection to the microprocessor.

Figure II-28. Electronic controller.

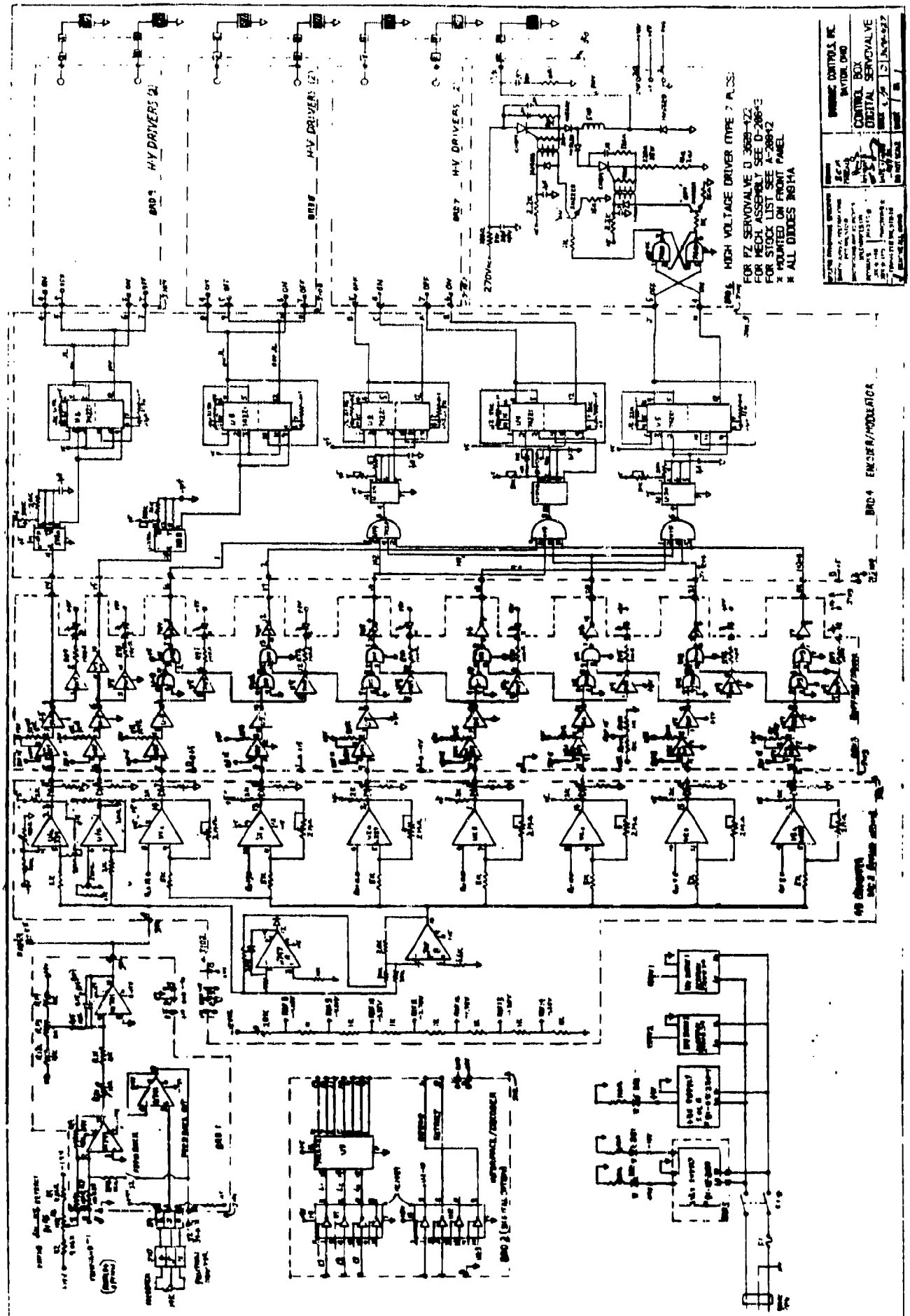

Figure II-29. Electronic controller.

Digital Control Design

For Phase II, a microprocessor was applied to provide real-time control of the digital servoactuator. The processor was designed to accept three analog inputs: command, command bias, and actuator position. The sum of their inputs determined the system error and was analyzed logically to drive the appropriate PZ poppet valves controlling the actuator direction and velocity. Software variables included in the program were forward loop gain, system threshold, and the system update rate. The variables were set from panel-mounted, hexadecimal-coded thumbwheel switches. The program was interrupt-driven from a programmable hardware timer. The controllers input-output requirements were as follows:

INPUTS

Command:	± 10.0 VDC to 200 Hz
Source:	panel-mounted input jacks
Bias:	± 10.0 VDC
Source:	panel mounted 10 Turn potentiometer
Actuator Position:	± 4.0 VDC to 100 Hz
Source:	linear potentiometer mounted on the actuator

OUTPUT

Analog:	The D/A conversion of the error signal ± 10.0 VDC
Digital:	9-position TTL Logic signals 2-directional + 7 flow levels (The BCD conversion is in the analog controller.)

SCALE FACTORS

Update rate:	1.0 millisecond/increment
Threshold:	5.0 millivolt/increment
Gain:	5.0 millivolt/increment

Hardware Design

A Z-80 microprocessor was selected as the CPU for the controller because of the availability of an existing macro-assembler and editing-support software in the Actuation Development Laboratory. An S-100 bus system was selected to provide commonality for other laboratory projects. Figure II-30 is the hardware diagram for the microprocessor. The main components of the system were purchased from the Prolog Company. A Xicor *2816 EEPROM* was installed on the CPU board as an accessible memory. The serial I/O board was used to interface with a terminal for programming and debugging. A write-lock switch was installed on the utility I/O board to prevent non-initiated memory changes.

The hexadecimal thumbwheel switches, bias pot, terminal connector, position monitor, command input jack, and error monitor were breadboard-mounted on a panel attached to the card cage. Figure II-31 is a photograph of the microprocessor hardware used to control the digital servovalve.

Software Design

The goals of the software design were:

- to provide real-time control of the servoactuator
- to run as fast as possible
- to accept gain, threshold, and update-rate variables.

Figure II-32 is the software structure diagram. The variables were input from two-digit hexadecimal switches providing the capability of 256 settings. Their set values were stored in memory during power-up or reset with the *initialize* routine.

The *initialize* routine first read the threshold and stored the value for the first flow step. The preset gain (representative of the incremental flow level value) was read and added to the threshold value and stored in memory as the second flow step. The flow gain was added to the last calculated flow step until all eight steps were stored in memory, creating a look-up table. The last function of the initialize routine was to set the programmable countdown timer with the data set on the update rate switches. When the timer reached zero, it provided the interrupt that the main program waited for to restart the main program sequence.

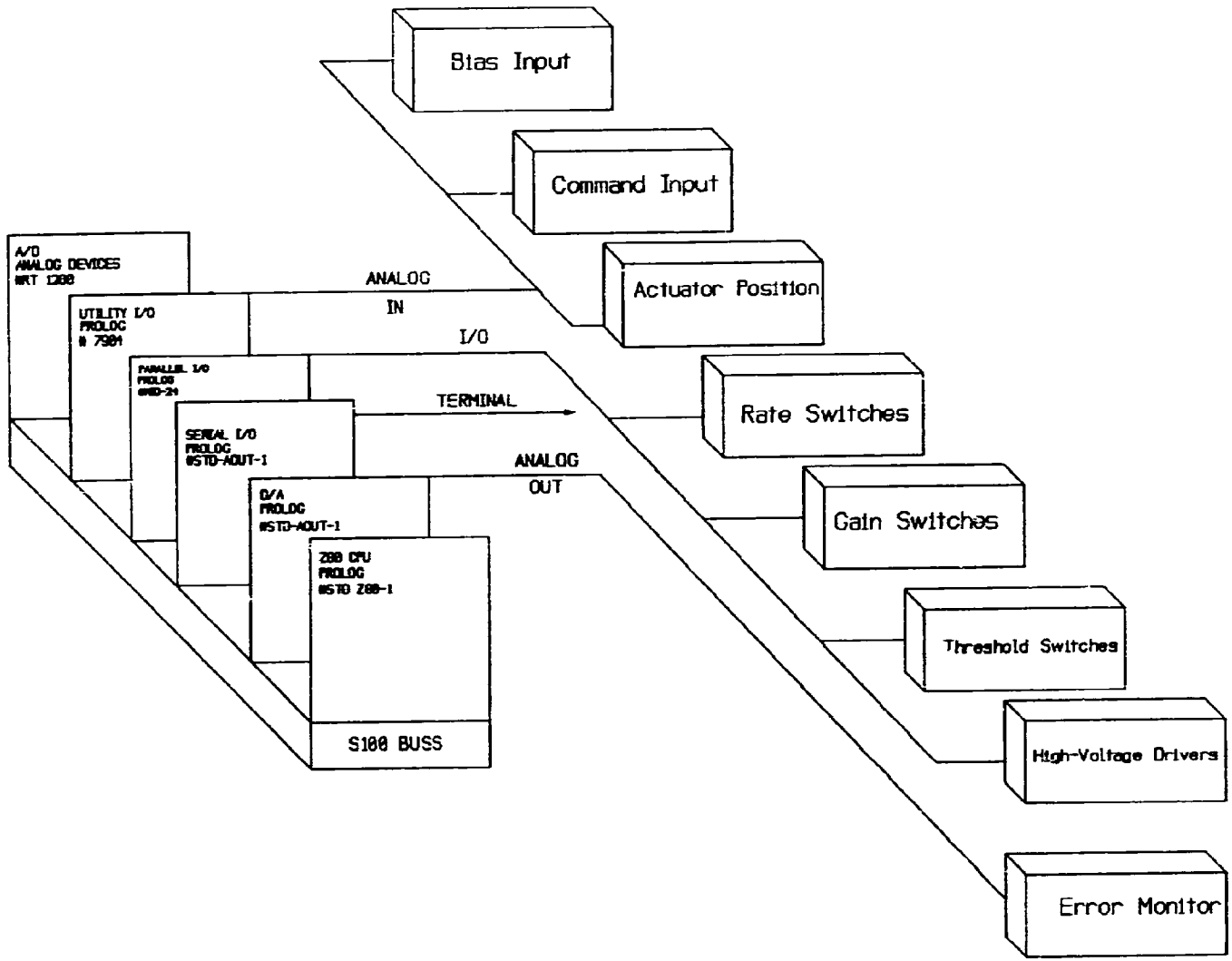

Figure II-30. Microprocessor hardware diagram - digital servovalve.

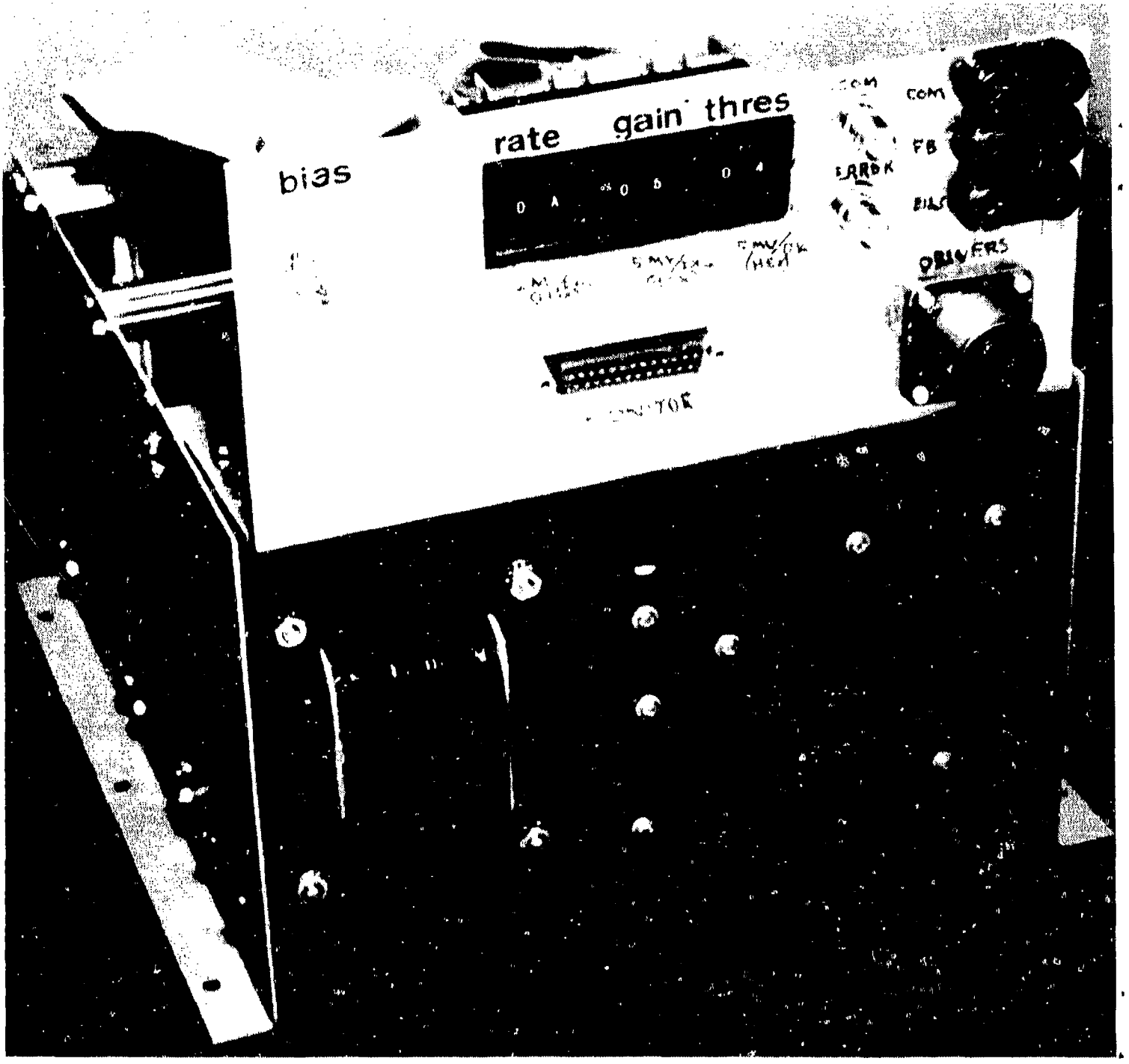

Figure II-31. Microprocessor hardware package.

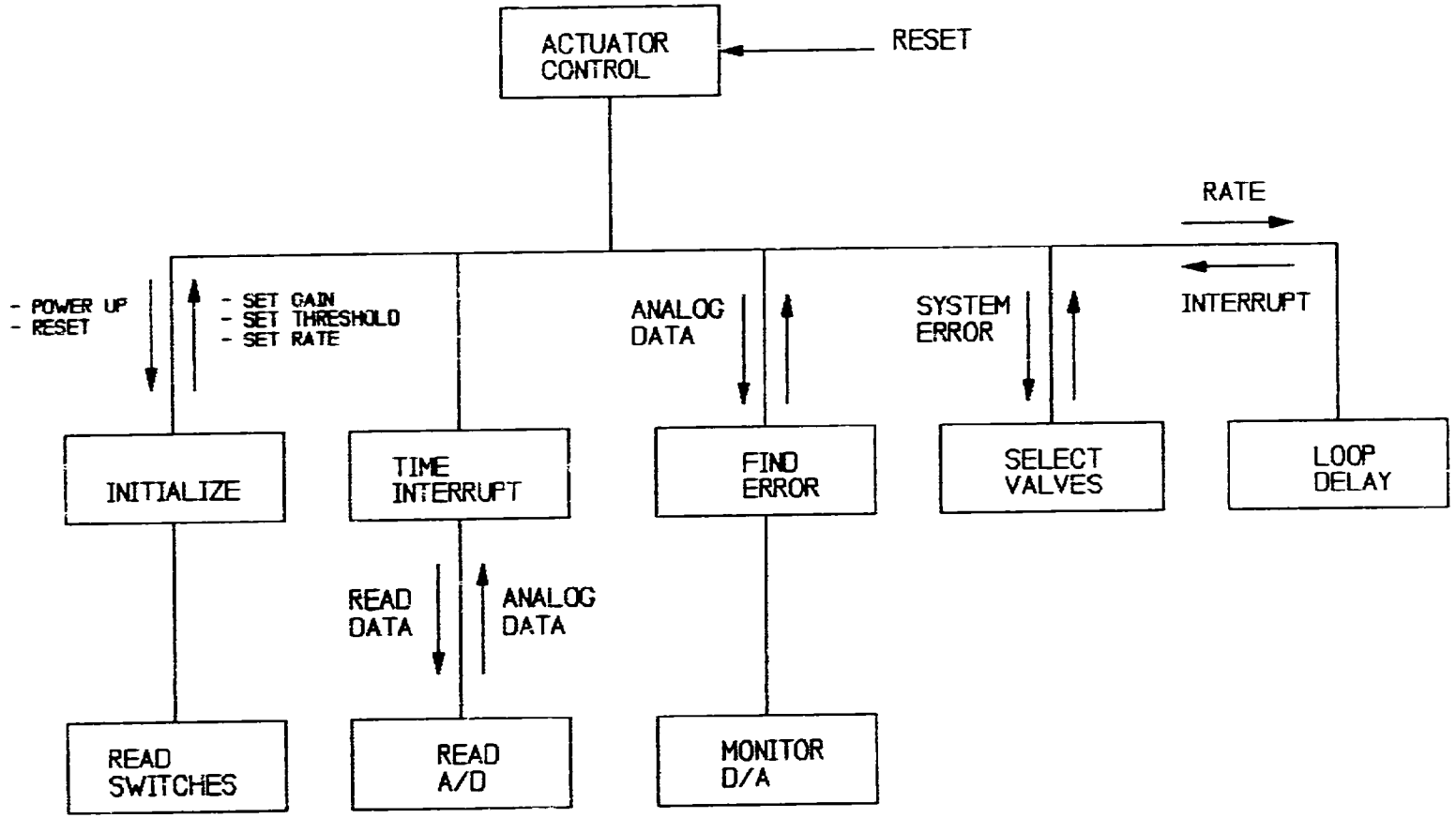

Figure II-32. Digital servovalve software structure diagram.

The main program started by reading the analog input values from a multiplexed 12-bit analog-to-digital convertor which was scaled to -10 VDC = 0000H and +10 VDC = OFFFH. The command and bias were summed. The control system error was determined by finding the difference between the command sum and the actuator position. The polarity of the error was checked to select extend or retract poppet valves. The amplitude of the error was first compared to the table threshold value. If it was less than threshold, the program jumped to the end and no action was taken. If greater than threshold, the magnitude was checked against the gain table starting at the highest value. The direction and magnitude information was used to develop an output code that operated the required poppet valves. The program waited for the timer interrupt before it cycled again.

The program used straight-line code throughout to enhance the operating speed. The total memory requirement was 556 bytes. Appendix A-1 contains the complete program as used in this control system.

Test Actuator and Manifold Design

Figure II-33 is the assembly drawing of the digital PZ servovalve/actuator. The actuator and manifold were designed as an integral unit to minimize the package size and interface porting hardware. The internal fluid porting of the manifold was sized as large as possible to keep the internal pressure drops to a minimum.

The body was manufactured from 7075-T6 aluminum. The actuator was designed to have a drive area of 0.77 square inches and a total stroke of 4.00 inches. The 304 stainless steel piston used two sets of Green Tweed *7-214* teflon cap-type seals to provide low friction and long life. The close-tolerance end caps were constructed from AMPCO-18, an aluminum-bronze bearing material. The end caps had low-friction Shambam teflon Delta seals installed as the dynamic rod seals. A Beckman *421-600* precision linear film potentiometer was designed into the package. The linear transducer was used to measure the actuator position with an accuracy of ± 0.25 percent of full scale.

An anti-rotation guide pin was mounted opposite the transducer and coupled through a yoke to prevent shaft rotation from damaging the transducer. Adjustment of the position transducer was provided by the integral body clamp for the course setting and a double nut design provided the fine-position transducer adjustment. Figure II-33 is a photograph of the disassembled components of the actuator/manifold. Figure II-34 is a photograph of the assembled actuator/manifold.

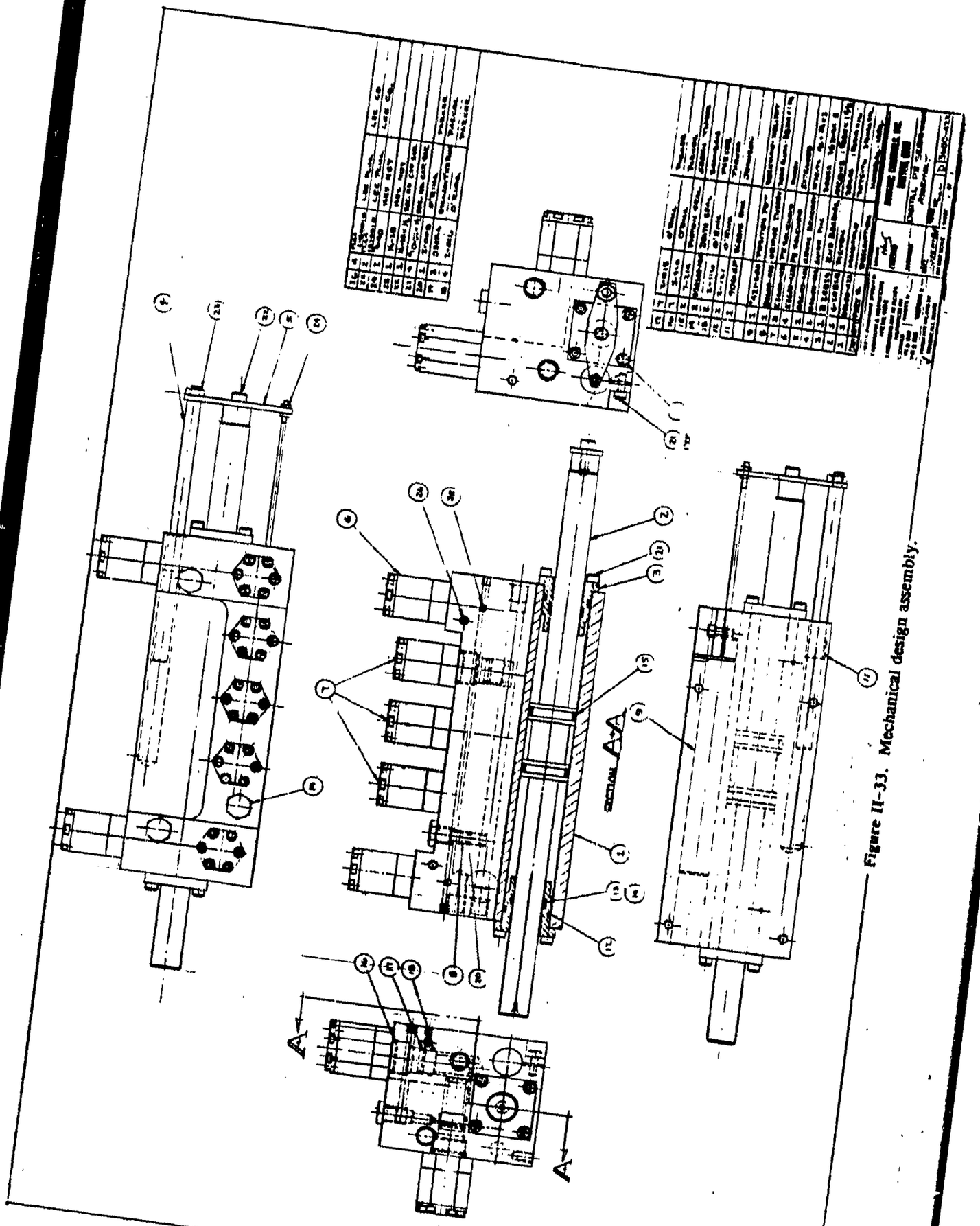

Figure II-33. Mechanical design assembly.

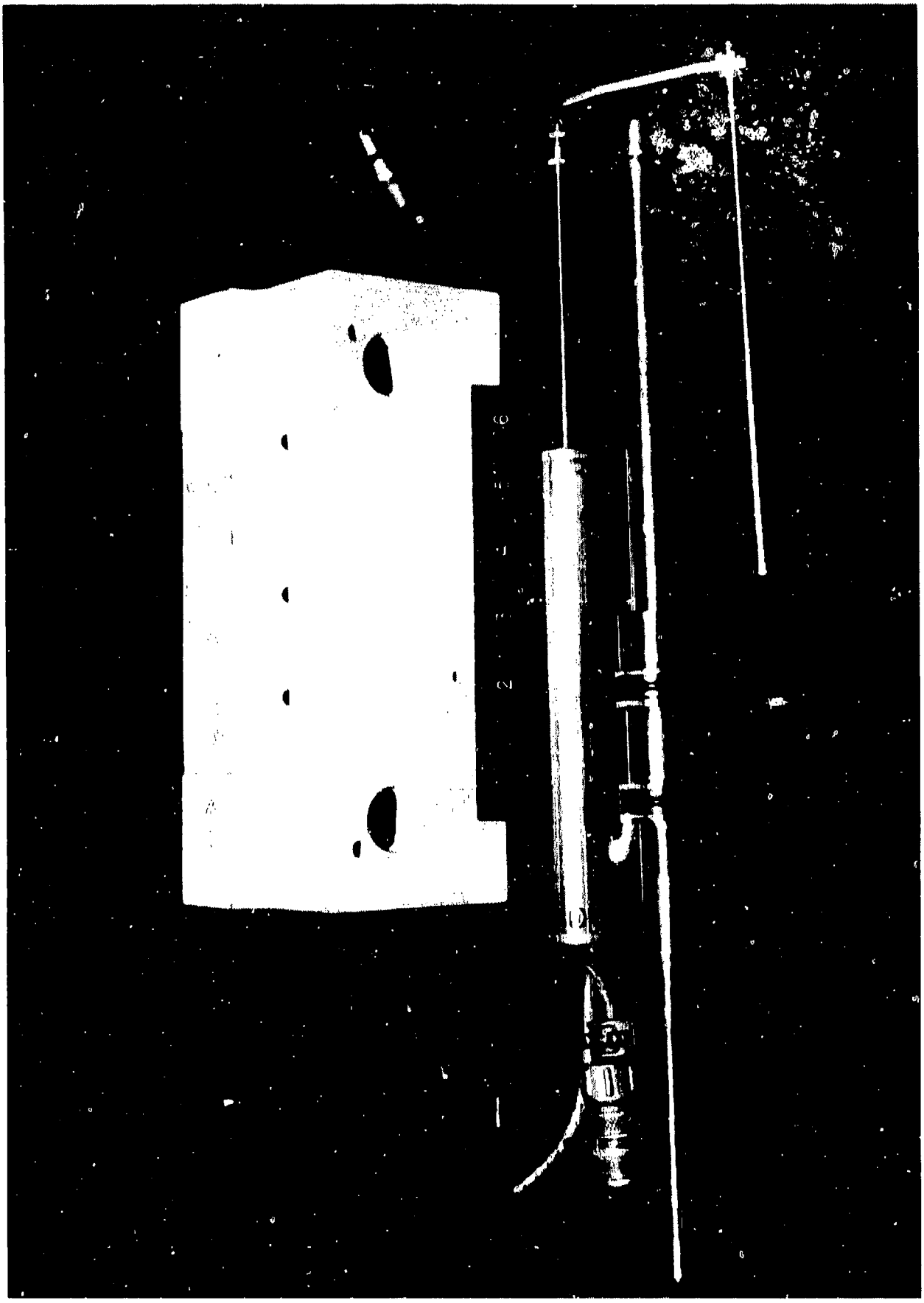

Figure II-34. Actuator/manifold components.

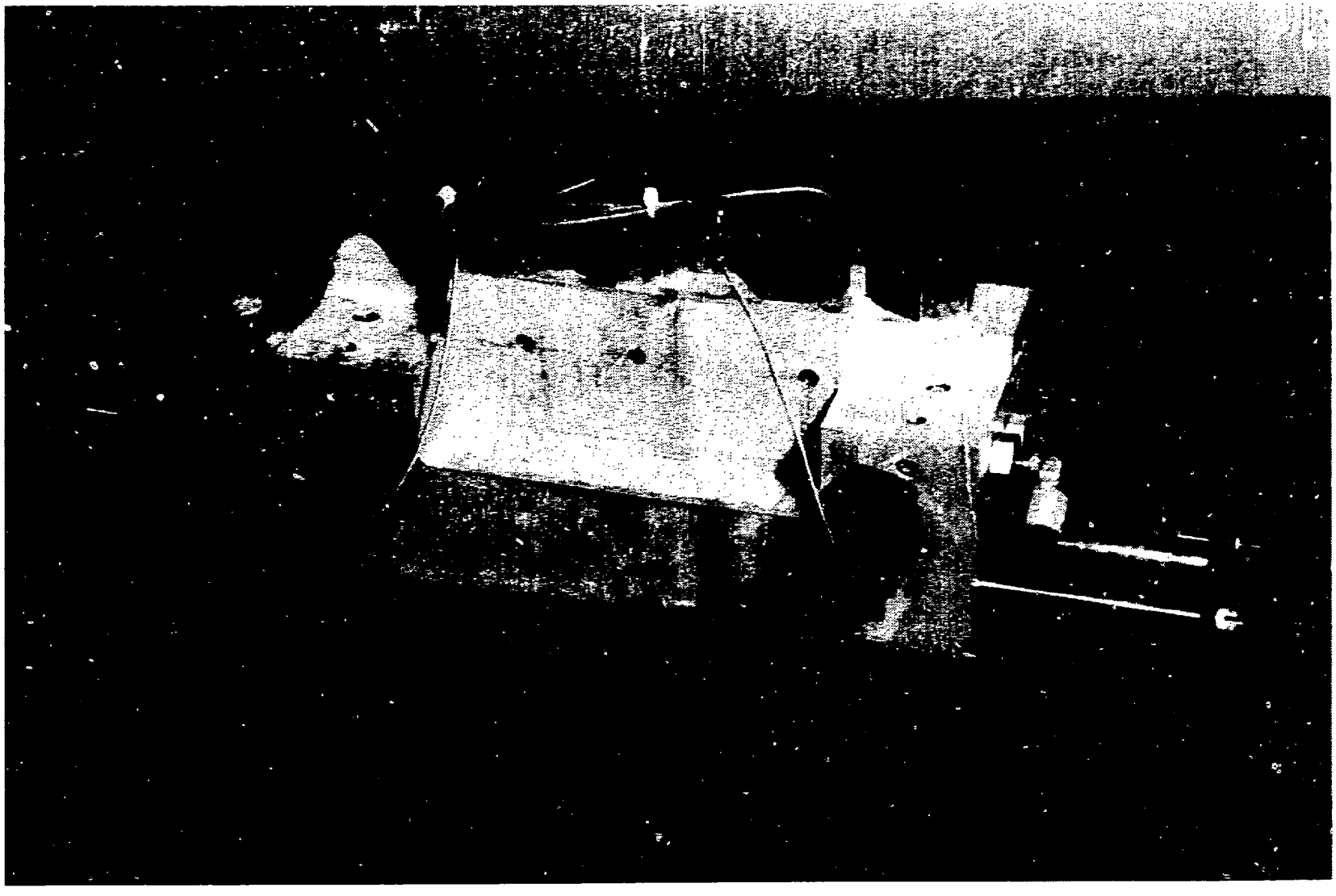

Figure II-35. Assembly of digital servovalve/actuator.

III. TEST PROCEDURE AND RESULTS

General

The performance of the PZ digital servovalve was indirectly evaluated by measuring the input-output (I/O) characteristics of the control system in which the valve was applied. The performance measurements performed were consistent with those used to define the control parameters of any electrohydraulic position feedback control system. The approach of measuring I/O characteristics was used because it was consistent with previous digital servovalve testing and it addressed the intended application of the digital servovalve.

The testing was divided into two phases. For Phase I, the system with analog control was evaluated and used as the baseline test. Phase II evaluated the control system with digital loop control. The microprocessor control evaluation included some parametric variations of the control system. The microprocessor's baseline setup was to duplicate the analog control baseline parameters. The evaluation test's performed on the hardware were the following:

- Flow Gain
- Static Threshold
- Dynamic Threshold
- Linearity/Hysteresis
- Saturation Velocity
- Frequency Response
- Step Response
- Waveform Characteristics

Flow Gain Test and Setup

The flow gain of the digital servovalve was determined with the servo/actuator configured in an open-loop mode (by disconnecting the position feedback). The error-voltage values that would energize specific flow steps were used as step inputs to the system. The step was applied with the actuator in the full-retract position and the stop-to-stop time was measured. Figure II-36 is representative of the PZ poppet valve configuration where directional valves 2 and 4 control the extend motion, directional valves 1 and 3 control the retract motion, and flow valves 5, 6, and 7 control the flow amplitude. The flow amplitude weighing-factor goals were to have valve 5 to be equivalent to 1 flow unit, valve 6 equal to 2 flow units, and valve 7 to equal 4 flow units. These values provide a binary weighing system as previously discussed.

The initial evaluation indicated that there was sufficient leakage through the flow control valves 5, 6, and 7, such that the fixed orifice could be eliminated. Also the PZ poppet valve development

produced values with less than one-third of the desired flow. This reduced the first flow step so low that it gave the fixed orifice a .004-inch diameter (which was too small for reliable in-house fabrication). Table II-6 is a tabulation of the flow step data and Figure II-37 shows a plot of output flow in cis versus the commanded flow step. The linearity curve shows saturation at the top of the curve. This was caused by the small difference in flow capability between the direction control and the flow control valves. The flow control valves were flow adjusted using the mechanical spool stops as a coarse setting and drive pulse width modulation as a fine adjustment. Desirable linearity was achieved through the lower 75 percent of the flow curve.

Analog Control Test Results

Test Setup

The gain of the error amplifier was adjusted to a gain of 27 volts per volt. The analog-to-digital converter was set up to have 0.66 volts of error per step, which converted to 4.65 volts for maximum flow or actuator velocity. At the input, this related to 0.66/27 = .024 volts per flow step and 4.65/27 = 0.172 volts for maximum velocity. The gain was set to obtain the best low-amplitude frequency response and maintain a well-damped control system. The directional threshold was set up at ± .050 volts at the convertor which would appear as 1.8 millivolts at the input. A 100-Hz filter was inserted on the gain amplifier to eliminate some of the inherent high-frequency noise.

Linearity

The linearity of a control system is defined as *the deviation from a straight line of the output to the input relationship*. The procedure used to measure linearity is to apply an input varying from the most negative to the most positive and back to the most negative while recording the input command and output position. The input must be varied at a rate that is less than one-tenth of the system's maximum rate to eliminate dynamic errors.

Figure II-38 shows a plot of the full-scale linearity recorded from the analog-controlled system. The linearity is better than 1.0 percent of full scale. This result is expected since a 0.5 percent linearity potentiometer was used for the system feedback. A ± 5.0-percent input-amplitude linearity plot is shown in Figure II-39. Deviation from the straight line is not yet detectable at this lower input amplitude. Hysteresis is usually noticed on low-amplitude linearity plots, although none is evident on this plot. The threshold starts to be evident in the very small stepping function recorded on the plot. This stepping has an amplitude of 4 per division or 1.25×10^{-3} inches.

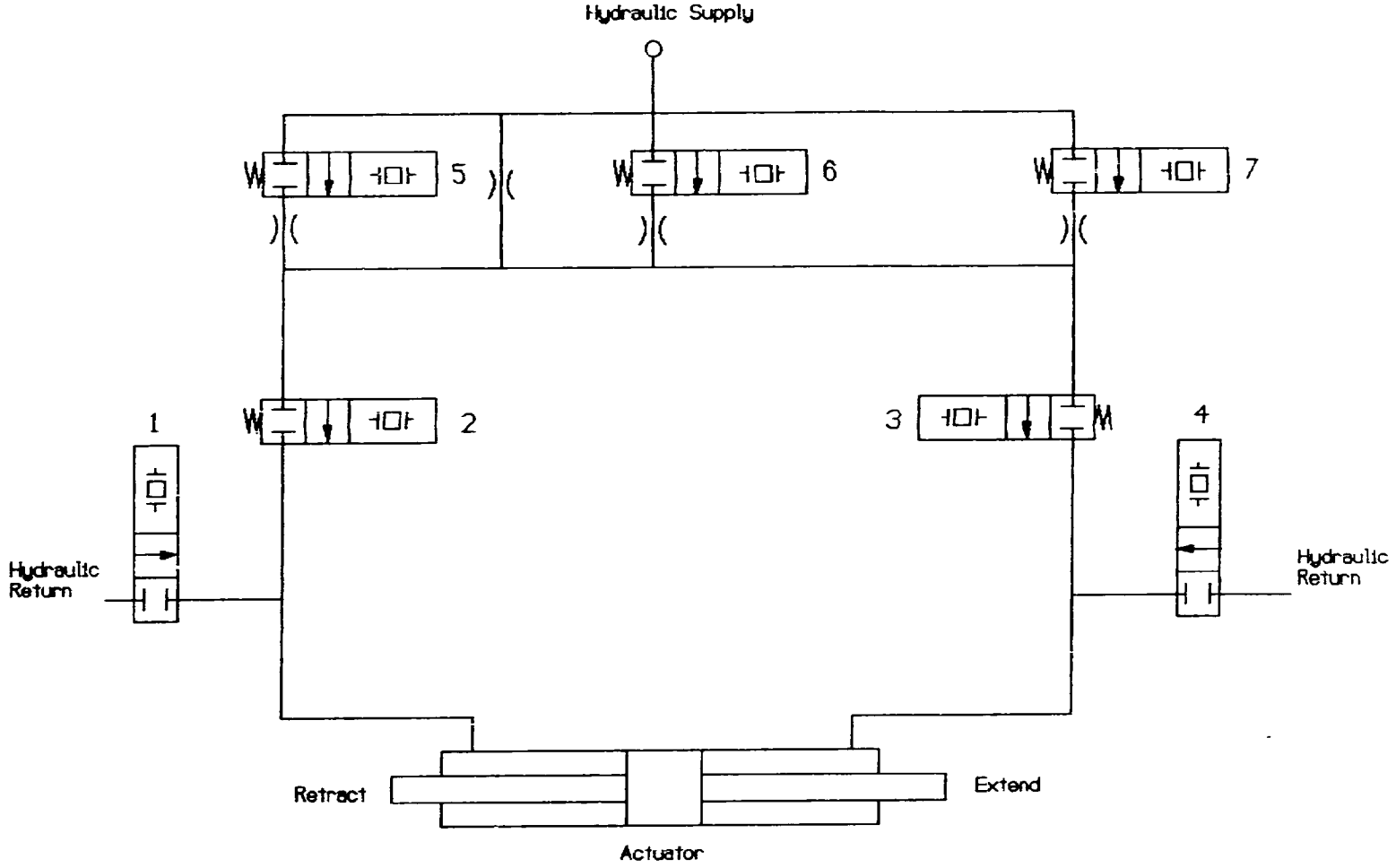

Figure II-36. Digital servovalve control.

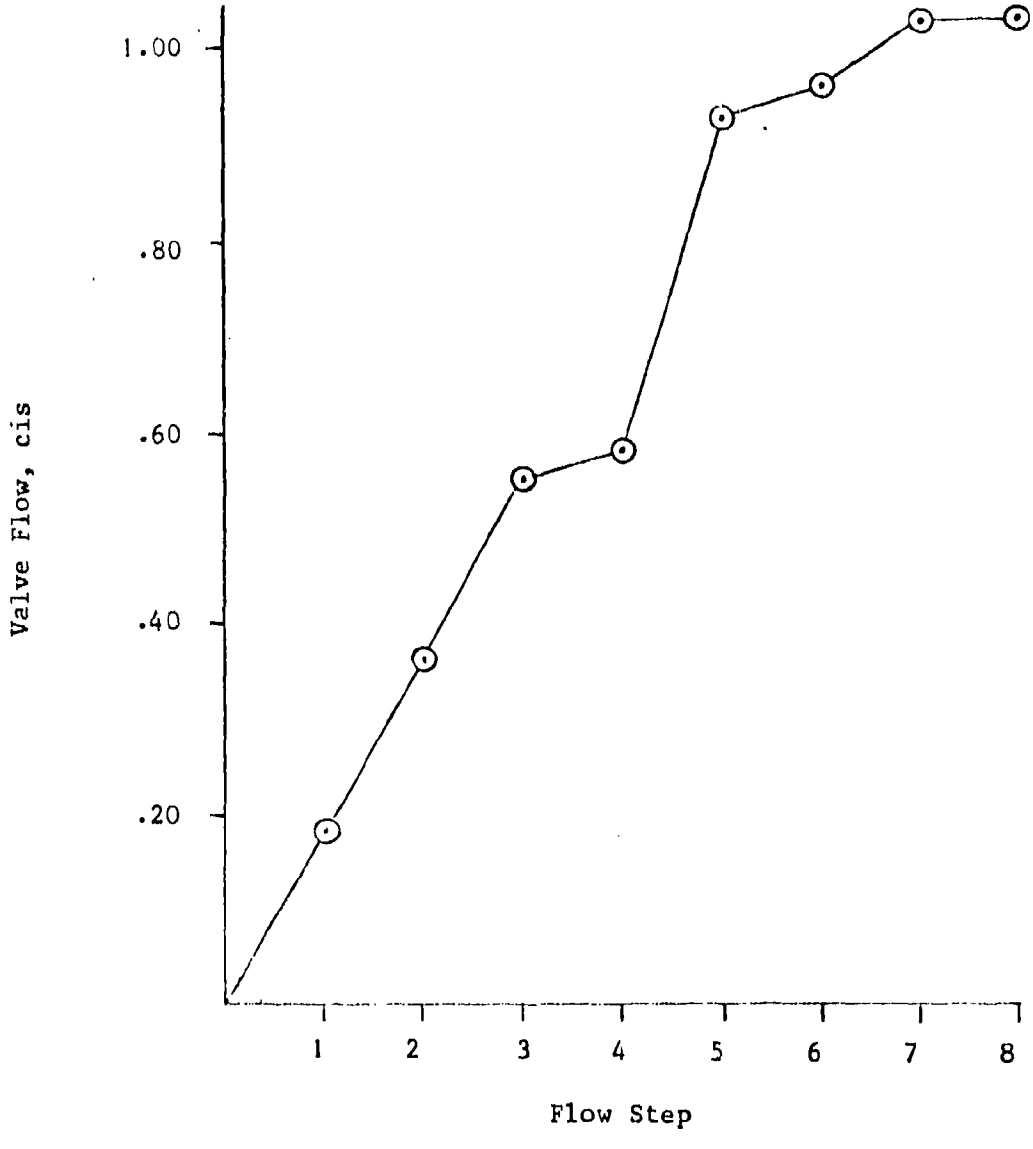

Figure II-37. Digital valve flow linearity.

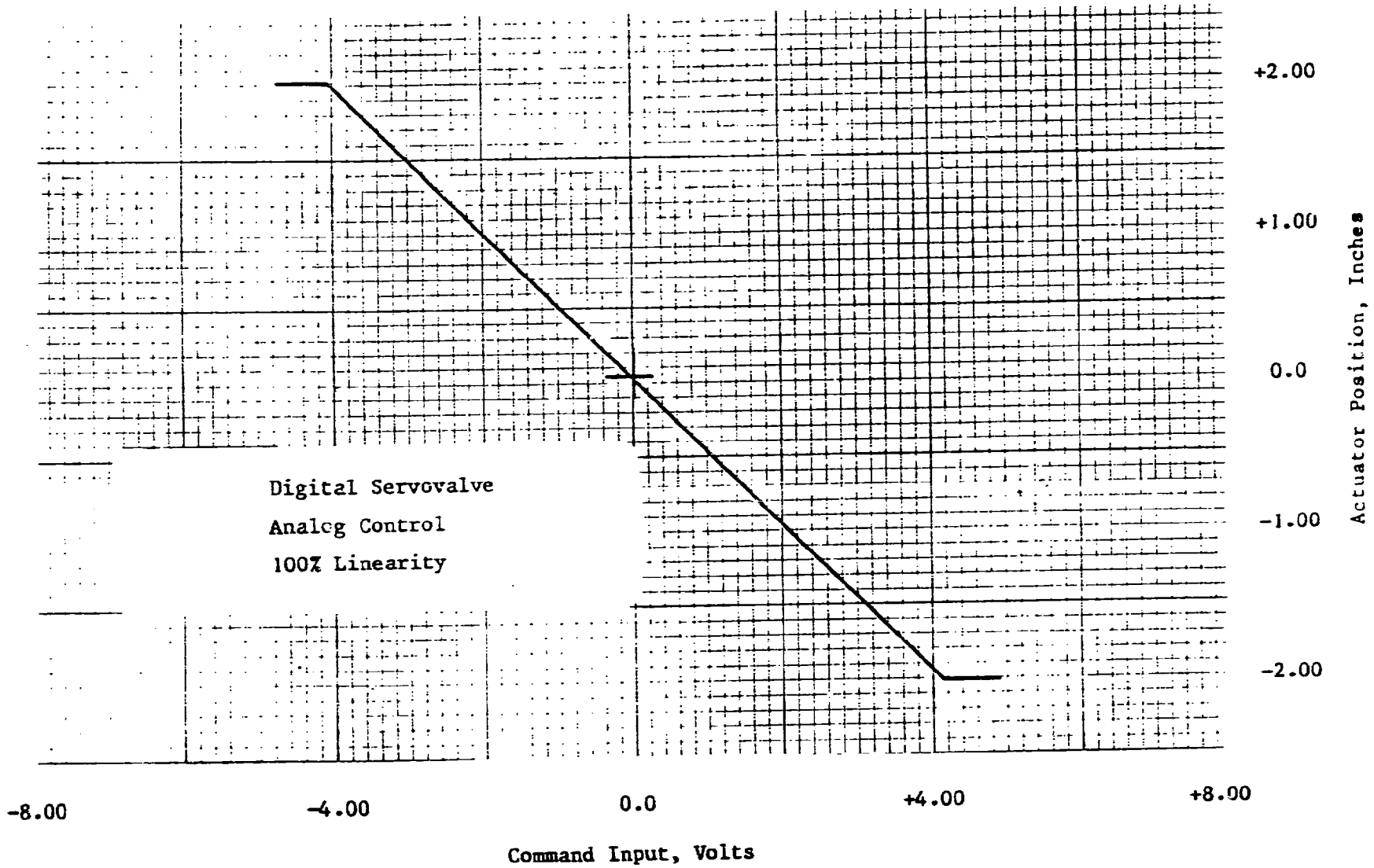

Figure II-38. Linearity - 100 percent - analog.

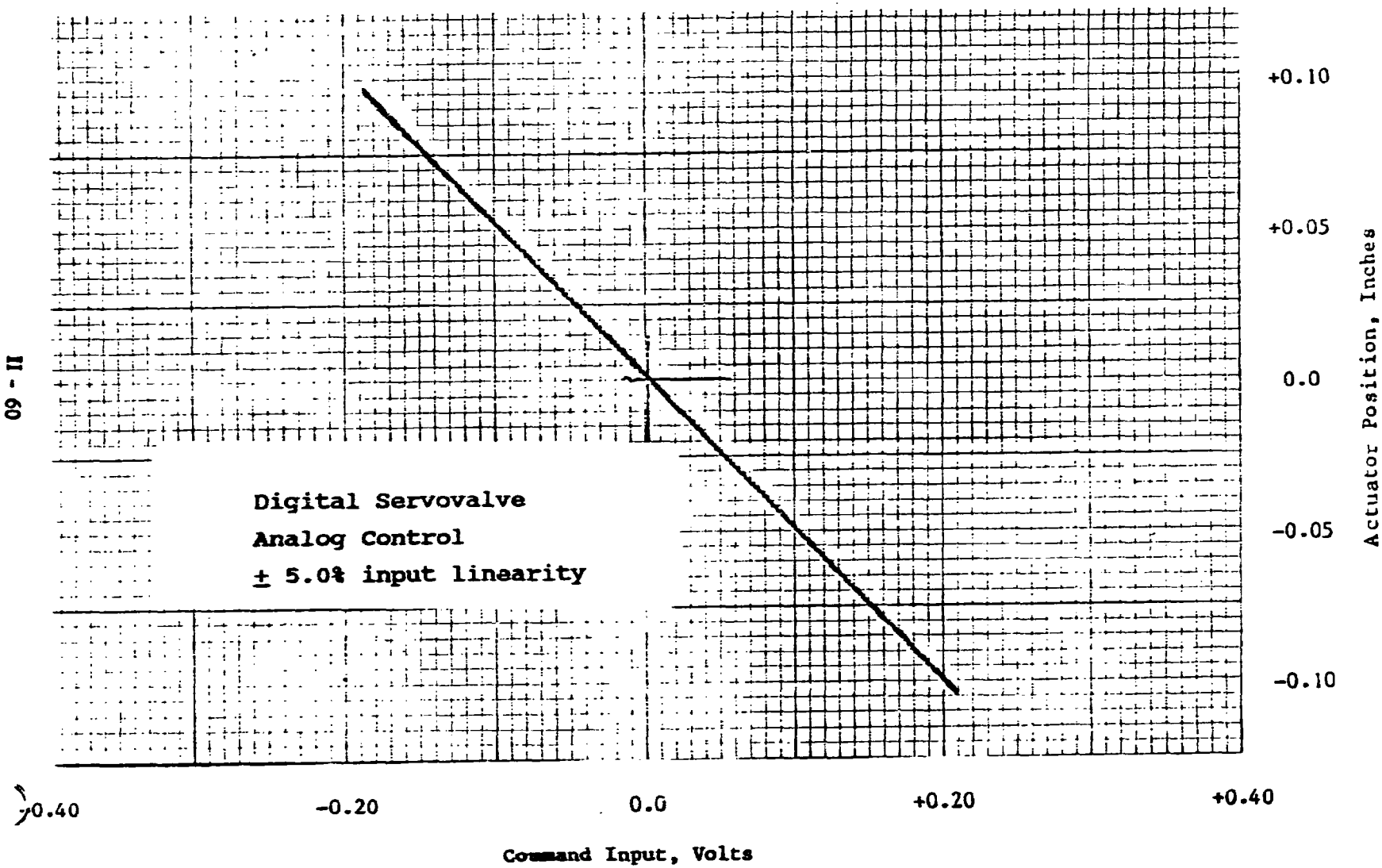

Figure II-39. Linearity - 5 percent input - analog.

Table II-6. Flow step table.

STEP #	VALUE COMBINATION	STOP-STOP TIME, SEC	AVERAGE VELOCITY IN/SEC	AVERAGE FLOW CIS
1	DIR-ONLY	17.0	.235	.18
2	5	8.56	.468	.36
3	6	5.6	.714	.550
4	5+6	5.3	.755	.581
5	7	3.3	1.21	.933
6	5+7	3.2	1.25	.963
7	6+7	3.0	1.33	1.03
8	5+6+7	3.0	1.33	1.03

Static Threshold

Static threshold is defined as "the minimum input change from zero which will cause a measurable output change". This procedure used a 0.10-Hz triangular wave as the command with the amplitude slowly increased from zero volts. The results shown in Figure II-40 were recorded on a time-history chart. The static threshold measured to be ± .003 volts or ± .0015 inches (scale factor = 2.0 volts per inch). This is ± .0075 percent of the ± 2.0-inch actuator stroke. Another approach to express threshold is to relate it as a percent of the system input required to generate full actuator rate. As a percent of rate command, 0.172 volts, the threshold is 1.7 percent. The electronics has 1.08-percent threshold (by design) to separate the direction control functions. The remainder of the threshold percentage is caused by actuator friction and the valve drive electronics.

Dynamic Threshold

The dynamic threshold is defined as "the sinusoidal frequency input level required to cause a measurable output". The frequency of the sinusoidal input is generally selected as 50 percent of the control system's bandpass frequency. The bandpass frequency is the frequency at which the amplitude is attenuated by -3 db or where the phase shift reaches -90° of phase shift, whichever frequency is lower. The input frequency was set at 5.0 Hz for this measurement. As shown on

TEST DATA

Test Item - Dynamic Controls, Inc.
Digital Servovalve

Date Prepared: 11-7-86

Test - Static Threshold
Analog Control

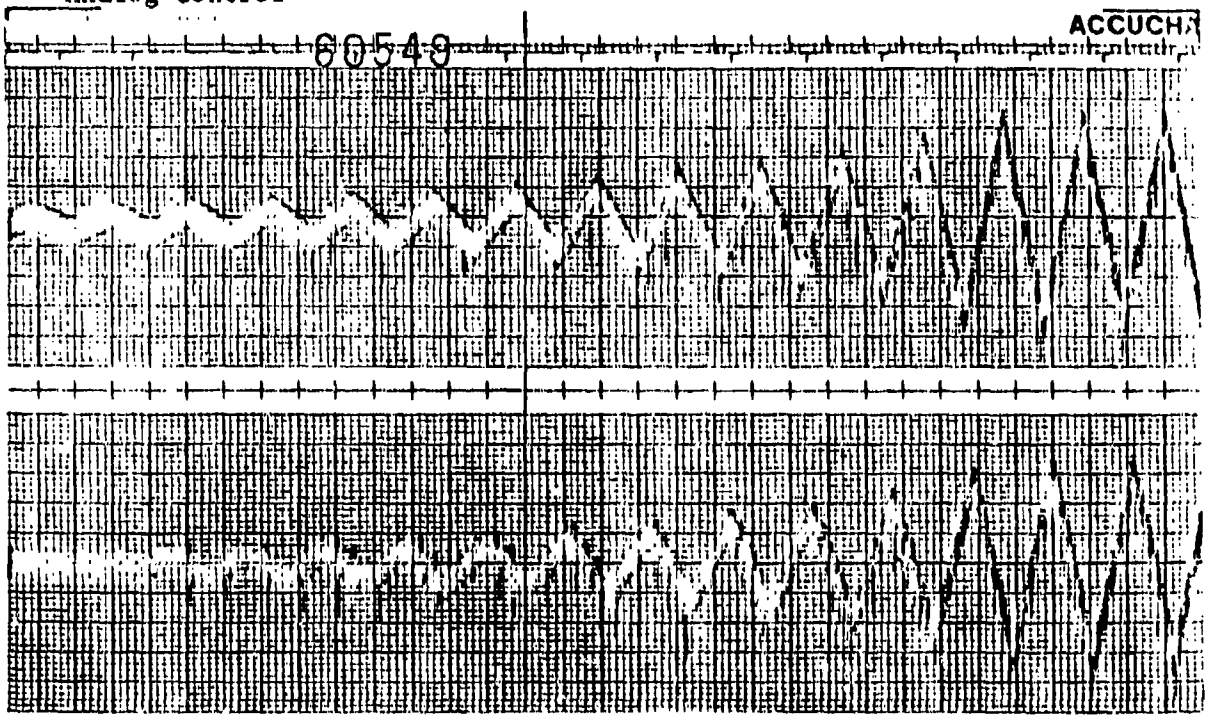

Time ⟶ 1.0 div/sec

Upper Trace: Command
Scale: 1.0 mv/div

Lower Trace: Actuator Position
Scale: 1.0 mv/div

Figure II-40. Static threshold, analog.

Figure II-41, the dynamic threshold is ± .002 volts or ± .001 inches when tracking. This is .05 percent of full stroke or 1.16 percent of full rate command. One of the reasons for the very low measured-threshold value is that the small amplitude stepping of the high-pressure gain digital servovalve provides a dither-like signal to the actuator, reducing the effect of seal friction.

Step Response

The step response of a system is obtained by applying a step input at a voltage level that will not exceed the error voltage that commands maximum flow. The output position response to the step input indicates the system's time delay and relative stability.

Figure II-42 shows a ± 100-millivolt step applied to the digital servovalve control system and the resulting output response. Upon the application of the negative step, a few milliseconds time delay occurs, partially because of the 100-Hz filter in the forward loop and partially due to the drive logic's pulse modulators. The effect of the drive logic is more evident when the positive step is applied. The logic contains electronic circuitry that ensures that the PZ actuator has ample time (2 milliseconds) to fully charge and discharge to prevent latching of the high-voltage drivers. When operating the drivers asynchronously, there can be a small overlap when all directional valves are open at the same time. Since the extend (positive) velocity is greater than the retract velocity, the actuator extends about .002 inches before retracting to its commanded negative value. Upon reaching the final position, both the negative and positive steps show good stability with no overshoot or ringing. The low-amplitude output motion is caused by the noise generated by electromagnetic interference.

Saturation Velocity

The lower half of Figure II-42 shows the extend (negative) and retract (positive) saturation velocity obtained by commanding the actuation control system with a ± 10.0 volt square-wave input. The extend velocity of 1.21 inches per second is obtained from traveling the 4-inch stroke excursion in 3.3 seconds. The retract velocity of 0.91 inches per second is somewhat slower than the extend velocity. The discrepancy between the extend and retract velocities was caused by leakage from the extend directional valve 4 (see Figure II-36). Reworking the valve was considered but not accomplished because of the impact on the investigation's schedule. This leakage was not considered to be a negative factor in the feasibility demonstration of this concept.

TEST DATA

Test Item - Dynamic Controls, Inc.
Digital Servovalve

Date
Prepared: 11-7-86

Test - Dynamic Threshold
Analog Control

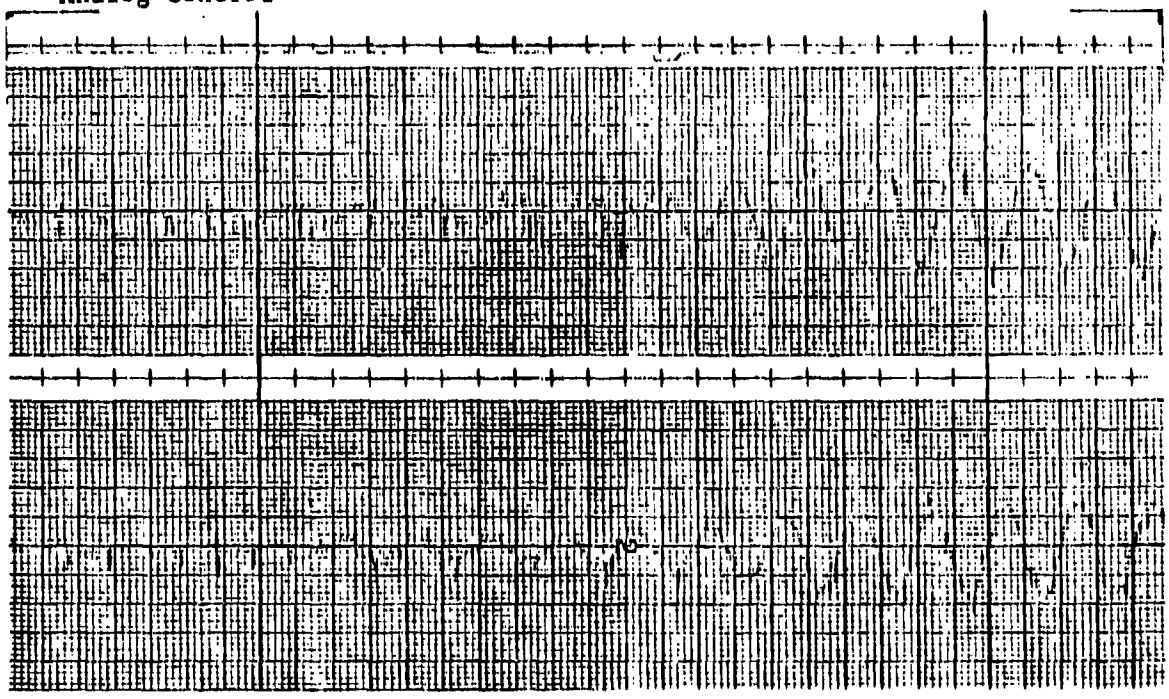

Time ⟶ 50 div/sec

Upper Trace: Command
Scale: 2.0 mv/div

Lower Trace: Actuator Position
Scale: 2.0 mv/div

Figure II-41. Dynamic threshold - analog.

Test Item - Dynamic Controls, Inc.
Digital Servovalve

Date Prepared: 4 Dec 86

Test - Step Response and Saturation Velocity
Analog Control

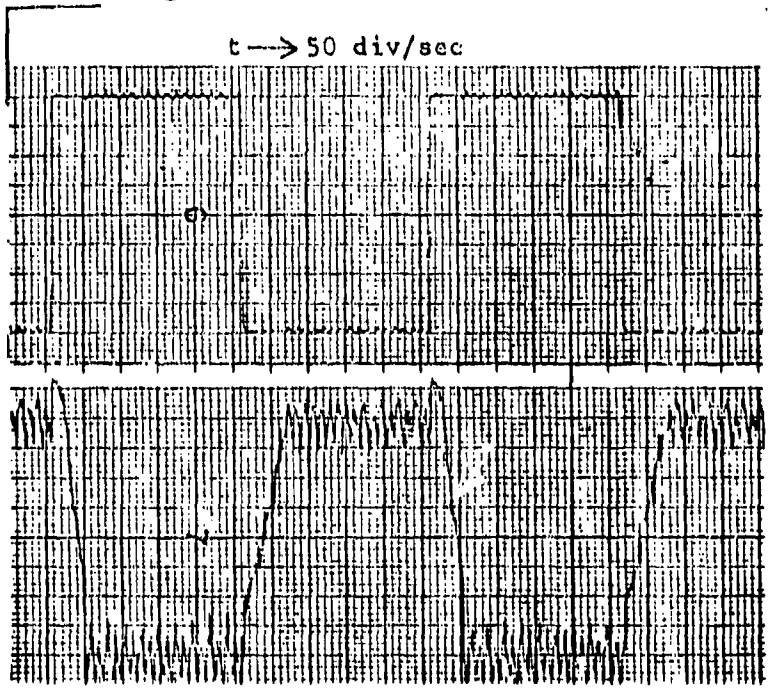

Step Response

Command
Scale: 5 mv/div

Actuator Position
Scale: 5 mv/div

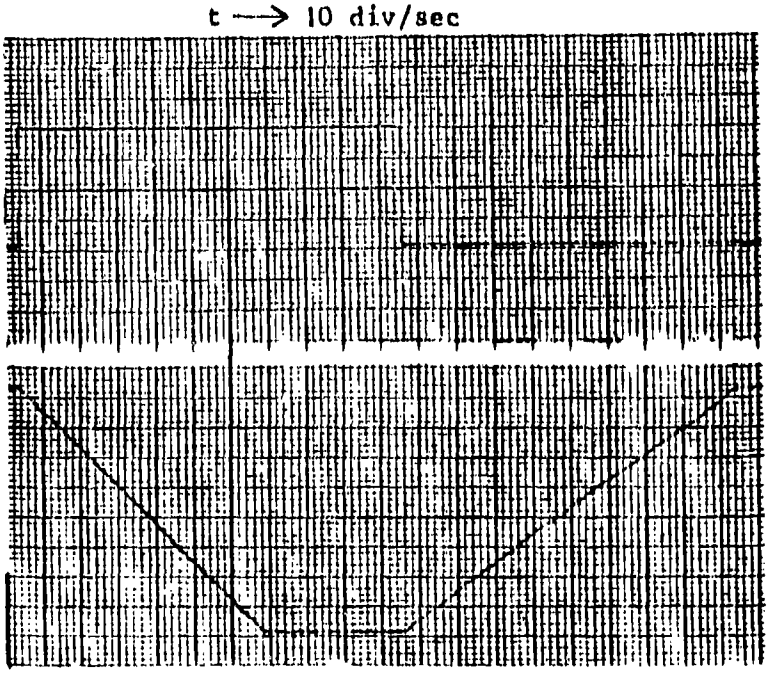

Saturation Velocity

Command
Scale: 500 mv/div

Actuator Position
Scale: 200 mv/div

Figure II-42. Step response and saturation velocity - analog.

Frequency Response

The frequency response of a control system is defined as *the amplitude ratio and phase shift of the output relative to the input as a function of frequency*. The input amplitude used should be large enough to minimize the non-linearities introduced by hysteresis and threshold, yet small enough to avoid saturation over the frequency range of interest.

A Hewlett-Packard 5423 signal analyzer was used for the frequency-response testing. The instrument generates a random noise signal for the system input, samples the output, computes the response from a Fourier Transform digital program, and plots the result using an X-Y plotter. Experience in operating the signal analyzer has indicated that the unit has a minor problem when measuring response below 0.5 Hz, generating erroneous information (especially with amplitude ratio) when there is a steady-state offset in the system's output. The data has been formatted in an A-over-B mode, with the amplitude ratio appearing on the top half of the figure and the phase angle occupying the bottom half.

The frequency response shown in Figure II-43 is the 10-percent of full-scale input data. At this amplitude, the system is velocity-saturated as can be observed on the amplitude ratio plot. The saturation on the amplitude plot has the expected 20 db per decade slope, typical of rate saturation. From this data, it was determined that the input should be reduced by 26 db or to 0.5-percent full-scale input to obtain 10-Hz system response. The 0.5-percent input amplitude would be in the system noise level and was not considered to be a usable input level. The measured phase shift is typical of a first-order system, where it rolls off and flattens to a constant value of 90° phase lag.

The 5-percent full-scale frequency response in Figure II-44 has a -3 db point at 1.5 Hz and -45° phase angle at 1.5 Hz (where velocity saturation starts to affect the response). The amplitude was reduced to 2.5 percent full scale, improving the response to -3 db at 2.5 Hz and -45° at 2.5 Hz (shown in Figure II-45). This is consistent with analysis which indicate that a saturation velocity of 1.15 inches per second should provide linear response to about 2.0 Hz at this amplitude. Figure II-46 is an example of the lowest input amplitude (1.25-percent, full-scale) frequency response measured. Predictably, it shows the amplitude response extended to 6 Hz for -3 dB and 5.6 Hz for - 45° phase shift.

All of the analog-controlled frequency response measurements are well-damped and do not indicate any resonant frequency modes through the frequency band of interest.

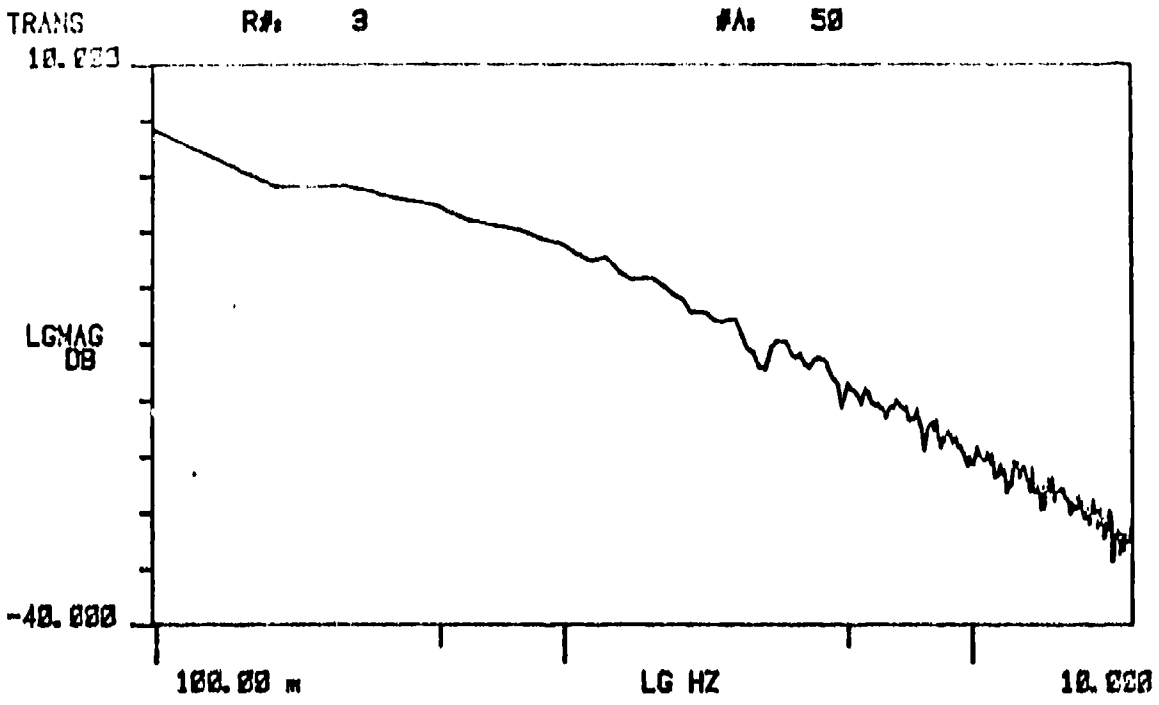

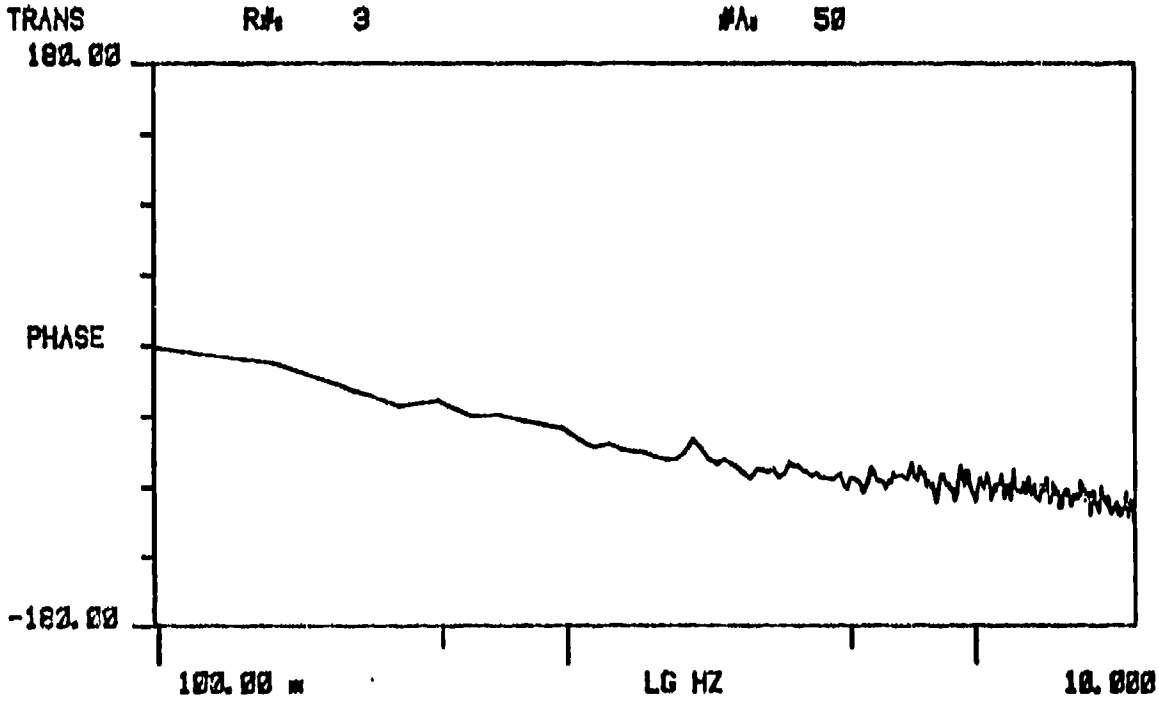

0 Db Input: ± 0.4 volts
Control Mode: Analog

Figure II-43. Analog frequency response - 10 percent.

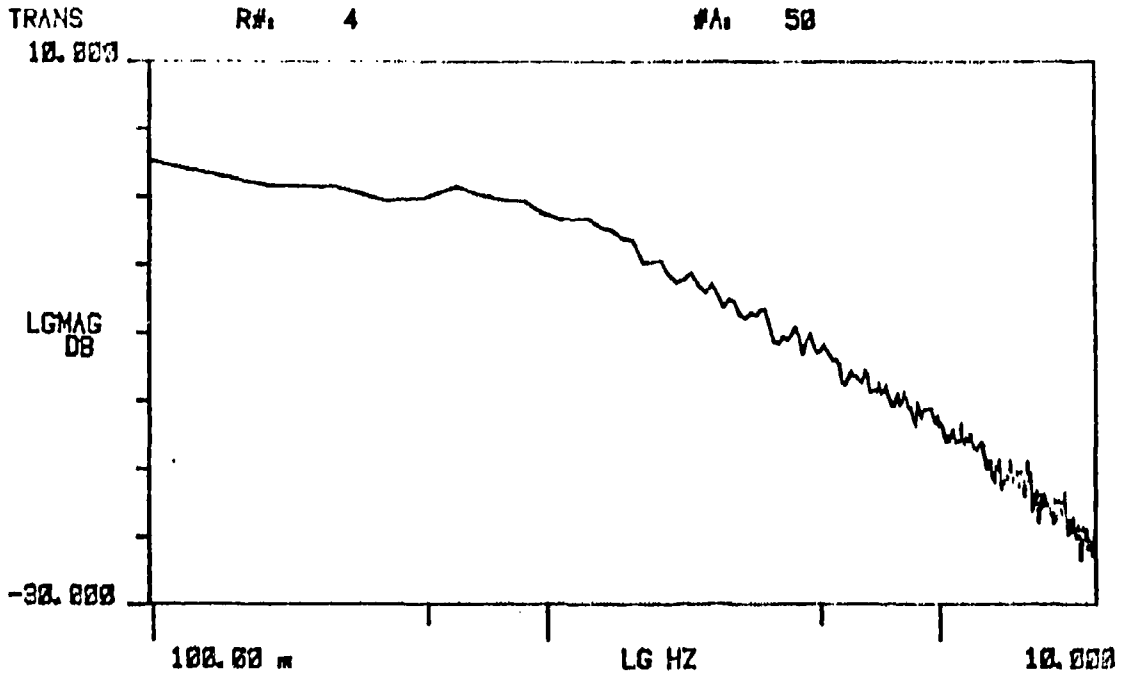

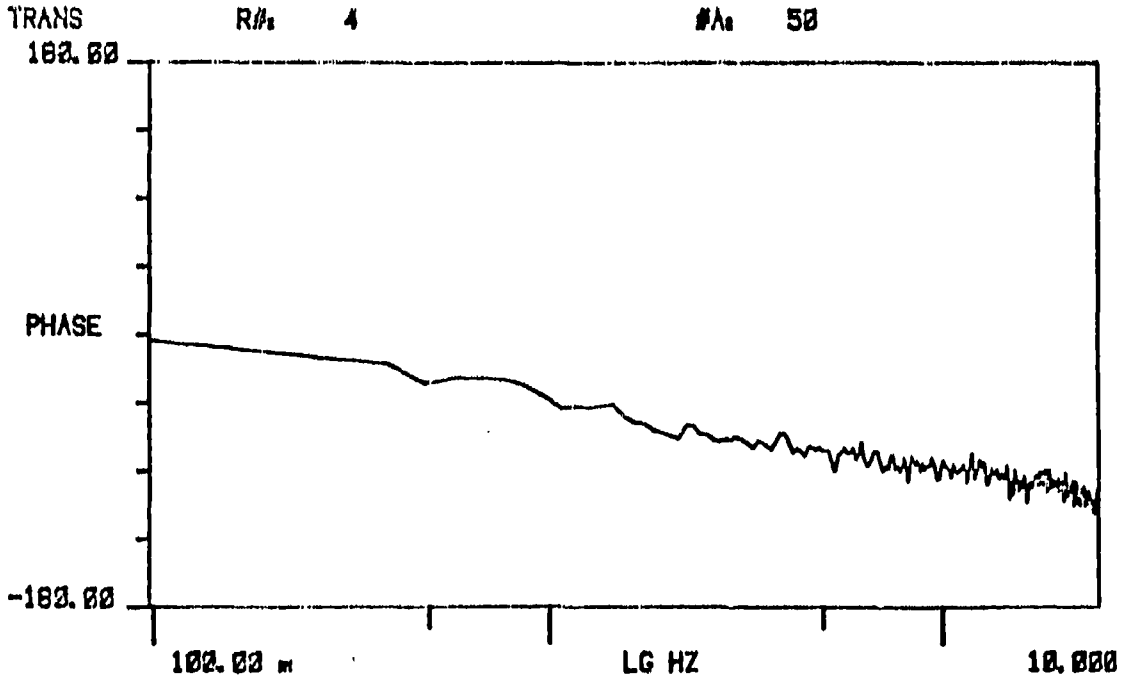

0 Db Input: ± 0.2 volts

Control Mode: Analog

Figure II-44. Analog frequency response - 5 percent.

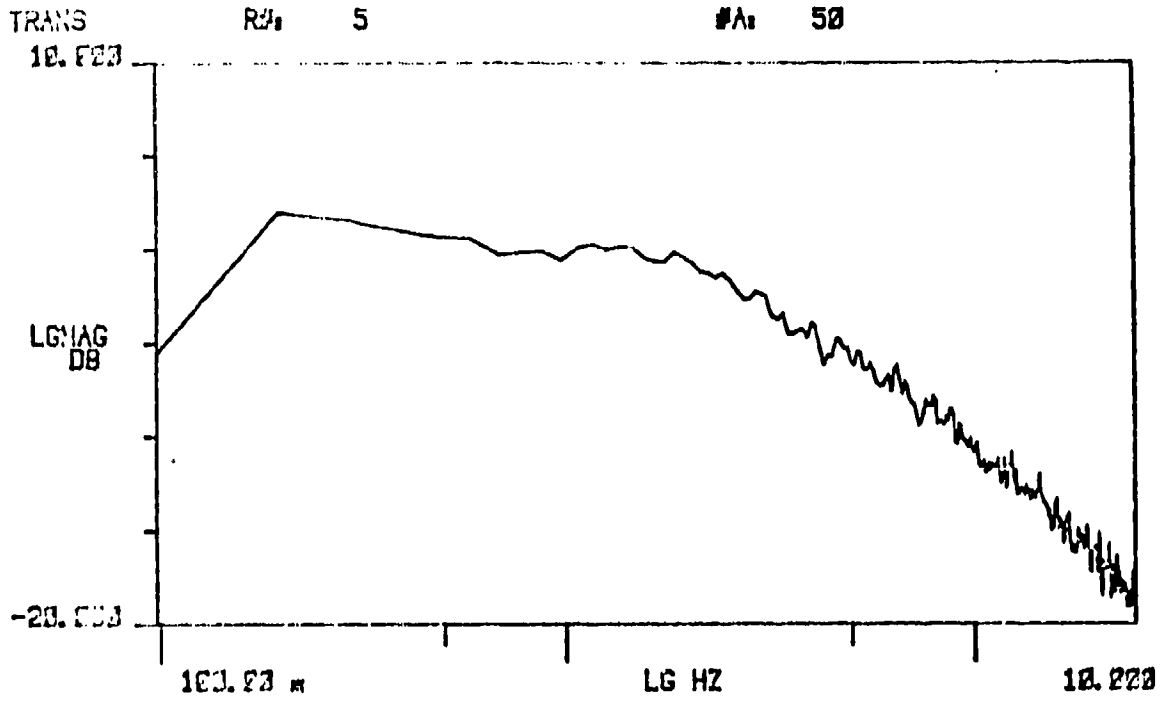

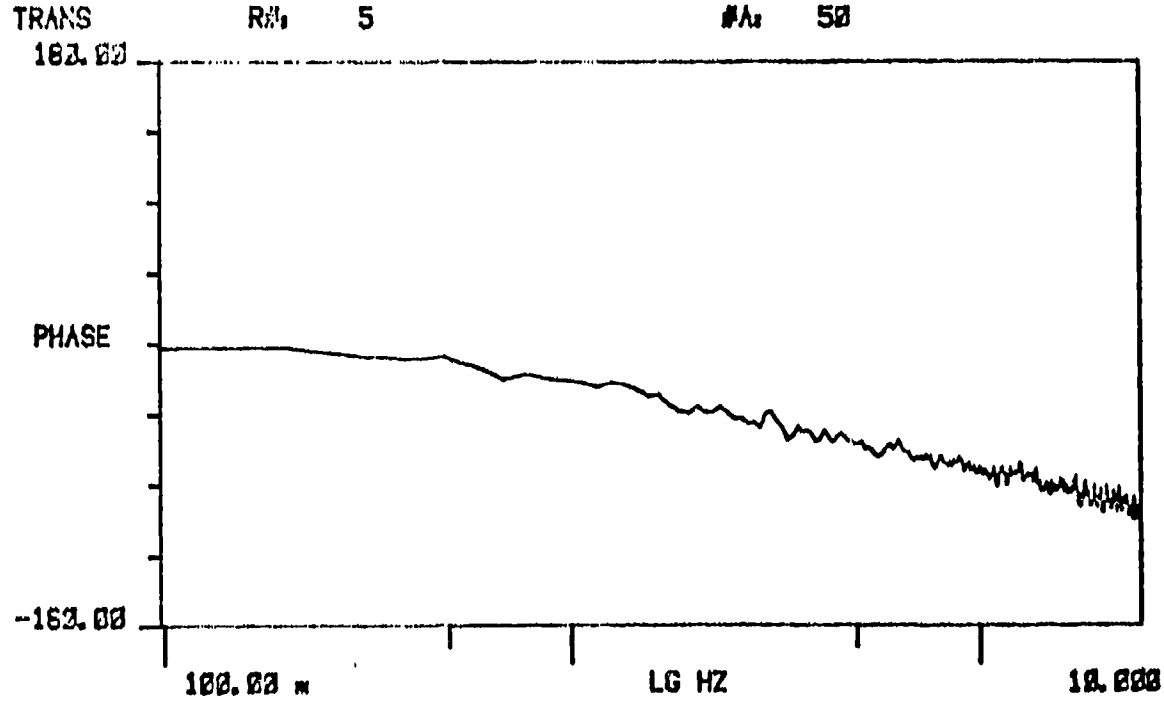

0 Db Input: ± 0.1 volts

Control Mode: Analog

Figure II-45. Analog frequency response - 2.5 percent.

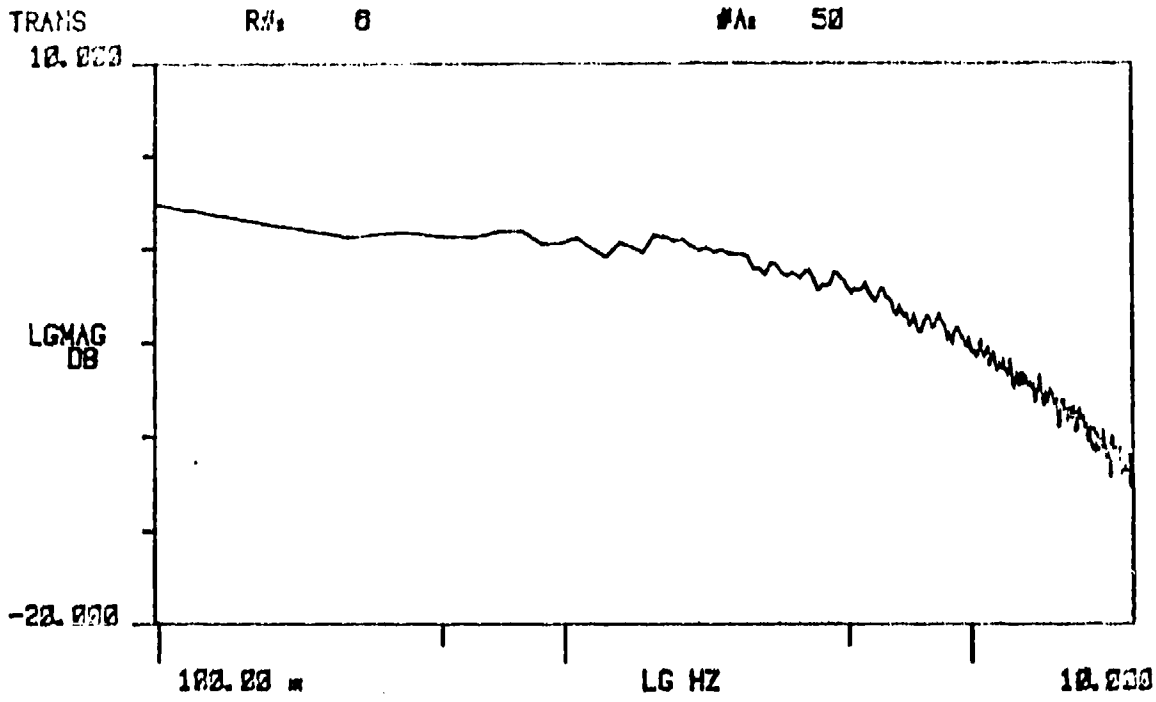

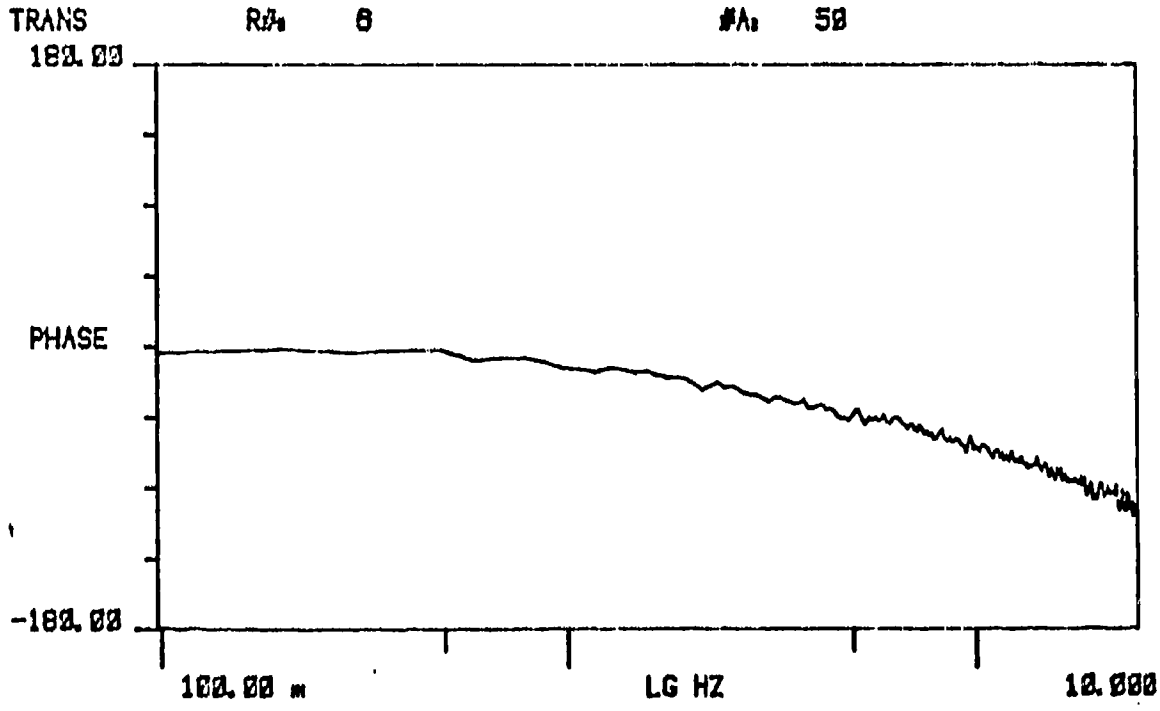

0 Db Input: ± .05 volts

Control Mode: Analog

Figure II-46. Frequency response - 1.25 percent - analog.

Waveform Characteristics

To indicate the distortion of the control system output in response to a sinusoidal input, time-history records at ± 2-percent, ± 5-percent, and ± 10-percent input levels were recorded. The frequencies recorded at these amplitudes were 0.3 Hz, 1.5 Hz, 3.0 Hz, and 10 Hz.

Figure II-47, with the 10-percent input level, indicates good output fidelity at 0.3 Hz. At 1.5 Hz velocity saturation is observable, caused by the flow limitation of the digital servovalve. The velocity limitation affects the output when the frequency is 3.0 Hz and 10.0 Hz.

Figure II-48 is the ± 5.0-percent full-scale command waveform characteristics. The output tracks the input well at the 0.3 Hz and 1.5 Hz frequencies. Velocity saturation becomes evident on the 3.0 Hz recording. There is a noticeable output bias shift in both the 5-percent and 10-percent data, because of the difference between the extend and retract saturation velocities.

Figure II-49 shows the waveform characteristics when a ± 2.0-percent full-scale command signal is applied to the analog-controlled digital servovalve system. When commanded at 0.3 Hz, 1.5 Hz, and 3.0 Hz, the output indicates good signal tracking. The band of noise impressed on the output is electrical noise generated by the high-voltage PZ drivers. The 3.0 Hz trace indicates a search for direction information at the peaks of the sine wave. Distinct slope changes are observed when flow level valves are energized and de-energized. The actuator position at 10 Hz is only -3 db down and continues to indicate velocity changes because of valve switching. The main part of the indicated signal distortion is the effect of the electrical noise, not actuator motion.

Test Item - Dynamic Controls, Inc.
Digital Servovalve

Date Prepared: 1 Dec 86

Test - Waveform Characteristics - Analog Control
± 10% F.S. Input

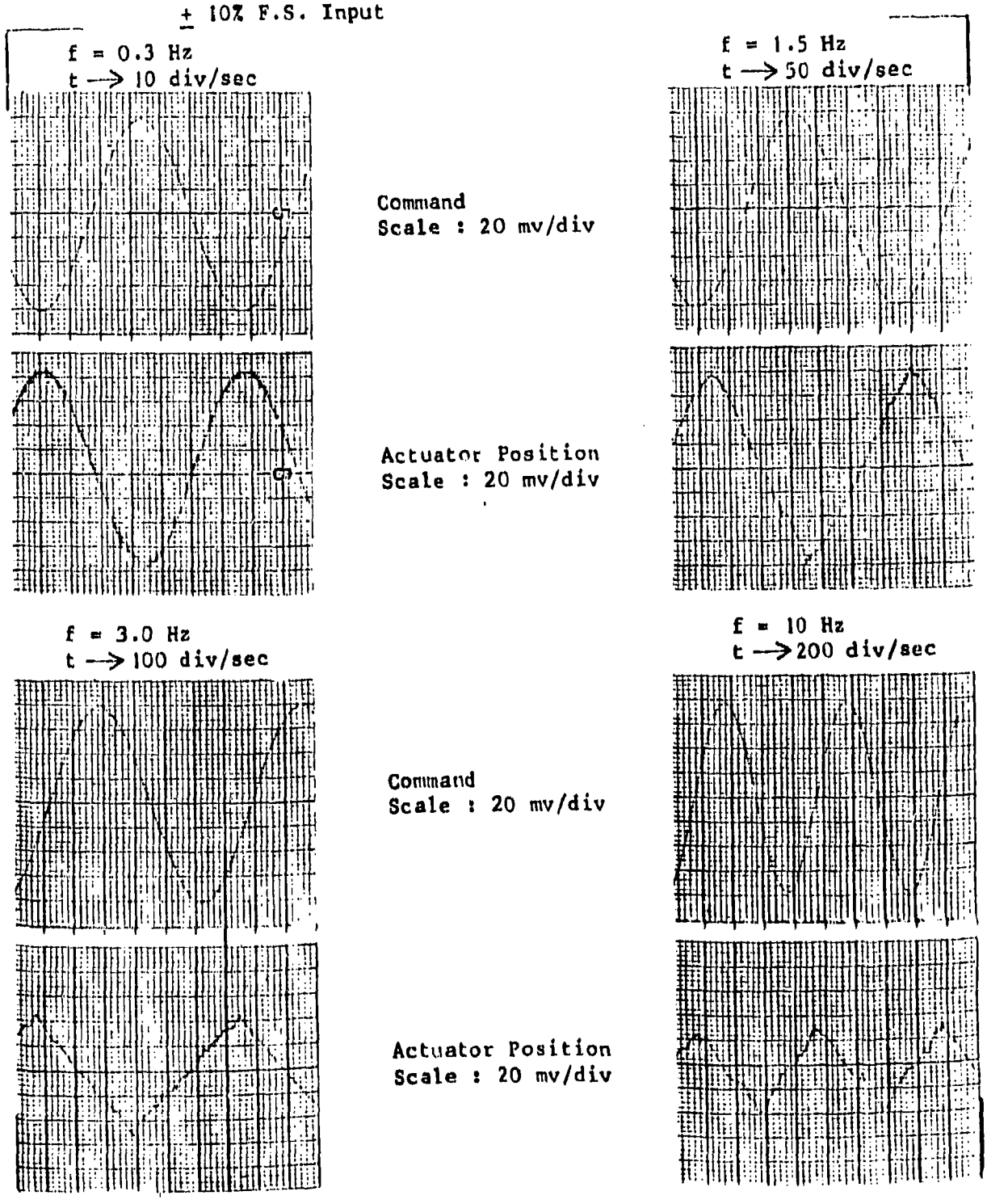

Figure II-47. Waveform characteristics - 10 percent - analog.

Test Item - Dynamic Controls, Inc.
Digital Servovalve

Date Prepared: 1 Dec 86

Test - Waveform Characteristics - Analog Control
± 5.0% F.S. Input

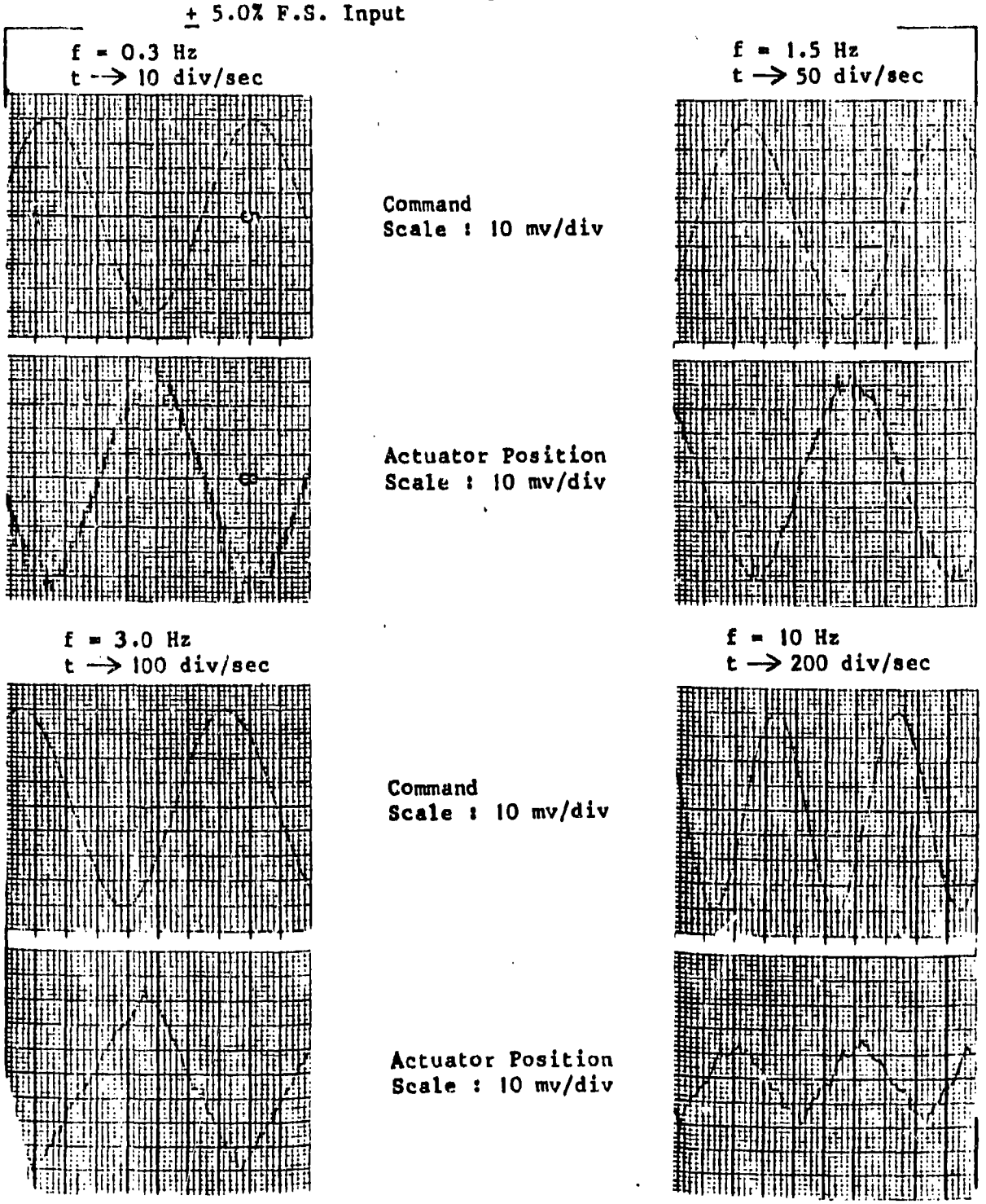

Figure II-48. Waveform characteristics - 5 percent - analog.

Test Item - Dynamic Controls, Inc.
Digital Servovalve

Date Prepared: 1 Dec 86

Test - Waveform Characteristics - Analog Control
± 2.0% F.S. Input

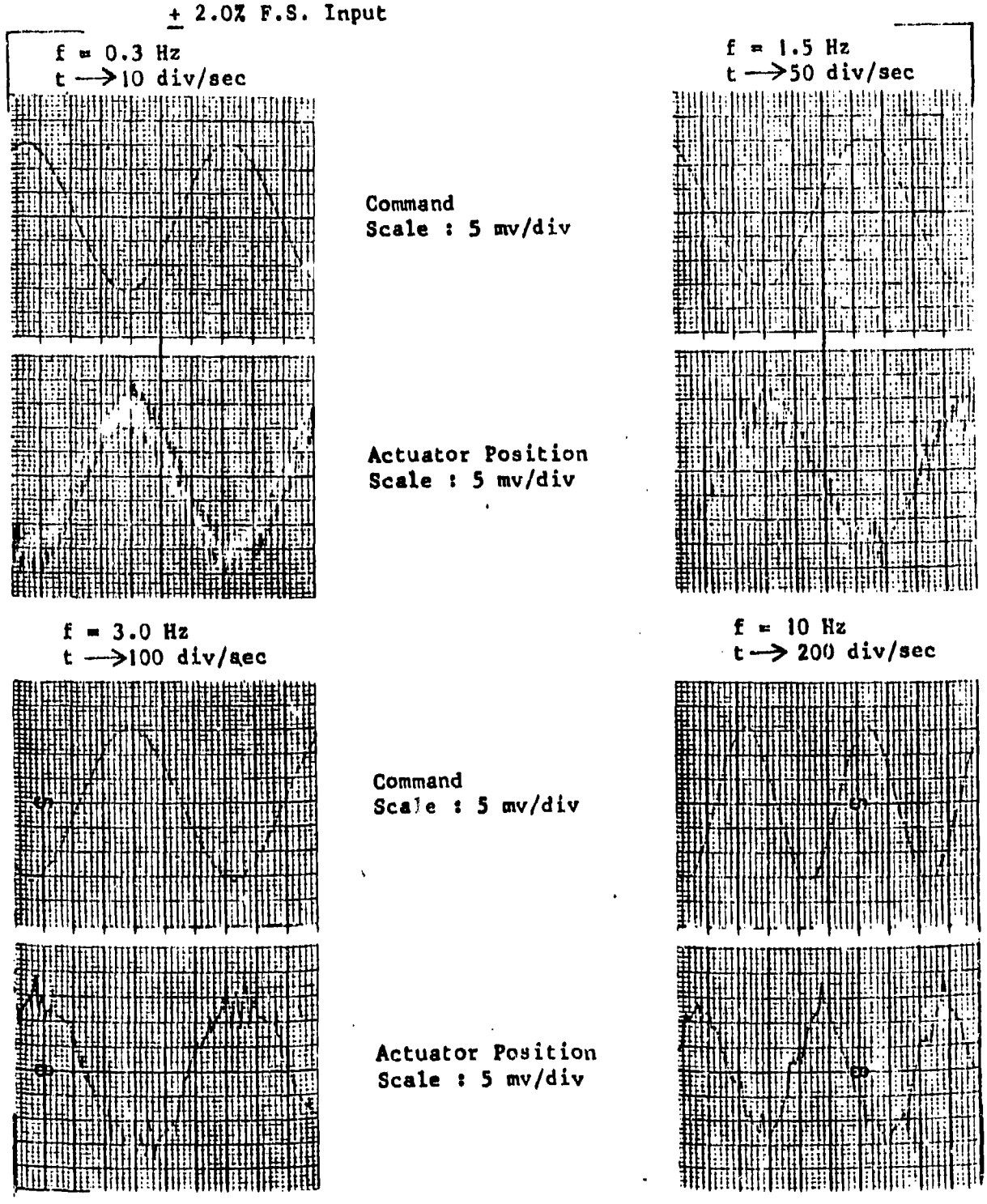

Figure II-49. Waveform characteristics - 2 percent - analog.

Microprocessor Control Evaluation

The basic test set up to evaluate the microprocessor-controlled, digital-servovalve-driven actuation system was the same as for the analog control evaluation. In the processor-controlled mode, the processor replaced every analog control function except the high-voltage PZ drivers and the modulation logic directly associated with the drivers. Variable control of the system update rate, gain, and threshold were provided on the processor control panel in the form of thumbwheel switches. To evaluate the effect of these parameters, eight configuration test cases were established.

The test cases with the associated parameters are listed in Table II-7. Case 1 was used as the base line and configured to closely matched the gain and threshold of the analog control system evaluated. Cases 2, 3, and 4 are variations in the update rate. Cases 5 and 6 are gain variations. Cases 7 and 8 are changes in the threshold level.

The overview description of each function test such as linearity, threshold, etc., discussed through the analog test results section are not repeated in the following discussion of the test results.

Table II-7. Test case identification list.

Case	Up-Date Rate	Gain	Threshold
1	1000/sec	25mv/step	15mv
2	100/sec	25mv/step	15mv
3	50/sec	25mv/step	15mv
4	25/sec	25mv/step	15mv
5	1000/sec	15mv/step	15mv
6	1000/sec	50mv/step	15mv
7	1000/sec	25mv/step	40mv
8	1000/sec	25mv/step	50mv

Linearity

The input-output linearity obtained from the system controlled with the microprocessor is shown in Figure II-50. This is the baseline setup, case 1, commanded at 100 percent full scale. Linearity deviation is not measurable on this plot and is determined basically by the feedback transducer's linearity. The resolution is barely noticeable on the 100-percent plot but is quite noticeable on the ± 5.0-percent full-scale input plot on Figure II-51. The output resolution is .015 inches or 0.37 percent of full scale. This is the result of the analog-to-digital (A/D) converter resolution and the preset threshold. The 12-bit convertor has a resolution of 4.9 millivolts based on 20 volts full scale and the set threshold is 15 millivolts. The plotted linearity correlates with the sum of the A/D converter resolution and set threshold.

Figures II-52 and II-53 are the 100 percent and 5 percent linearity plots run with the processor set up for case 3 (update rate = 50/sec). These plots indicate that the update rate has no effect on linearity or resolution. Since the linearity plots were recorded with .05 Hz triangular wave as the command, the rate of amplitude change was slow enough that a theoretical error of only 0.4 percent full scale would be incurred at the slowest update rate, case 4.

Static Threshold

The static threshold data recorded from the digital servoactuator under microprocessor control is shown in Figures II-54, II-55, and II-56. The variations are cases 1, 5, 6, 7, and 8. All of these cases show the static threshold to be between ± 3 and ± 4 millivolts. This includes cases 7 and 8 where the preset electrical threshold is 40 and 50 millivolts (see Table II-8). The explanation for this anomaly is found in the software of the microprocessor combined with a leak in one of the directional control valves. The leak allows the actuator to slowly drift until the threshold is overcome, then an opposing directional valve is triggered to drive the actuator back to just below threshold. The actuator will drift off to repeat the cycle. This action creates a constant offset in the forward loop error signal. The software assumes that the error is zero when the velocity is zero. When the system error is processed, first the polarity is determined, then the error level is checked as an absolute value against the look-up table created for gain and threshold.

Since any drift- or velocity-related offset will allow the loop error to sit at the electronic threshold level, any bipolar input will cause output motion. In this case, the 0.1 Hz command signal and the drift rate seem fairly well-matched. When driven with a dynamic signal as shown in the dynamic threshold testing, the 5 Hz signal has a much higher rate than the drift. The output signal will move off the set zero-point and center its amplitude about the command sum or real error signal.

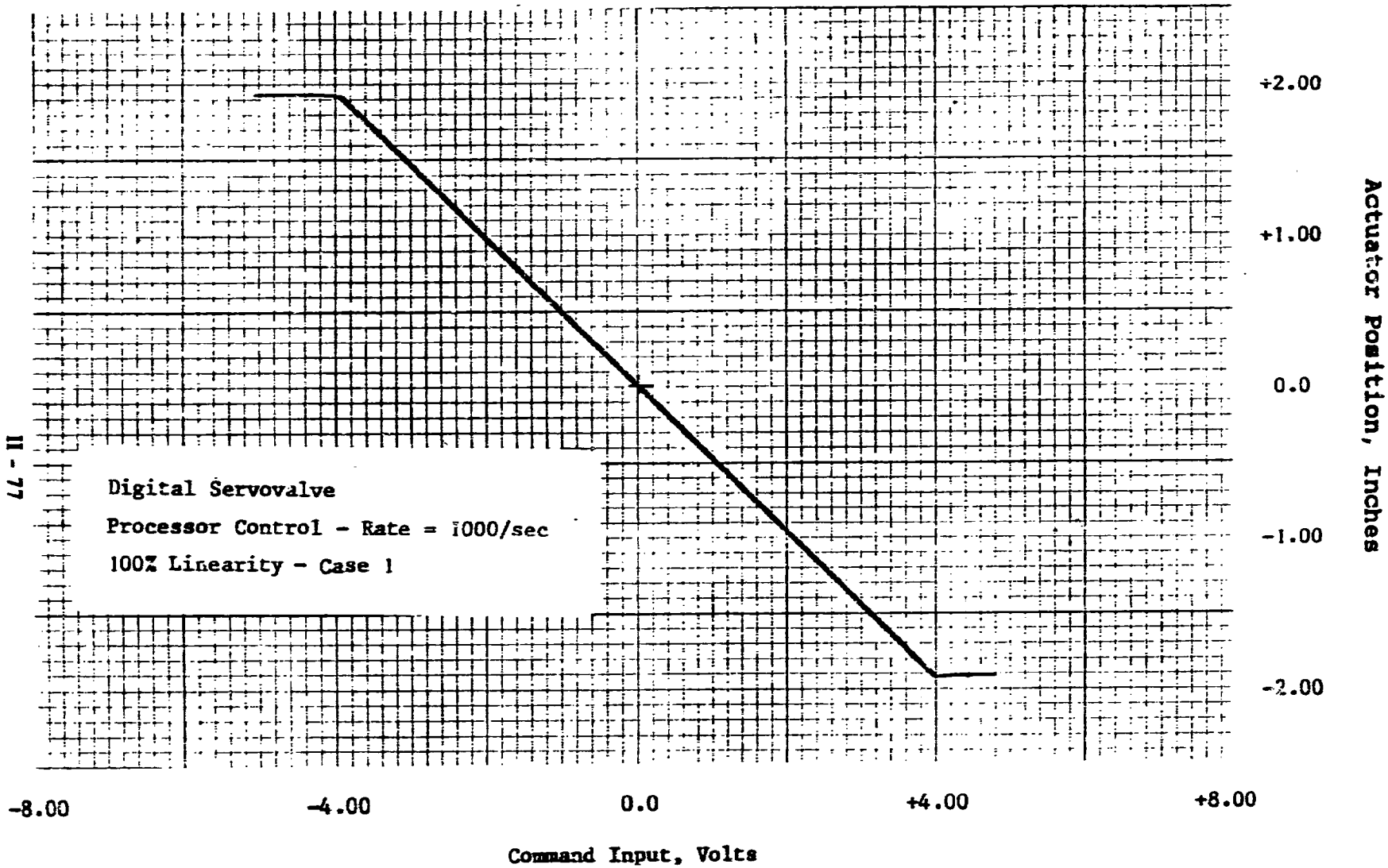

Figure II-50. Linearity - 100 percent - digital - case 1.

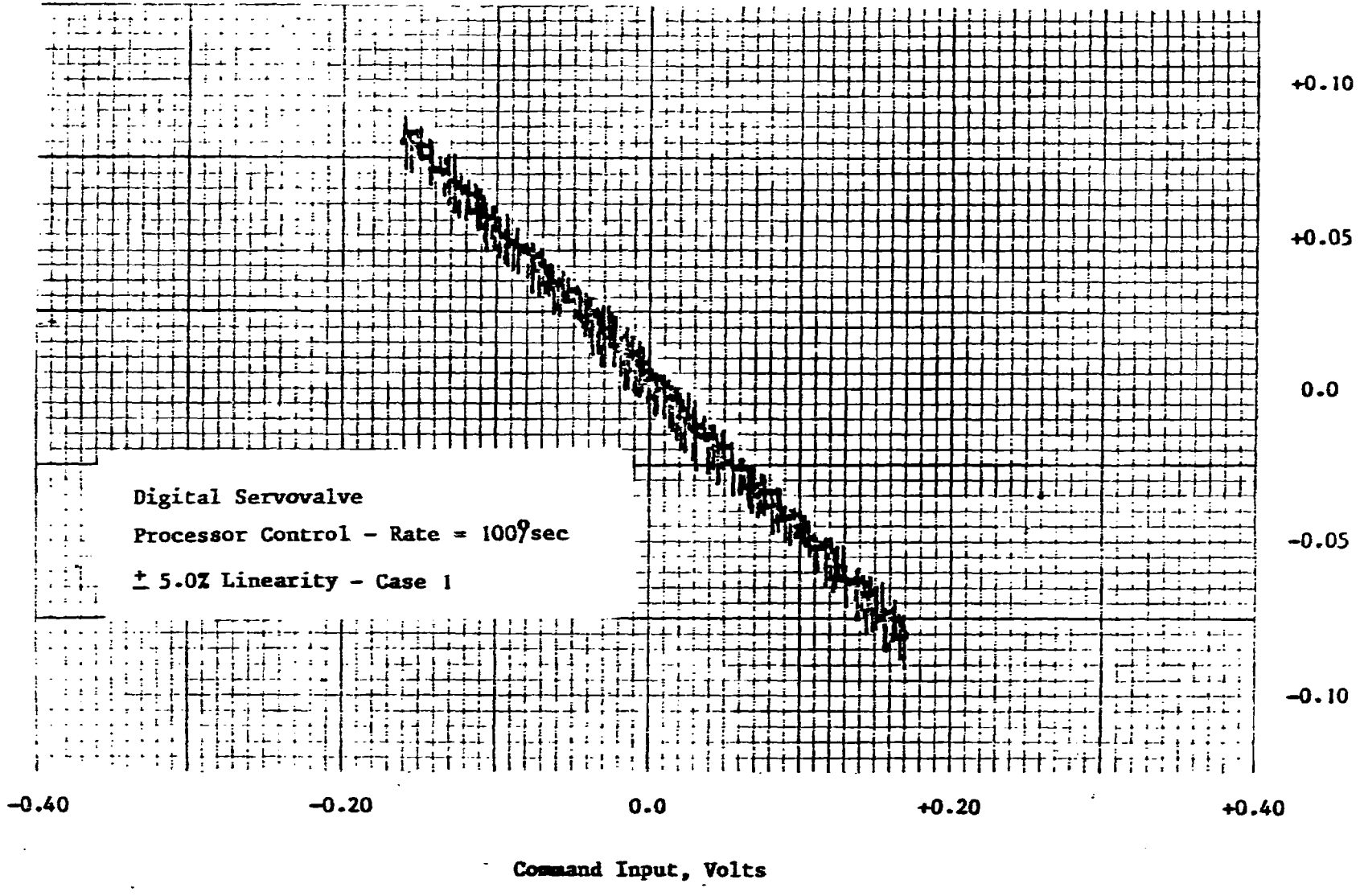

Figure II-51. Linearity - 5 percent - digital - case 1.

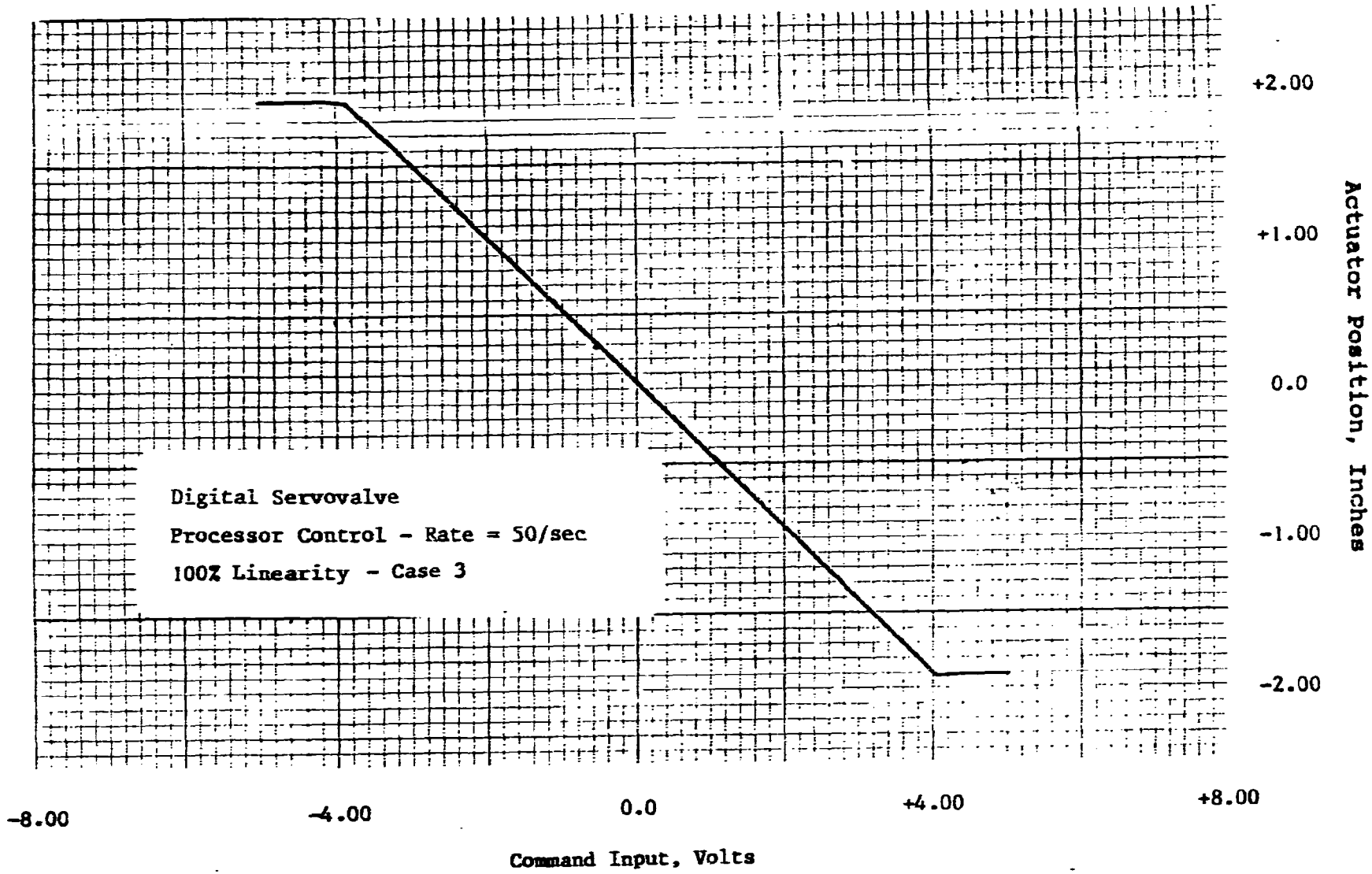

Figure II-52. Linearity - 100 percent - digital - case 3.

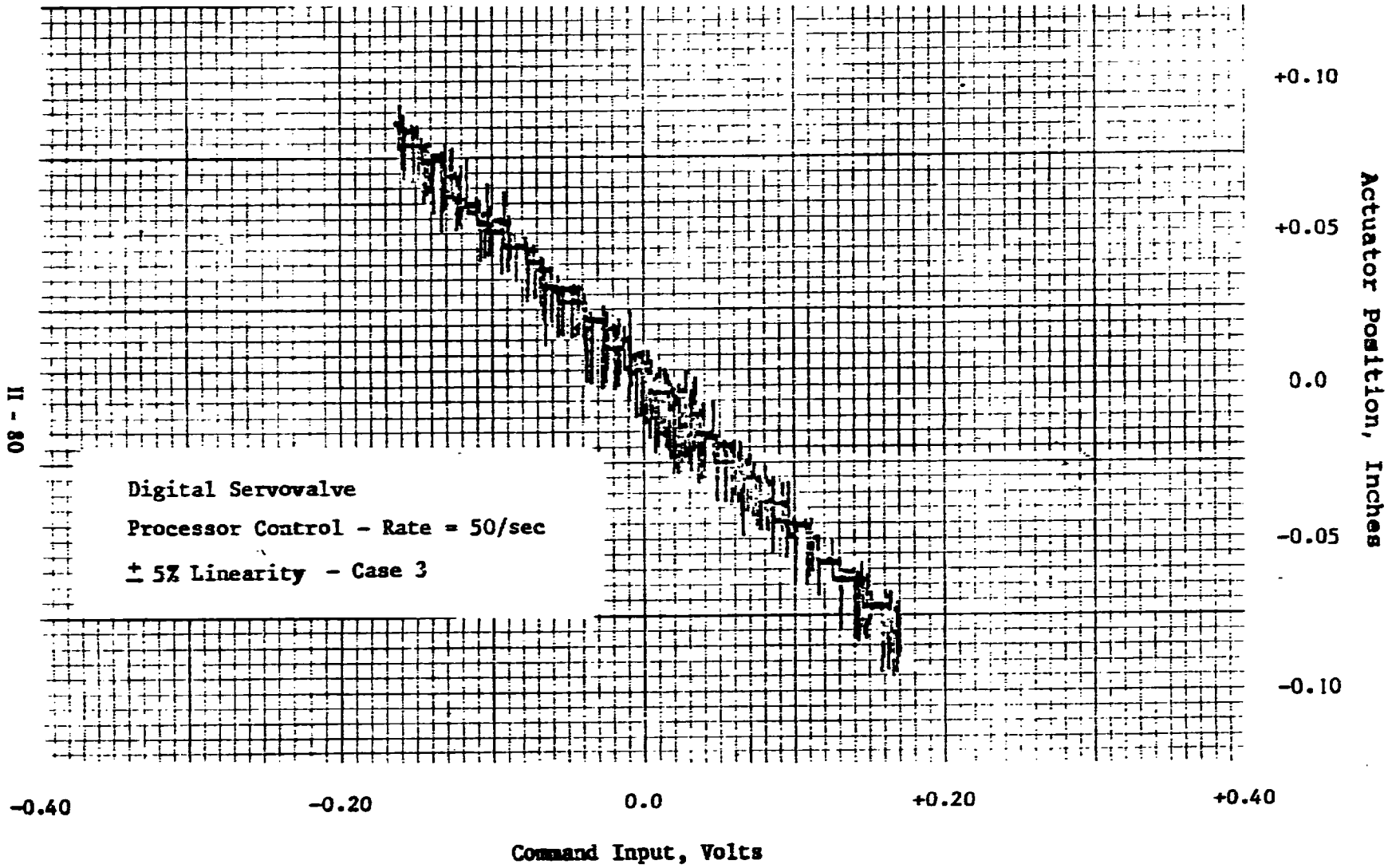

Figure II-53. Linearity - 5 percent - case 3.

Test Item - Dynamic Controls, Inc.
Digital Servovalve

Date Prepared: 5-Dec-86

Test - Static Threshold - Processor Control
.10 Hz Triangle Wave Input

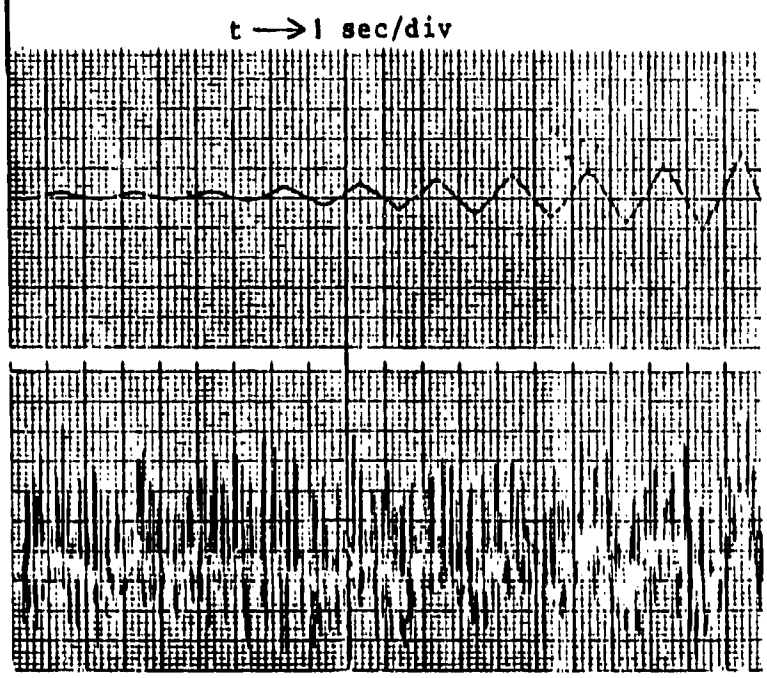

Case 1

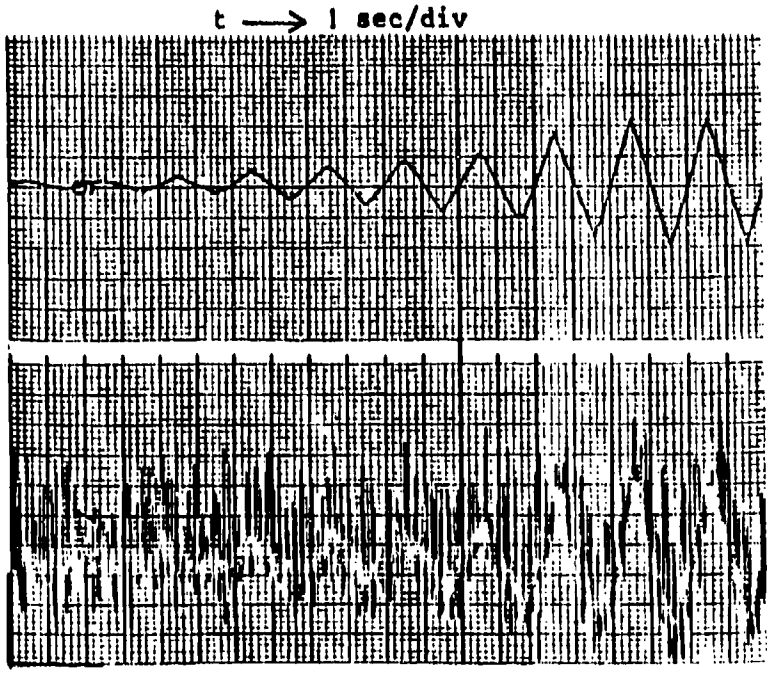

Case 5

Figure II-54. Static threshold - cases 1 and 5.

Test Item - Dynamic Controls, Inc.
Digital Servovalve

Date Prepared: 5-Dec-86

Test - Static Threshold - Processor Control
.10 Hz Triangle Wave Input

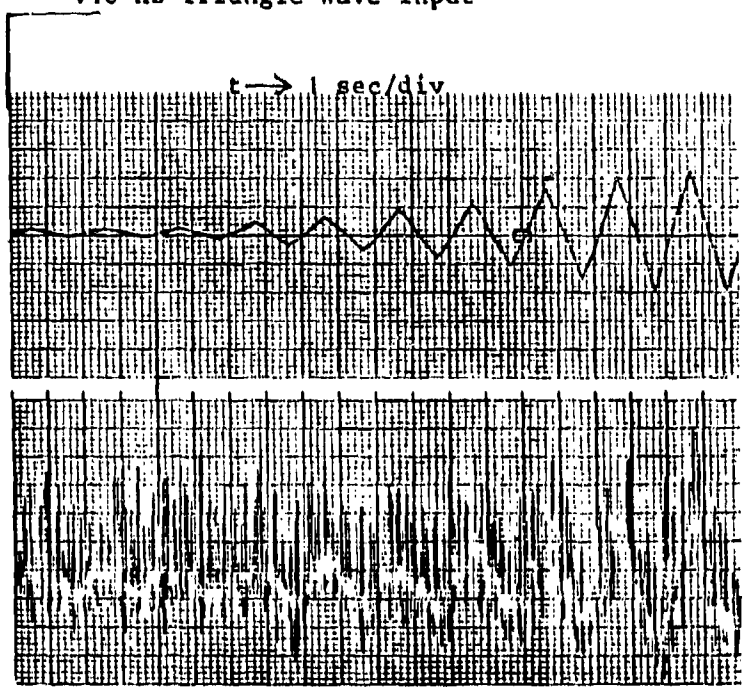

Case 6

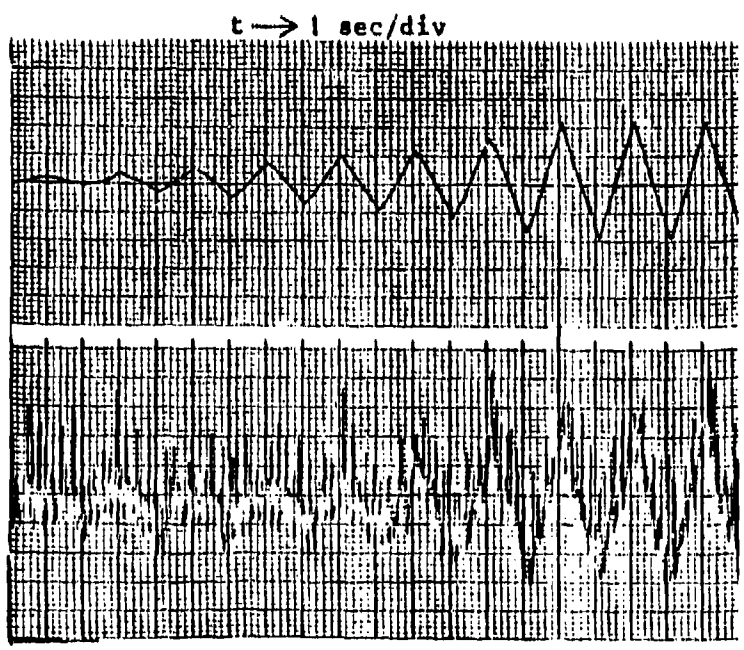

Case 7

Figure II-55. Static threshold - cases 6 and 7.

Test Item - Dynamic Controls, Inc.
Digital Servovalve

Date Prepared: 5-Dec-86

Test - Static Threshold - Processor Control
.10 Hz Triangle Wave Input

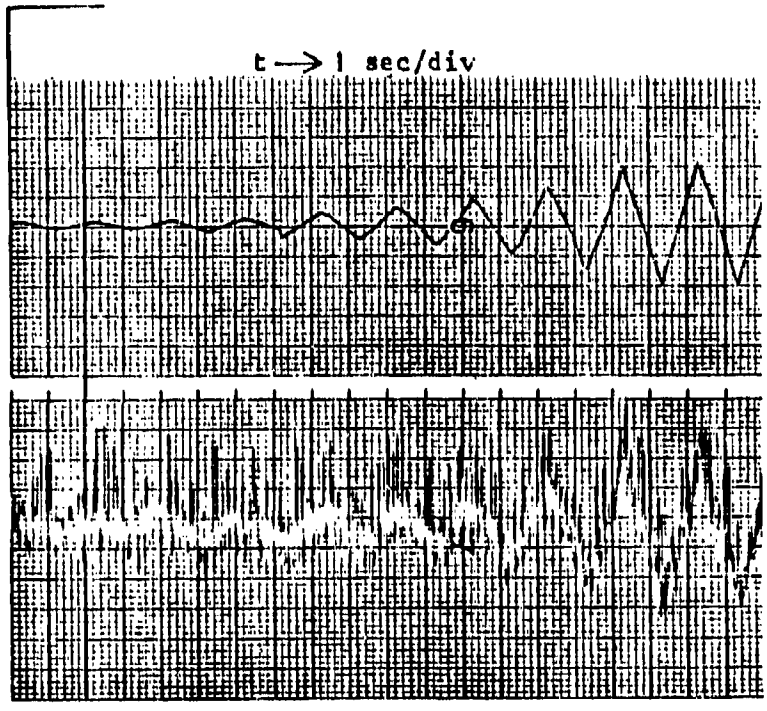

Case 8

Figure II-56. Static threshold - case 8.

Dynamic Threshold

The dynamic threshold was measured using a 5-Hz sine wave input with its amplitude slowly increasing from a minimum value until the output resembled the input. Figures II-57, II-58, and II-59 are the dynamic threshold measurements with the microprocessor set up for cases 1, 5, 6, 7 and 8. Cases 1, 5, and 6 are set up with respective gains of 25, 15 and 50 millivolts per gain step. For each of these cases, the dynamic threshold is measured to be ± 4.0 millivolts or ± 0.1 percent of full scale. The processor-set threshold was ± 15 millivolts. Signal noise accounts for the lower measured threshold value. The change in gain is difficult to notice at this low amplitude input where the signal to noise ratio is unfavorable. However, if the ascending slope of the actuator position is carefully examined, slope changes which are proportional to the set gain can be observed. Case 7 (Figure II-58) had a set threshold of ± 40 millivolts and a measured value of ± 30 millivolts or 0.8 percent full scale. Increasing the set threshold to ± 50 millivolts for case 8, shown in Figure II-59, has a measured value of ± 42 millivolts or 1.1-percent full-scale dynamic threshold.

Step Response

The step response was recorded with a 2.5-percent full-scale square-wave input at 1.0 Hz. The data displayed in Figures II-60 and II-61 was recorded for all of the preset processor test cases 1 through 8. Figure II-60 represents sample times of 1, 10, 20, and 40 milliseconds for cases 1, 2, 3 and 4, respectively. Little difference is detected between cases 1 and 2 where desirable stable response is observed. The sample-rate time delay can be measured for cases 3 and 4 at 20 and 40 milliseconds after the input is applied. Case 4 indicates a 7-percent overshoot at this input level creating the effect of an under-dampened control system. This is typical of a sampled (digital-controlled) control system when the sample rate approaches the system's frequency response.

The effect of loop gain changes are depicted in cases 5 and 6 on Figure II-61. The measured time for the output to reach its final value is 60 milliseconds for the highest gain of case 5, 140 milliseconds for the lowest gain in case 6, and 80 milliseconds for the baseline case 1. The differences in the system damping is apparent when the roundness of the output step corner is observed as it approaches its final value.

Saturation Velocity

The saturation velocity recording in Figure II-62 was obtained by applying ± 10 volt steps to provide full stop-to-stop excursions of the control actuator. The rate for the extend (negative) direction is 1.29 inches per second; for the retract (positive) direction, 1.05 inches per second. As in the analog

Test Item - Dynamic Controls, Inc.
Digital Servovalve

Date Prepared: 5-Dec-86

Test - Dynamic Threshold - Processor Control
5.0 Hz Sine Wave Input

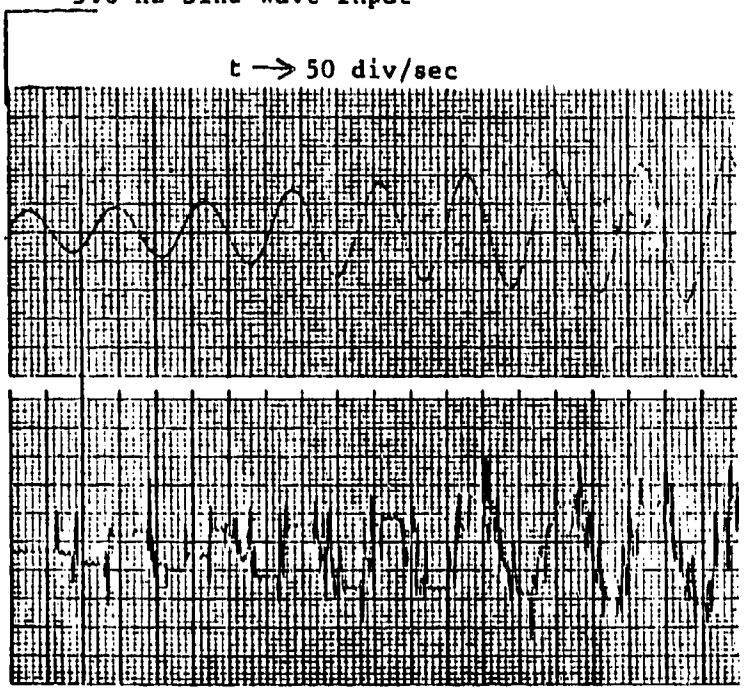

Command
Scale : 2.0 mv/div

Actuator Position
Scale : 2.0 mv/div

Case 1

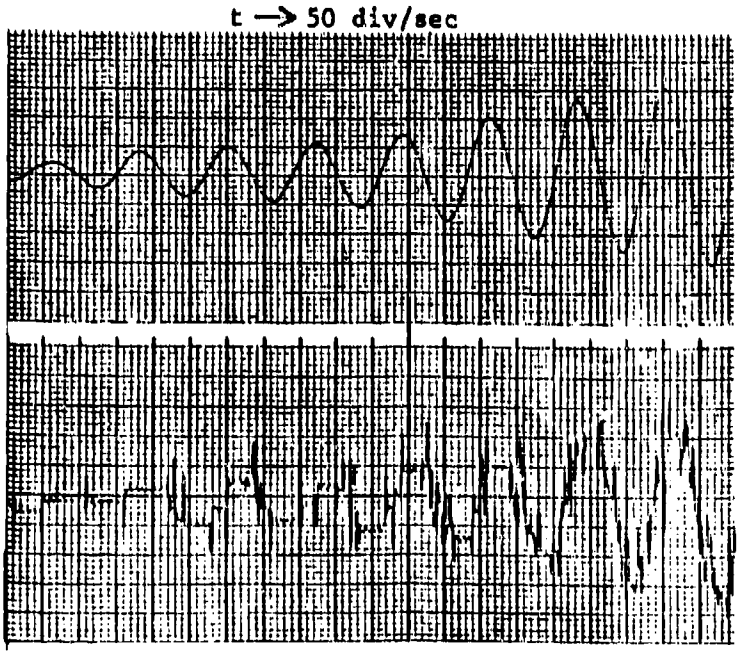

Command
Scale : 2.0 mv/div

Actuator Position
Scale : 2.0 mv/div

Case 5

Figure II-57. Dynamic threshold - cases 1 and 5.

Test Item - Dynamic Controls, Inc.
Digital Servovalve

Date Prepared: 5-Dec-86

Test - Dynamic Threshold - Processor Control
5.0 Hz Sine Wave Input

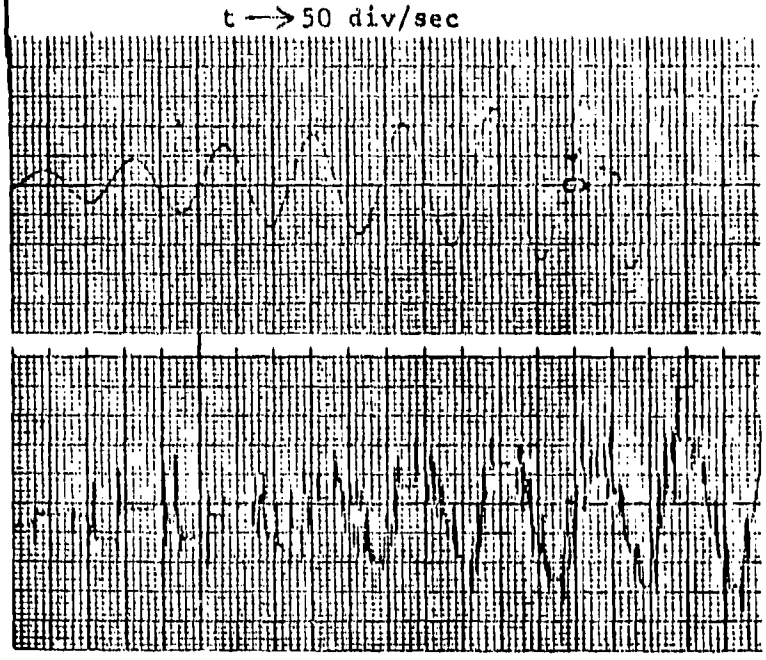

Command
Scale : 2.0 mv/div

Actuator Position
Scale : 2.0 mv/div

Case 6

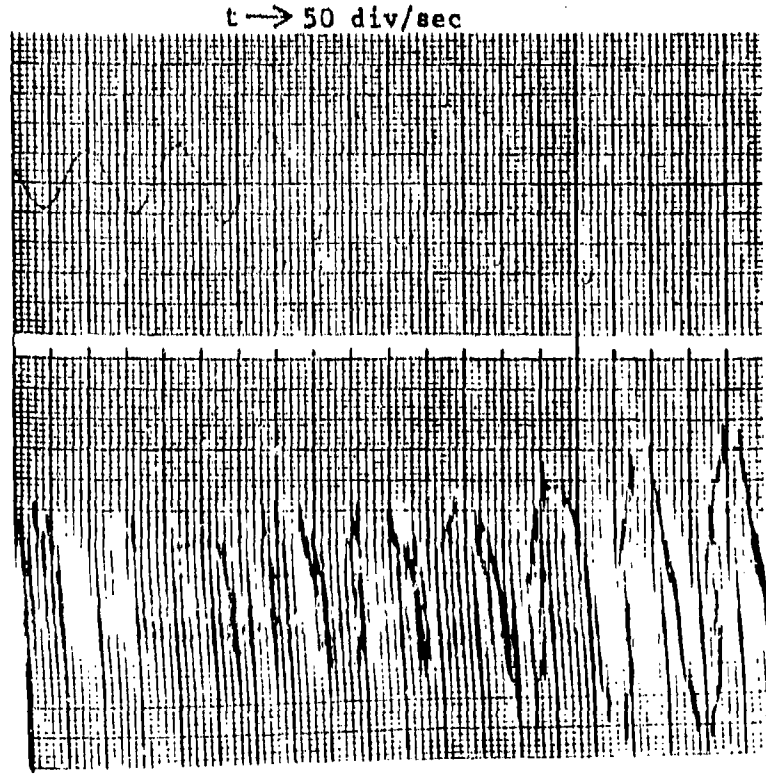

Command
Scale : 5.0 mv/div

Actuator Position
Scale : 5.0 mv/div

Case 7

Figure II-58. Dynamic threshold - case 6 and 7.

TEST DATA

Test Item - Dynamic Controls, Inc.
Digital Servovalve

Date Prepared: 5-Dec-86

Test - Dynamic Threshold - Processor Control
5.0 Hz Sine Wave Input

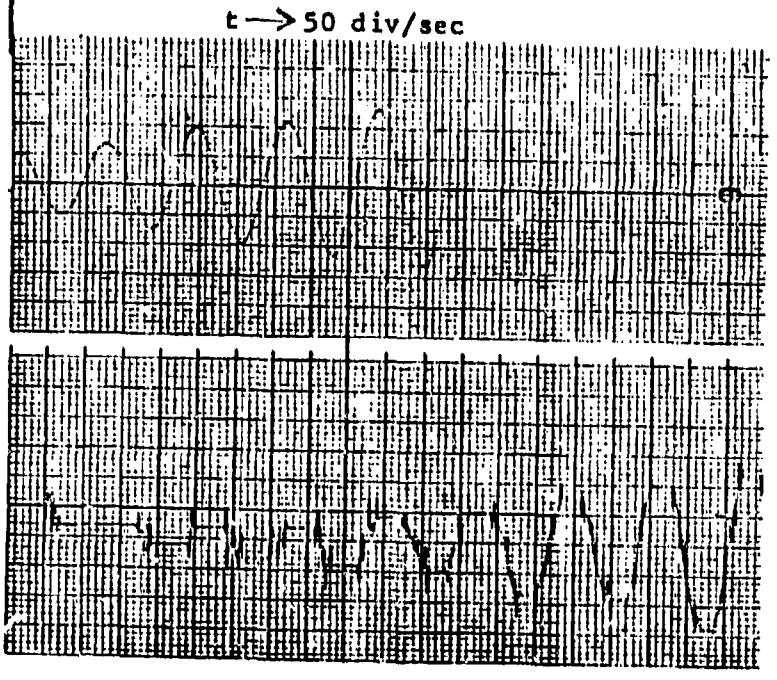

Command
Scale : 5.0 mv/div

Actuator Position
Scale : 5.0 mv/div

Case 8

Figure II-59. Dynamic threshold - case 8.

Test Item - Dynamic Controls, Inc.
Digital Servovalve

Date Prepared: 5-Dec-86

Test - Step Response - Processor Control
± 2.5% F.S. Input Step @ 1.0 Hz

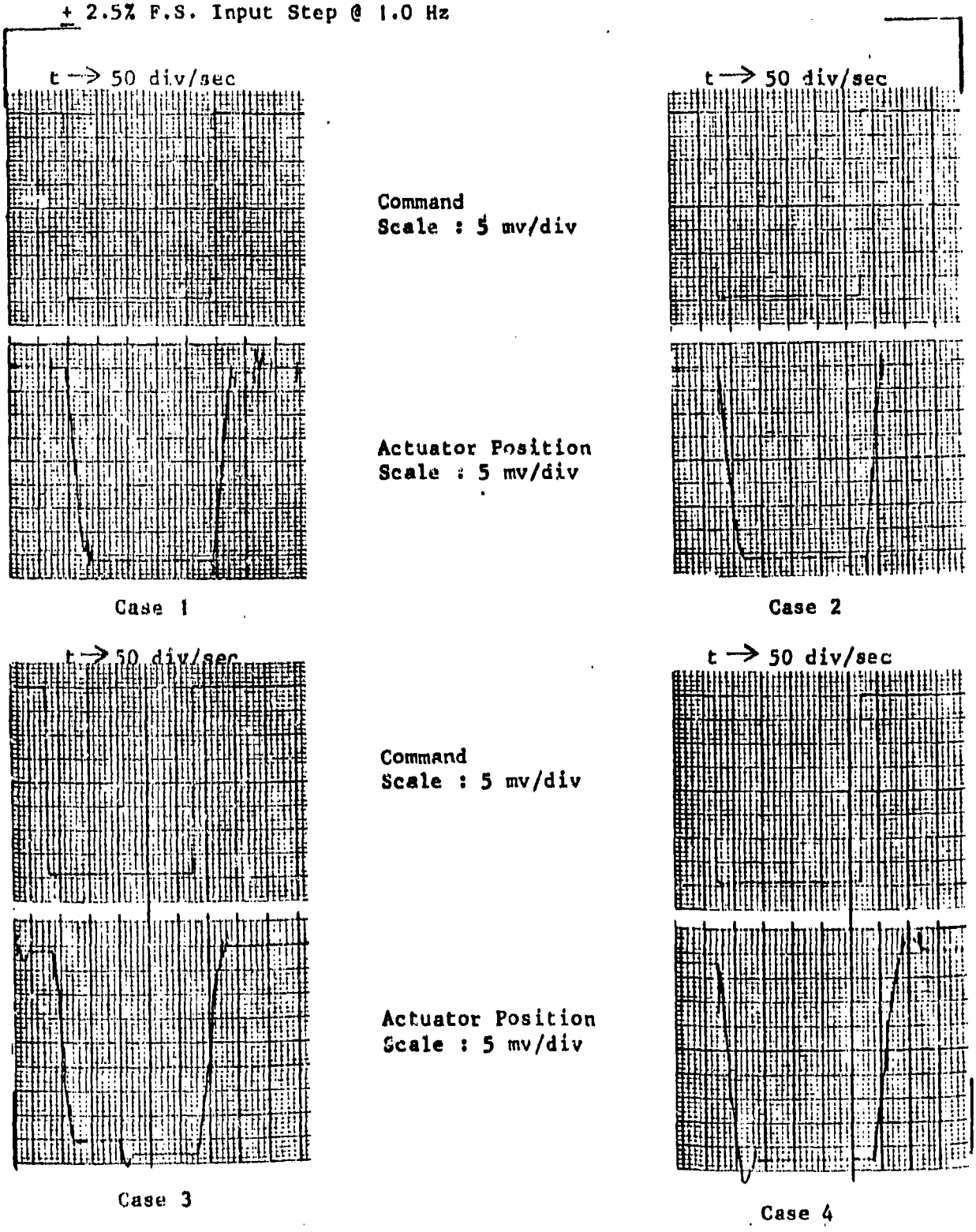

Figure II-60. Step response - cases 1 through 4.

Test Item - Dynamic Controls, Inc.
Digital Servovalve

Date Prepared: 5-Dec-86

Test - Step Response - Processor Control
± 2.5% F.S. Input Step @ 1.0 Hz

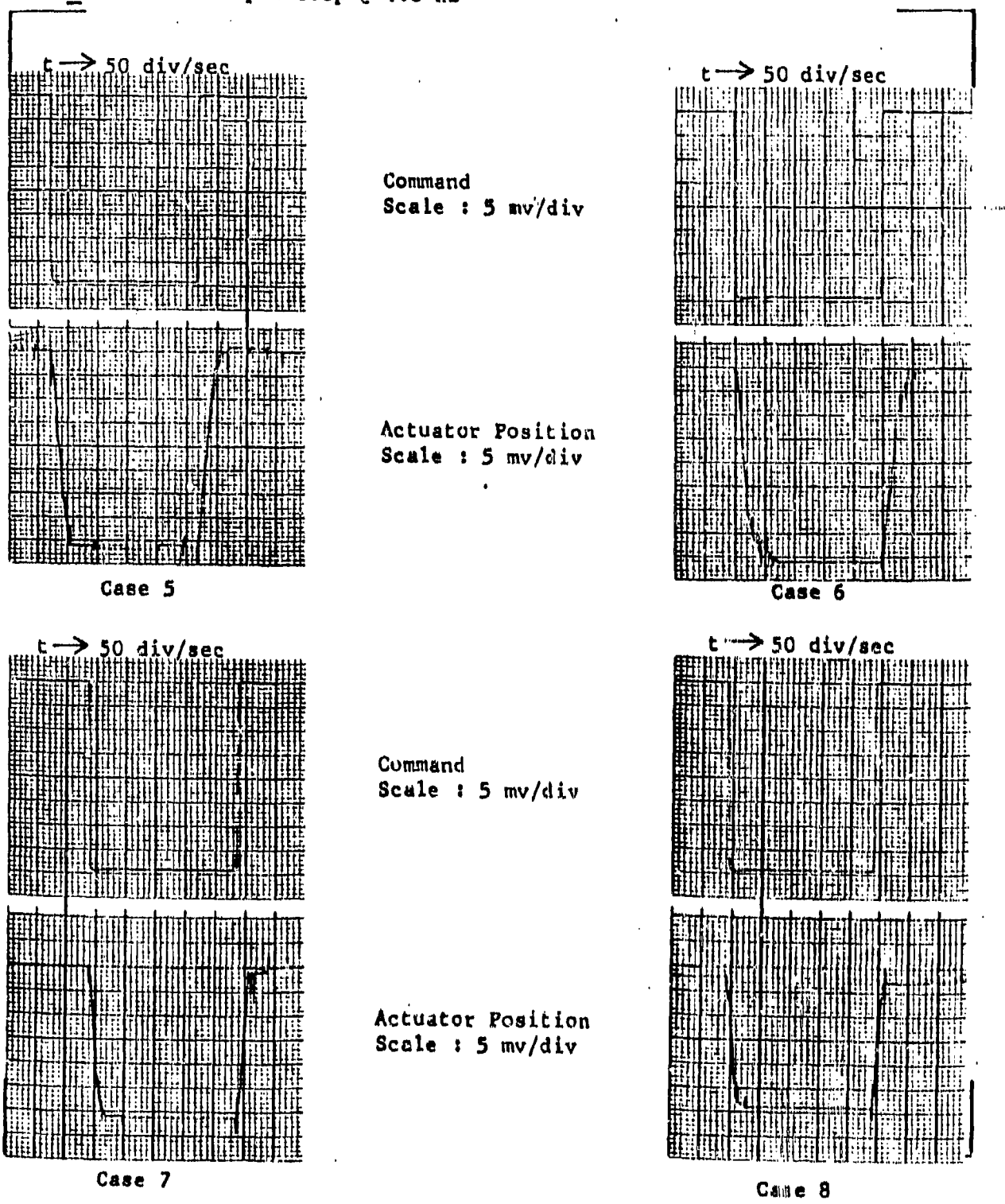

Figure II-61. Step response - cases 5 through 8.

TEST DATA

Test Item - Dynamic Controls, Inc.
Digital Servovalve

Date Prepared: 5-Dec-86

Test - Saturation Velocity - Processor Control
± 10.0 v Step Input - Case 1

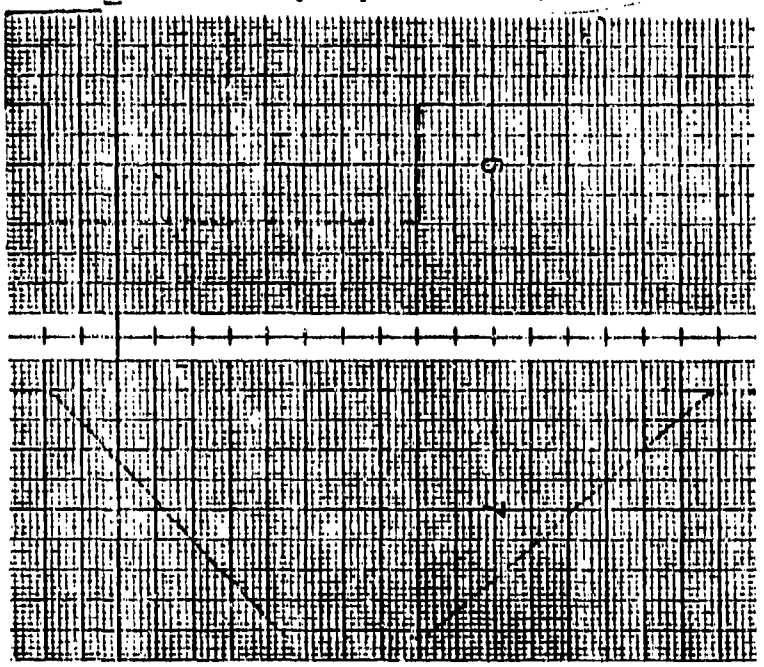

Figure II-62. Saturation velocity - digital.

Frequency Response

The frequency response of the digital servovalve/actuator system having the loop closed with the microprocessor was measured with a Hewlett-Packard signal analyzer. As with the response data obtained when the system had analog control, the very low-frequency amplitude and phase response is erroneous and can be ignored. The high signal-to-noise ratio accounts for some of that problem as well as limiting the lowest amplitude to 5 percent of full scale to obtain a meaningful plot.

Figure II-63 (the 10-percent full-scale frequency response plot recorded with the processor set up at the baseline case 1) shows that velocity saturation is occurring at about 2 Hz and that by 5 Hz, the log magnitude slope is a predictable -20 db per decade. The phase plot shows a phase shift of -135° at 16 Hz, greater than the -90° the analog control did at the same input amplitude and frequency. This indicates that adding processor control produces a higher-order control system, even when the system is being updated at 100 times the frequency of interest, which is 10 Hz.

The ± 5-percent full-scale frequency response with the baseline (case 1) is shown in Figure II-64. The -3 db and -45° phase shift occurs at 5.5 Hz which is typical of a first-order system when these two points agree. The 90° phase lag point occurs at 16 Hz. Overall, the response for case 7 shows good performance and stability.

Figures II-65, II-65, and II-67 represent the effect of slower sample rates at the 5-percent input level recorded with the processor set at cases 2, 3, and 4. Case 2 is 100 samples per second, case 3 is 50 samples per second, and case 4 is 25 samples per second. The time delay contributed by the processor is the reciprocal of the sample rate. Therefore, 1/100 = .01 seconds, 1/50 = .02 seconds, and 1/25 = .04 seconds would be the equivalent processor delay times. Table II-8 lists the frequencies at which the -3 db, -6 db, -45° and -90° points were measured for cases 1, 2, 3 and 4.

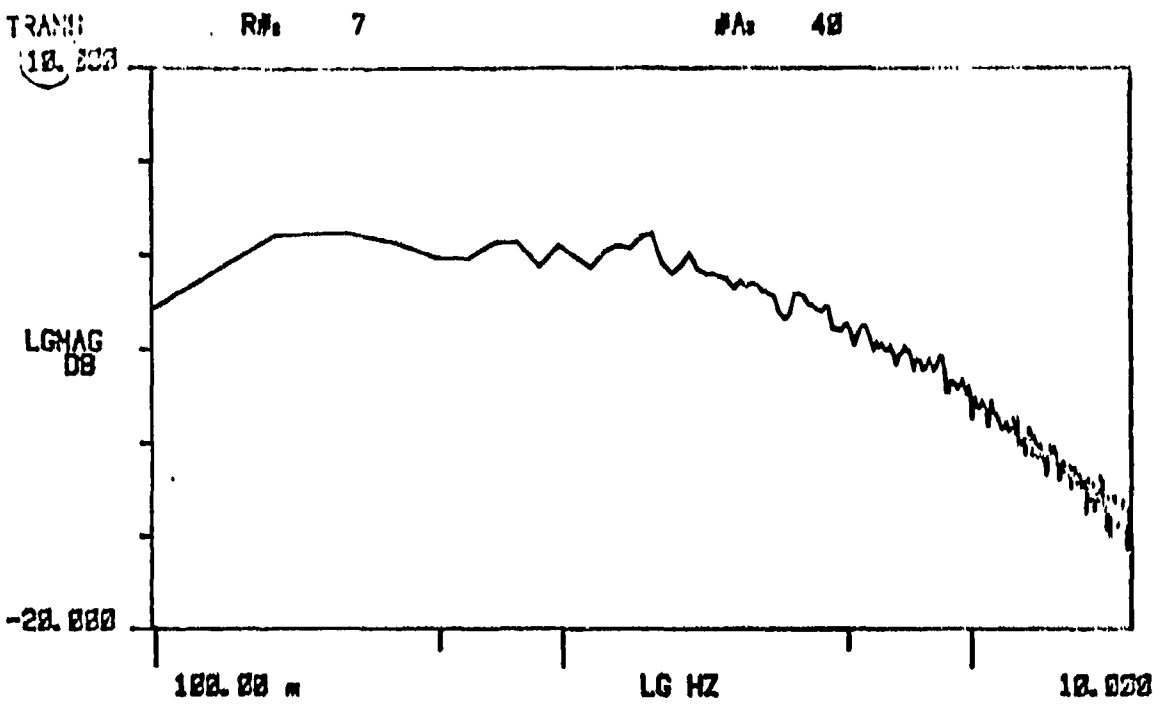

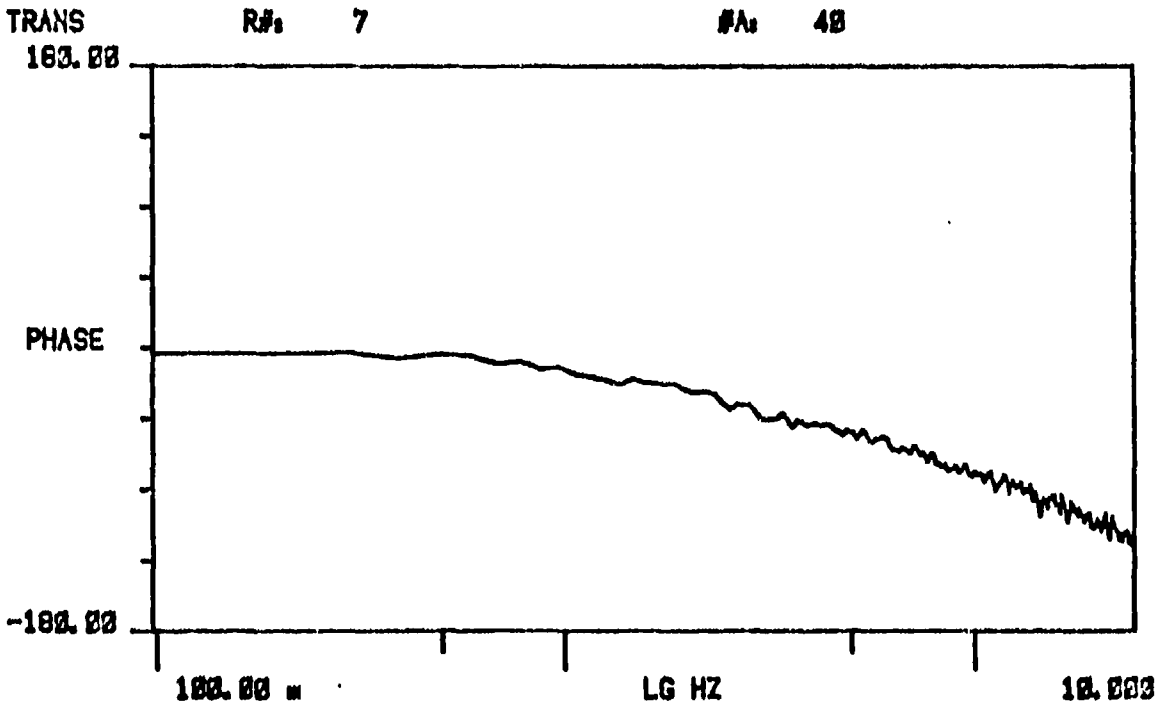

0 Db Input: ± 0.4 volts
Control Mode: Processor - Case 1

Figure II-63. Frequency response - ± 10 percent - case 1.

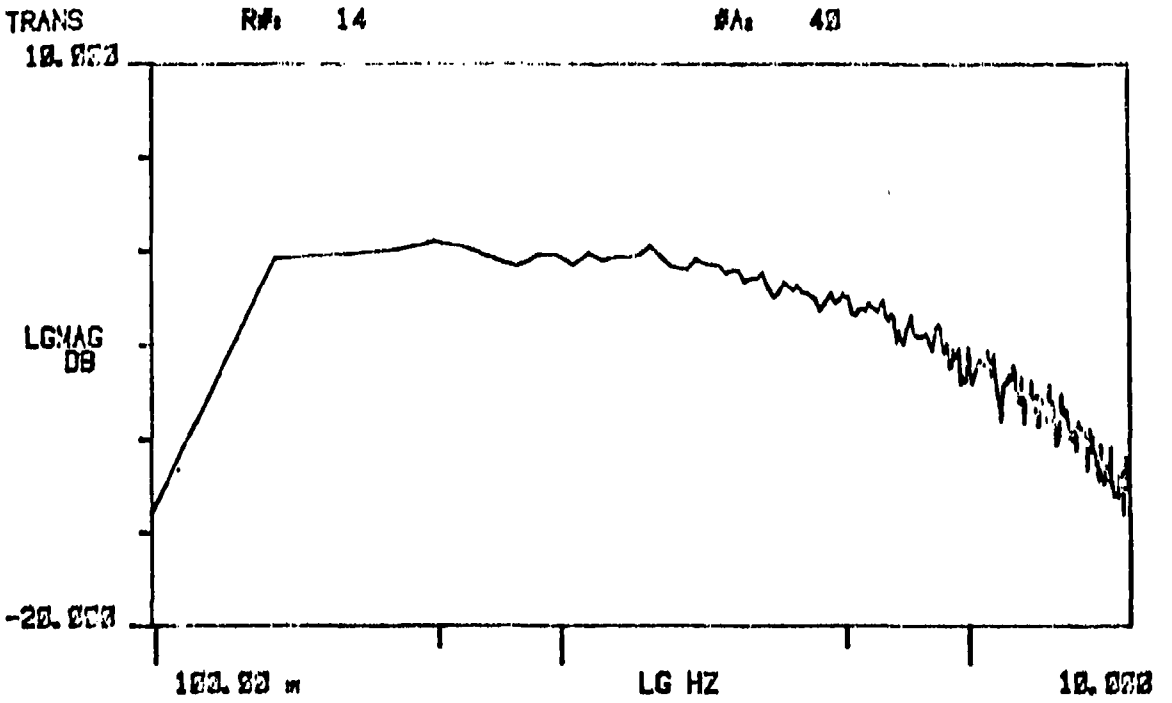

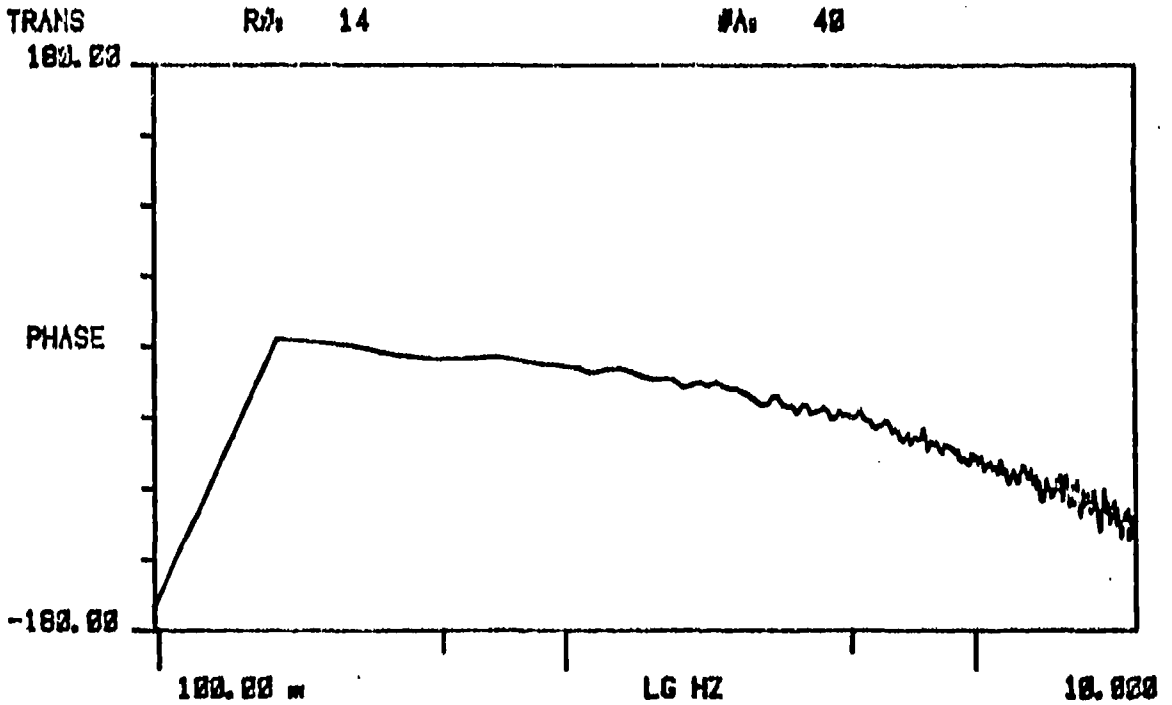

0 Db Input: ± 0.2 volts
Control Mode: Processor - Case 1

Figure II-64. Frequency response - ± 5 percent - case 1.

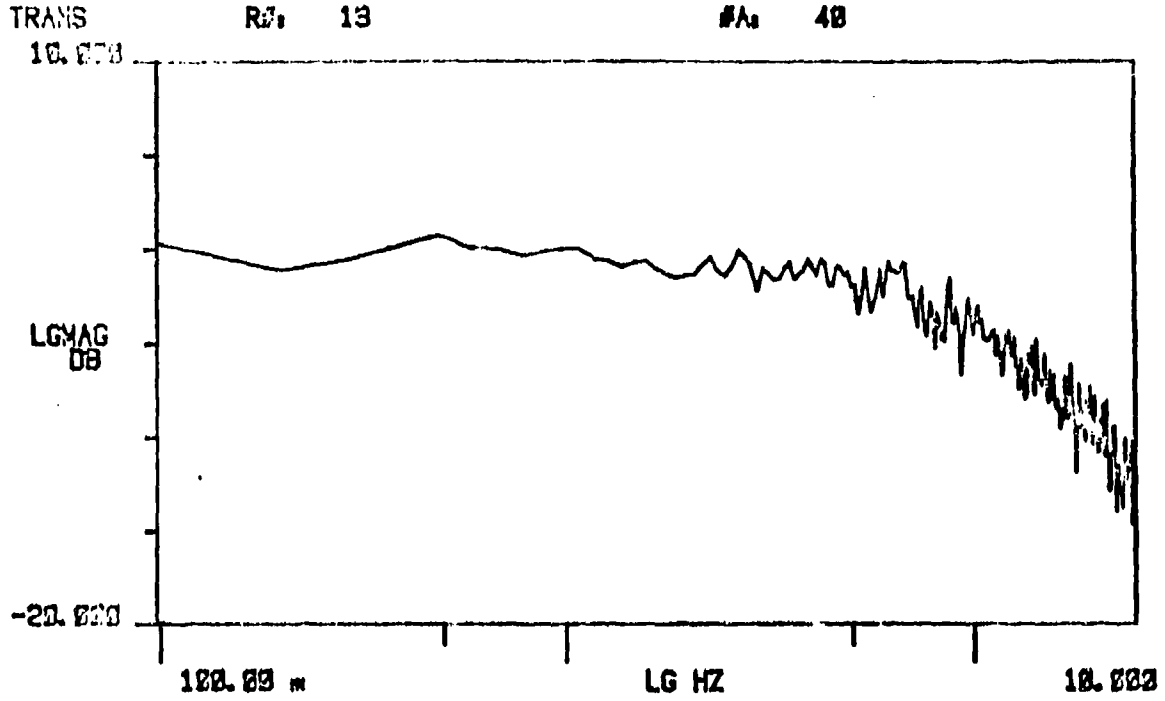

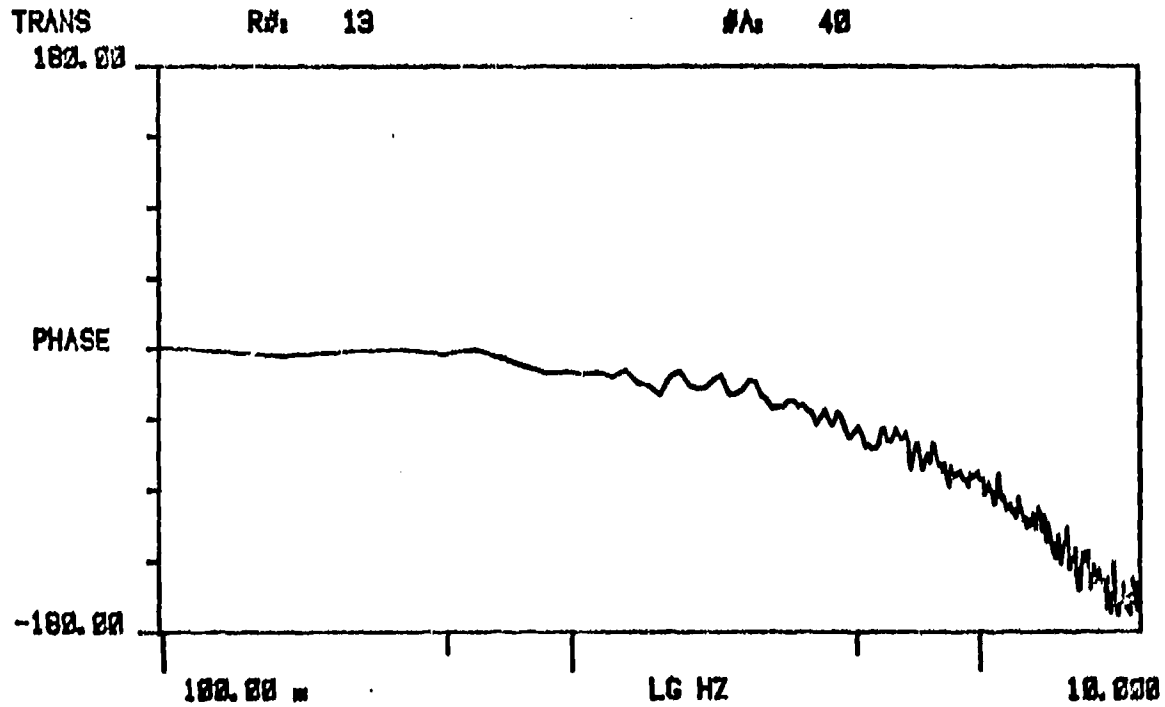

0 Db Input: ± 0.2 volts
Control Mode: Processor - Case 2

Figure II-65. Frequency response - ± 5 percent - case 2.

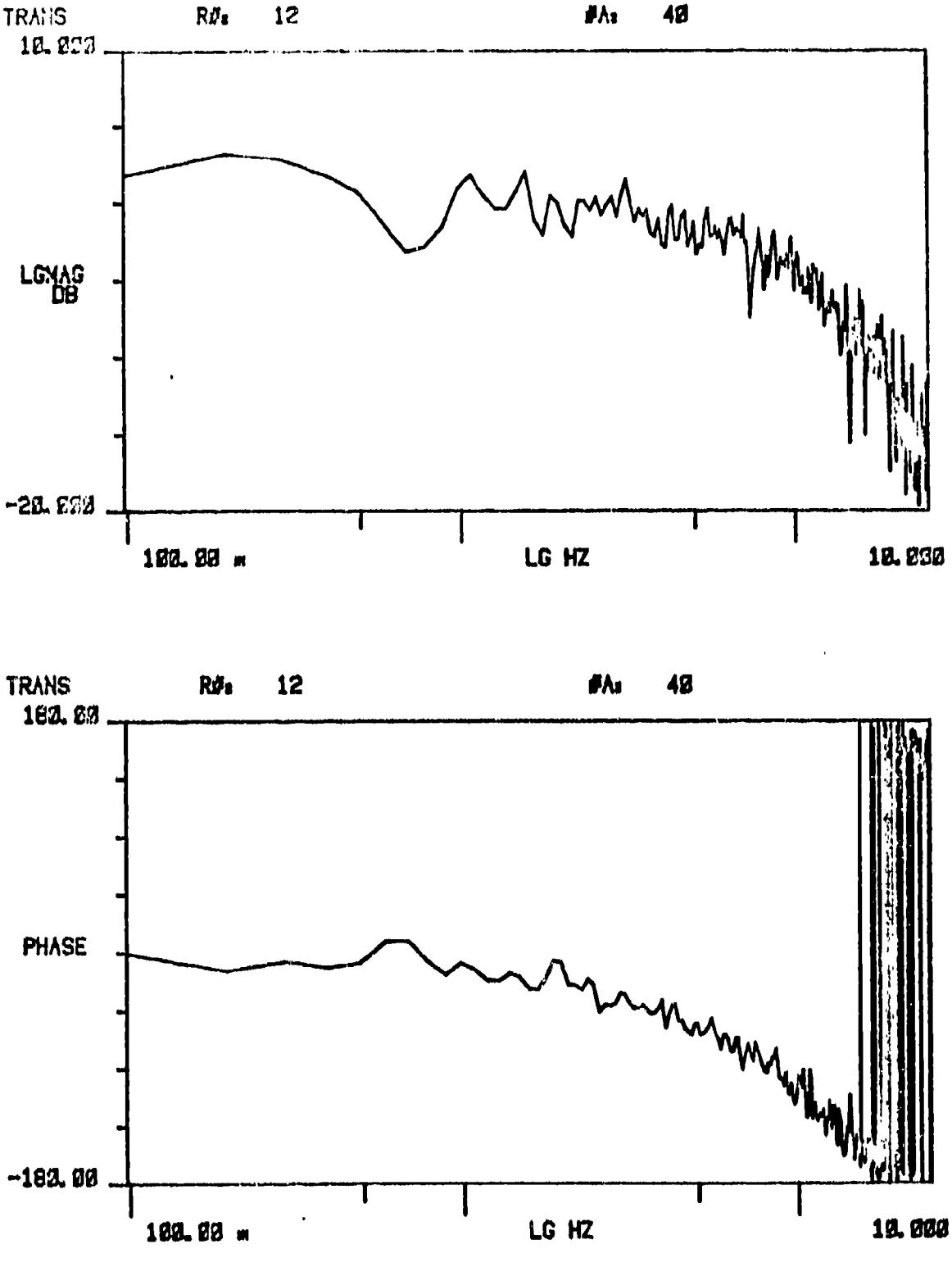

0 Db Input: ± 0.2 volts
Control Mode: Processor - Case 3

Figure II-66. Frequency response - ± 5 percent - case 3.

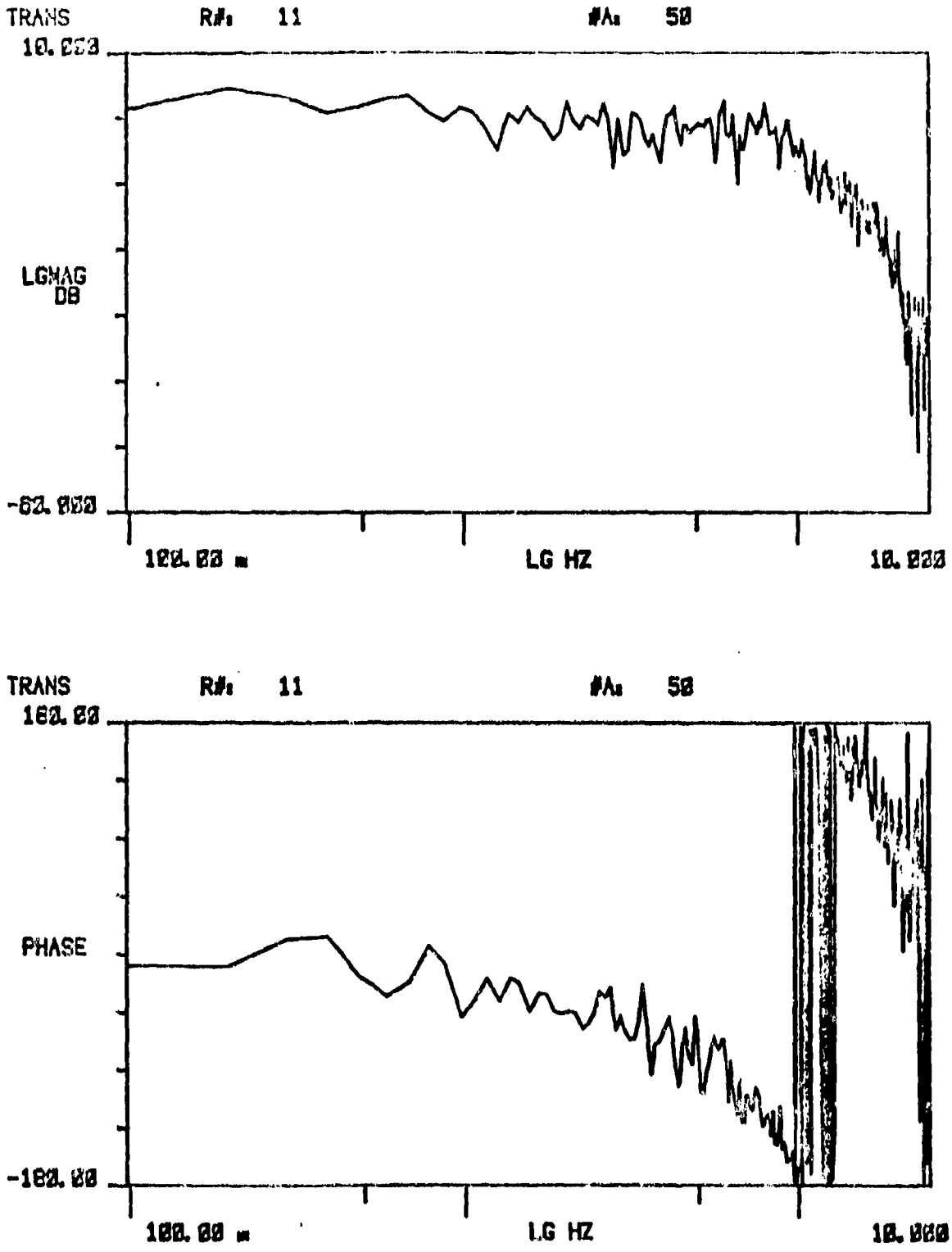

0 Db Input: ± 0.2 volts
Control Mode: Processor - Case 4

Figure II-67. Frequency response - ± 5 percent - case 4.

Table II-8. Tabulation of frequency response measurement.

	Case Numbers			
	1	2	3	4
-3db, Hz	5.5	8.0	8.0	8.5
-6db, Hz	10.4	13.5	12.0	10.5
-45°, Hz	5.5	4.5	4.0	2.5
-90°, Hz	16.0	11.0	8.5	6.0

As indicated by the tabulated response data, when the sample rate is decreased, the -3 db point frequency increases and the -90° phase shift frequency shows a significant decrease. The plots for cases 3 and 4 (Figures II-66 and II-67) show the phase shift exceeding 180°. The frequency response for case 4 also indicates the amplitude ratio holding near the 0 db level longer and the phase rolling off at a lower frequency than the other cases. Normally, the combination of extended amplitude ratio with increased phase angle would produce peaking of the amplitude. It does not peak in this case because the system is operating at velocity saturation. The phase lag is typical of the time delay effect on a control system because of the sampling rate. The case 4 frequency response plot is characteristic of signal aliasing. The low damping effect is consistent with the step response data recorded with the slowest sampling rate.

Waveform Characteristics

The output waveform of the control system was recorded to provide an indication of the system's signal distortion. The output was recorded with input levels of 10 percent, 5 percent, and 2 percent

at frequencies of 0.3 Hz, 1.5 Hz, 3.0 Hz, and 10.0 Hz. All of these amplitudes and frequencies were first recorded with the microprocessor set for case 1 as baseline.

The 10-percent full-scale input (Figure II-68) indicates that there is good output signal fidelity at 0.3 Hz. Velocity saturation becomes prevalent at 1.5 Hz where the waveform is triangular.

The 5-percent full-scale input (Figure II-69) shows the input signal being followed with low distortion out to the 3.0-Hz input frequency. Some effects of velocity saturation can be observed at this frequency. At the 10-Hz input, the signal triangulates and indicates a 90° phase lag. The small amplitude output signal perturbations were determined to be signal noise, not actuator motion. Velocity steps can be observed at the 10-Hz output frequency recording.

Figure II-70 is the input of 2.0 percent of full scale, the lowest amplitude input recorded. As with the 5-percent recording, the output signal follows the input with low distortion. One aspect of the system that is recognized on the 3-Hz recording is the difference between the ascending and descending slope. This is caused by a difference in the extend and retract flow gain. The preset threshold at this lower input amplitude is noticeable at the 0.3-Hz and 1.5-Hz input frequencies. The actuator position plot shows desirable tracking with noticeable flow-switching points.

Variations of update rate, gain, and threshold were introduced into the control system when the input signal was a 5-percent full-scale sine wave at 1.5 Hz. This input amplitude was selected because the baseline recording indicates good fidelity. It also was within the dynamic response envelope and an amplitude greater than the baseline threshold.

The time-history recordings in Figure II-71 are the result of update variations when preset for case 2 (100/sec), case 3 (50/sec) and case 4 (25/sec). The case 2 actuator-position signal follows the input command in the same manner as the baseline case 1 testing. When the update rate is reduced, significant signal distortion can be observed as in the case 4 data recording. The signal-to-update-rate ratio for this case is still 16:1. Further reduction of this ratio introduces more output distortion.

The result of loop gain variations when changed to case 5 (where the gain is equal to 15 millivolts per step) and case 6 (where the gain is equal to 50 millivolts per step) are not presented. The highest gain waveform characteristics (case 5) are similar to the baseline data of case 1. The recorded low gain waveform of case 6 implied velocity saturation occurred. This is actually a situation where the full valve flow is not being commanded. The seven flow steps at 50 millivolts each plus the 15 millivolts threshold will total 350 millivolts. The command input voltage for 5-percent full scale is 200

Test Item - Dynamic Controls, Inc.
Digital Servovalve

Date Prepared: 1 Dec 86

Test - Waveform Characteristics - Processor Control
± 10% F.S. Input - Case 1

f = 0.3 Hz
t → 10 div/sec

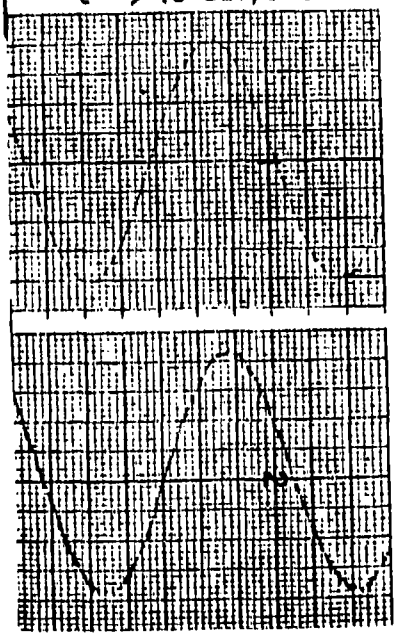

Command
Scale : 20 mv/div

Actuator Position
Scale : 20 mv/div

f = 1.5 Hz
t → 50 div/sec

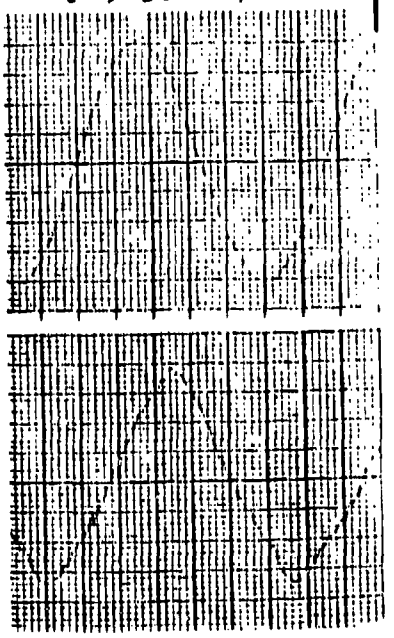

f = 3.0 Hz
t → 100 div/sec

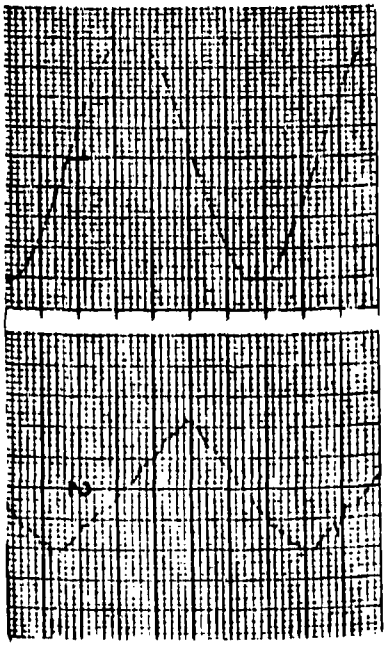

Command
Scale : 20 mv/div

Actuator Position
Scale : 20 mv/div

f = 10 Hz
t → 200 div/sec

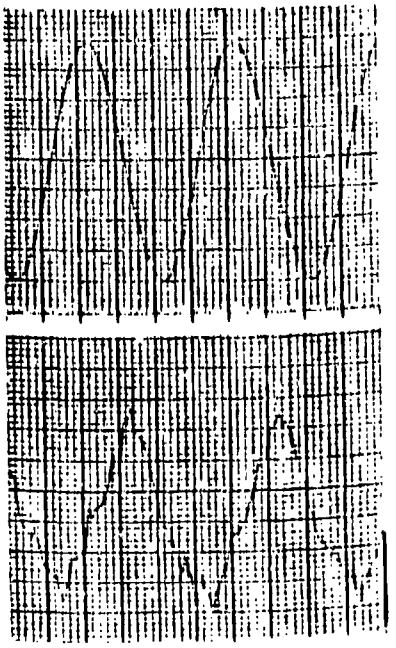

Figure II-68. Waveform characteristics - 10 percent - case 1.

Test Item - Dynamic Controls, Inc.
Digital Servovalve

Date Prepared: 1 Dec 86

Test - Waveform Characteristics - Processor Control
± 5.0% F.S.Input - Case 1

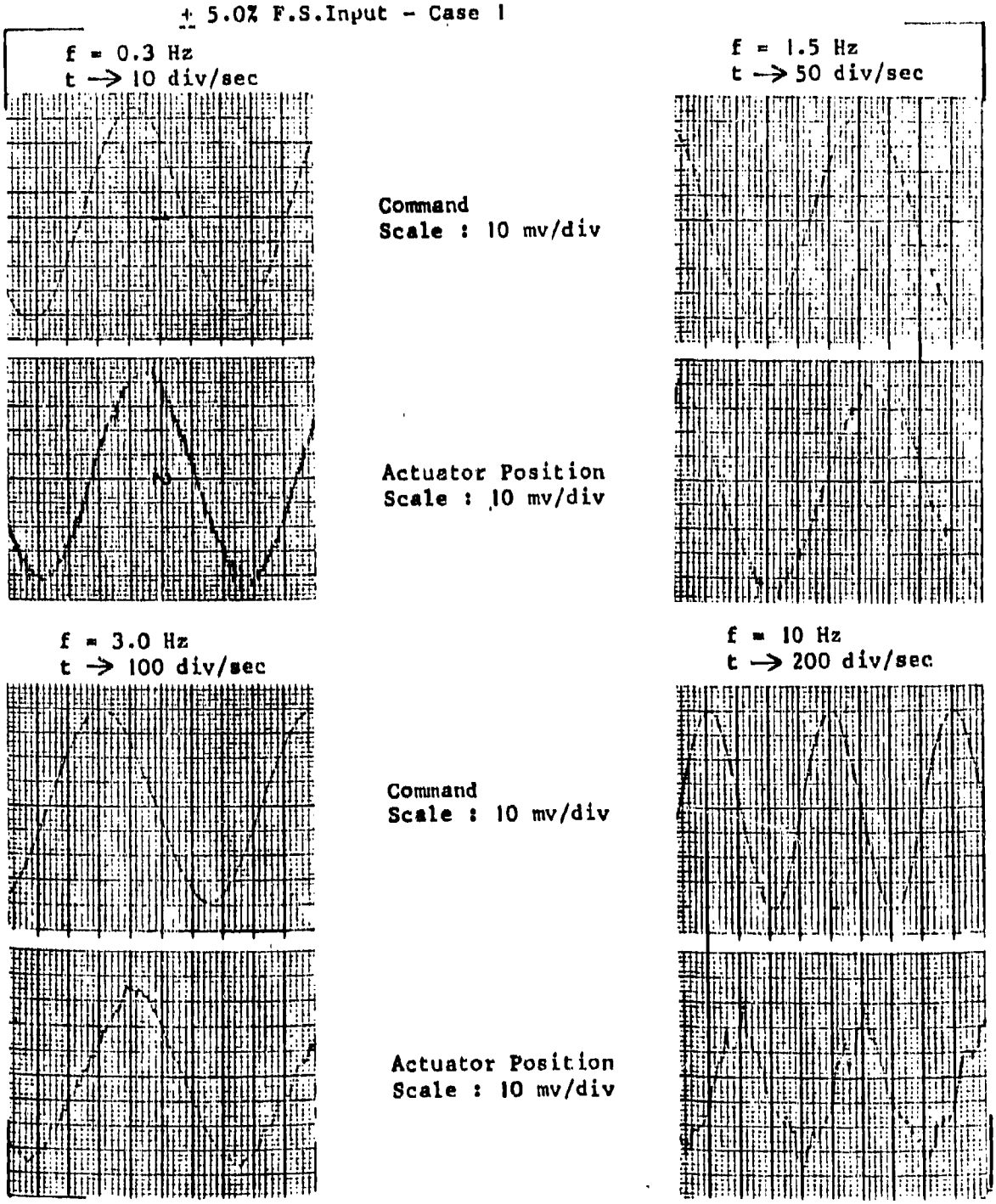

Figure II-69. Waveform characteristics - 5 percent - case 1.

Test Item - Dynamic Controls, Inc.
Digital Servovalve

Date Prepared: 1 Dec 86

Test - Waveform Characteristics - Processor Control
± 2.0% F.S. Input - Case 1

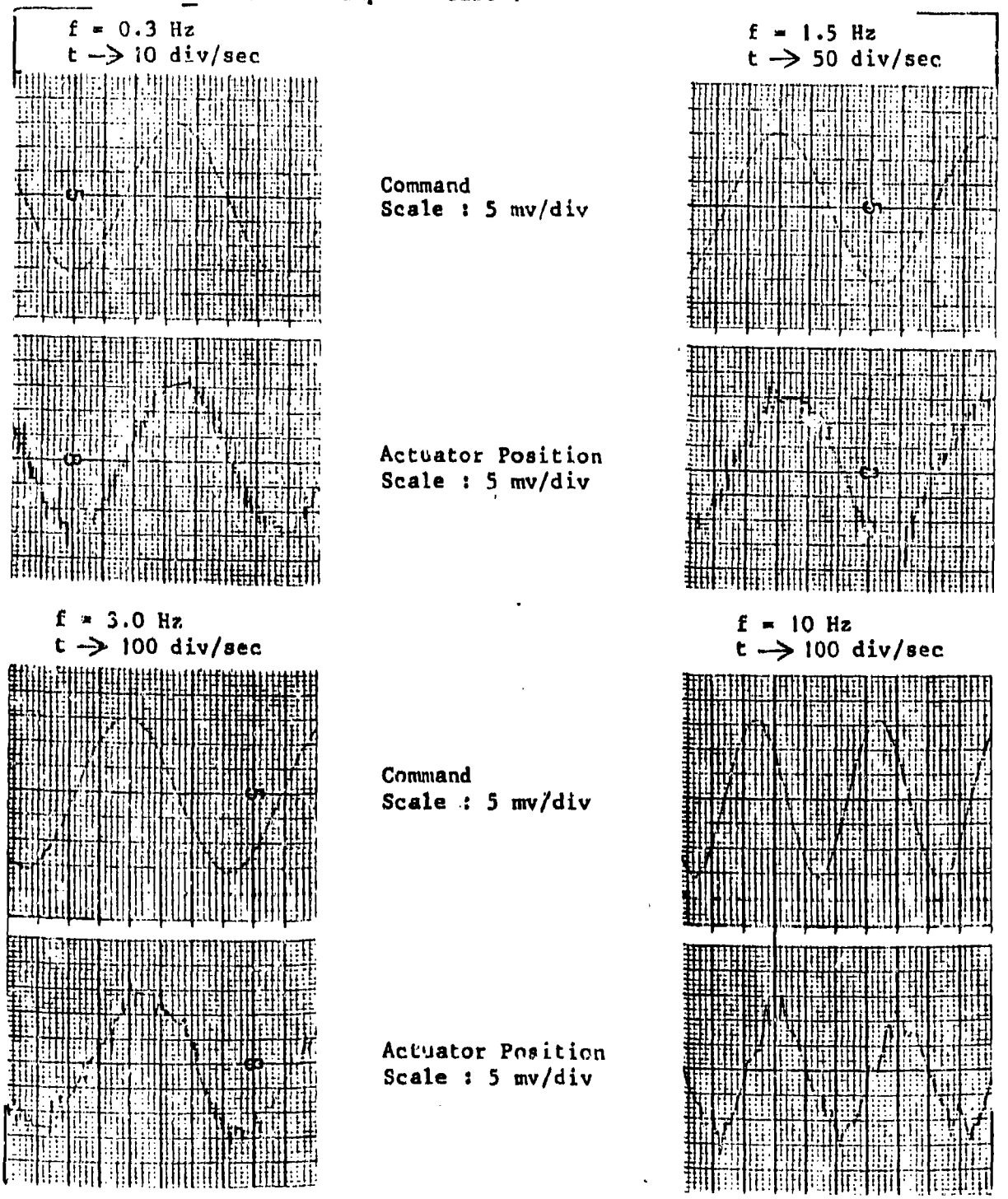

Figure II-70. Waveform characteristics - 2 percent - case 1.

Test Item - Dynamic Controls, Inc.
Digital Servovalve

Date Prepared: 1 Dec 86

Test - Waveform Characteristics - Processor Control
± 5.0% F.S. Input - Up-Date Variations

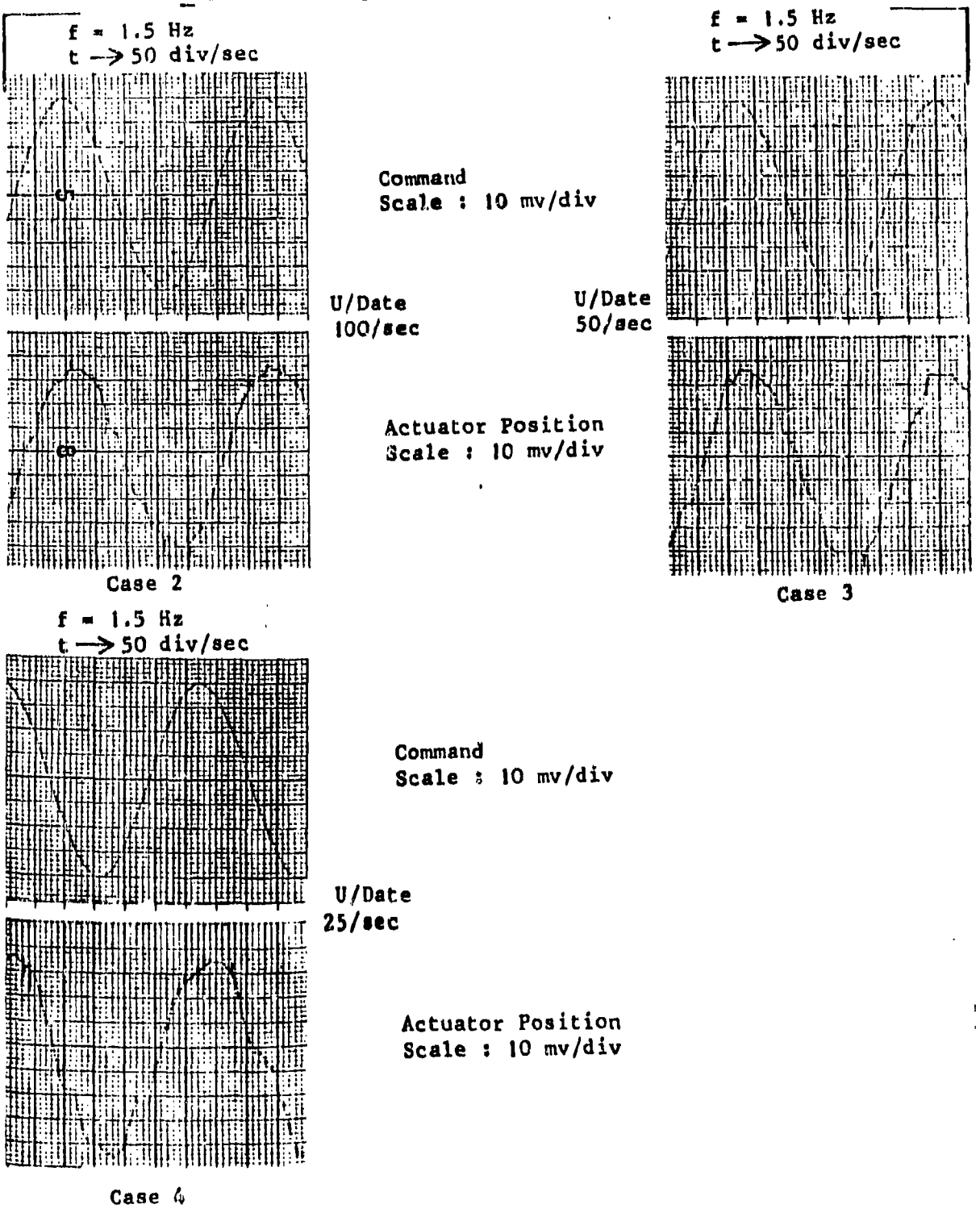

Figure II-71. Waveform characteristics - ± 5 percent - cases 2 through 4.

millivolts. The 5-percent input could only command 57 percent of the full valve flow with the 50 millivolt/step gain setting.

The effect of threshold variations is evident in Figure II-72 (cases 7 and 8). The measured value for case 7 is + 35 millivolts and for case 8 the threshold is + 45 millivolts. This empirical data has favorable agreement with the preset threshold of + 40 and + 50 millivolts. The effect of threshold in the microprocessor software does not provide the same effect as observed in the analog system evaluation. It could be more properly termed *error dead band* as that is the function that it provides.

TEST DATA

Test Item - Dynamic Controls, Inc.
Digital Servovalve

Date Prepared: 1 Dec 86

Test - Waveform Characteristics - Processor Control
± 5.0% F.S. Input - Threshold Variations

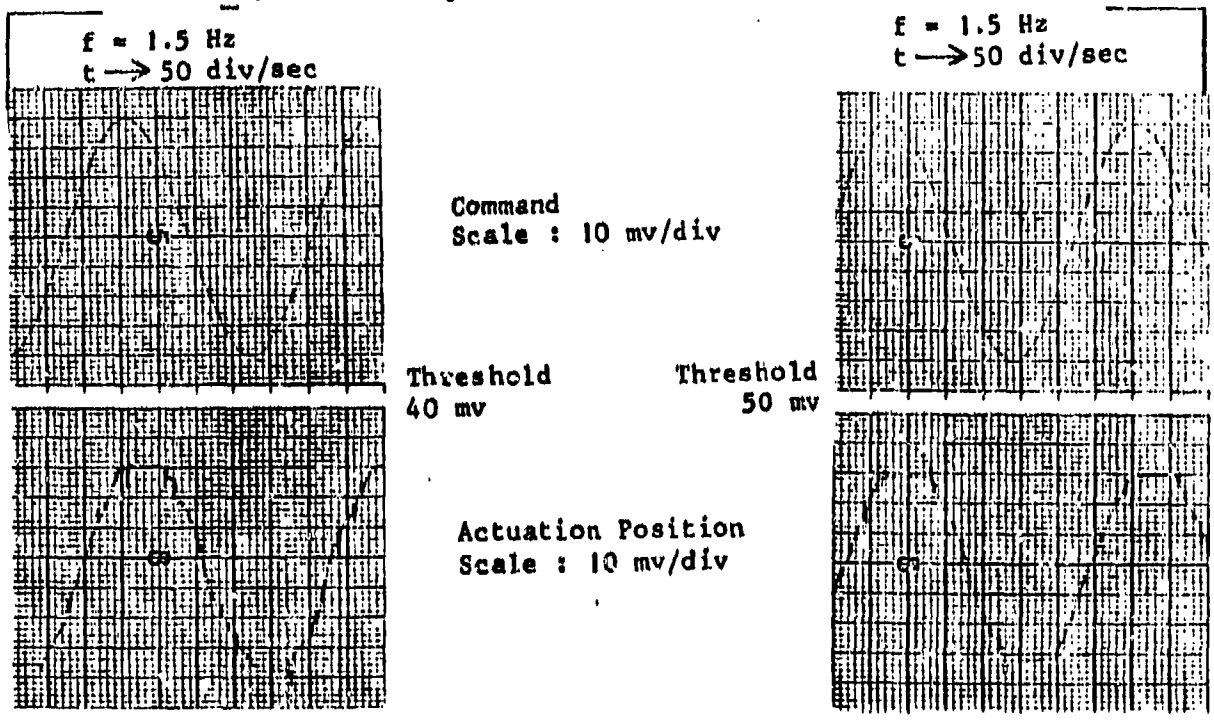

Case 7

Case 8

Figure II-72. Waveform characteristics - 5 percent - cases 7 and 8.

IV. CONCLUSIONS AND RECOMMENDATIONS

The results obtained from the evaluation testing demonstrated that the digital servovalve operated as intended by the design concept. The maximum flow output was the only parameter that failed to meet the original goals. This is because the final flow obtained from the piezoelectric poppet valves was one third of the design goals. The flow limitation affected the slew rate and frequency response of the actuator.

The 500-microsecond operating speed of the piezoelectric poppet valve is very impressive when compared to the fastest-available hydraulic poppet valve (having an operate time of greater than 5 milliseconds). The speed of the piezoelectric-actuated hydraulic valves could provide a solution to time-critical control system problems.

Through the development phase of this project, critical PZ design parameters were identified. Some of these are the effect of high-stress preloads on the piezoelectric element; the importance of the hydraulic amplifier design and the effect of its volume, critical design tolerances for conical poppet valves, and the interfacing of high-voltage pulse drivers to control circuits while maintaining EMI immunity.

The use of a microprocessor to control the digital servovalve system proved to be very successful. Even when using off-the-shelf Z80 hardware, the maximum processing time for the real-time program was 600 microseconds. The fast processing time was the result of efficient straight-line machine-code programming. The processor provided the flexibility of varying the update rate, gain, and threshold to evaluate the effect on system performance.

The high-speed and high-force capability of the piezoelectric actuators could be applicable to a direct-drive force motor design that could be applied to a spool-type servovalve. The on-off drive requirement provides excellent compatibility for interfacing a digital control system.

SECTION III

F-15 RUDDER ACTUATOR EVALUATION

I. INTRODUCTION

Test Specimen

The test specimen evaluated in this report is a rotary hydraulic servoactuator used to drive the rudder surfaces of McDonnell Douglas F-15 fighter aircraft. The test specimen submitted to the Air Force Flight Dynamics Laboratory at Wright-Patterson Air Force Base was built by Hydraulic Units, Incorporated (HUI) of Duarte, California and bore the following identification: Part No. 3U3151-5E, Serial No. 2376. The submitted specimen, mounted in its load fixture, is shown in Figure III-1.

Specimen Description

The specimen is a rotary hinge-line servoactuator capable of accepting mechanical inputs, electrical inputs, or both. The actuator's output shaft is rotated by a controlled differential hydraulic pressure acting on internal vanes. The vanes are directly attached to the output shaft of the servoactuator.

The actuator is designed to have the following three distinct modes of operation:

1. The Control Augmentation System (CAS) mode
2. The CAS-off mode
3. The damping mode

The CAS mode of operation accepts both a mechanical input from the pilot and an electrical input from the Automatic Flight Control System (AFCS). The actuator position and the pilot input are summed together to drive the main control valve to the actuator. The electrical inputs (CAS inputs) position the main control valve sleeve. As shown in Figure III-2, the CAS mode of operation energizes the solenoid valve and connects the drive end of the CAS-mode switch valve to hydraulic return. Spring force retains this valve in the blocked position. The CAS-mode switch valve also takes the output ports of the electrohydraulic servovalve out of bypass and de-energizes the CAS servo-lock mechanism. Electrical feedback from the CAS position (the main control valve sleeve) is obtained from a Linear Variable Differential Transformer (LVDT). Mechanical feedback for the actuator is obtained by a screw arrangement which converts rotary motion to linear motion. The

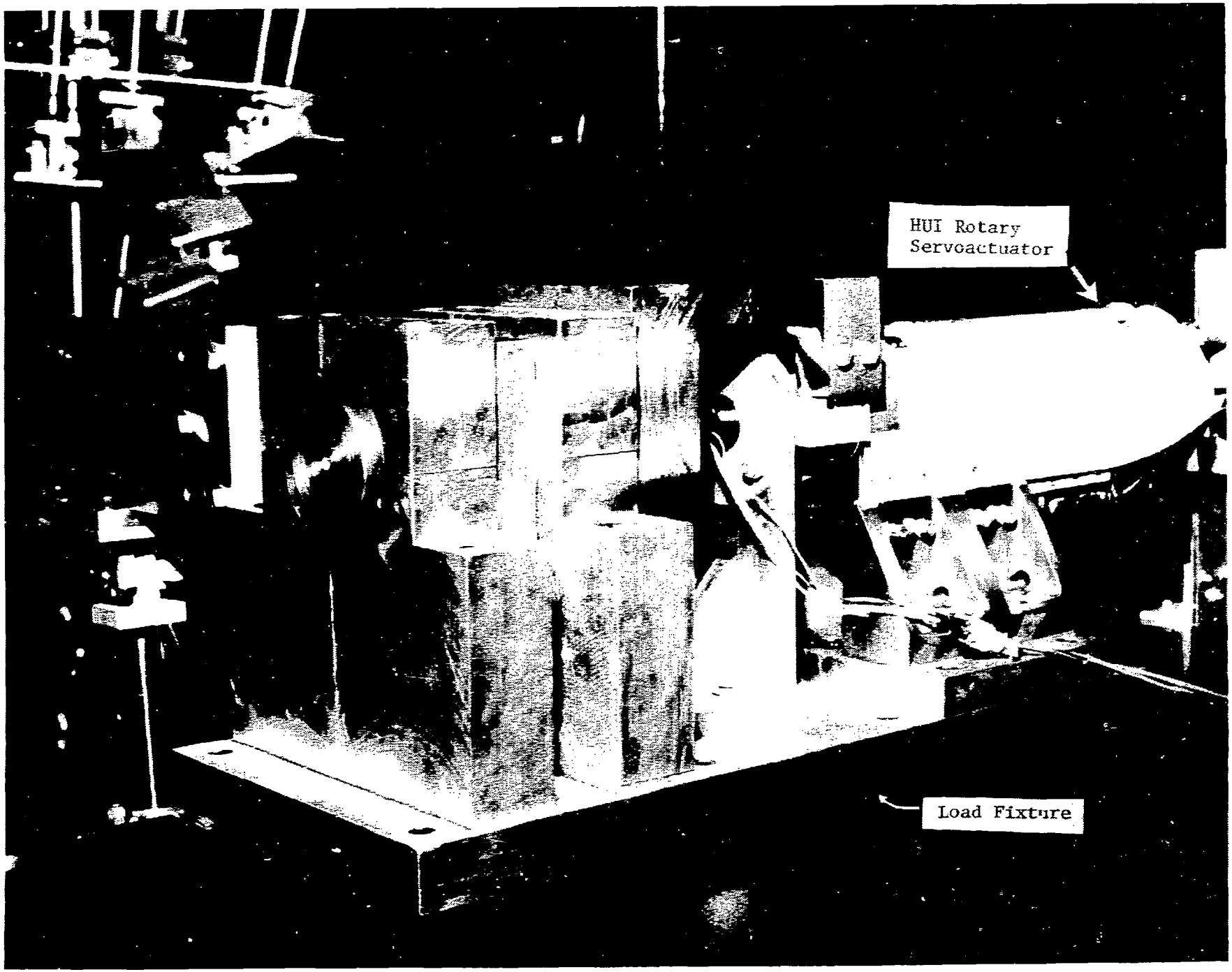

Figure III-1. Rotary servoactuator by Hydraulic Units, Incorporated (HUI).

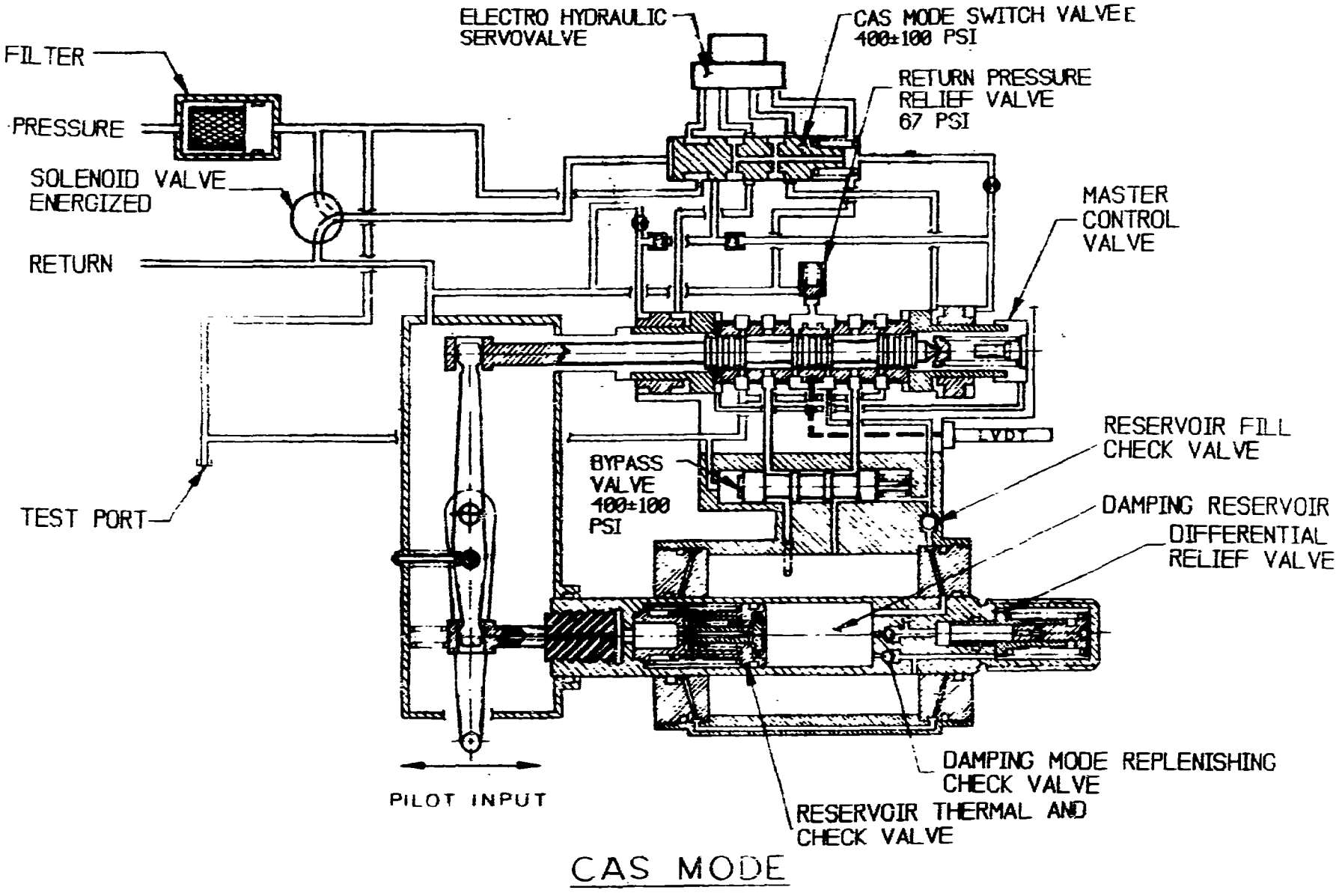

Figure III-2. CAS mode hydraulic schematic.

actuator (from a pilot input) by centering the main control valve spool. Flow to the actuator in response the CAS piston motion is cancelled by actuator motion in the same way.

The CAS-off mode of operation accepts only mechanical inputs from the pilot. With energizing of the solenoid valve, the CAS mode switch is driven to the right (as shown in Figure III-3), blocking off hydraulic supply pressure from the servovalve. The mode switch also bypasses the output ports of the servo-valve and energizes the CAS servo-lock mechanism. The servo-lock mechanism is energized by applying hydraulic pressure to cavities behind the two sleeves which ride on the master control valve. The sleeves lock the CAS piston to the body of the actuator, preventing the piston from moving the main control valve sleeve and driving the actuator.

The third mode of operation (shown in Figure III-4) is the damping mode which is used when supply pressure to the actuator drops below 400 ± 100 psi. At that point, the bypass valve shuttles to block the control ports from the main control spool. A damper accumulator is mounted on actuator body to prevent cavitation while operating in the damper mode.

The parameter characteristics for the actuator (as listed by HUI) are as follows:

1. Actuator operating pressure: 3000 psi
2. Actuator maximum travel:
   - Mechanical input: 63° ± 2° full travel or 31.5° ± 1° in each direction from mid-stroke
   - Electrical input: 30° ± 1.2° full travel or 15° ± 0.6° in each direction from mid-stroke
3. Actuator output torque: 22,000 ± 450 in-lbs
4. Nominal loop gain: 28.9 sec^{-1}
5. Maximum angular velocity:
   - Mechanical input: 150° ± 15° per second
   - Electrical input: 150° ± 15° per second
6. Master control valve stroke: ± 0.040 inches

Figure III-5 is a block diagram of the overall control system for one actuator.

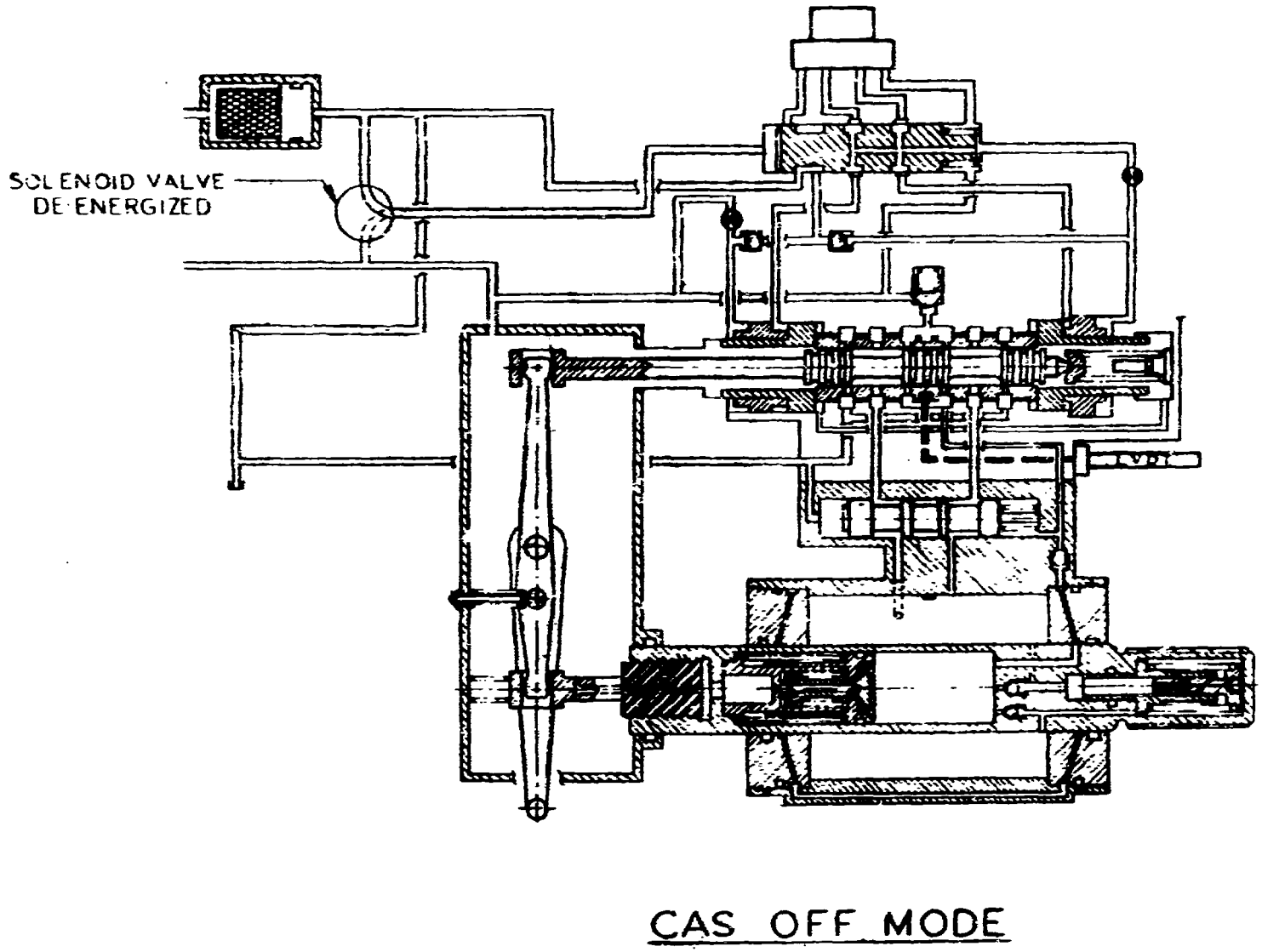

Figure III-3. CAS-off mode hydraulic schematic.

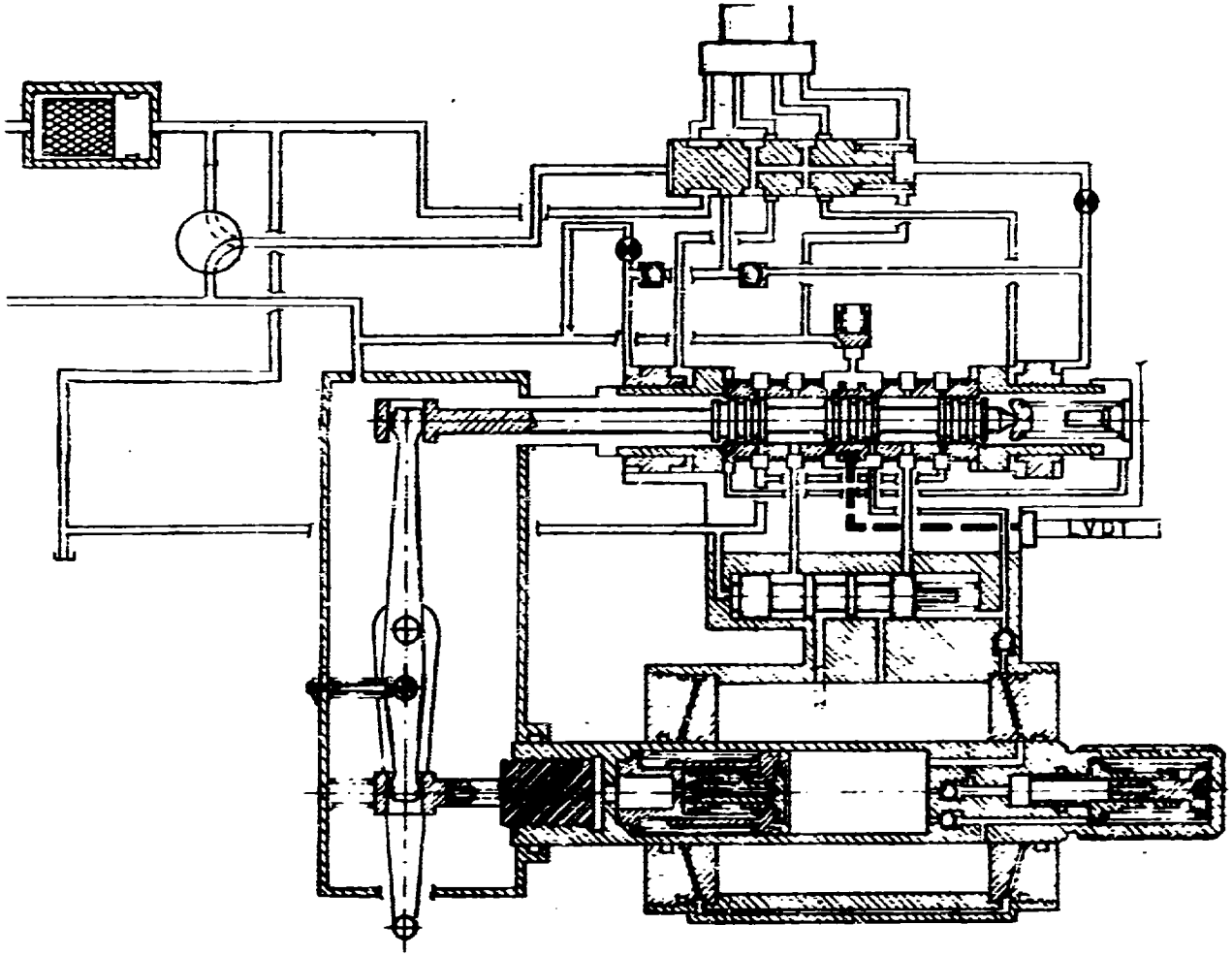

Figure III-4. Damping mode hydraulic schematic.

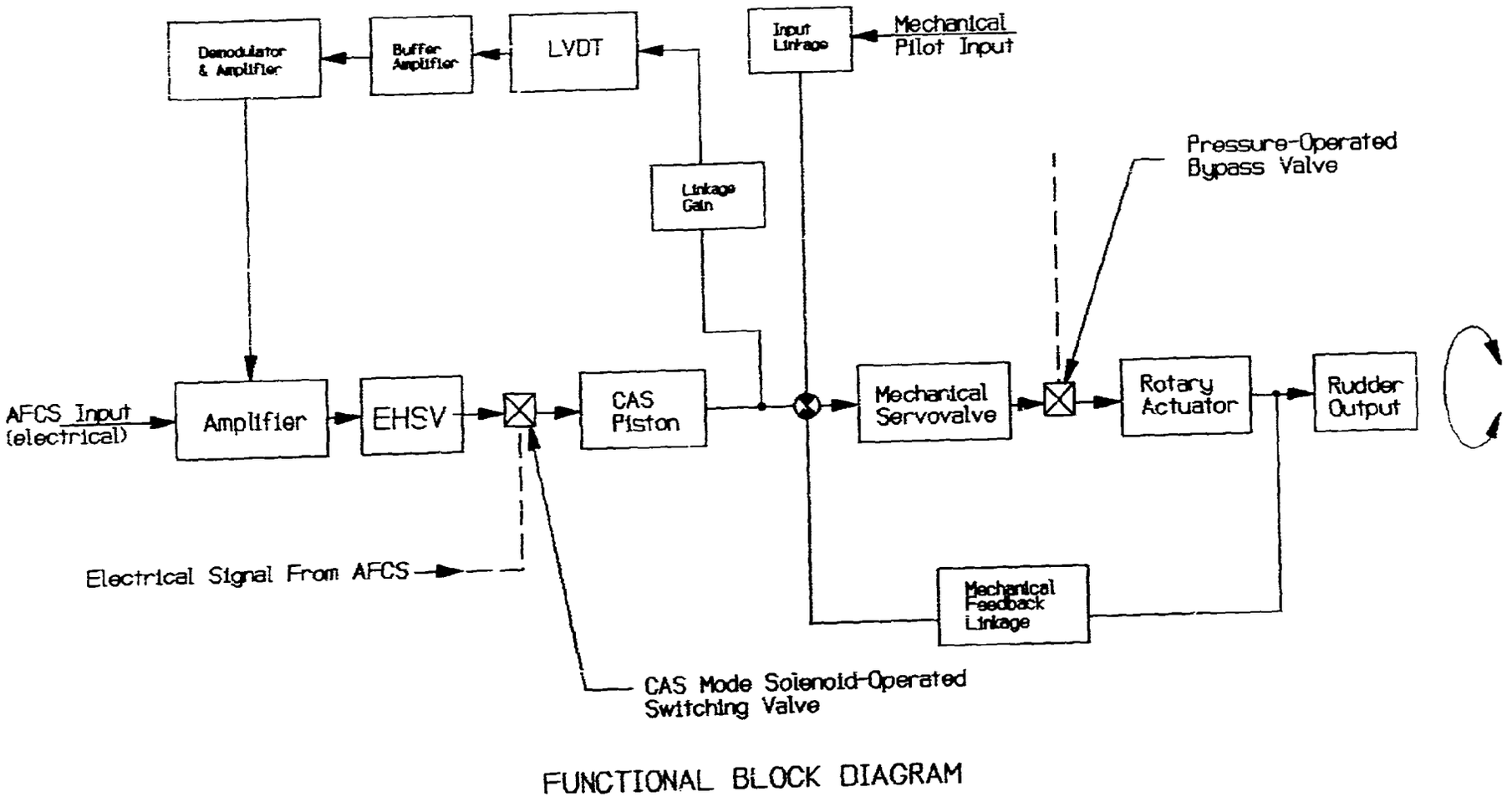

Figure III-5. Block diagram of overall control system.

II. TECHNICAL APPROACH

General

The objective in testing the HUI rotary servoactuator was to determine the performance parameters of the actuator as a control element in an a fly-by-wire control system. The unique design of this actuator (i.e., the use of vanes and long linear seals to control the output shaft of rotary actuators) provided an opportunity to establish a baseline against which future hingeline actuators (both electro-hydraulic and electro-mechanical) could be compared.

Therefore, for all testing, the mechanical input shaft was mechanically grounded at null and only electrical commands were used to drive the actuator. An electronic console was designed and constructed to command the test specimen and to output pertinent data.

A portion of the testing was conducted with simulated aerodynamic loads applied to the specimen. A test fixture was designed and constructed to hold the actuator during application of these loads. The actuator was tested in the Multipurpose Actuation System Test Rig (MASTR) in the Actuation Laboratory at Wright-Patterson Air Force Base, Ohio.

Actuator Installation and Instrumentation

The rotary servoactuator was installed in its test fixture and connected to its command console. Hydraulic power (30 gpm at 3000 psi) was connected to hydraulic ports located on the test actuator. A linear rotary potentiometer was connected directly to the output shaft of the actuator and was used to measure output shaft displacement. Applicable voltages were used to electrically power the actuator. Instrumentation and all external inputs to the specimen are shown in Figure III-6. The Wavetek 144 generator and the Hewlett Packard X-Y plotter were used to record linearity and hysteresis data. The Brush 200 chart recorder, in conjunction with the Wavetek 144 generator, were used to record static and dynamic thresholds along with step response and saturation velocity data. The Hewlett Packard 5423A frequency analyzer and the Hewlett Packard digital plotter were used for amplitude response and phase shift measurements.

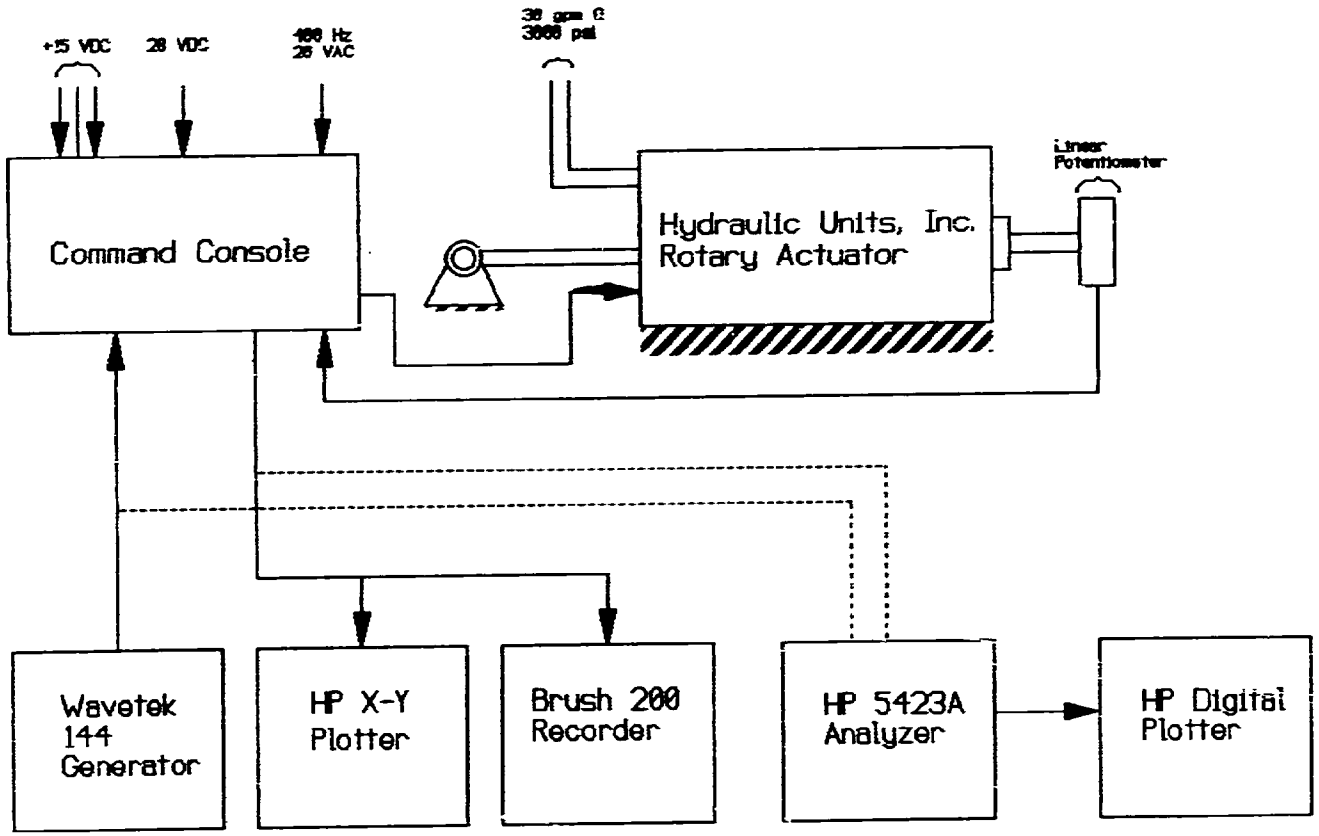

Figure III-6. Instrumentation block diagram.

Test Procedure

The measurements used to evaluate the HUI rotary actuator were based on a series of input/output tests used by Dynamic Controls, Incorporated (DCI) for testing other actuation systems for the Flight Dynamics Laboratory at Wright-Patterson Air Force Base, Ohio.

The HUI rotary servoactuator was evaluated with the measurement series first in the unloaded configuration to establish baseline performance, then in the loaded configuration to measure performance characteristics with simulated aerodynamic loads.

Specific Performance Measurements

Linearity

Definition: *The deviation of output-versus-input from a straight line relationship.*

Test: The input was commanded to > 100 percent at 0.1 Hz with a sawtooth waveform. The output of the rotary position potentiometer-versus-input command was recorded.

Hysteresis

Definition: *The non-coincidence of loading and unloading curves at large and small input command levels.*

Test: The input was commanded to ± 1.0 and ± 10.0 percent of maximum amplitude at a frequency of 0.1 Hz with a sawtooth waveform. The output of the rotary position potentiometer-versus-input command was recorded.

Frequency Response

Definition: *With a random noise actuator input, the frequency response for the actuator is the relationship of the output to input expressed as an amplitude ratio and phase shift as a function of frequency.*

Test: The input was commanded to ± 3.0 percent of maximum amplitude using a white noise input with the bandwidth set at 0.03 to 12.5 Hz. The response and phase shift of the rotary position potentiometer-versus-input command were plotted. The test was repeated with an input command of ± 1.0 percent.

Static Threshold

Definition: *The minimum change from zero level which causes a measurable output change.*

Test: The input was commanded to zero amplitude. The amplitude of a sawtocth waveform at 0.1 Hz was slowly increased until a measurable output was recorded. The input command and the output of the rotary position potentiometer were recorded.

Dynamic Threshold

Definition: *The input level at a frequency of 50 percent of the actuator's bandpass required to cause a measurable output level.*

Test: Starting at zero amplitude, a sinusoidal waveform at a frequency of 2.0 Hz was slowly increased until a measurable output was recorded. The input command and the output of the rotary position potentiometer were recorded.

Saturation Velocity

Definition: *The maximum velocity at which the actuator is capable of moving in each direction.*

Test: The input was commanded to 110 percent of maximum amplitude with a square waveform at a frequency of 0.3 Hz. The input command and the output of the rotary position potentiometer were recorded.

Transient Response

Definition: *The time response of the actuator output to an applied step input whose amplitude minimizes the nonlinear distortions of threshold and hysteresis, yet avoid velocity saturation.*

Test: The input was commanded to 10 percent of maximum amplitude with a square waveform at a frequency of 0.3 Hz. The input command and the output of the rotary position potentiometer were recorded.

III. UNLOADED TEST RESULTS

Unloaded Tests

General

The following data was recorded from the HUI rotary servoactuator by using the measurement methods presented previously in Section II. The splined-hinge assembly used to drive the load actuator and the output position potentiometer were attached to the output shaft of the servoactuator. Unloaded data was recorded with the test actuator in this configuration (with the load actuator bypassed).

Specific Unloaded Test Results

Linearity

Figure III-7 shows data recorded in establishing the actuator output linearity. Note the presence of hysteresis in the linearity plot. This hysteresis is assumed to be caused by the directional change of the linear vane-tip seals internal to the actuator. The percentage of hysteresis (referred to maximum output motion) is 2.54 percent. The maximum deviation from a straight line is 2.37 percent referred to the output. The nonlinearity observed in Figure III-7 may be attributed to the linearity of the mechanical feedback linkage. Normally, with an actuator (which is an integrator) position linearity is primarily a function of the actuator's feedback linearity. However, since the CAS input positions the sleeve of the power spool (and the sleeve has its own LVDT for position feedback), nonlinearities in the CAS LVDT feedback also appear in the output position linearity of the actuator. The 2.54 percent (of maximum CAS output motion) hysteresis corresponds to an uncertainty of 45 minutes of angle at the rudder surface.

Hysteresis

Hysteresis was measured at ± 1 percent and ± 10 percent input command levels around the null position of the servoactuator's output shaft. Figure III-8 shows the ± 1 percent data. The hysteresis at this input level was 17.8 percent referred to the ± 1 percent command, and 0.42 percent as referred to total actuator output. Hysteresis resulting from the ± 10 percent input level is shown in Figure III-9. Hysteresis at this input level was 5.61 percent referred to the ± 10 percent input command, and 1.25 percent (referred to total actuator output).

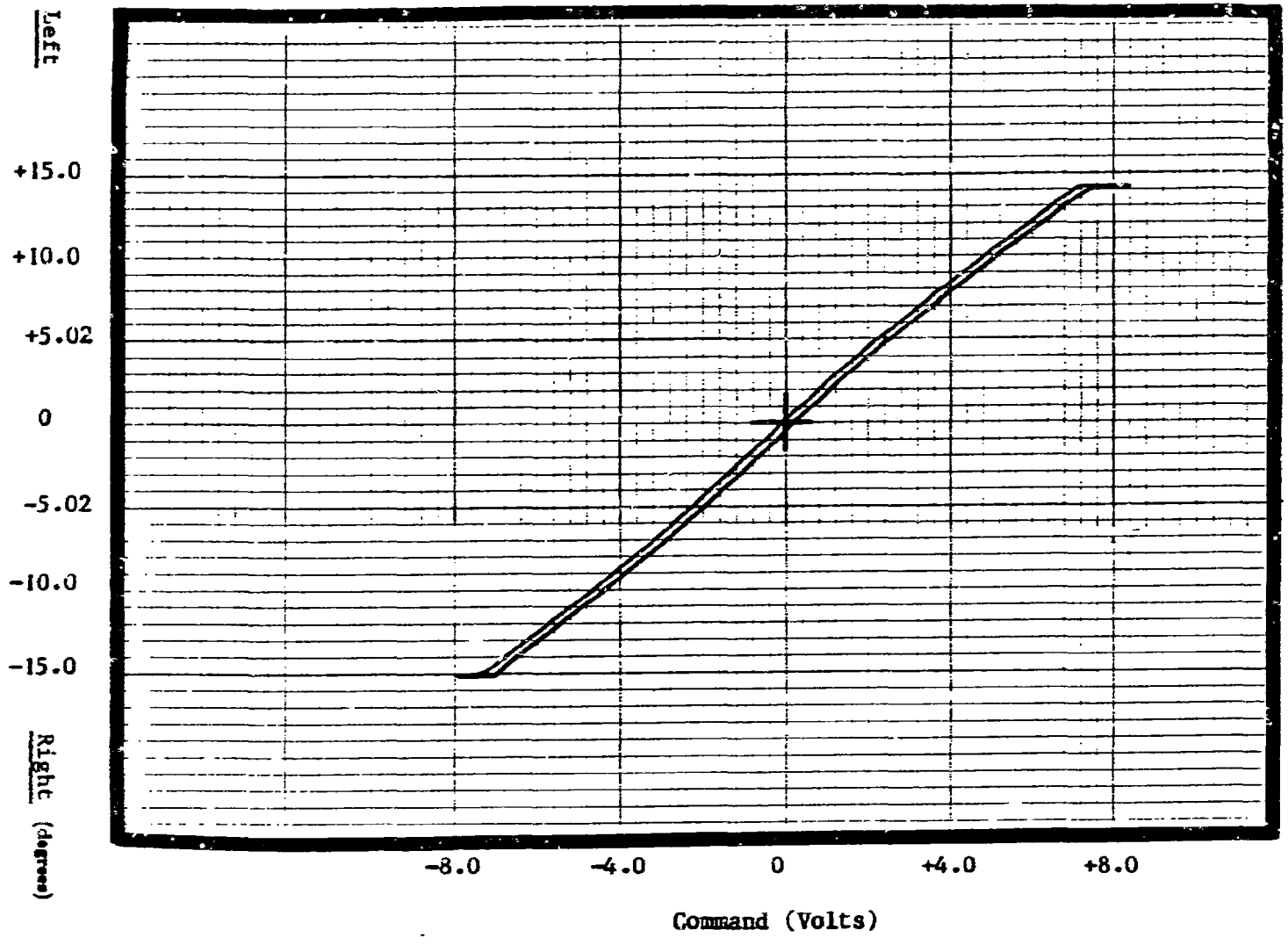

Figure III-7. Linearity - unloaded.

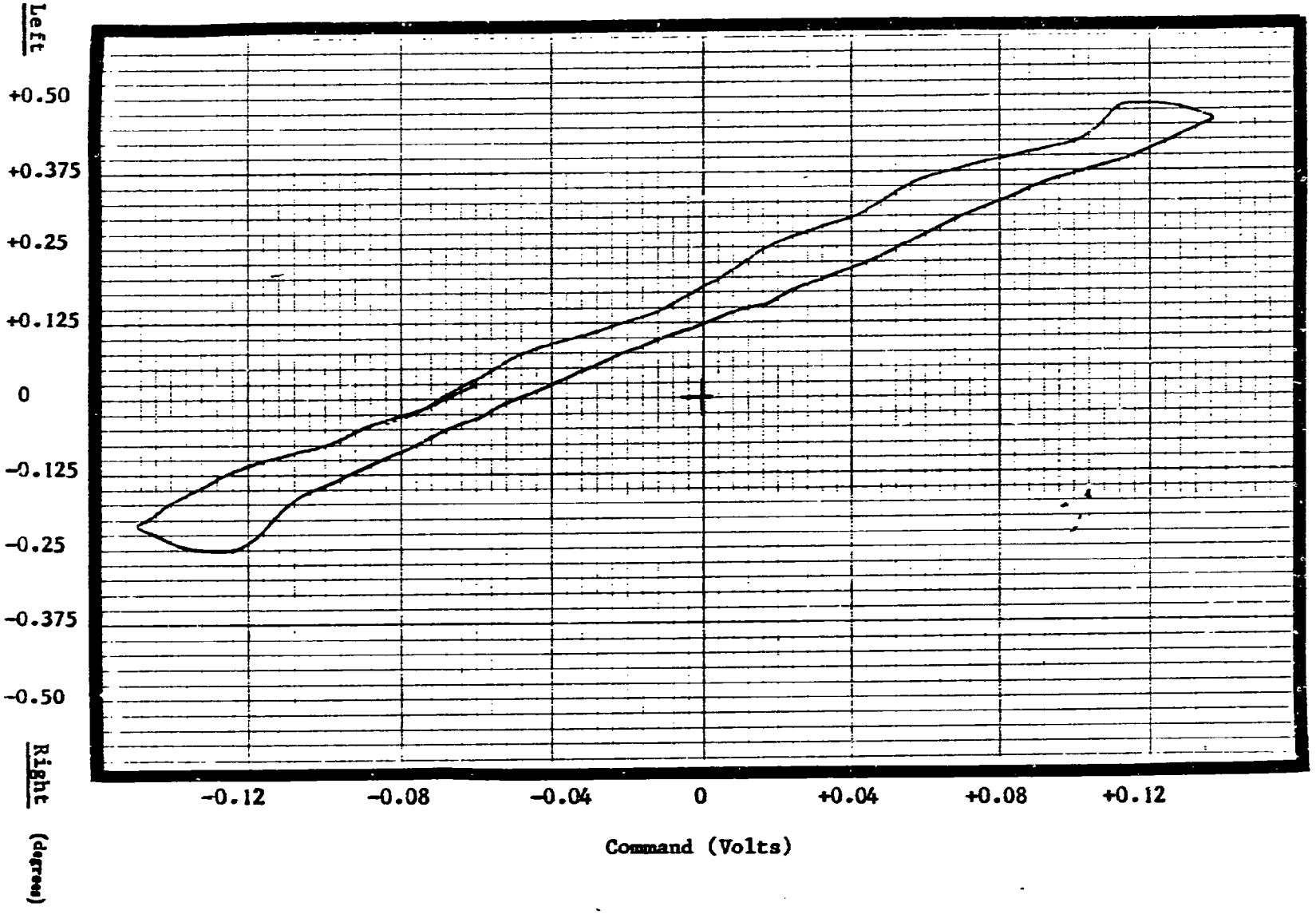

Figure III-8. Hysteresis - unloaded - ± 1 percent command.

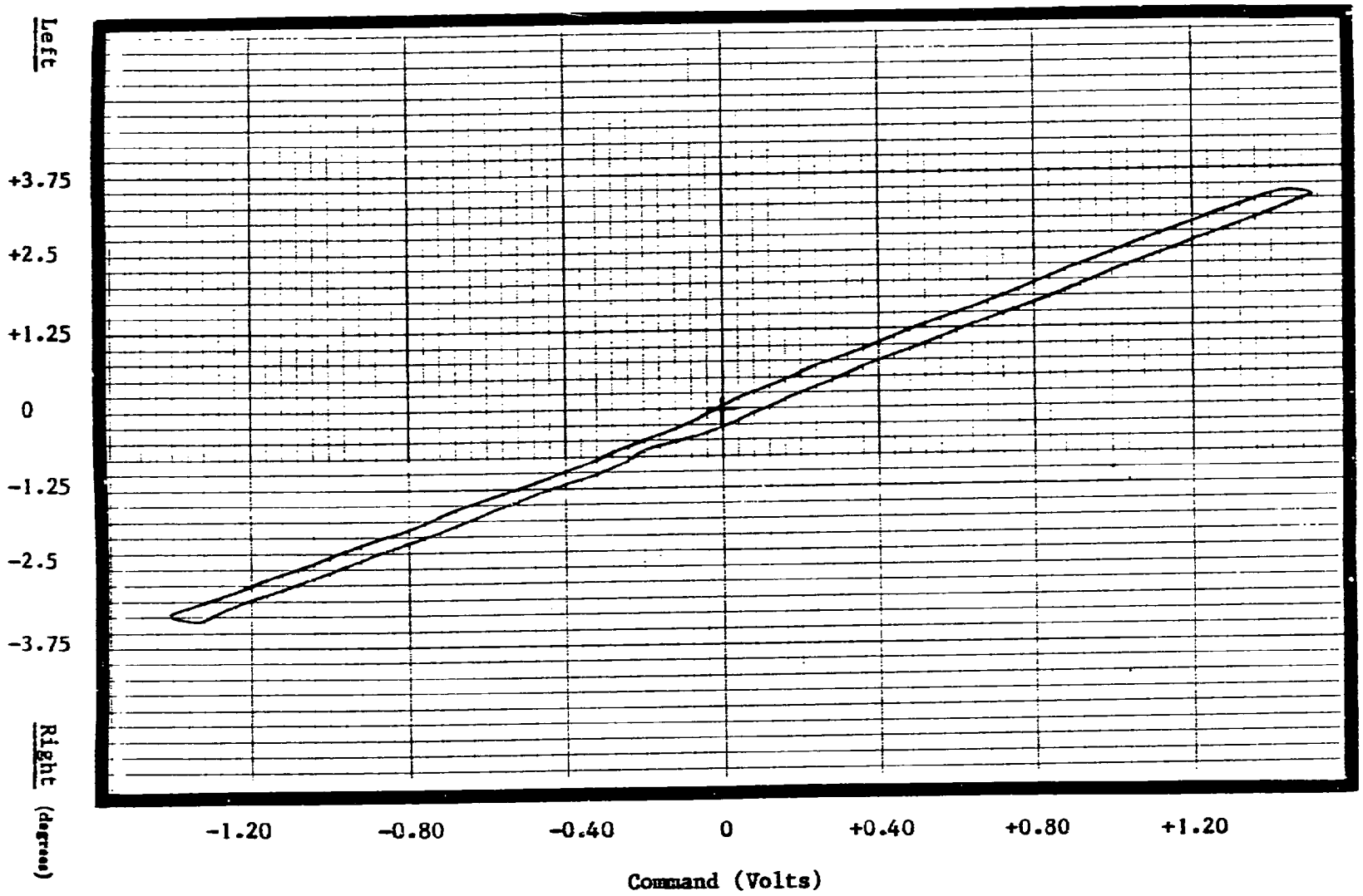

Figure III-9. Hysteresis - unloaded - ± 10 percent command.

Frequency Response

Frequency response and phase shift were measured at two input command levels, ± 1 percent and ± 3 percent. Results of this test are compiled in Table III-1. Actual data recorded is shown in Figures III-10 through III-12. The measurement were made with the test specimen's output shaft operating around the null position.

Table III-1. Results of frequency response, unloaded testing.

Input Command	-3 db Frequency	Phase Shift Frequency -45°	-90°
± 1 percent	4.88 Hz	2.39 Hz	4.27 Hz
± 3 percent	3.68 Hz	2.74 Hz	6.70 Hz

The frequency response change between the 1 percent and 3 percent input command amplitudes is probably due to the effect of the low-amplitude nonlinearities of threshold and hysteresis on the response measurement. The frequency response analyzer uses band-limited white noise as an excitation signal for the actuator. The input signal resembles a train of square waves having a fixed time base and a variable amplitude. To perform the response measurement, the peak amplitude of the input signal is adjusted to the desired command amplitude. The amplitude of part of the input signal train does not exceed threshold and hysteresis input levels. With larger input levels, less of the input signal train is at or below the threshold and hysteresis input levels and the frequency response changes from the lower input level measurement.

Static Threshold

Static threshold data is shown in Figure III-14. Note that the input command is a sawtooth waveform with an increasing amplitude. Note that the actuator's output motion is almost a square waveform. This distortion of the output waveform can again be attributed to the valve seal reversal which was noted in the linearity test. Note also that the static threshold level is ± 0.016 volts. This is 0.23 percent of the maximum input command of ± 7 volts.

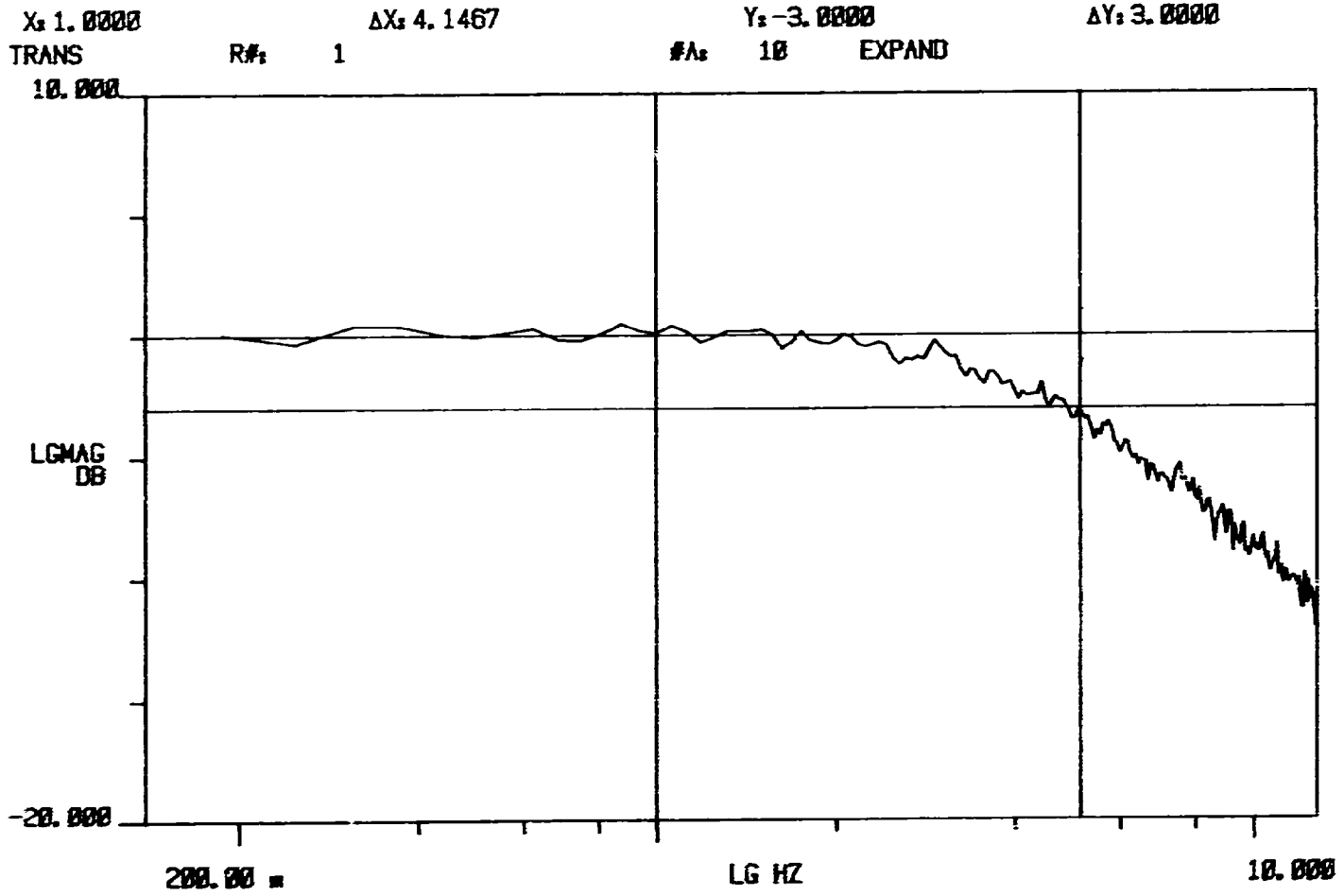

Figure III-10. Frequency response, rudder centered, unloaded, ± 1 percent command.

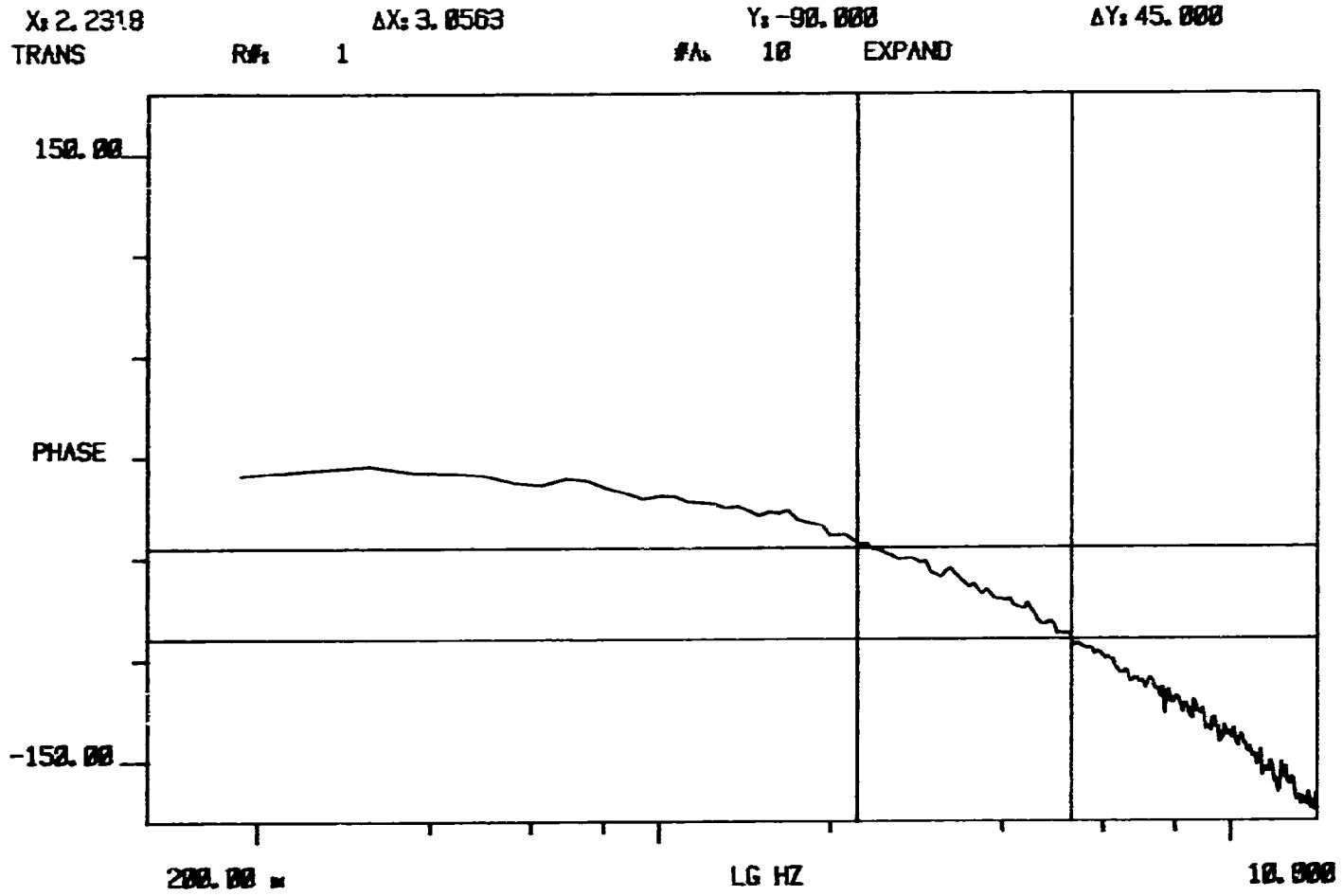

Figure III-11. Phase measurement, rudder centered, unloaded, ± 1 percent command.

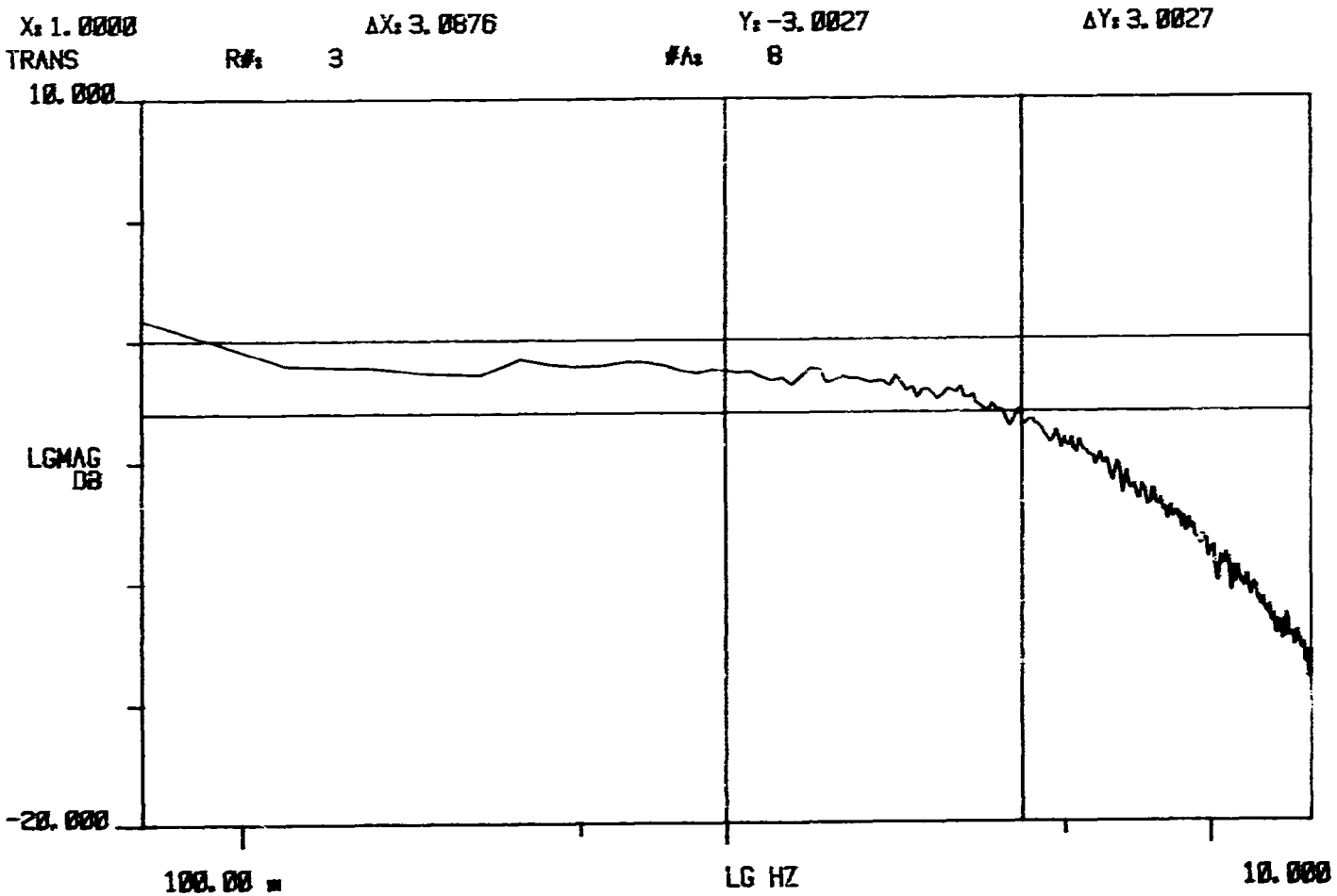

Figure III-12. Frequency response, rudder centered, unloaded, ± 3 percent command.

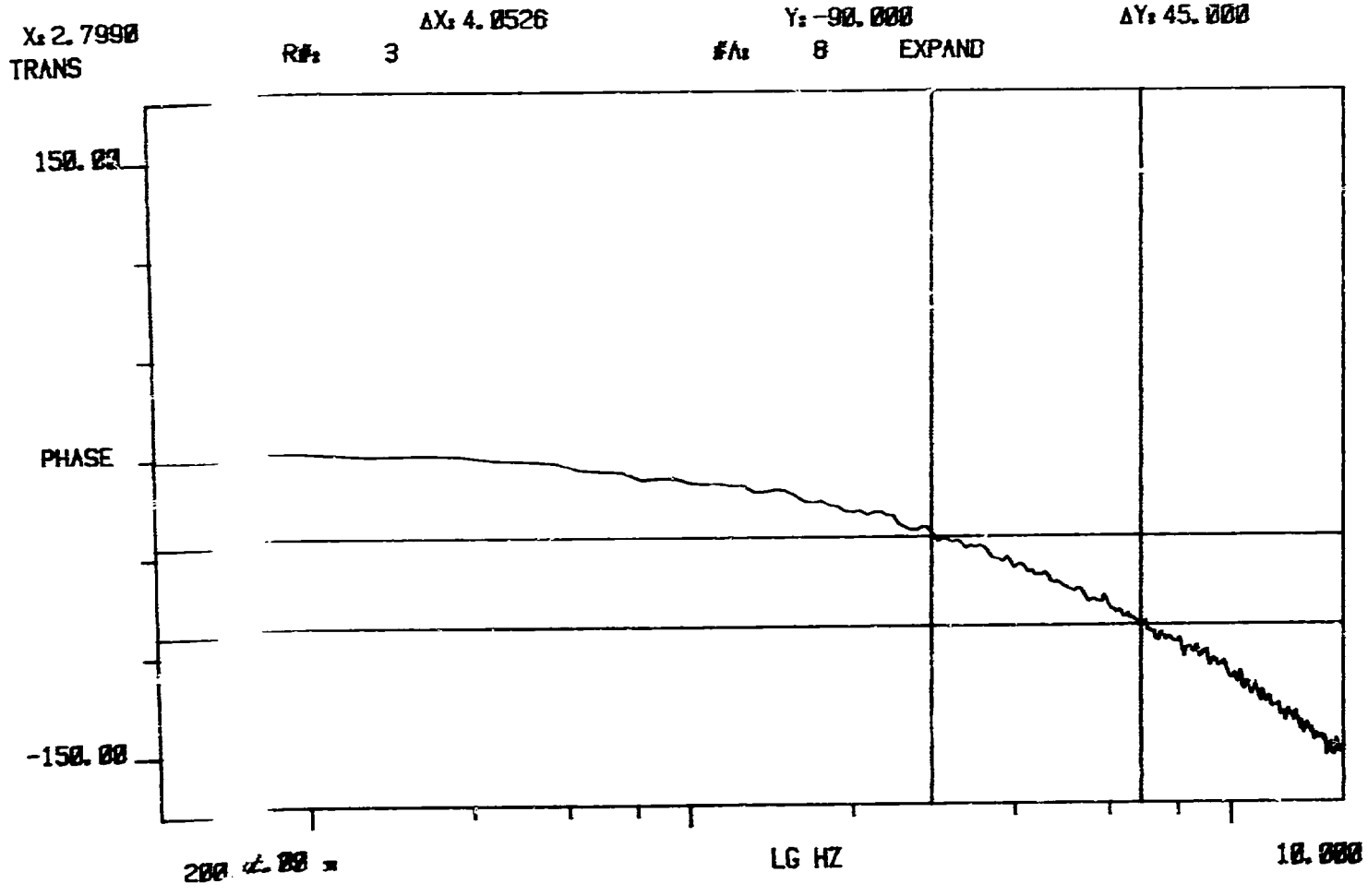

Figure III-13. Phase measurement, rudder centered, unloaded, ± 3 percent command.

Test Item - Hydraulic Units, Inc.
F-15 Rotary Rudder Servoactuator
P/N 3U3151-5E; S/N 2376

Date Prepared: 9/17/86

Test - Static Threshold
Surface Position - 0°
Load - 0 lbs.

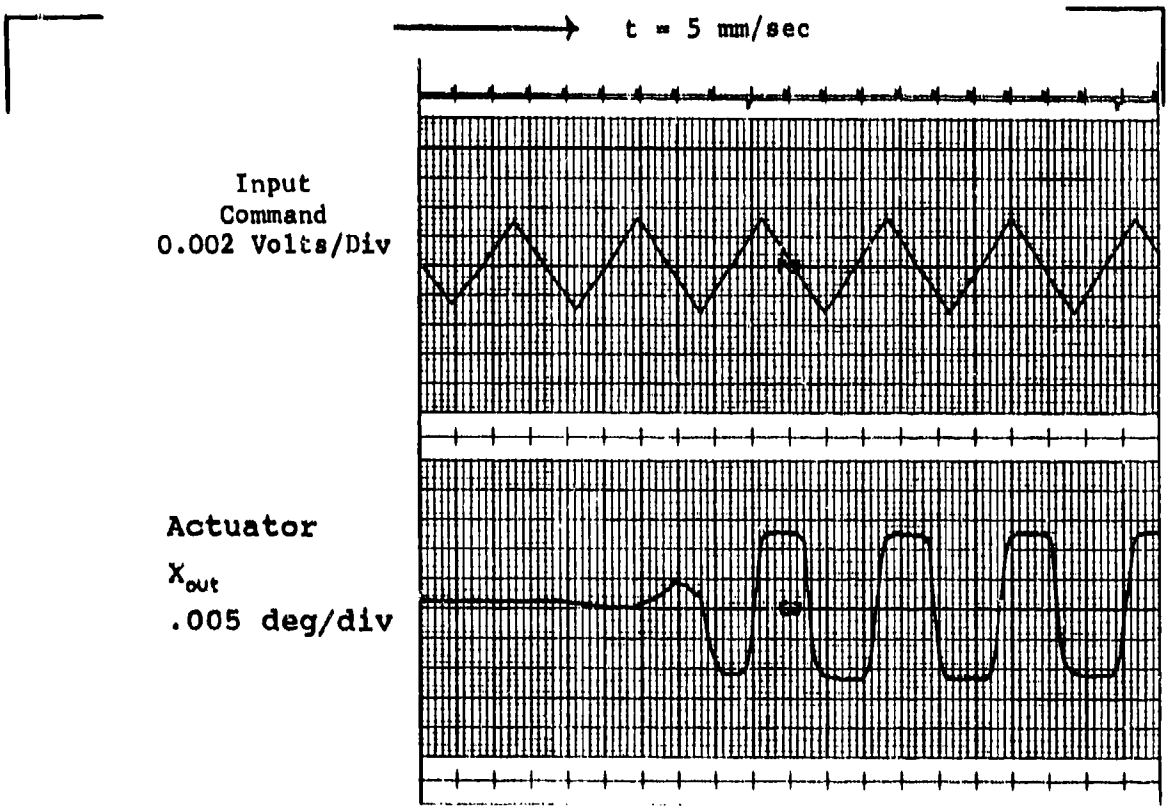

Figure III-14. Unloaded static threshold.

Dynamic Threshold

Figure III-15 shows the data recorded during the dynamic threshold test. Note the position offset which occurred at a command level of 0.015 volts. Note that this is the same value as the static threshold. The actuator did not respond to the 2 Hz input command until the amplitude reached a level of ± 0.021 volts (± 0.3 percent of maximum command).

Transient Response

Data for the step response test is shown in Figure III-16. Input command amplitude was ± 10 percent of full scale. The *rudder left* trace shows a time delay of .005 seconds and a time of .055 seconds to reach 63 percent of its final value. The *rudder right* trace shows a time of .005 second delay and the same .055 second to reach 63 percent of its final value. The slight slope of the input command exhibited in both traces is because of the response characteristics of the brush recorder. The step responses show that the actuator's control loop is well-damped with no ringing.

Saturation Velocity

Figures III-17 and III-18 show data recorded for the saturation velocity test. Figure III-17 shows a velocity for 172.6 degrees per second for the rudder full-left to full-right trace. Figure III-18 shows a velocity of 169.43 degrees per second for the rudder full-right to full-left trace. The slope of the step input command in both figures is again due to response characteristics.

Test Item - Hydraulic Units, Inc.
F-15 Rotary Rudder Servoactuator
P/N 3U3151-5E; S/N 2376

Date Prepared: 9/17/86

Test - Dynamic Threshold
Surface Position - 0°
Load - 0 lbs.

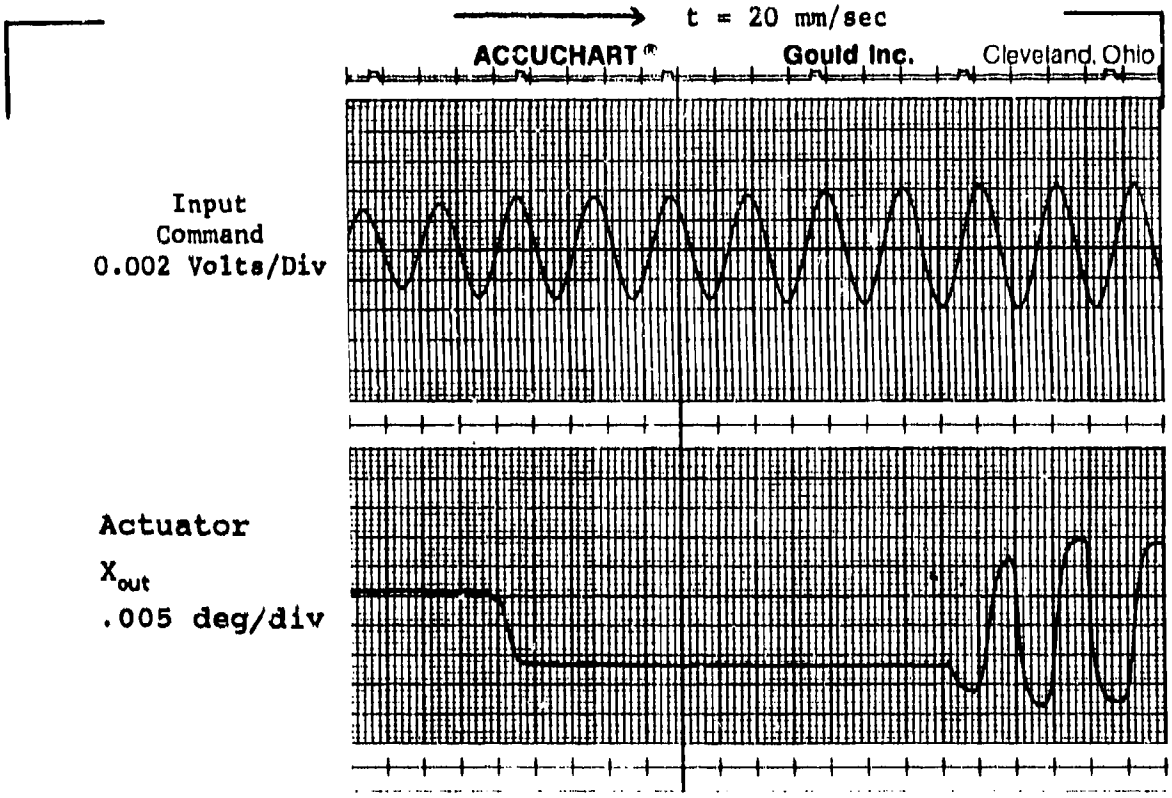

Figure III-15. Unloaded dynamic threshold.

Test Item - Hydraulic Units, Inc.
F-15 Rotary Rudder Servoactuator
P/N 3U3151-5E; S/N 2376

Date Prepared: 9/18/86

Test - Transient Response
Surface Position -
Load - 0

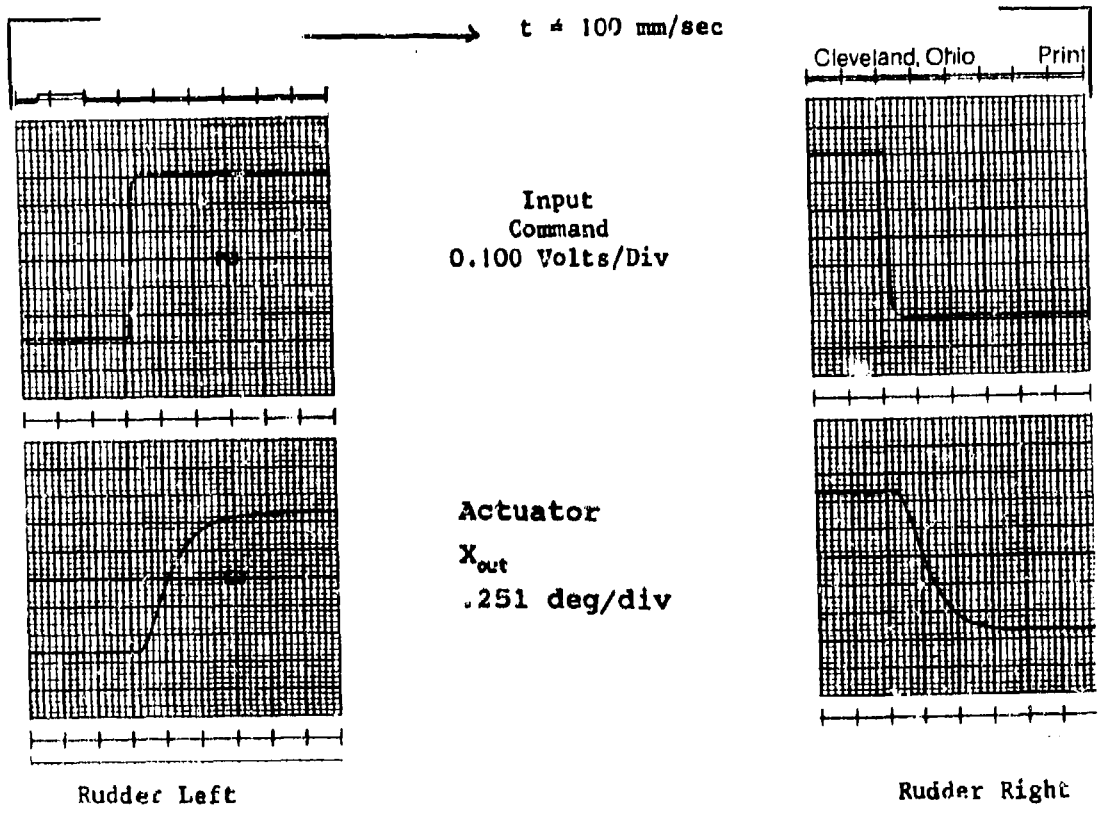

Figure III-16. Unloaded step response.

Test Item - Hydraulic Units, Inc.
F-15 Rotary Rudder Servoactuator
P/N 3U3151-5E; S/N 2376

Date Prepared: 9/18/86

Test - Saturation Velocity
Surface Position -
Load - 0 lbs.

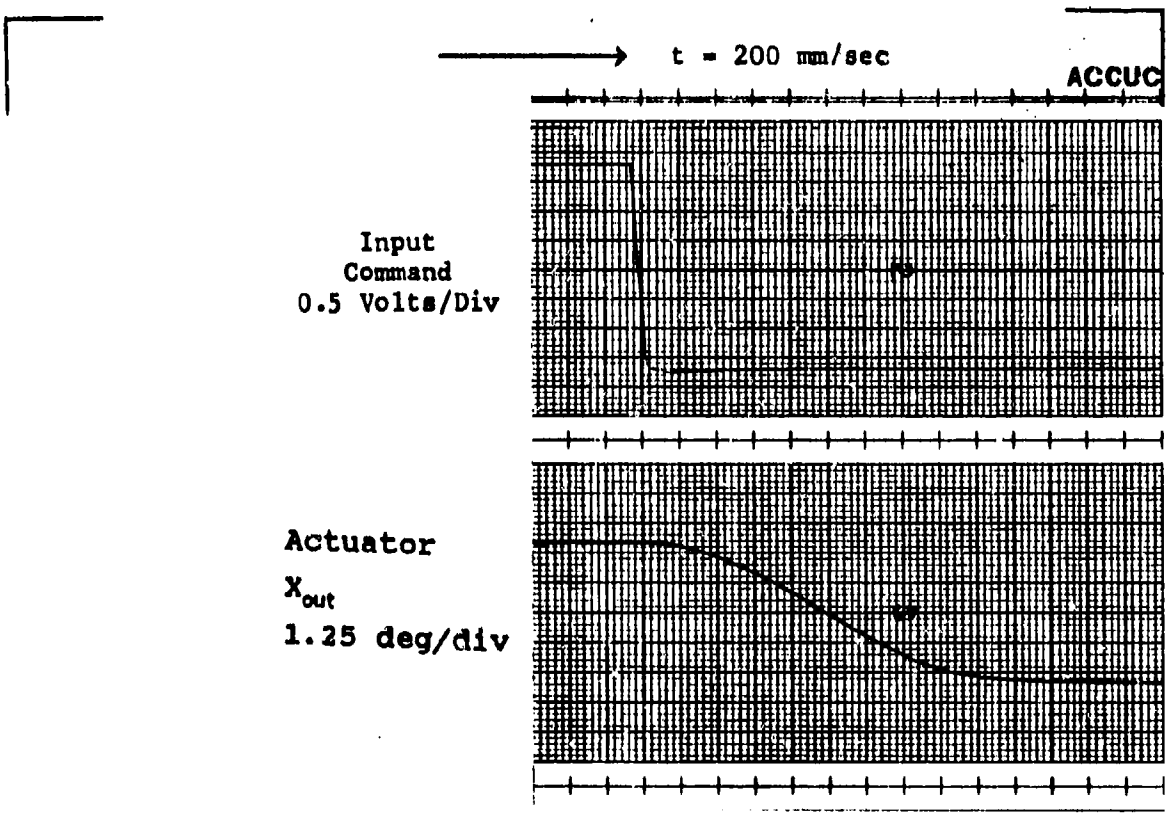

Rudder Left to Right

Figure III-17. Unloaded left-to-right saturation velocity.

Test Item - Hydraulic Units, Inc.
F-15 Rotary Rudder Servoactuator
P/N 3U3151-5E; S/N 2376

Date Prepared: 9/18/86

Test - Saturation Velocity
Surface Position -
Load - 0 lbs.

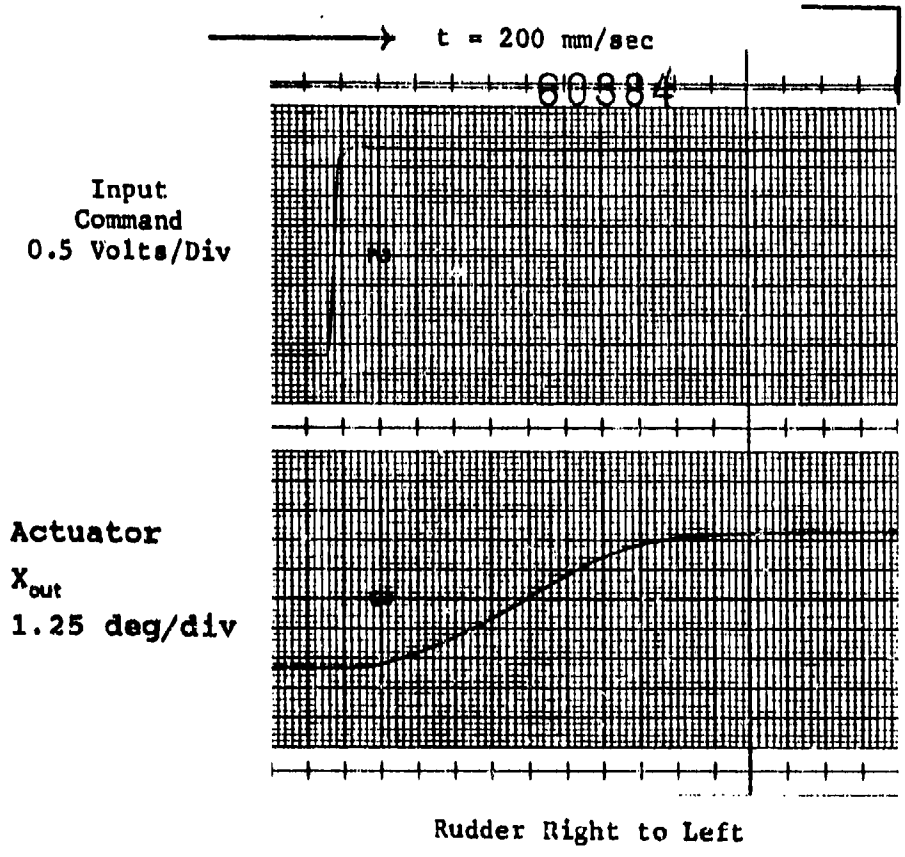

Rudder Right to Left

Figure III-18. Unloaded right-to-left saturation velocity.

IV. LOADED TEST RESULTS

Loaded Tests

General

Loaded testing was accomplished by utilizing the Multipurpose Actuation System Test Rig (MASTR) in the single-channel mode. The single load actuator was attached to the torque arm of the actuator's test fixture. The torque arm was short and stiff and enabled the angular travel of the arm to stay within the stroke limits of the load actuator. Figures III-19 and III-20 show the load actuator and test actuator assembly in the MASTR.

Load Application and Data Presentation

The maximum load applied to the test actuator was 13,200 in-lbs or 60 percent of the stall torque rating for the actuator. The loading actuator was attached to the torque arm at a distance of 15 inches from the rotation axis of the test actuator. The 60 percent of the 22,000 in-lb stall torque of the actuator corresponded to a load force of 880 lbs from the load actuator. To simulate an aerodynamic load, the load actuator was programed to apply the load proportional to deflection of the test actuator. Table III-2 lists the load versus actuator position for both the 60- and 30-percent aero load.

Two aerodynamic load profiles were used, one at 30 percent of the maximum load and one at 60 percent of the maximum load.

To simulate crosswind conditions, the test actuator was evaluated at positions of 7° left and 7° right rudder as well as 0° rudder for hysteresis and frequency response measurements. Transient response and saturation velocity measurements were made with a constant 13,200 in-lb loads (both aiding and opposing) applied.

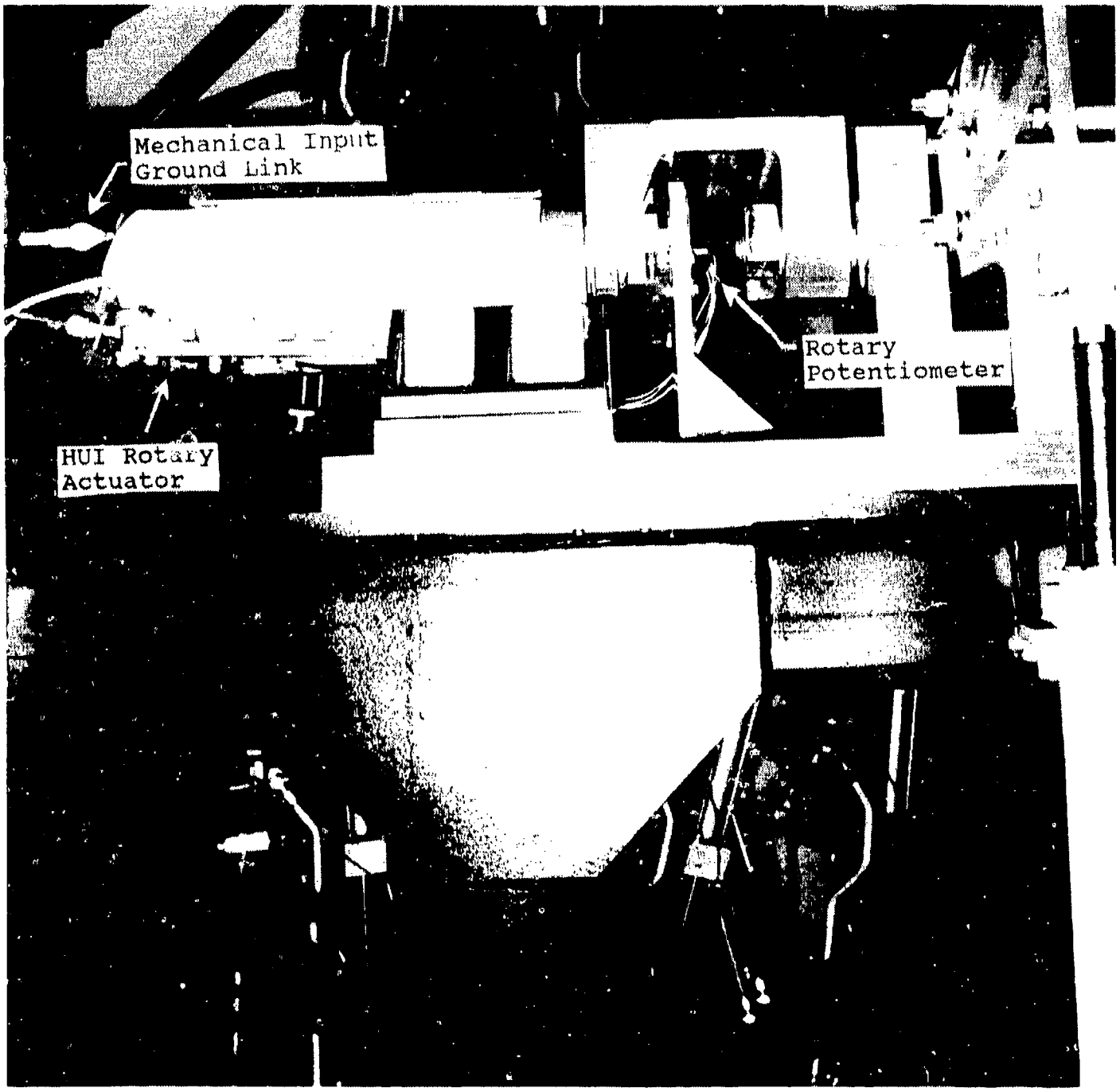

Figure III-19. Loaded test setup, View A.

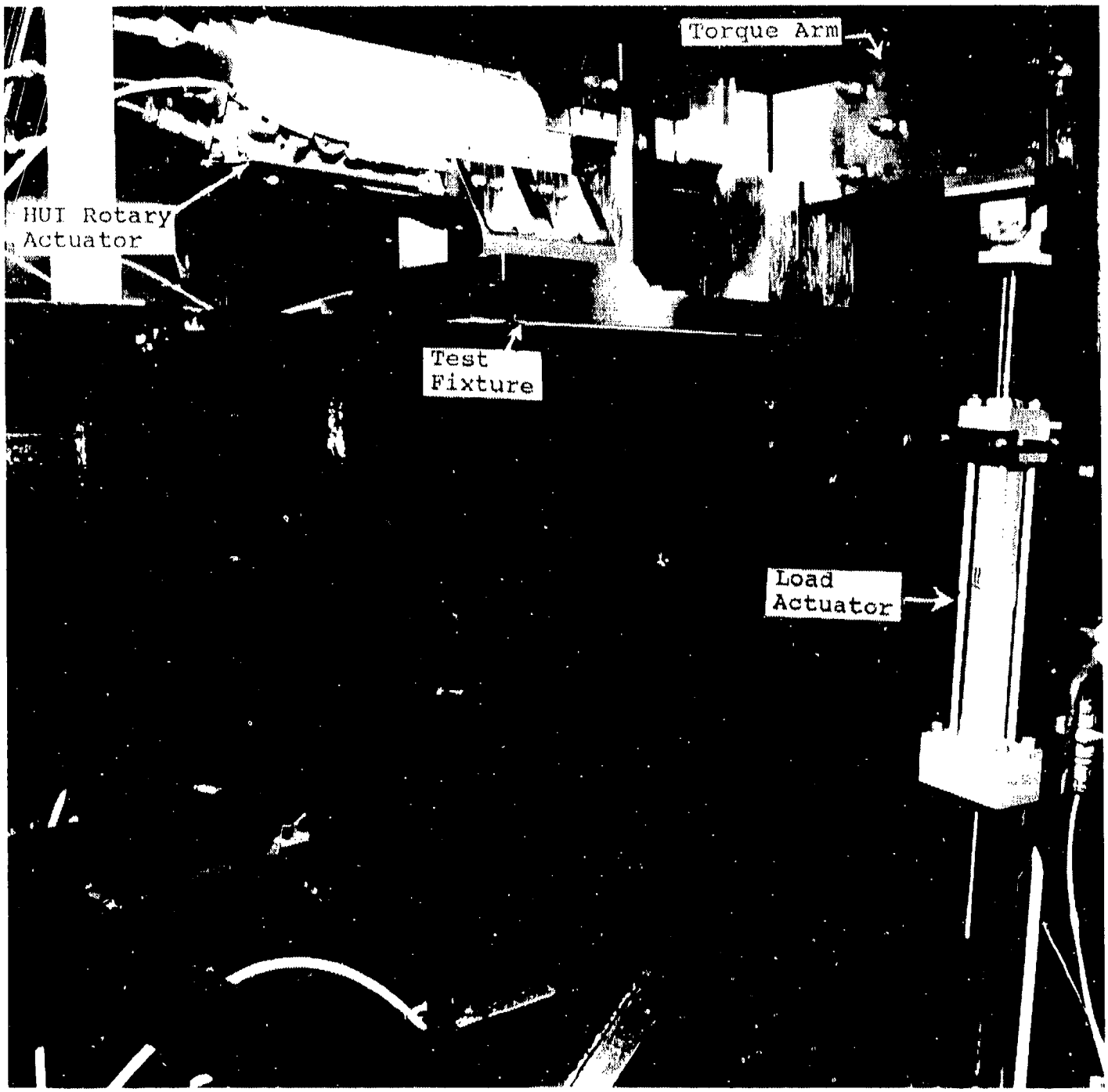

Figure III-20. Loaded test setup, View B.

Table III-2. Applied loads-versus-actuator position.

60-PERCENT LOAD

Actuator Position	In-lb Load
15°	13,200
10.5°	9,240
7°	6,160
3.5°	3,080
0°	0

30-PERCENT LOAD

Actuator Position	In-lb Load
15°	6,600
10.5°	4,620
7°	3,080
3.5°	1,540
0°	0

Loaded Linearity

Linearity tests were conducted with both 30 and 60 percent of maximum stall load applied to the specimen at maximum travel. Figure III-21 shows the results of the 30-percent load test, while Figure III-22 shows the 60-percent load test results.

As shown in Figure III-21, for a 30-percent load, the linearity deviation is 3.33 percent referred to maximum output motion. Hysteresis is 3.0 percent referred to the maximum output motion.

Referring to Figure III-22 for a 60-percent load, linearity deviation is 4.0 percent referred to the maximum output. Hysteresis is 3.33 percent referred to the maximum output motion.

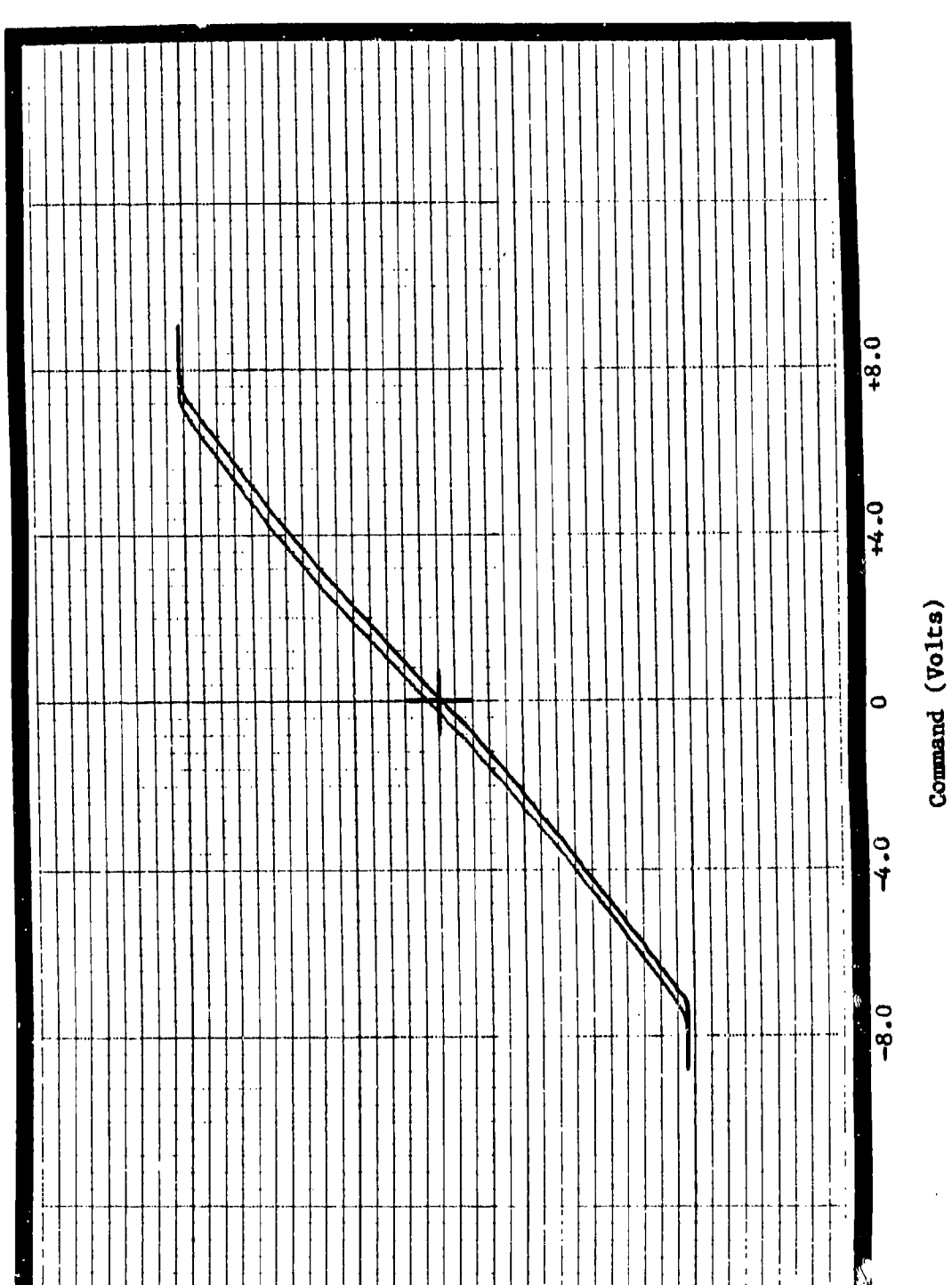

Figure III-21. Linearity - 30-percent aero load.

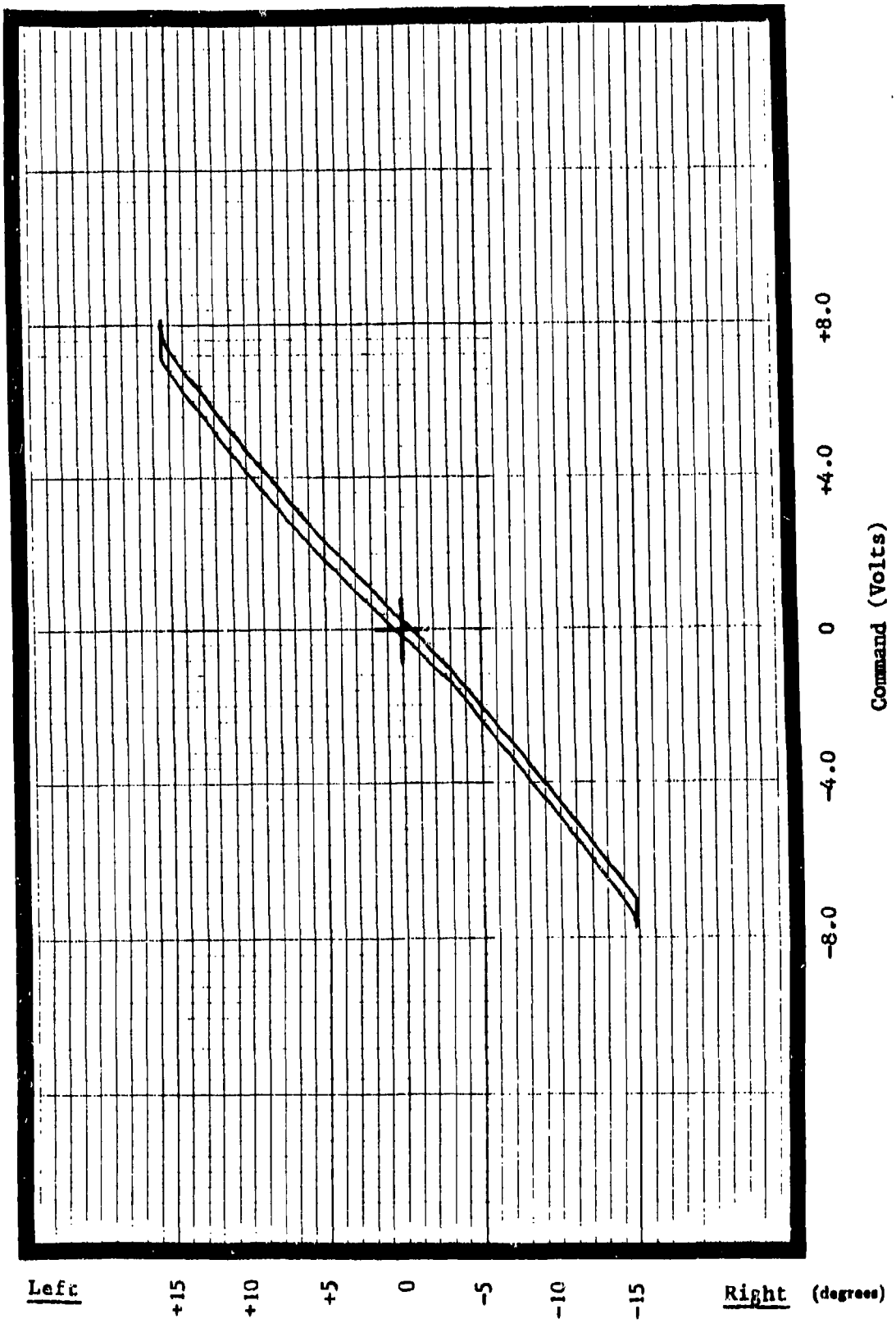

Figure III-22. Linearity - 60-percent aero load.

The aero loads increase the nonlinearity and hysteresis by nominally 20 to 30 percent more than the unloaded values. The 60-percent load causes an increase in hysteresis of 11 percent and nonlinearity of 20 percent over the 30-percent load.

Loaded Hysteresis

Figures III-23 through III-28 show data recorded during the loaded hysteresis testing. These plots were made with ± 1 percent inputs and ± 10 percent inputs at the 7° left rudder, 0° rudder, and 7° right rudder positions. Two aero load levels were applied, 30 and 60 percent. The figures illustrate the hysteresis data for the ± 1 and ± 10 percent inputs for the 30 percent aero loads. The data is representative of the 60 percent aero loads.

Figure III-23 is the data for 7° left rudder, 30 percent aero load, and ± 1 percent command test results. Hysteresis is 35 percent referred to the 0.500° output travel and 0.58 percent referred to maximum output travel.

Figure III-24 shows hysteresis at 0° rudder position with 30 percent load and 1 percent command. Hysteresis is 50 percent referred to the 0.488° output travel and 0.818 percent referred to maximum output travel.

Figure III-25 shows the hysteresis measurement for 7° right rudder, 30 percent aero load, and ± 1 percent command. Hysteresis is 61.2 percent referred to the 0.238° output travel and 0.48 percent referred to maximum output travel.

Figure III-26 shows the hysteresis data for 7° left rudder position, 30 percent load and ± 10 percent command. Hysteresis is 4.4 percent referred to the 5.7° output travel and 0.84 percent referred to maximum output travel.

Figure III-27 shows the hysteresis measurement for 0° right rudder, 30 percent load and ± 10 percent command. Hysteresis is 8.48 percent referred to the 5.6° output travel and 1.58 percent referred to maximum output travel.

Figure III-28 shows the hysteresis measurement for 7° right rudder, 30 percent and ± 10 percent command. Hysteresis is 9.5 percent referred to the 5.0° output travel and 1.58 percent referred to maximum output travel.

Table III-3 lists the results of the hysteresis tests with applied loads.

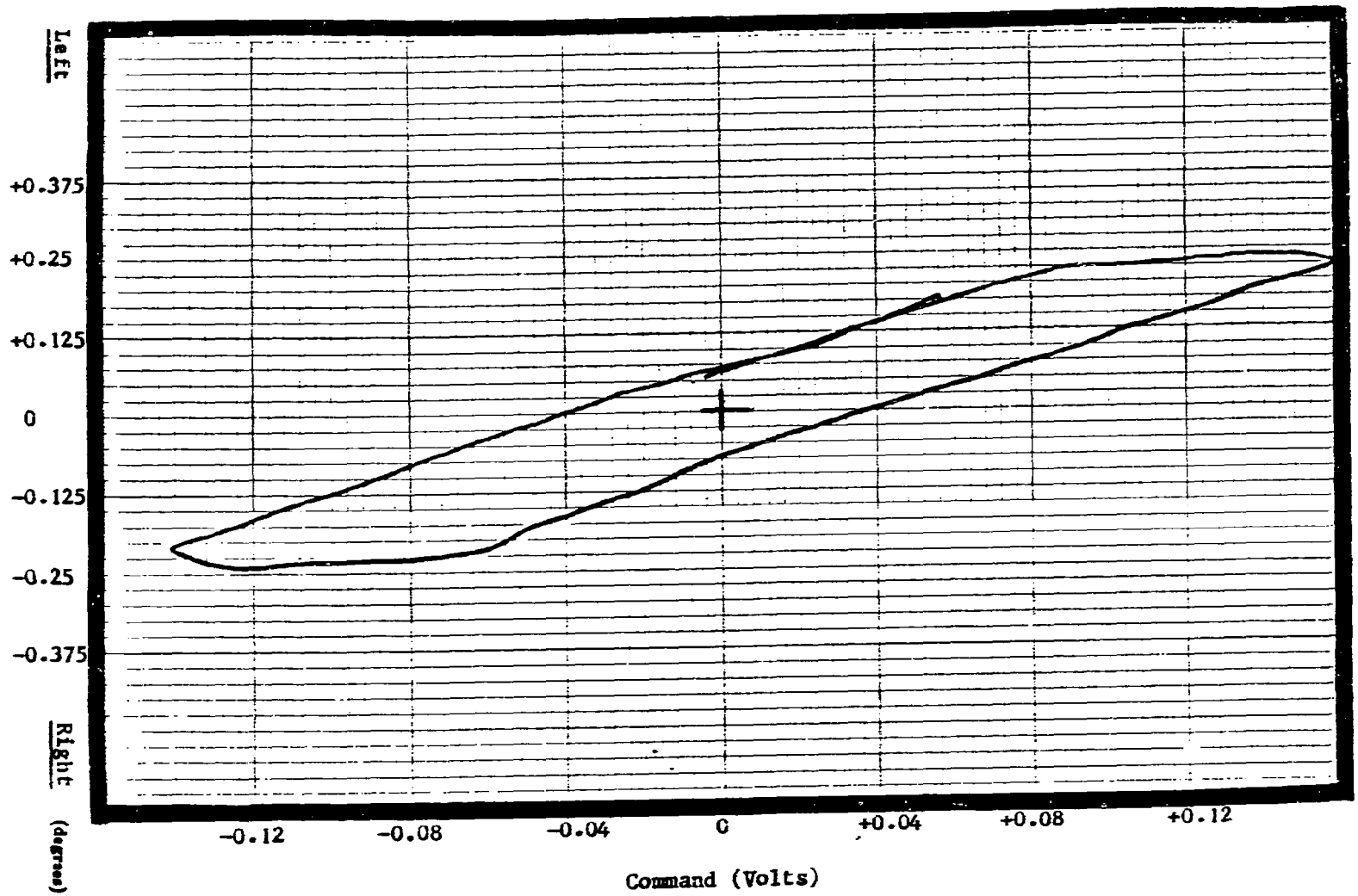

Figure III-23. Hysteresis, ± 1 percent command, 7° left rudder, 30-percent aero load.

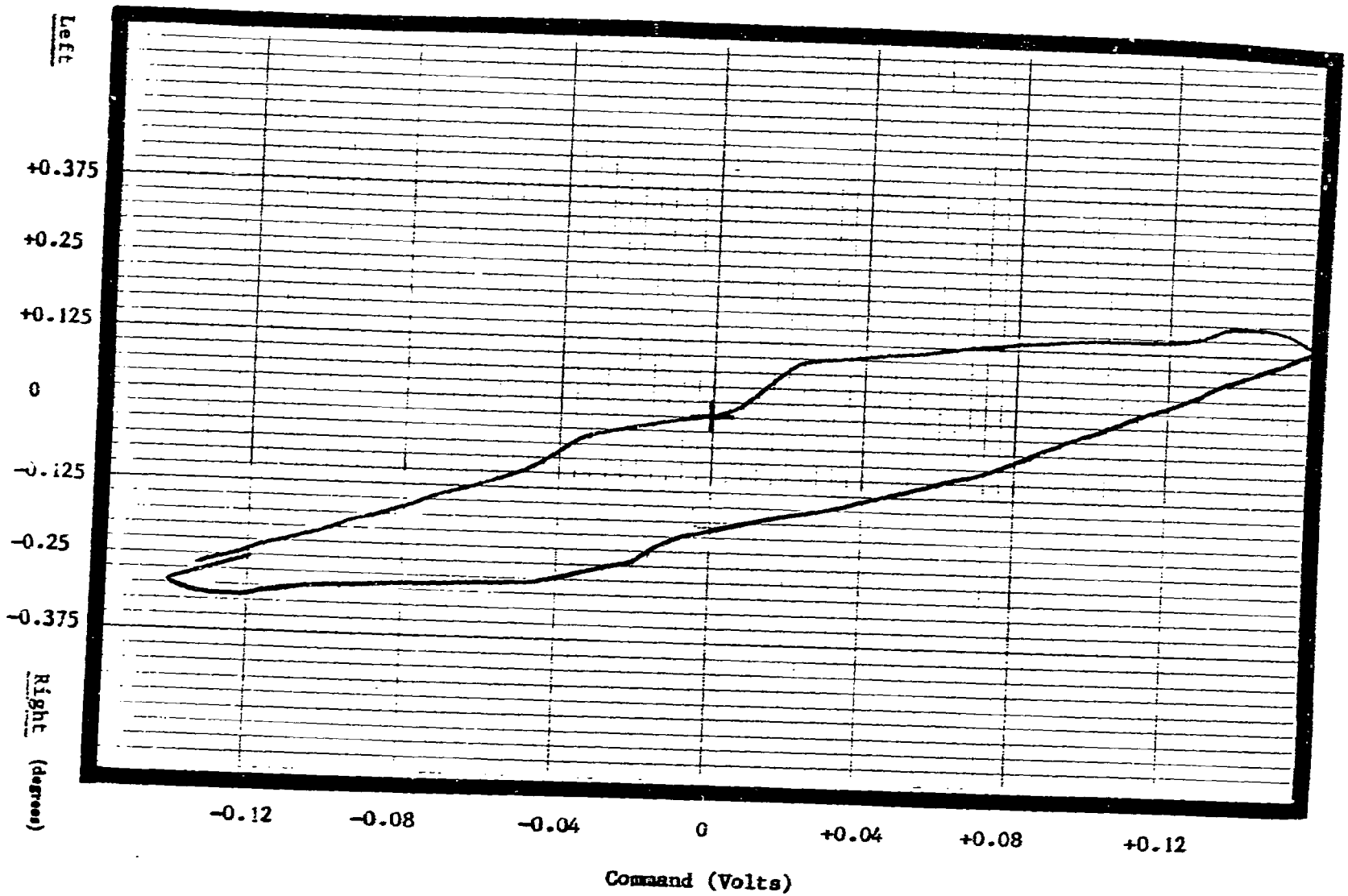

Figure III-24. Hysteresis, ± 1 percent command, 0° rudder, 30-percent aero load.

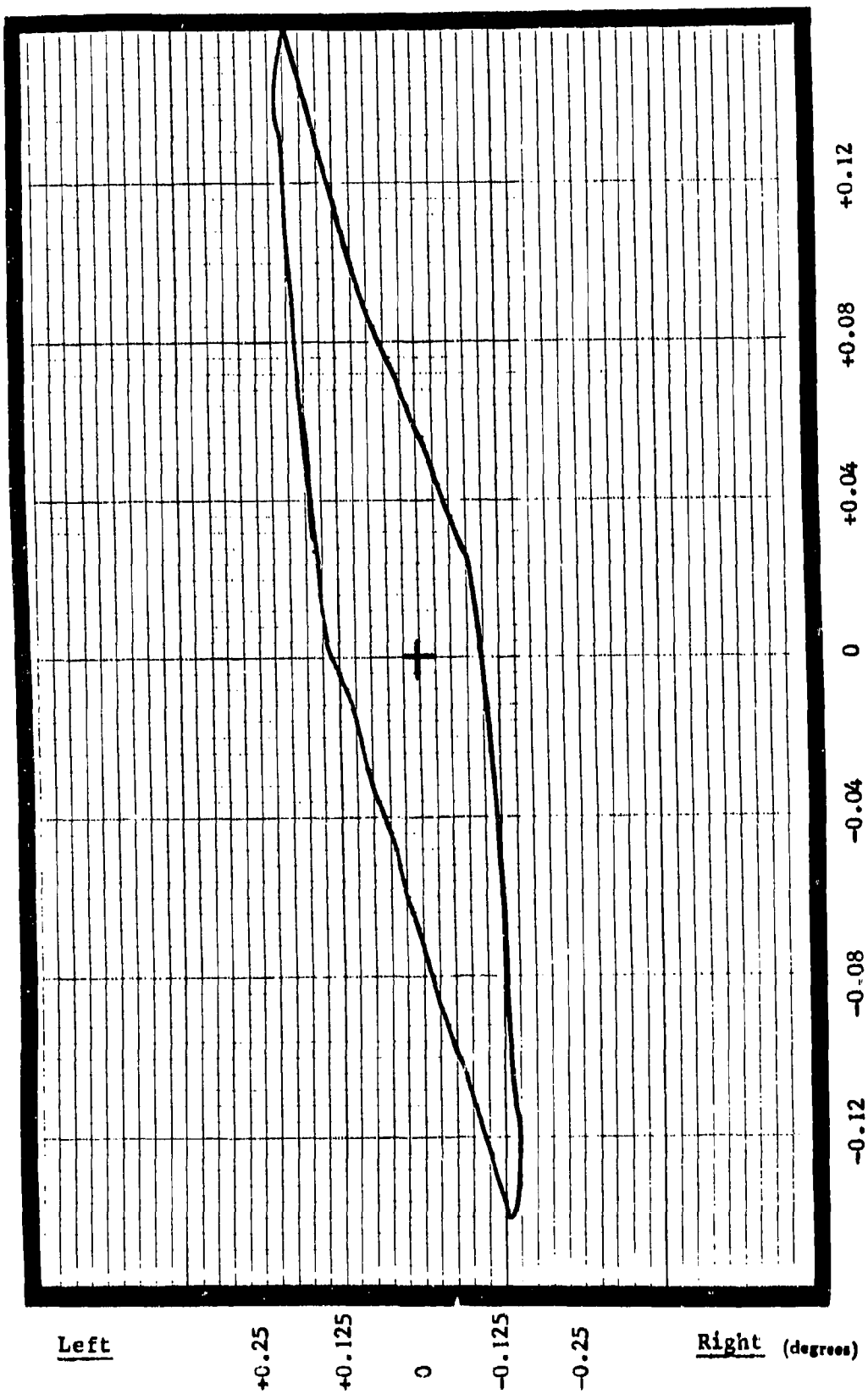

Figure III-25. Hysteresis, ± 1 percent command, 7° right rudder, 30-percent aero load.

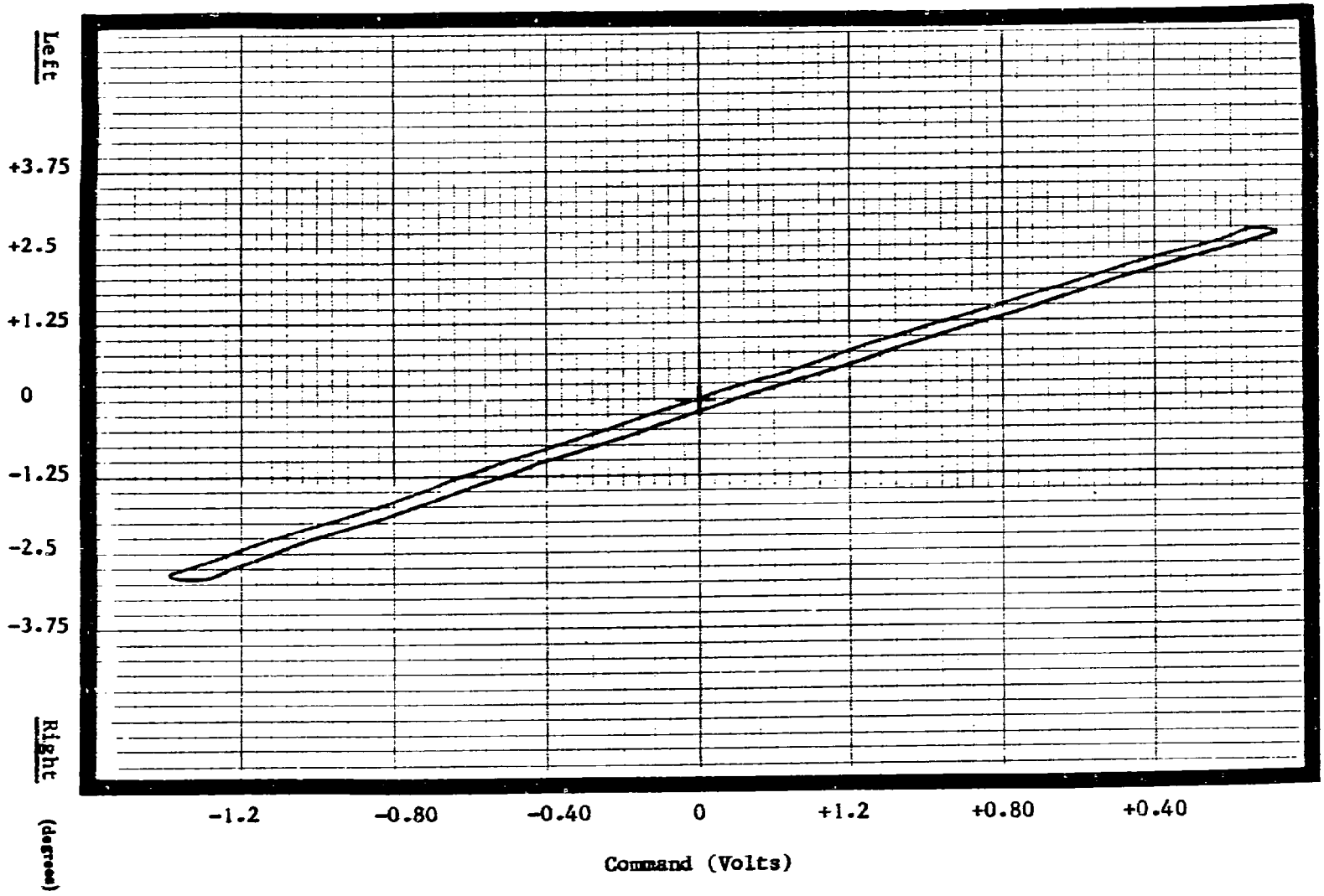

Figure III-26. Hysteresis, ± 10 percent command, 7° left rudder, 30-percent aero load.

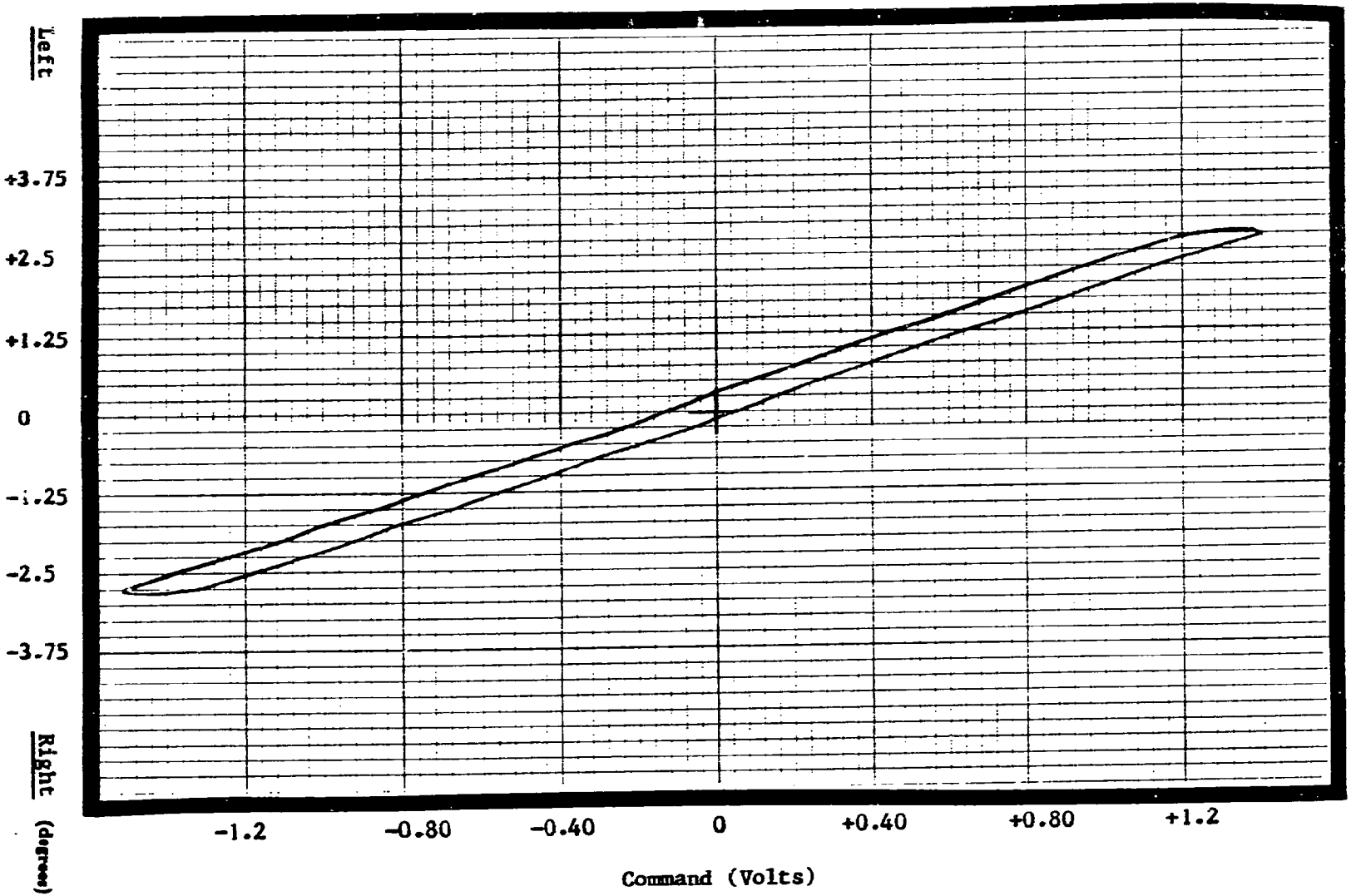

Figure III-27. Hysteresis, ± 10 percent command, 0° rudder, 30-percent aero load.

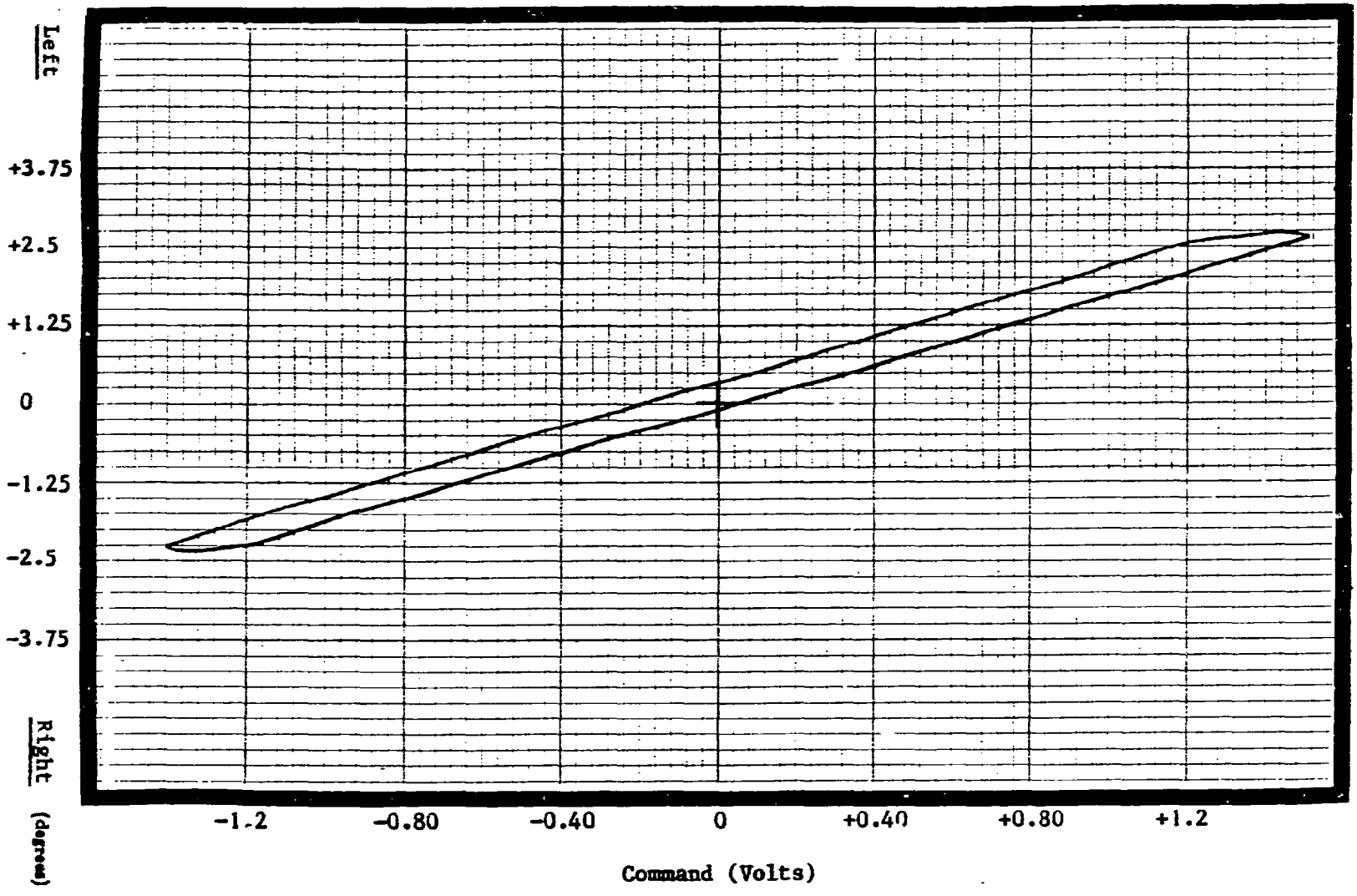

Figure III-28. Hysteresis, ± 10 percent command, 7° right rudder, 30-percent aero load.

Table III-3. Results of hysteresis tests with applied loads.

Command %	Load %	Rudder Position (°)	Hysteresis as % of Output Travel	Hysteresis as % of Max. Travel	Rudder Travel at Command Level (°)
± 1.0	30.0	7° left	35.0	0.58	0.500
± 1.0	30.0	0°	50.0	0.488	0.81
± 1.0	30.0	7° right	61.2	0.48	0.238
± 1.0	60.0	7° left	21.6	0.42	0.578
± 1.0	60.0	0°	29.1	0.54	0.558
± 1.0	60.0	7° right	62.5	0.42	0.20
± 10.0	30.0	7° left	4.4	0.84	5.7
± 10.0	30.0	0°	8.48	1.58	5.60
± 10.0	30.0	7° right	9.5	1.58	5.00
± 10.0	60.0	7° left	4.44	0.83	5.6
± 10.0	60.0	0°	3.8	0.73	5.80
± 10.0	30.0	7° right	6.70	1.29	5.6

Loaded Frequency Response

The frequency response measurements were made with the test actuator operating in three positions: 7° left rudder, 0° rudder and 7° right rudder. The load system for all the frequency response measurements was programmed for the aero load of 60 percent of stall at 15 degrees deflection from 0° position as previously listed in Table III-2.

Figures III-29 through III-40 are plots of the amplitude ratio and phase angle for each of the six test conditions. Table III-4 lists 3 frequencies for each test condition. The frequencies correspond to where the amplitude ratio is -3 dB, where the phase angle is -45° and where the phase angle is -90°.

Note that the frequency response measurements with the ± 1 percent command input show a better response for the 7° right position than for the 0° or 7° left position. This is probably due to threshold and hysteresis effects on the response measurements at the low input level. The irregularity of the amplitude response at the 1 percent input level also indicates nonlinearity effects. The frequency response at ± 3 percent command input provides a more consistent trend. The frequency response at the 0° position is slightly greater than at either the 7° right or left rudder positions.

Table III-4. Results of frequency response, loaded testing.

Command Input	Load %	Rudder Position	-3 db Frequency Hz	Phase Shift -45° Hz	-90°Hz
± 1.0	60.0	7° right	5.18	2.48	5.44
± 1.0	60.0	0°	3.18	1.92	4.79
± 1.0	60.0	7° left	2.26	1.64	4.07
± 3.0	60.0	7° right	3.35	1.87	4.15
± 3.0	60.0	0°	4.81	2.28	5.28
± 3.0	60.0	7° left	3.61	2.03	3.98

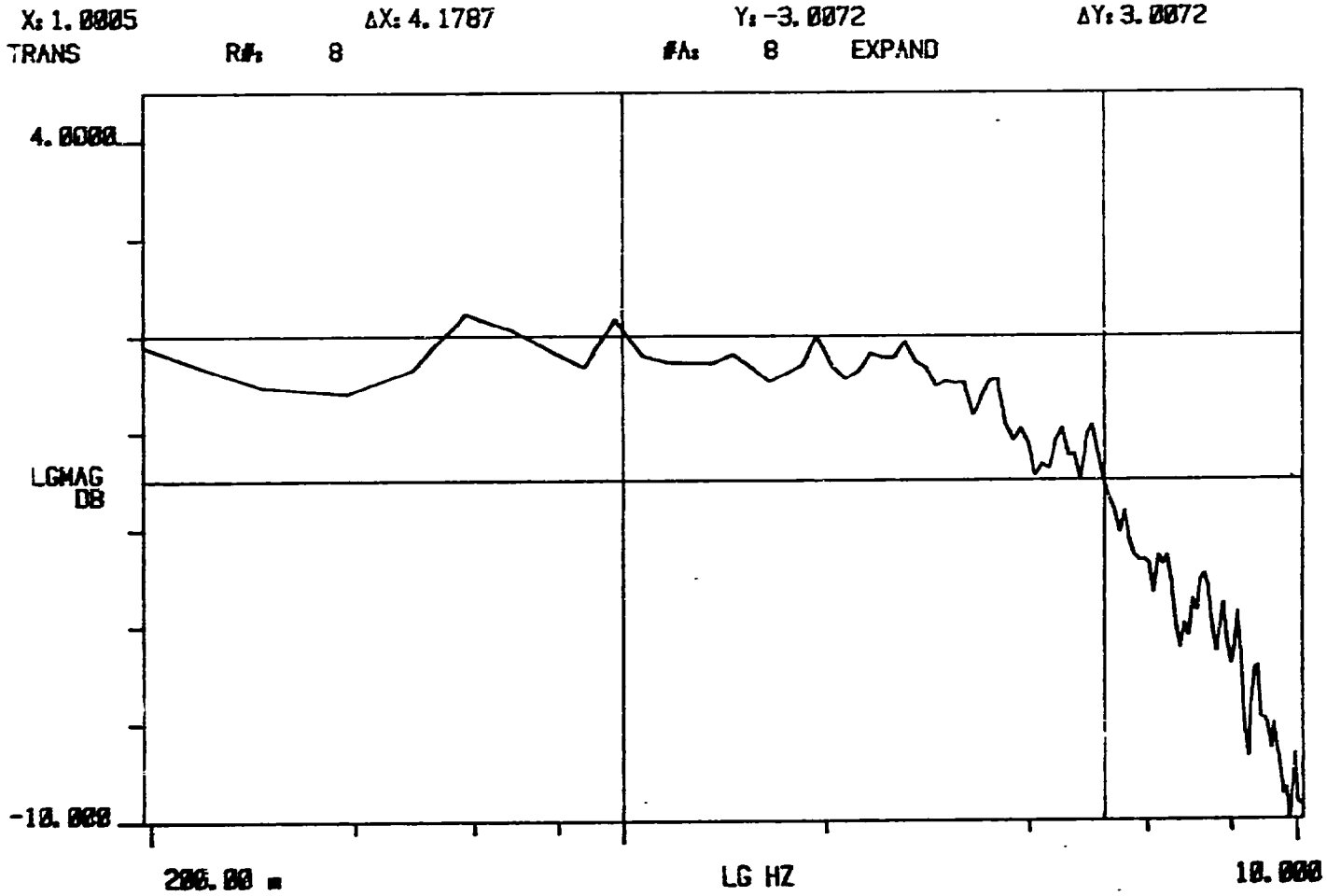

Figure III-29. Amplitude response: 7° right rudder, 60-percent aero load, ± 1 percent command.

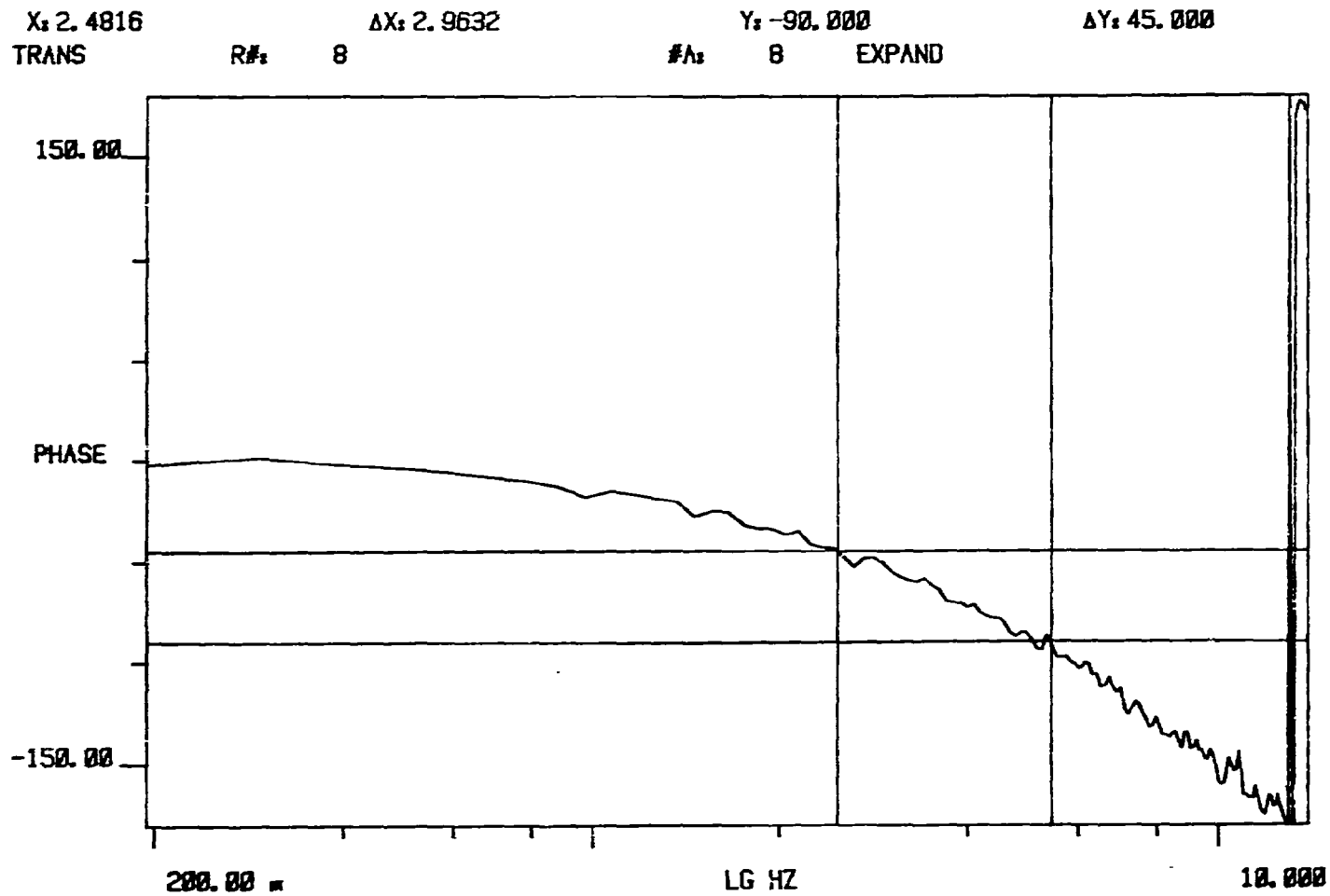

Figure III-30. Phase response: 7° right rudder, 60-percent aero load, ± 1 percent command.

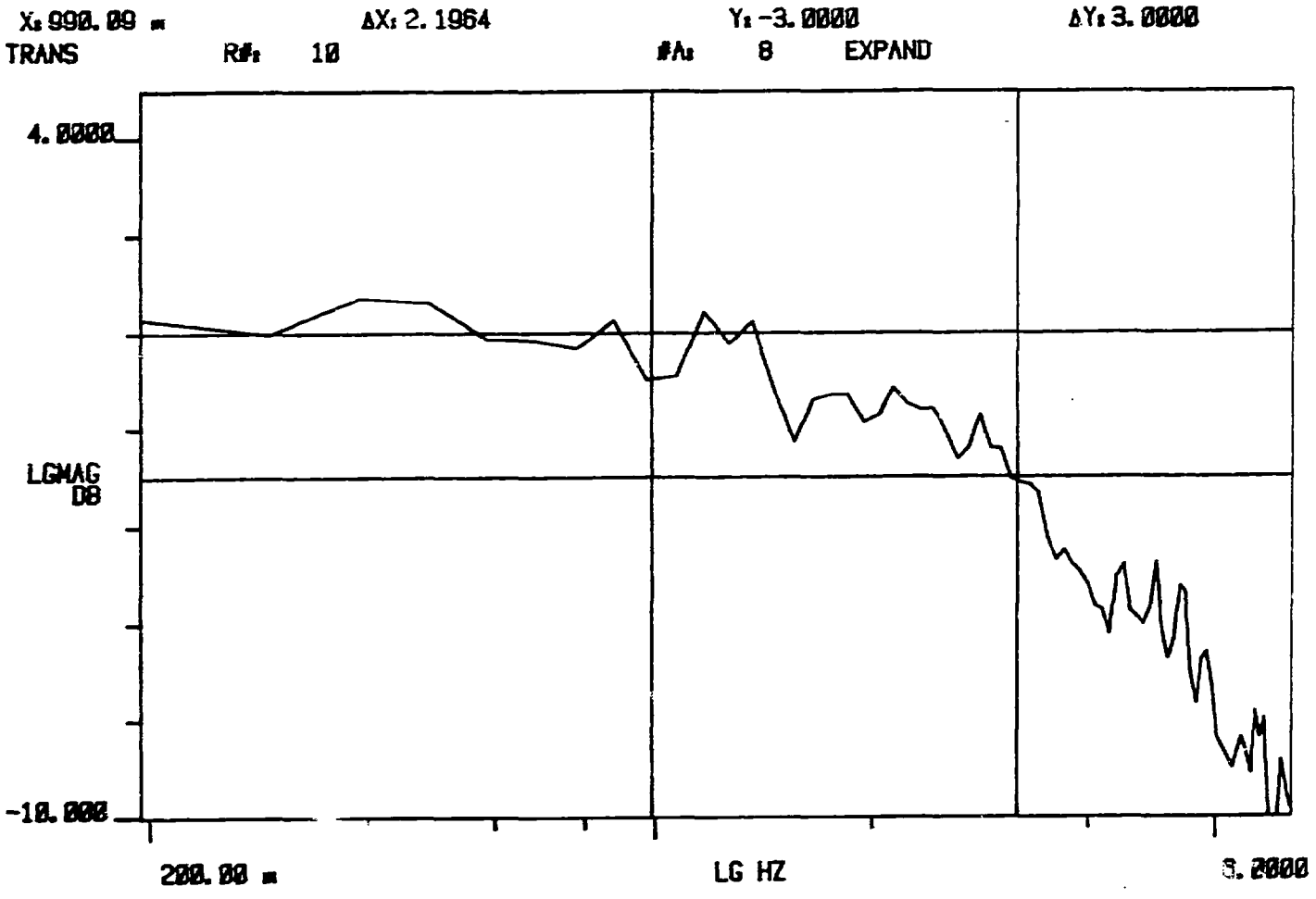

Figure III-31. Amplitude response: rudder centered, 60-percent aero load, ± 1 percent command.

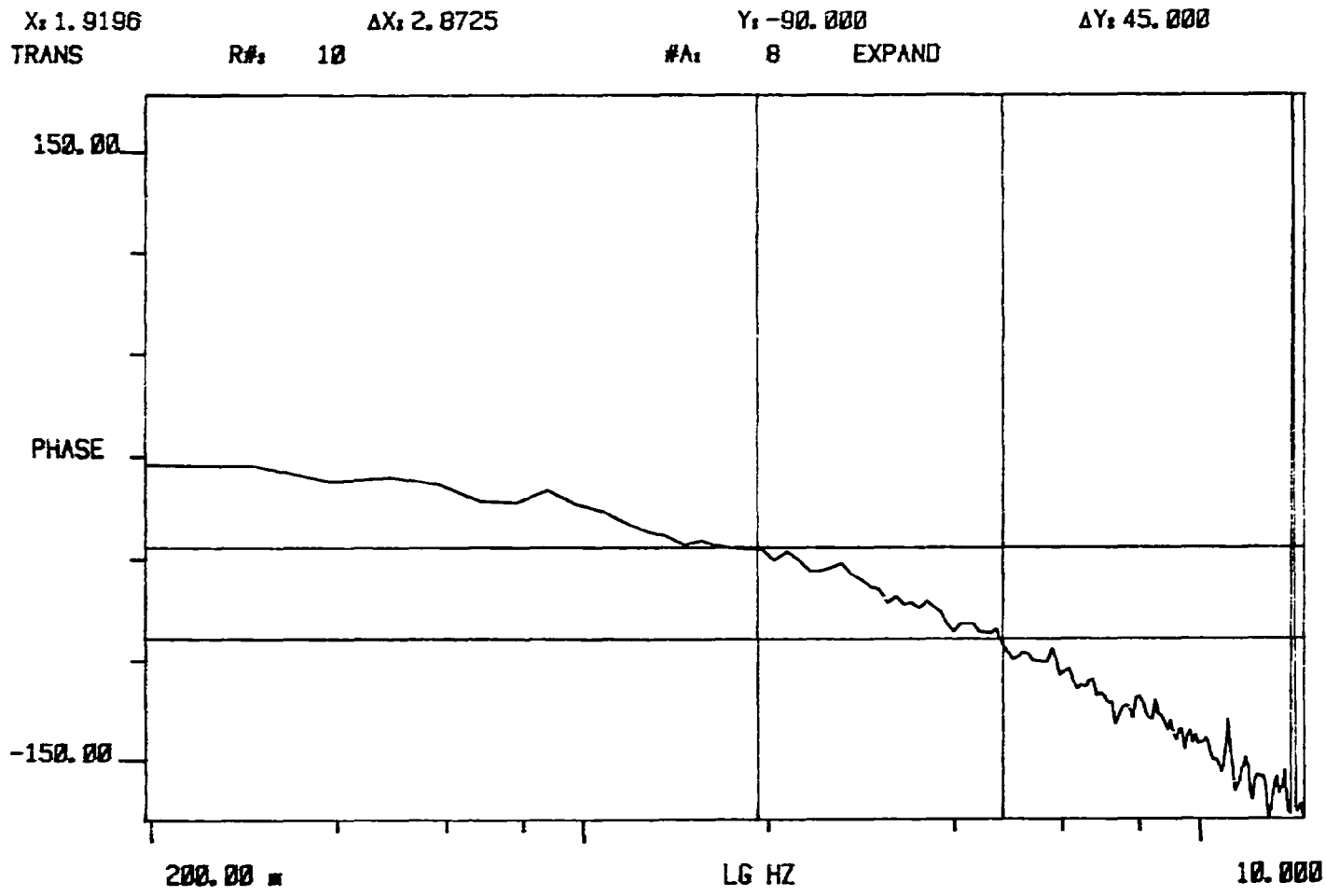

Figure III-32. Phase response: rudder centered, 60-percent aero load, ± 1 percent command.

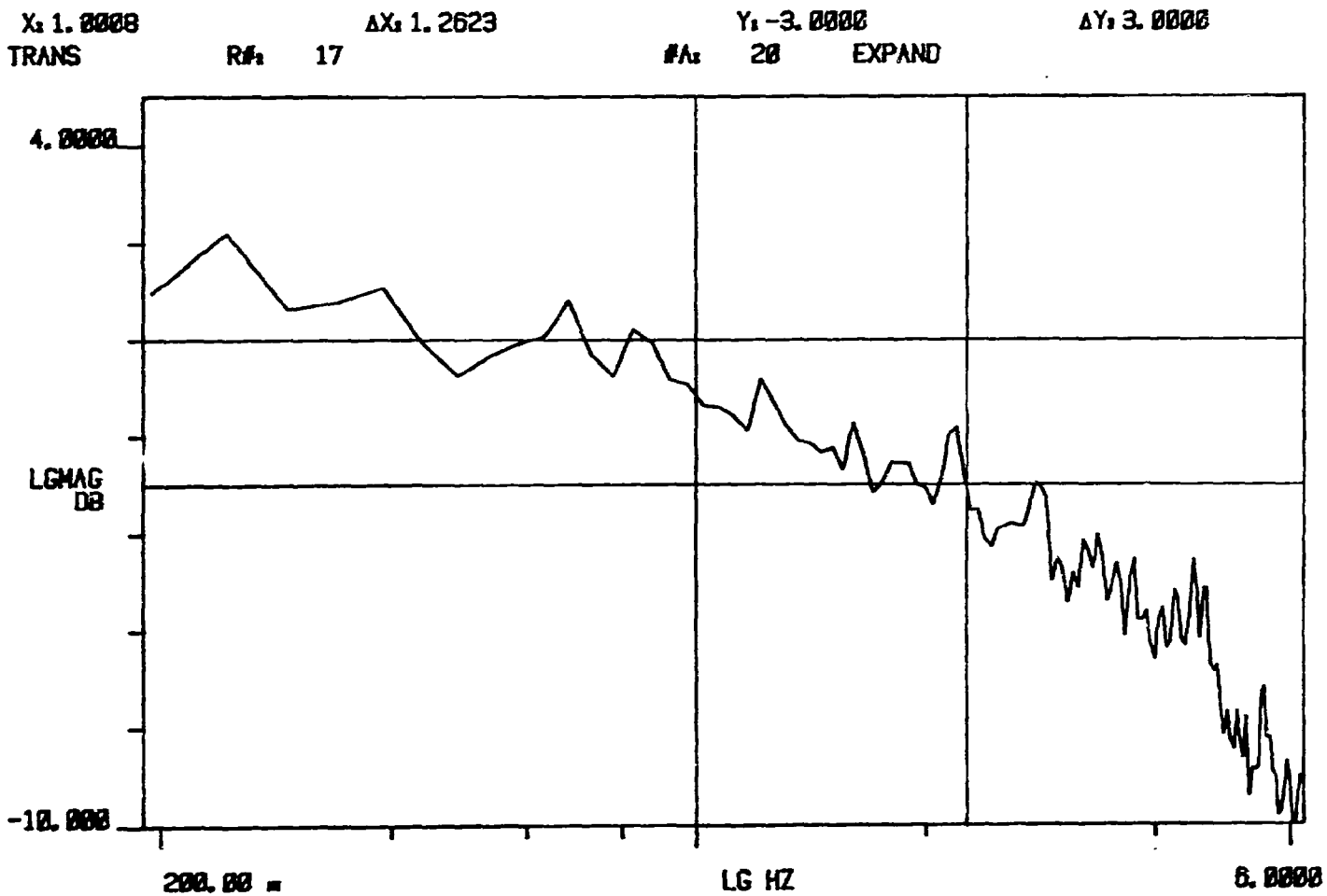

Figure III-33. Amplitude response: 7° left rudder, 60-percent aero load, ± 1 percent command.

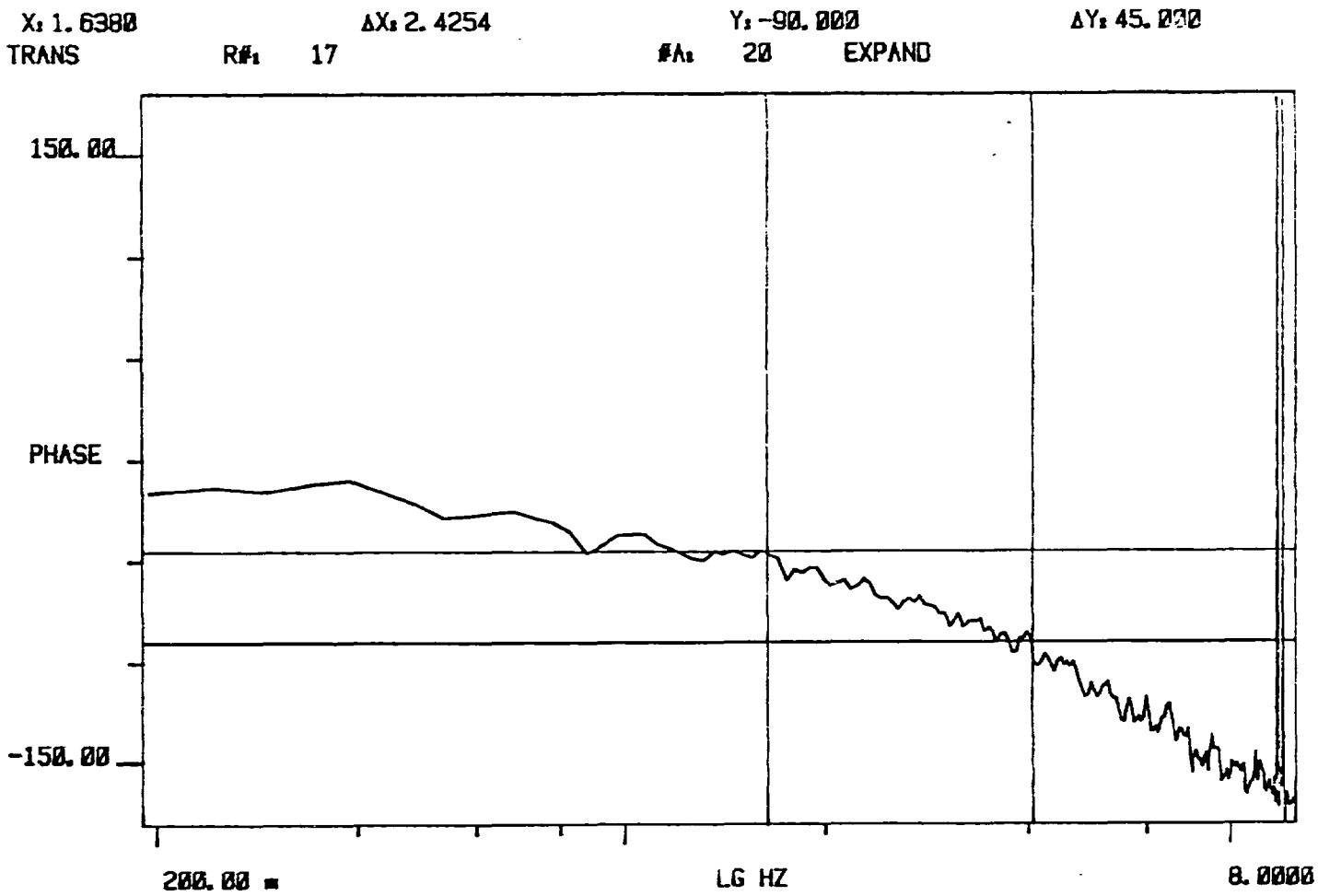

Figure III-34. Phase response: 7° left rudder, 60-percent aero load, ± 1 percent command.

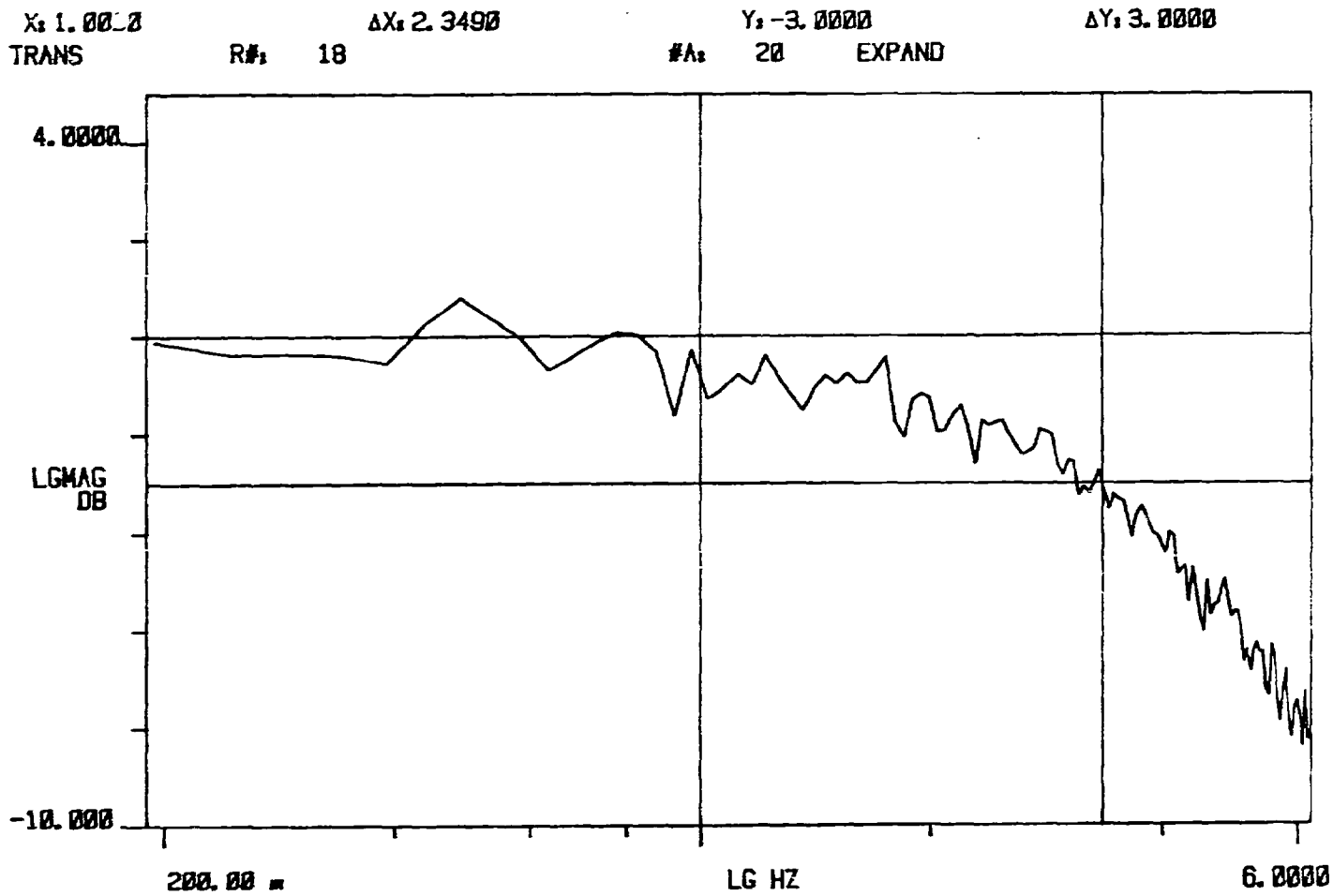

Figure III-35. Amplitude response: 7° right rudder, 60-percent aero load, ± 3 percent command.

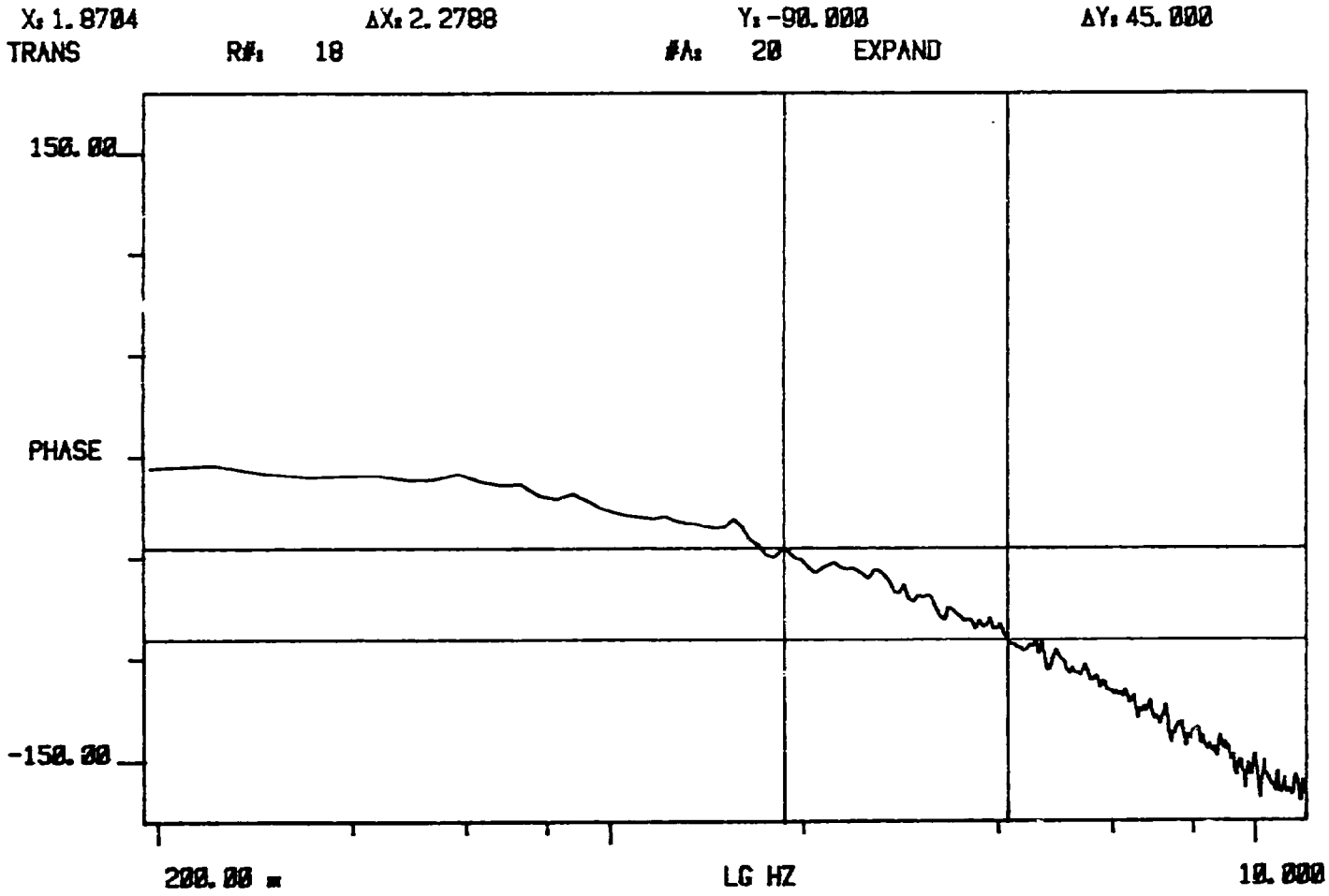

Figure III-36. Phase response: 7° right rudder, 60-percent aero load, ± 3 percent command.

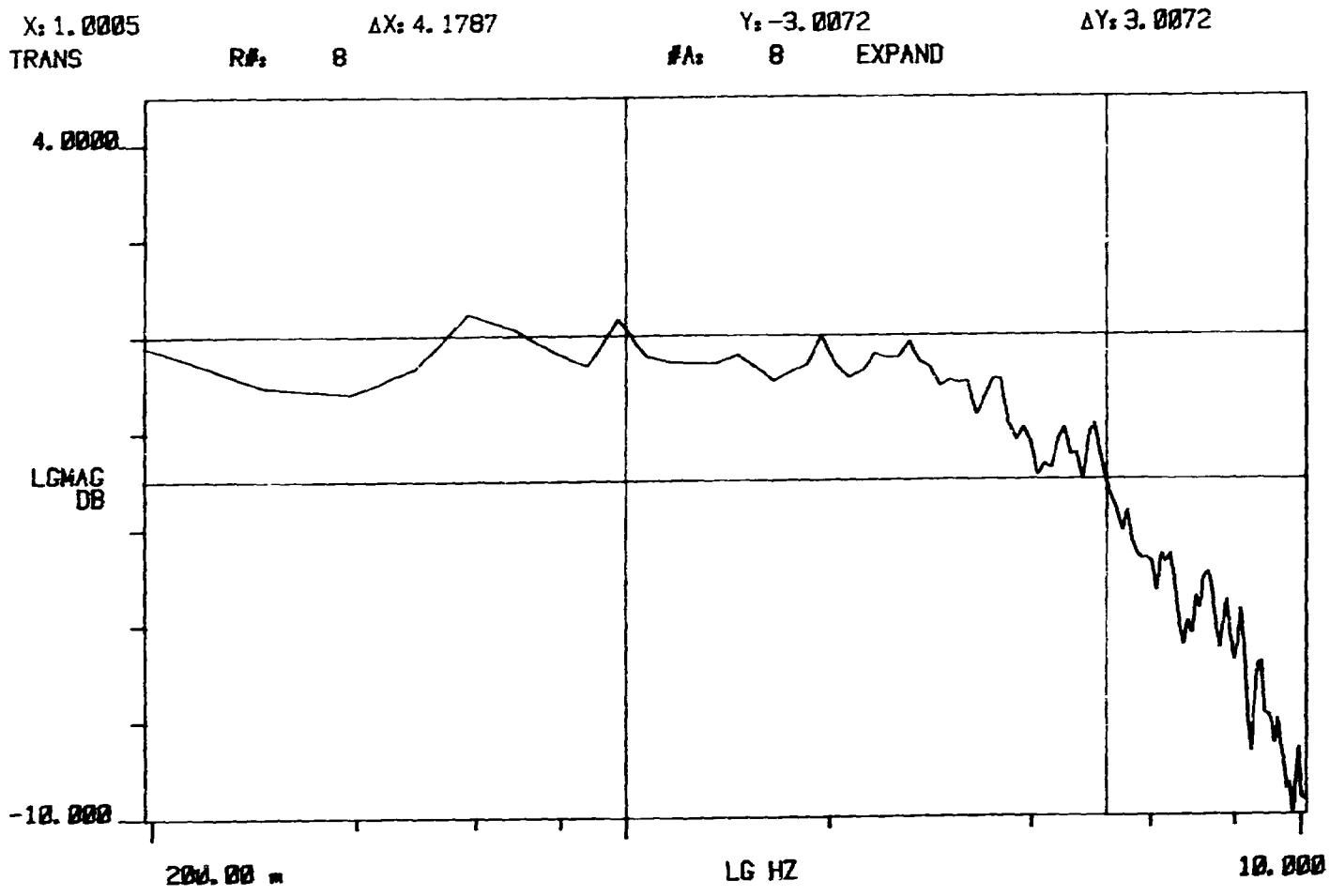

Figure III-37. Amplitude response: rudder centered, 60-percent aero load, ± 3 percent command.

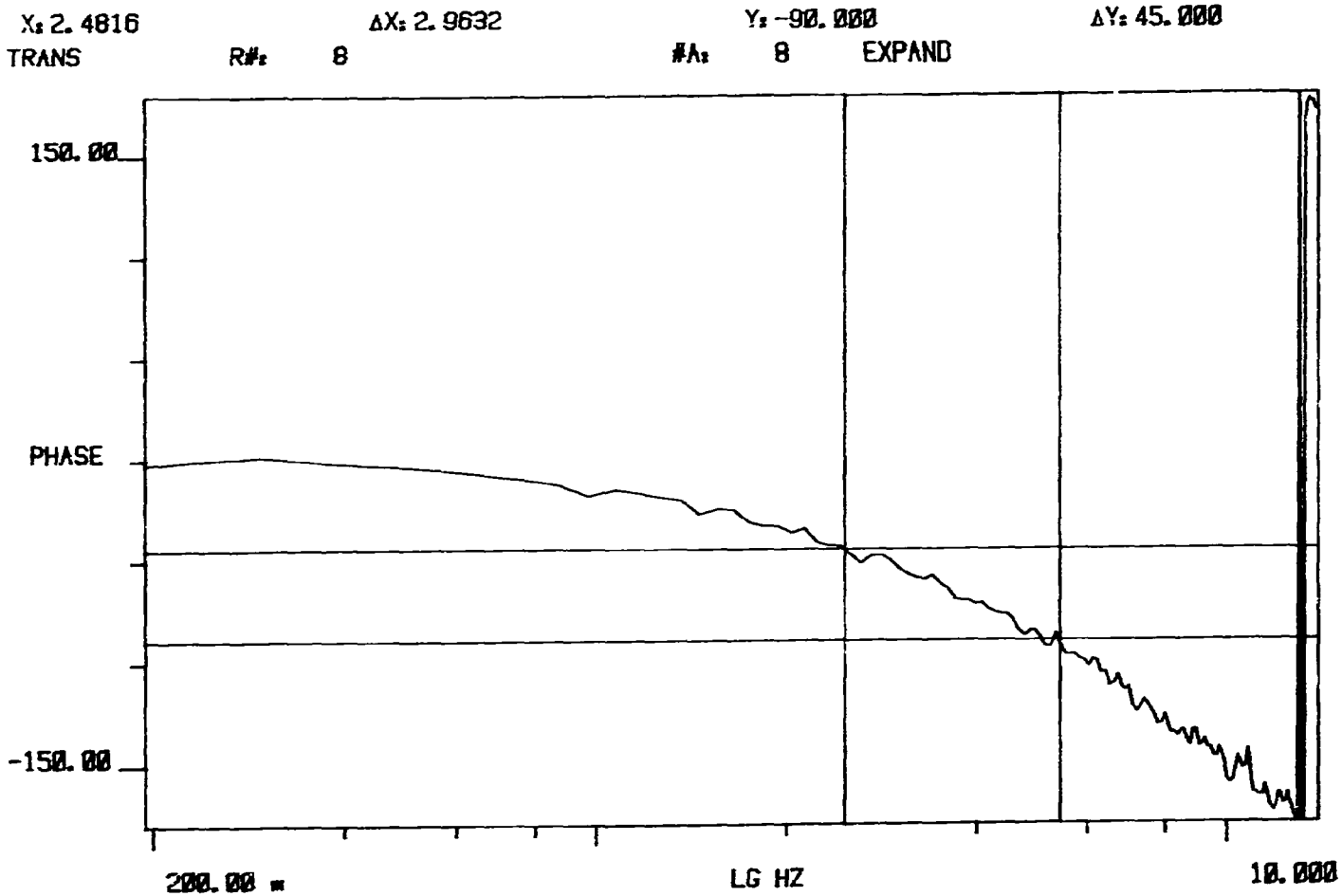

Figure III-38. Phase response: rudder centered, 60-percent aero load, ± 3 percent command.

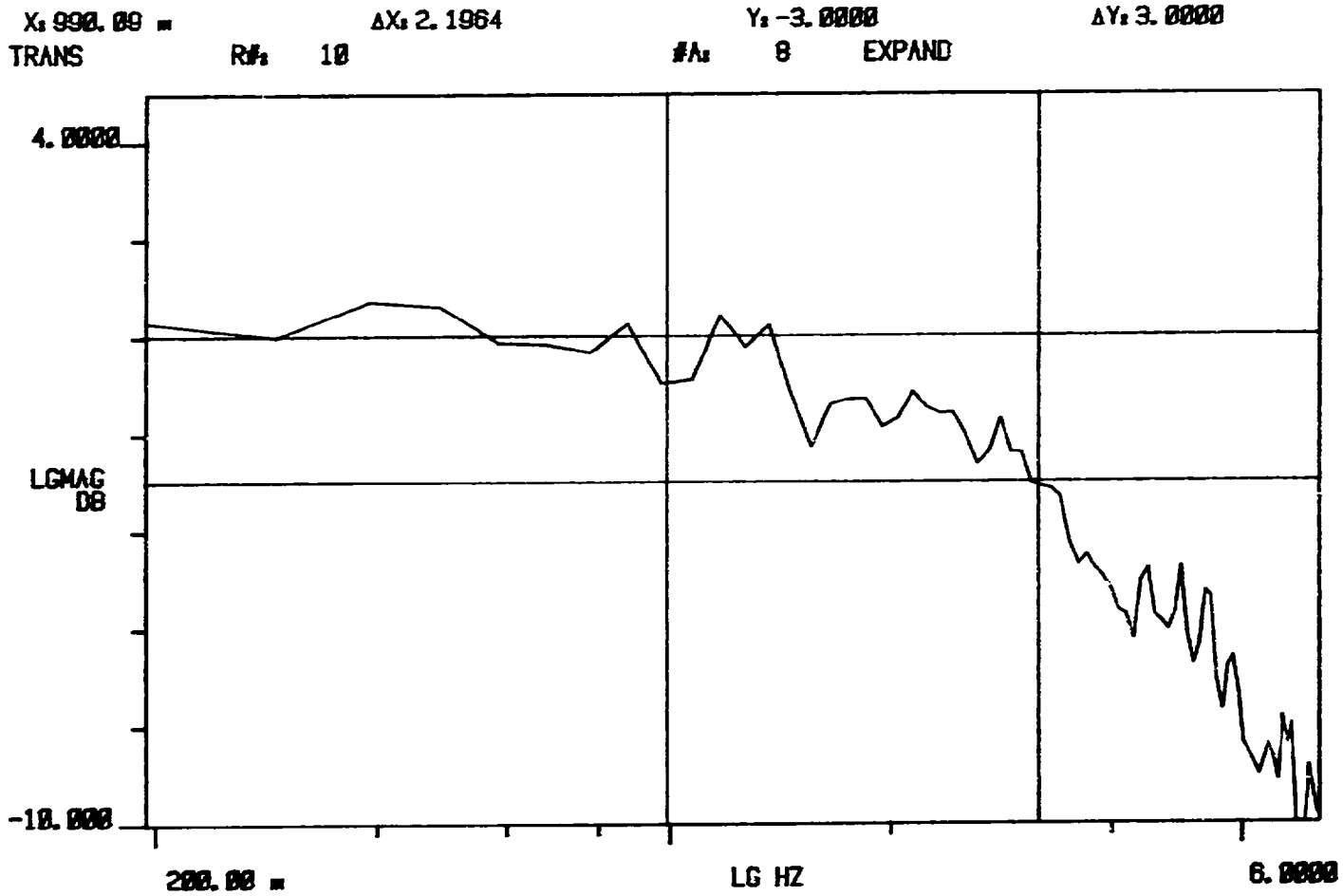

Figure III-39. Amplitude response: 7° left rudder, 60-percent aero load, ± 3 percent command.

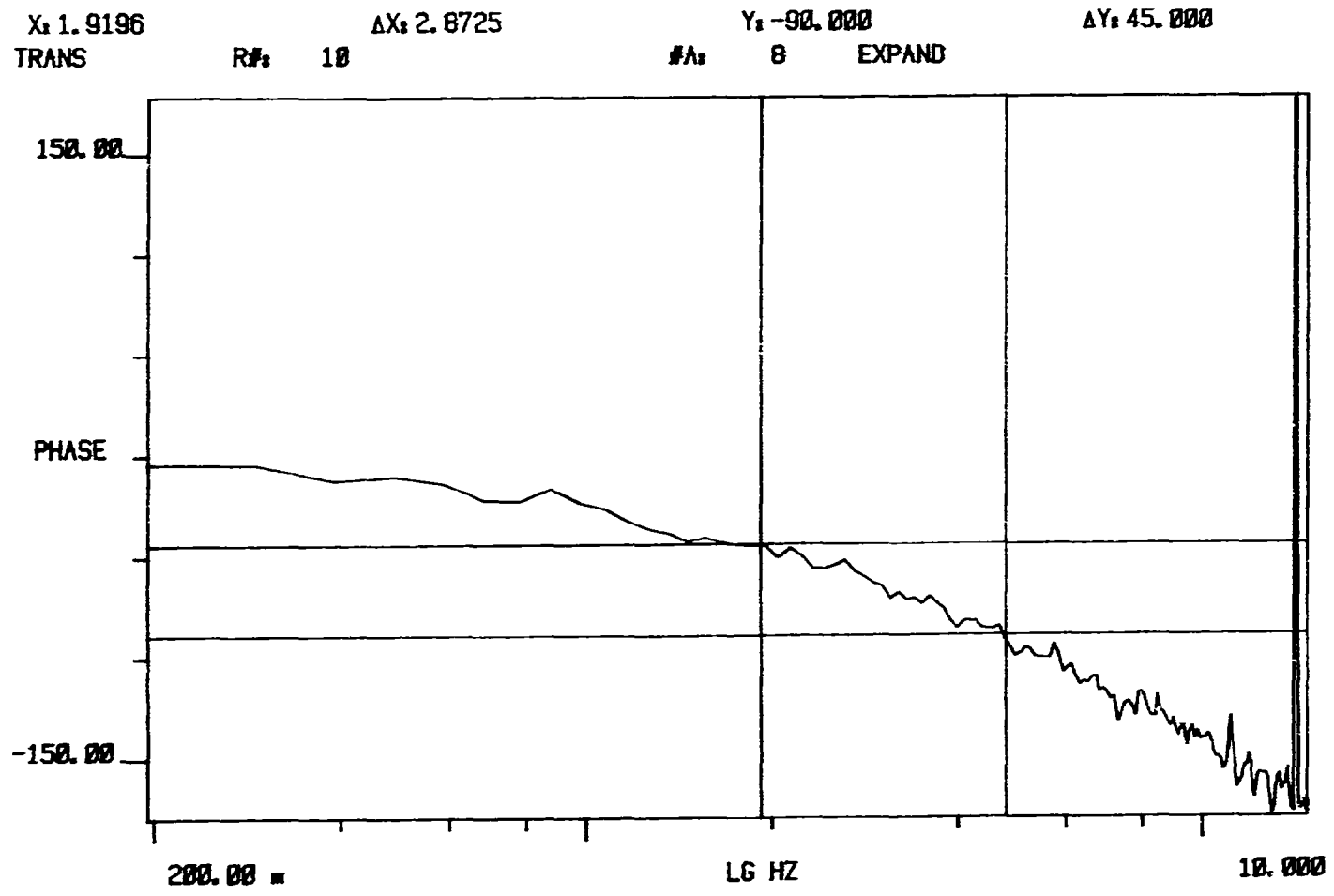

Figure III-40. Phase response: 7° left rudder, 60-percent aero load, ± 3 percent command.

Loaded Static Threshold

The static threshold tests were conducted around the 0° rudder position with a 13,200 in-lb load applied uni-directionally, first from the left side of the actuator, then from the right side. This load remained constant regardless of actuator position.

Figure III-41 shows the loaded static threshold data with the load applied from the left side of the actuator. The static threshold level is ± 0.012 volts for this condition. This represents 0.171 percent of the maximum input command level of ± 7 volts.

Figure III-42 shows loaded static threshold data with the load applied from the right side of the actuator. The static threshold level is 0.011 volts for this condition and represents 0.157 percent of the maximum input command of ± 7 volts.

Loaded Dynamic Threshold

The dynamic threshold tests were conducted around the 0° rudder position with a 13,200 in-lb load applied uni-directionally to the output shaft of the specimen actuator. Load application was first from the left side of the actuator, then from the right side. This load remained constant regardless of actuator position.

Figure III-43 shows the data recorded during test with the load application from the left side. The dynamic threshold level is ± 0.030 volts for this condition which represents 0.28 percent of the maximum input command of ± 7 volts.

Figure III-44 shows data recorded during testing with application of the load from the fight side of the actuator. The dynamic threshold level is ± 0.019 volts which represents 0.27 percent of the input command level of ± 7 volts.

Note that there is a slow shift of the output position once the threshold value is exceeded. For both load directions, the output motion tracks the input waveform. The loaded dynamic threshold values agree with the unloaded test data previously obtained, indicating that load (at least the value used) did not affect the dynamic threshold value.

TEST DATA

DATE: 4 DEC 86

TEST ITEM: Hydraulic Units, Inc.
F-15 Rotary Rudder Servoactuator
P/N 3U3151-5E; S/N 2376

TEST: Static threshold - loaded
SURFACE POSITION: 0°
LOAD: 13,200 in-lb LEFT

----- t = 5 div/sec ------>

Input Command

.002 volts/division

x_{out}

.005 degrees/division

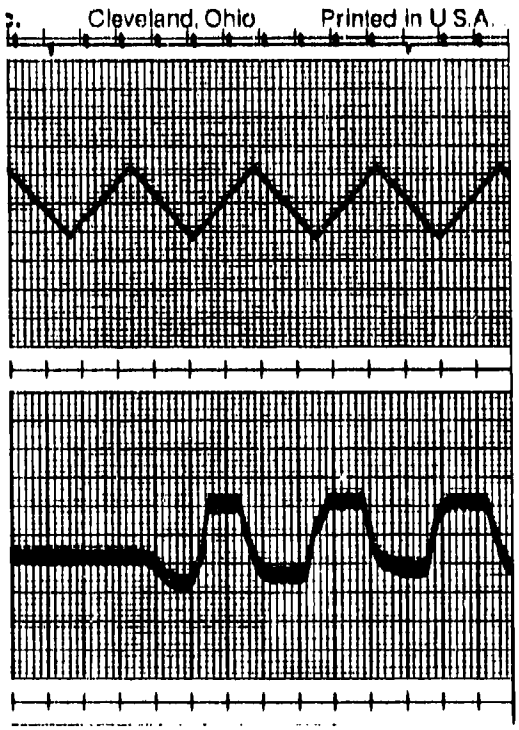

Figure III-41. Static threshold, loaded from the left.

TEST DATA

DATE: 4 DEC 86

TEST ITEM: Hydraulic Units, Inc.
F-15 Rotary Rudder Servoactuator
P/N 3U3151-5E; S/N 2376

TEST: Static threshold - loaded
SURFACE POSITION: 0°
LOAD: 13,200 in-lb RIGHT

----- t = 5 div/sec ------>

Input Command

.002 volts/division

X_{out}

.005 degrees/division

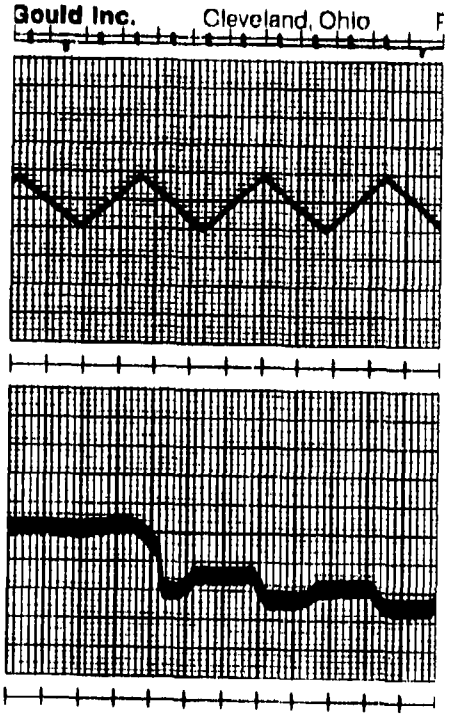

Figure III-42. Static threshold, loaded from the right.

TEST DATA

DATE: 3 DEC 86

TEST ITEM: Hydraulic Units, Inc.
F-15 Rotary Rudder Servoactuator
P/N 3U3151-5E; S/N 2376

TEST: Dynamic threshold - loaded
SURFACE POSITION: 0°
LOAD: 13,200 in-lb LEFT

----- t = 20 div/sec ------>

Input Command

.002 volts/division

X_{cut}

.005 degrees/division

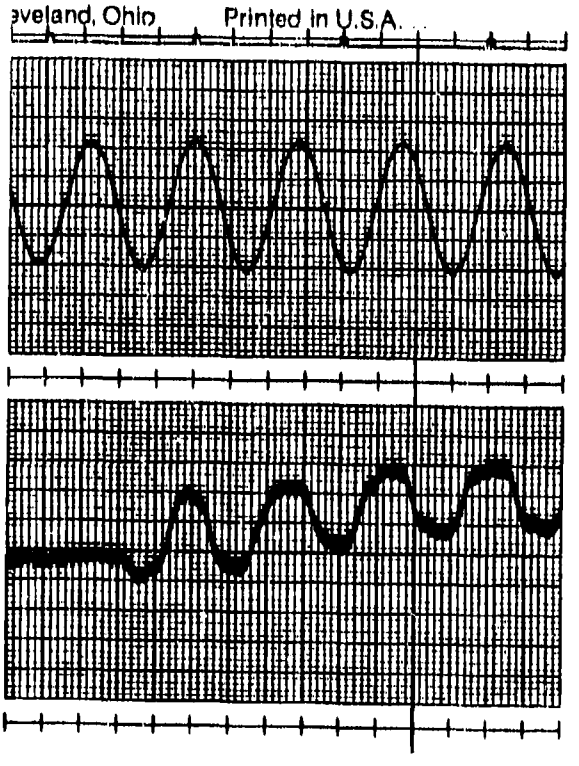

Figure III-43. Dynamic threshold, loaded from the left.

TEST DATA

DATE: 3 DEC 86

TEST ITEM: Hydraulic Units, Inc.
F-15 Rotary Rudder Servoactuator
P/N 3U3151-5E; S/N 2376

TEST: Dynamic threshold - loaded
SURFACE POSITION: 0°
LOAD: 13,200 in-lb RIGHT

----- t = 20 div/sec ------>

Input Command

.002 volts/division

X_{out}

.005 degrees/division

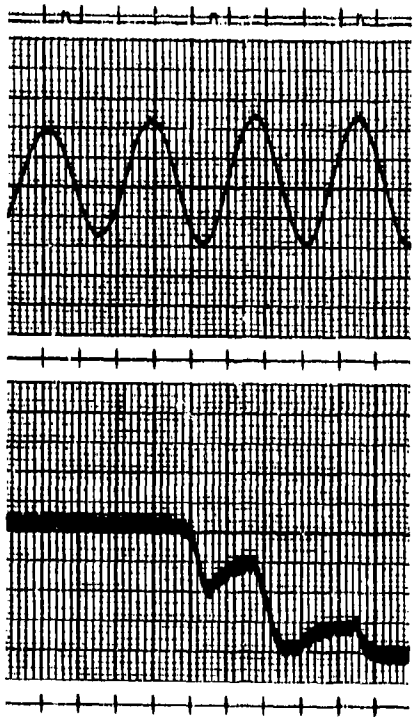

Figure III-44. Dynamic threshold, loaded from the right.

Loaded Saturation Velocity

Loaded saturation velocity measurements were made with a 13,200 in-lb load applied in each direction of rudder travel. Figure III-45 shows data taken with the load applied to the left side of the rudder actuator and motion from left to right (load aiding). The maximum velocity is 159.1 degrees per second.

Figure III-46 shows data taken with the load applied to the left side of the actuator and actuator motion from right to left (load opposing). The maximum velocity is 83.3 degrees per second.

Figure III-47 shows data taken with the load applied to the right side of the actuator and motion from right to left (load aiding). The maximum velocity is 166.7 degrees per second.

Figure III-48 shows data taken with the load applied to the right side of the actuator and motion from left to right (load opposing). The maximum velocity is 71.4 degrees per second.

The change in maximum velocity is consistent with the change in differential pressure across the flow control ports of the central control valve sleeve. The theoretical ratio of velocities is 2.00 (assuming sharp-edged orifices for the flow control ports) which agrees fairly well with the measured 1.91 change for left load and 2.33 for the right load.

Loaded Transient Response

The loaded transient response tests were conducted about the 0° actuator position with a constant load of 13,200 in-lbs applied uni-directionally (first from the right side, then from the left side). The input command was a square wave with an amplitude of 2.8 volts, 20 percent of the maximum command level of 14 volts.

Figures III-49 through III-52 is the data recorded during this test. The transient response time can be defined as time required for the actuator to reach 63 percent of its final value when commanded by a step input. Table II-5 lists the response times for the four test conditions of Figures III-49 through III-52. The response times with an *aiding* load are shorter than with an *opposing* load. The change in response is due to a change in the flow (and flow gain) of the control valving. Note that as shown in Figures III-49 to III-52, the step response input does not saturate the control valving. Saturation would be indicated by a straight line for the actuator motion.

TEST DATA

DATE: 5 Dec 86

TEST ITEM: Hydraulic Units, Inc.
F-15 Rotary Rudder Servoactuator
P/N 3U3151-5E; S/N 2376

TEST: Saturation velocity - loaded
SURFACE MOTION: Left to right
LOAD: 13,200 in-lb LEFT

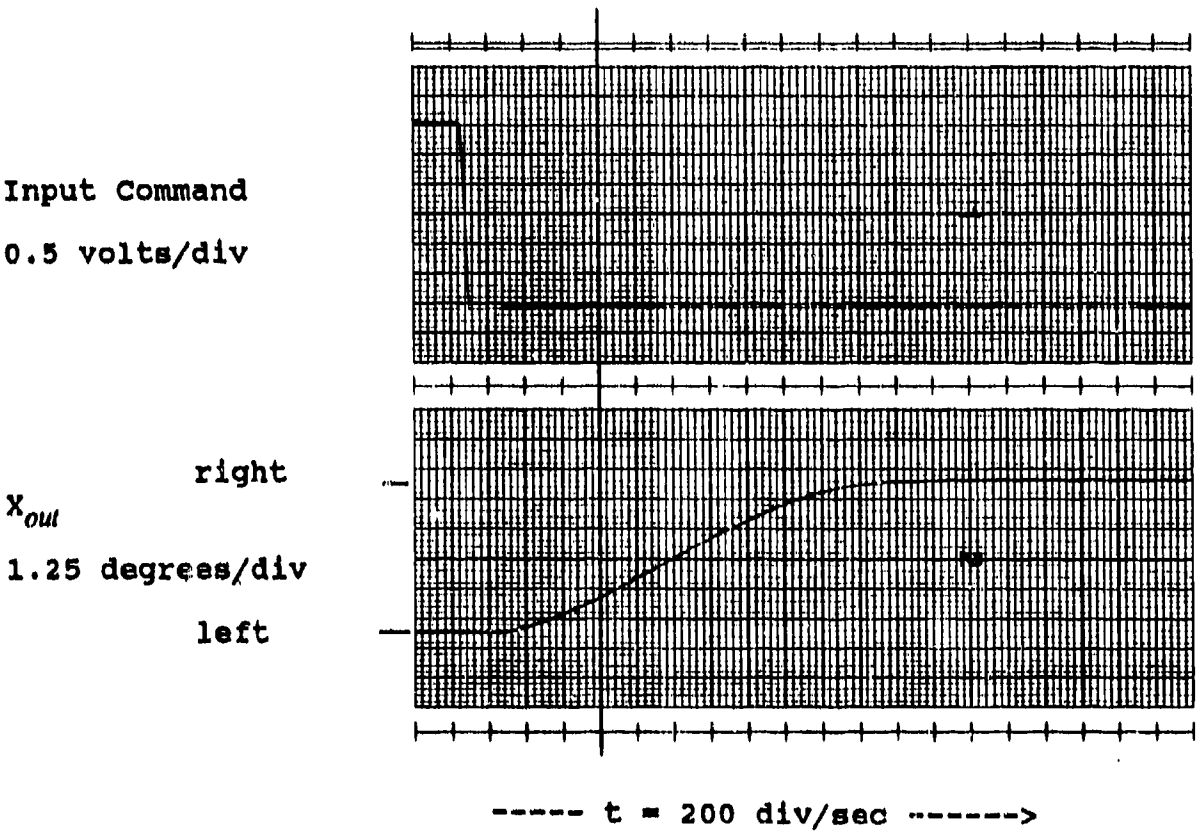

Figure III-45. Saturation velocity: loaded from left, rudder motion left to right.

TEST DATA

DATE:	5 DEC 86
TEST ITEM:	Hydraulic Units, Inc. F-15 Rotary Rudder Servoactuator P/N 3U3151-5E; S/N 2376
TEST:	Saturation Velocity - loaded
SURFACE MOTION:	Right to lft
LOAD:	13,200 in-lb LEFT

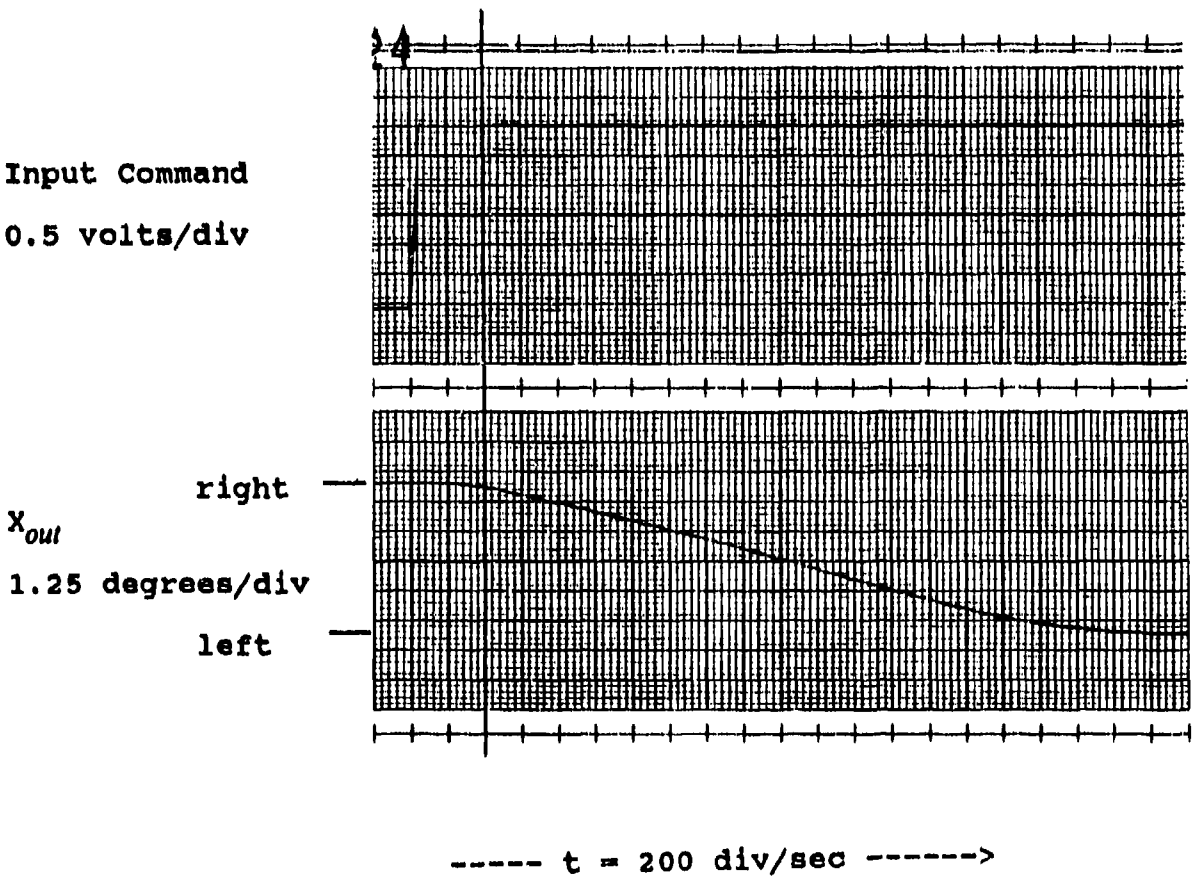

Figure III-46. Saturation velocity: loaded from left, rudder motion right to left.

TEST DATA

DATE: 9 DEC 86

TEST ITEM: Hydraulic Units, Inc.
F-15 Rotary Rudder Servoactuator
P/N 3U3151-5E; S/N 2376

TEST: Saturation Velocity - Loaded
SURFACE MOTION: Right to Left
LOAD: 13,200 in-lb RIGHT

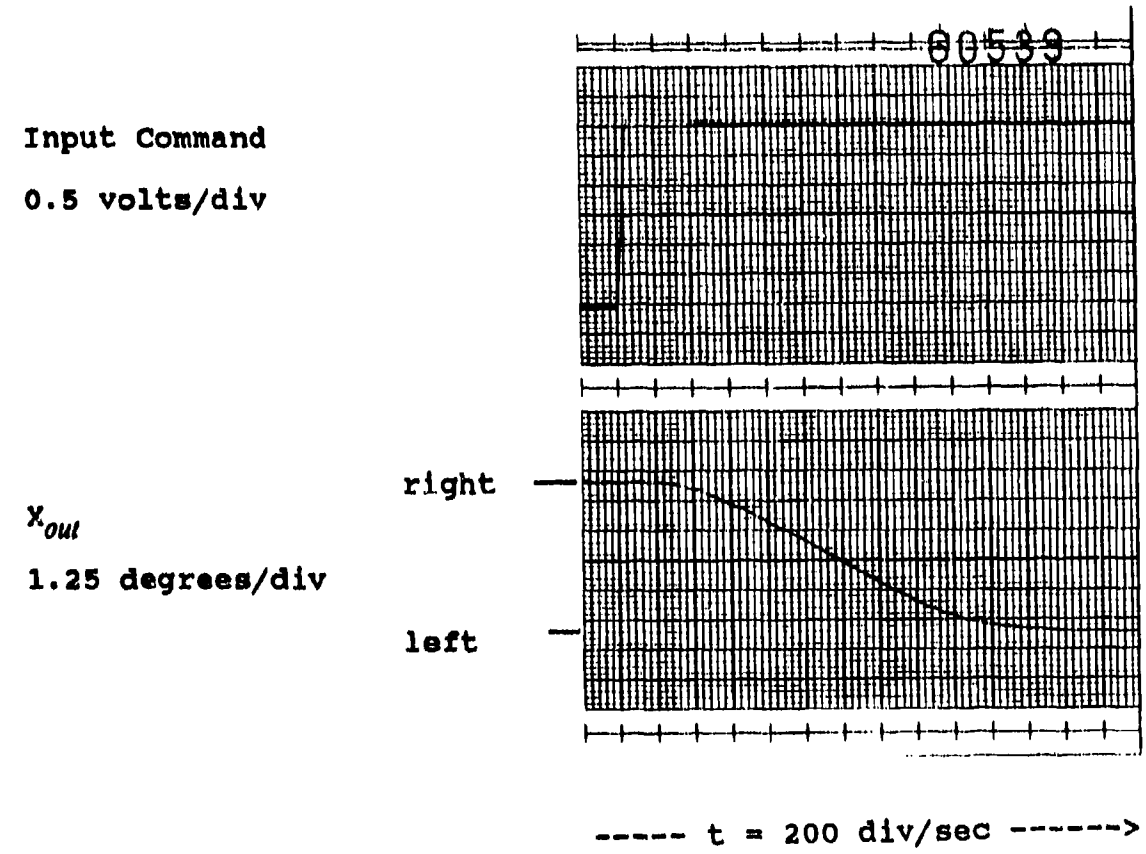

Figure III-47. Saturation velocity: loaded from right, rudder motion right to left.

TEST DATA

DATE: 5 DEC 86

TEST ITEM: Hydraulic Units, Inc.
F-15 Rotary Rudder Servoactuator
P/N 3U3151-5E; S/N 2376

TEST: Saturation Velocity - loaded
SURFACE MOTION: Left to right
LOAD: 13,200 in-lb RIGHT

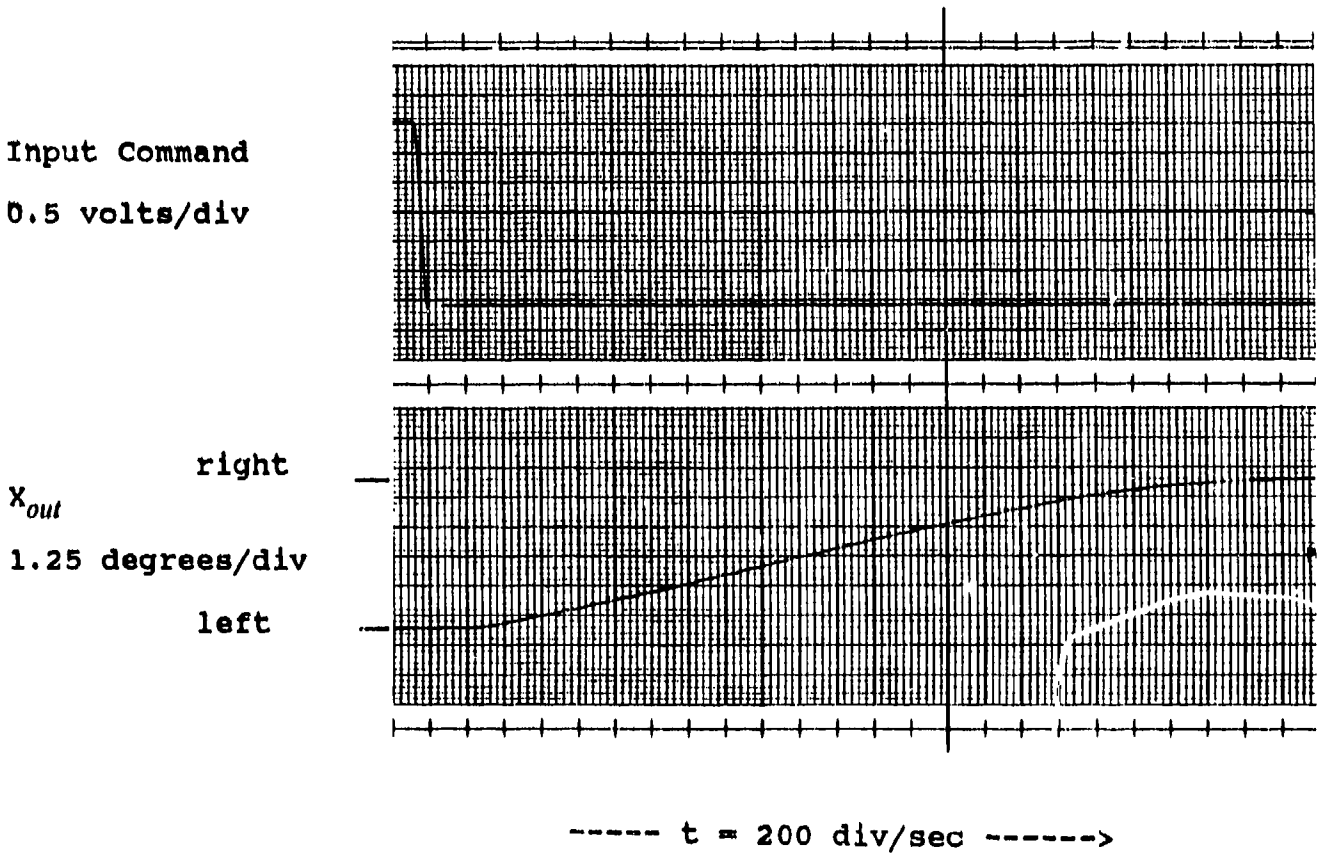

Figure III-48. Saturation velocity - loaded from right, rudder motion from left to right.

TEST DATA

DATE: 15 DEC 86

TEST ITEM: Hydraulic Units, Inc.
F-15 Rotary Rudder Servoactuator
P/N 3U3151-5E; S/N 2376

TEST: Transient Response - Loaded
SURFACE MOTION: Right to Left
LOAD: 13,200 in-lb RIGHT

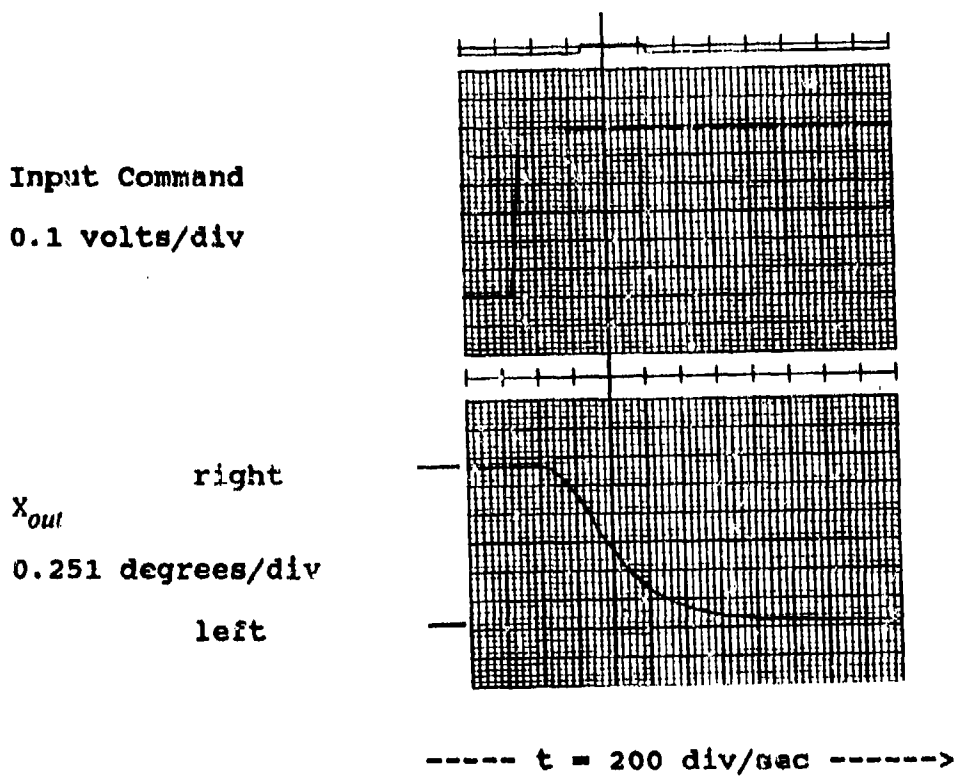

Figure III-49. Transient response - loaded from right, rudder motion from right to left.

TEST DATA

DATE: 15 DEC 86

TEST ITEM: Hydraulic Units, Inc.
F-15 Rotary Rudder Servoactuator
P/N 3U3151-5E; S/N 2376

TEST: Transient Response
SURFACE MOTION: Left to right
LOAD: 13,200 in-lb RIGHT

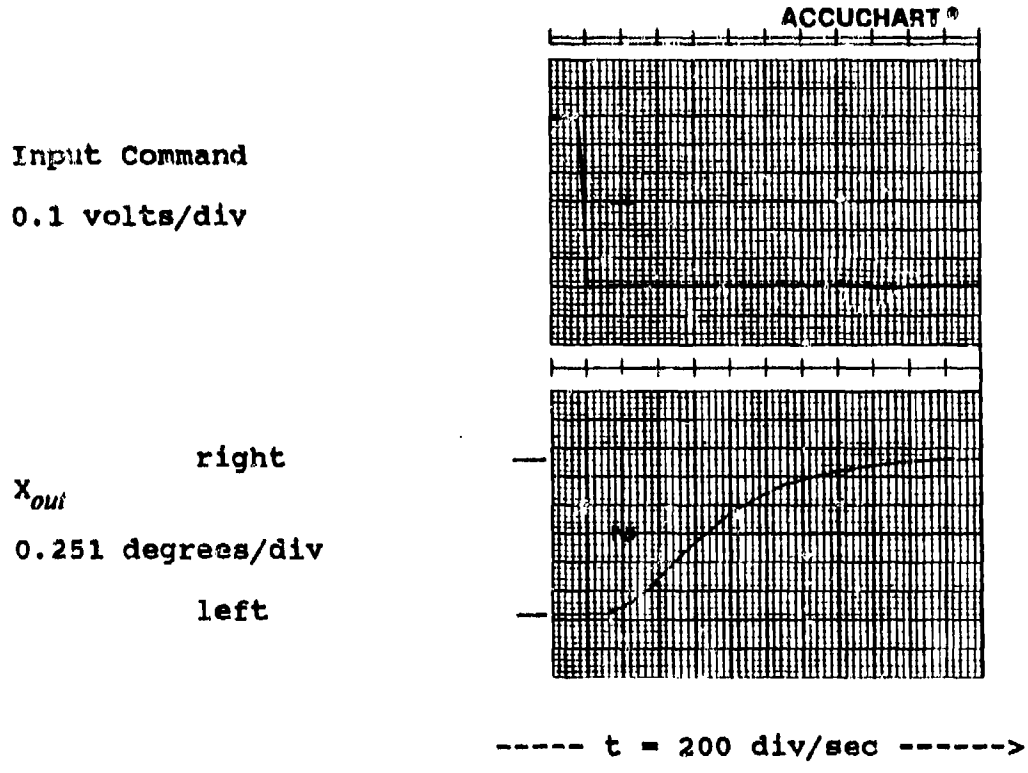

Figure III-50. Transient response - loaded from right, rudder motion from left to right.

TEST DATA

DATE: 15 DEC 86

TEST ITEM: Hydraulic Units, Inc.
F-15 Rotary Rudder Servoactuator
P/N 3U3151-5E; S/N 2376

TEST: Transient Response - loaded
SURFACE MOTION: Left to right
LOAD: 13,200 in-lb LEFT

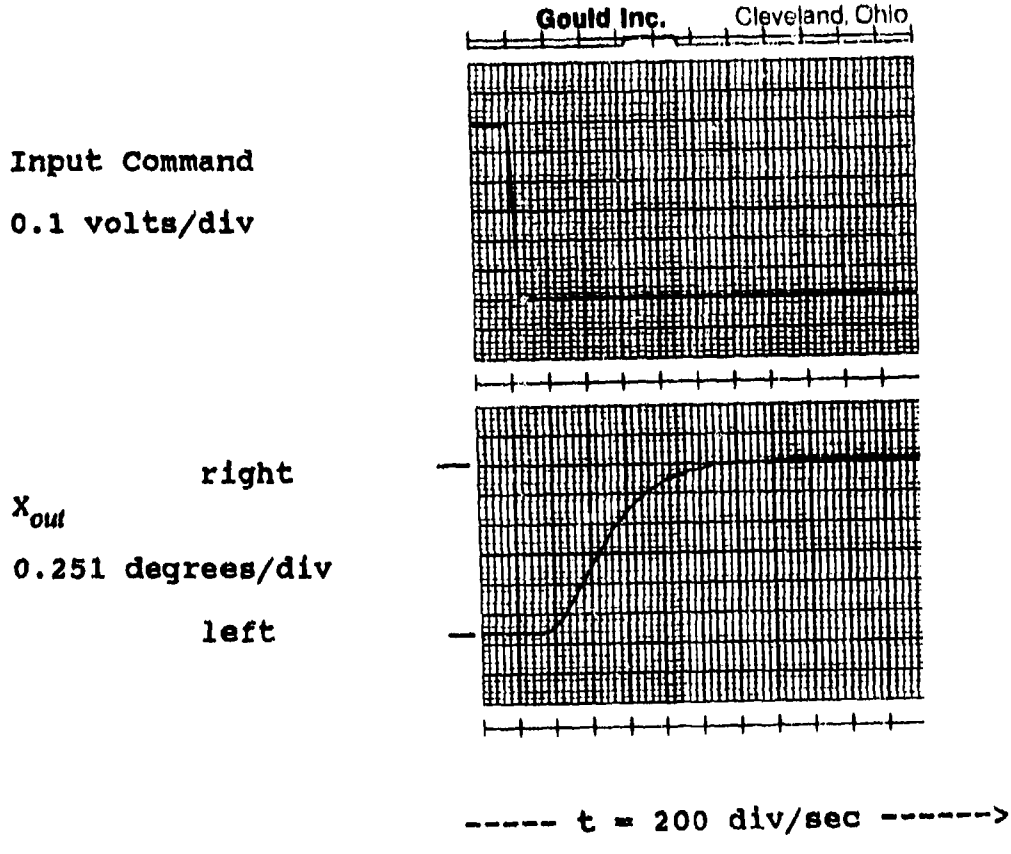

Figure III-51. Transient response - loaded from left, rudder motion from left to right.

TEST DATA

DATE:	15 DEC 86
TEST ITEM:	Hydraulic Units, Inc. F-15 Rotary Rudder Servoactuator P/N 3U3151-5E; S/N 2376
TEST:	Transient Response - loaded
SURFACE MOTION:	Left to right
LOAD:	13,200 in-lb LEFT

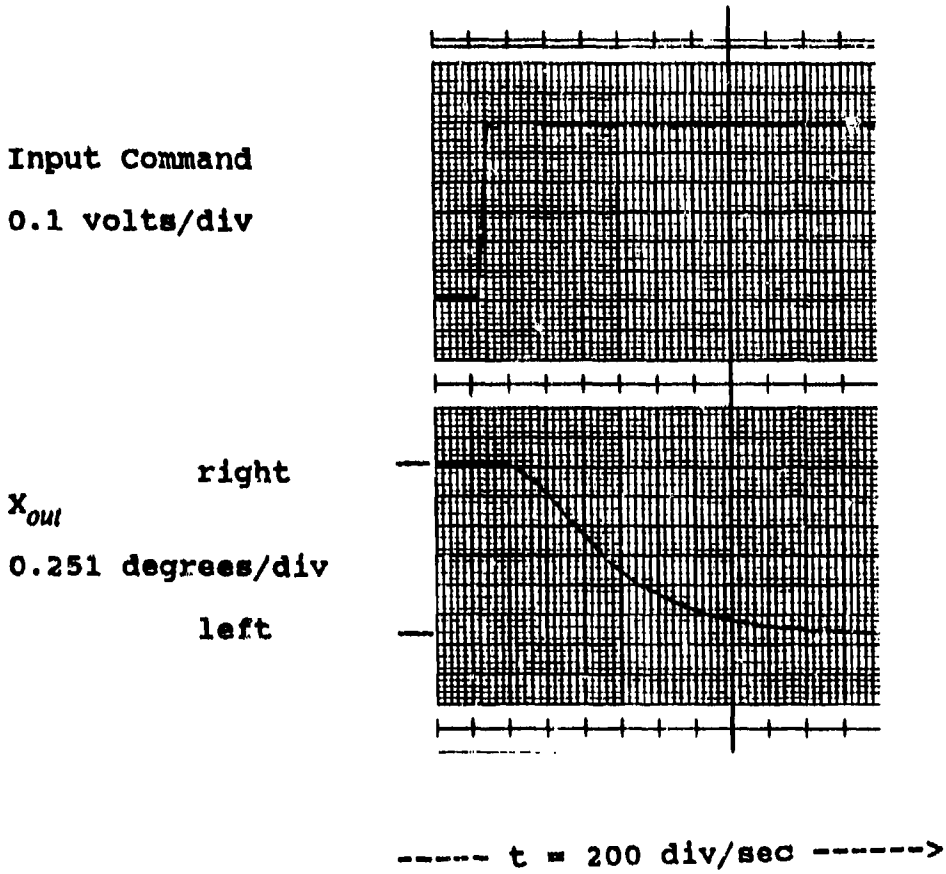

Figure III-52. Transient response - loaded from left, rudder motion from left to right.

Table III-5. Results of transient response, loaded testing.

Direction of Load Application	Direction of Actuator Travel	Response Time of Actuator (sec)
left	right to left	0.075
left	left to right	0.0575
right	right to left	0.055
right	left to right	0.080

V. CONCLUSIONS AND RECOMMENDATIONS

The actuator operated without problems for the entire test sequence. The actuator was designed as non-redundant so the operating characteristics evaluated were single input - single output relationships.

Of particular interest in the evaluation were performance characteristics that were peculiar to the use of a rotary output actuator using a vane construction. The static and dynamic threshold were the two characteristics that were expected to be different from a linear actuator, primarily because of the different actuator seal configuration required for a vane actuator. Both the dynamic and static thresholds were greater than the values measured on other fly-by-wire actuators (including an F-16 ISA) by at least a factor of 2. However, the values were well within the McDonnell Aircraft Company's (specification PS 68-690053) requirements for the actuator.

The other characteristic whose value appeared associated (at least in part) with the use of a vane actuator was the hysteresis. The hysteresis values were above 2 percent (referenced to the CAS-controlled actuator motion) as compared to less than 1 percent usually recorded for a fly-by-wire actuator. The measured input/output linearity was consistent with the use of mechanical feedback for actuator position.

All other measured performance characteristics were consistent with a well designed electrohydraulic actuator. Application of output loads did not improve the performance characteristics of the actuator or degrade the performance in other than a predictable manner.

The compact configuration of the actuator and the general performance characteristics make it a viable candidate as the basis of a pure fly-by-wire rotary actuator. Although the actuator is non-redundant as a fly-by-wire actuator (assuming the mechanical input is not used as a *back-up*), the simplicity of the design would allow it to be used in redundant applications where parallel redundancy extends to the control surface and *single-thread* actuators are used.

APPENDIX A-1

DIGITAL SERVOVALVE CONTROLLER PROGRAM

```
;DIGITAL SERVO-VALVE CONTROLLER
; Z-80 MACHINE CODE WITH MNEMONICS
;STEVE C. MURPHY  21 OCTOBER 1985
; LAST CHANGE 10/10/86
; THIS PRINT 10/10/86
   ;
   ; HARDWARE COMPONENTS
   ;    Z-80 CARD
   ;    MULTISTAGE TIMER
   ;    ANALOG TO DIGITAL CONVERTER
   ;    DIGITAL TO ANALOG CONVERTER
   ;    PARALLEL INTERFACE CARD
   ;    SERIAL INTERFACE CARD (FOR SETUP AND DEBUG ONLY)
   ;    THUMBWHEEL SWITCHES
   ;
```

********** BEGIN PROGRAM **********

```
;*****************  PROCEEDURE INTIIALIZE  ****************************

E000 F3            DI                ;PREVENT INTERUPTS
E001 3E C3         MVI A,C3          ;SET UP NMI INTERUPT VECTOR
E003 32 66 00      STA 0066H         ;STORE JUMP COMMAND
E006 21 00 E1      LXI H,0E100H
E009 22 67 00      SHLD 0067H        ;STORE THE JUMP ADDRESS
E00C 31 00 03      LXI SP,0300H      ;LOAD THE STACK-POINTER
E00F 00            NOP
E010 DB 20         IN 020H           ;GET THE RATE INPUT
     E012 0F               RRC             ;CORRECT FOR HARDWARE
     E013 0F               RRC
     E014 0F               RRC
     E015 0F               RRC
     E016 32 00 01         STA 0100H       ; SAVE IN MEMORY
E019 DB 21                 IN 021H         ;GET THE GAIN INPUT
     E01B 0F               RRC             ;CORRECT FOR HARDWARE
     E01C 0F               RRC
     E01D 0F               RRC
     E01E 0F               RRC
     E01F 32 01 01         STA 0101H       ;SAVE IN MEMORY
E022 DB 22         IN 022H           ;GET THE THRESHOLD
     E024 0F               RRC             ;CORRECT FOR HARDWARE
     E025 0F               RRC
     E026 0F               RRC
     E027 0F               RRC
     E028 32 02 01         STA 0102H       ;SAVE IN MEMORY

; MAKE LEVEL TABLE
E02B 6F    MOV L,A         ;SAVE THRESHOLD IN HL
E02E AF    XORA            ;CLEAR A
E02F 57    MOV D,A         ;CLEAR D
E030 67    MOV H,A         ;CLEAR H
E031 3A 01 01  LDA 0101H   ;GET THE GAIN INPUT
E032 5F    MOV E,A         ;PUT IT IN DE
E033 19    DAD D           ;ADD TO HL TO MAKE FLOW-LEVEL1
     E034 22 10 01         SHLD 0110H
E037 19    DAD D           ;FLOW LEVEL2
     E038 22 12 01   SHLD 0112H
E03B 19    DAD D           ;FLOW LEVEL3
     E03C 22 14 01         SHLD 0114H
E03F 19            DAD D           ;FLOW LEVEL4
     E040 22 16 01         SHLD 0116H
E043 19    DAD D           ;FLOW LEVEL5
     E044 22 18 01 SHLD 0118H
E047 19    DAD D           ;FLOW LEVEL6
     E048 22 1A 01         SHLD 011AH
E04B 19    DAD D           ;FLOW LEVEL7
     E04C 22 1C 01         SHLD 011CH
```

```
; SET UP THE  TIMER

E04F 3E 7F          MVI A,7F          ;INITIALIZE THE TIMER CHANNELS
    E051 D3 40          OUT 040H          ;TURN OFF TIMER 0
    E053 D3 41          OUT 041H          ;TURN OFF TIMER 1
    E055 D3 42          OUT 042H          ;TURN OFF TIMER 2
E057 3E CC          MVI A,0CCH        ;LOAD TIMER 0 TIME CONSTANT FOR 100uS
    E059 D3 40          OUT 040H          ;AND START TIMER 0
E05B 3E 0A          MVI A,0AH         ;LOAD THE FIRST MULTIPLIER FOR 1mS
    E05D D3 41          OUT 041H          ;AND START TIMER 1
E05F 3A 00 01       LDA 0100H         ;LOAD THE RATE MULTIPLIER IN mSEC's
    E062 D3 42          OUT 042H          ;AND START TIMER 2
E064 FB             EI                ;ENABLE THE INTERUPTS
E065 00 00 00 00 00 00 00 00 00 00 00 00  NOP
;
;************* END INITIALIZE ************************


;************** PROCEDURE WAIT *********************
;
  E070 64 E0        JMP 0E070H        ;LOOP HERE TILL INTERUPT
;
;************* END WAIT ****************************
```

```
;*************** PROCEDURE PRIMARY ***************************

; READ COMMAND INPUT
E100 3E 00          MVI A,00          ;LOAD CHANEL 1 (COMMAND)
E102 D3 8B          OUT 08BH          ;START CONVERSION
E104 DB 8D          IN 08DH           ;GET THE A/D STATUS
   E106 E6 80         ANI 080H            ;MASK OFF EXCESS
   E108 FE 80         CPI 080H            ;CHECK THE BUSY BIT
   E10A CA 04 E1    JZ 0E104H             ;GO BACK IF NOT DONE
E10D DB 8C          IN 08CH           ;ELSE GET THE LOW BYTE
E10F 32 00 02       STA 0200H         ;AND SAVE IT
E112 DB 8D          IN 08DH           ;NOW THE HIGH BYTE
   E114 E6 0F         ANI 0FH             ;MASK THE EXCESS OFF
E116 32 01 02       STA 0201H         ;SAVE THE UPPER BYTE

; READ BIAS INPUT
E119 3E 01          MVI A,01H         ;LOAD CHANEL 2 (BIAS)
E11B D3 8B          OUT 08BH          ;OPERATION SAME AS ABOVE
E11D DB 8D          IN 08DH           ;GET THE STATUS
   E11F E6 80         ANI 080H            ;MASK OFF EXCESS
   E121 FE 80         CPI 080H            ;CHECK BUSY BIT
   E123 CA 1D E1    JZ 0E11DH             ;GO BACK IF NOT DONE
E126 DB 8C          IN 08CH           ;ELSE GET THE LOW BYTE
E128 32 10 02       STA 0210H         ;SAVE LOW BYTE
E12B DB 8D          IN 08DH           ;GET THE HIGH BYTE
   E12D E6 0F         ANI 0FH             ;MASK OFF THE EXCESS
E12F 32 11 02       STA 0211H         ;SAVE HIGH BYTE

; READ FEEDBACK INPUT
E132 3E 02          MVI A,02H         ;LOAD CHANEL 3 (FEEDBACK)
E134 D3 8B          OUT 08BH          ;OPERATION SAME AS ABOVE
E136 DB 8D          IN 08DH           ;GET THE STATUS
   E138 E6 80         ANI 080H            ;MASK OFF THE EXCESS
   E13A FE 80         CPI 080H            ;CHECK BUSY BIT
   E13C CA 36 E1    JZ 0E136H             ;GO BACK IF NOT DONE
E13F DB 8C          IN 08CH           ;ELSE GET THE LOW BYTE
E141 32 20 02    STA 0220H ;SAVE LOW BYTE
E144 DB 8D          IN 08DH           ;GET THE HIGH BYTE
   E146 E6 0F         ANI 0FH             ;MASK THE EXCESS
E148 32 21 02       STA 0221H         ;SAVE HIGH BYTE
E14B 00 00 00 00 00    NOP
```

```
; *********  COMMAND_SUM = COMMAND + BIAS ********
E150 3A 21 02      LDA 0221H          ;LOAD BIAS
E153 CB 5F         BIT TEST A,(3)     ;TEST (+) OR (-)
E155 CA 70 E1      JZ 0E170H          ;JUMP IF NEGITIVE BIAS

;+ BIAS
E158 CB 9F         RESET BIT A,(3) ;BIAS IS POSITIVE (CLEAR OFF POLARITY B
E15A 57    MOV D,A                ;LOAD BIAS INTO DE
E15B 3A 20 02      LDA 0220H
E15E 5F    MOV E,A
E15F 2A 00 02      LHLD 0200H         ;LOAD COMMAND INTO HL
E162 19    DAD D                  ;ADD COMMAND AND BIAS
    ;CHECK FOR OVER FLOW
       E163 7C      MOV A,H
       E164 E6 F0   ANI 0F0H
    ;IF NOT READY FOR FEEDBACK
        E166 CA 86 E1       JZ 0E186H
    ;ELSE SET TO MAX VALUE FIRST THEN PROCEED TO FEEDBACK
        E169 21 FF 0F       LXI H,0FFFH
        E16C C3 86 E1       JMP 0E186H
        E06F 00             NOP
;- BIAS
E170 ED 5B 20 02  LD DE,(0220H) ;RELOAD
    ;SUBTRACT FROM 0800H TO NORMALIZE
       E174 21 00 08        LXI H,0800H
       E177 ED 52   SBC HL,DE
       E179 EB      XCHG
    ;NOW SUBTRACT FROM COMMAND
       E17A 2A 00 02        LHLD 0200H ;GET COMMAND
       E17D AF      XORA   ;CLEAR CARRY
       E17E ED 52   SBC HL,DE
       E180 D2 86 E1        JNC 0E186H       ;IF NO CARRY
    ;IF CARRY SET TO MIN. VALUE FIRST
       E183 21 00 00        LXI H,0000H
    ;ELSE ABOUT READY FOR FEEDBACK
E186 22 00 02      SHLD 0200H         ;SAVE THE COMBINED COMMAND AND BIAS

;********** ERROR = COMMAND_SUM - FEEDBACK *************
E189 ED 5B 10 02    LD DE,(0210H)  ;LOAD THE FEEDBACK
E18D AF    XORA                   ;CLAER THE CARRY

;COMMAND-FEEDBACK
   E18E ED 52       SBC HL,DE          ;(SUBTRACT) COMMAND_SUM - FEEDBACK
   E190 D2 A3 E1    JNC 0E1A3H         ;IF NO CARRY
;IF CARRY SWITCH BECAUSE FEEDBACK > COMM
   E193 EB          XCHG     ;SWAP
   E194 ED 5B 00 02  LD DE,(0200H) ;GET THE COMMAND AGIAN
   E198 AF          XORA               ;CLEAR CARRY
   E199 ED 52       SBC HL,DE          ;(SUBTRACT) FEEDBACK - COMMAND_SUM
   ;LOAD (-) FLAG
   E19B 3E 08       MVI A,08H
   E19D 32 0A 01    STA 010AH          ;SAVE IN POLARITY STORAGE
   E1A0 C3 A8 E1    JMP 0E1A8H         ;
```

```
;ELSE COMMAND_SUM > FEEDBACK
   E1A3 3E 10     MVI A,010H          ;LOAD (+) FLAG
   E1A5 32 0A 01  STA 010AH  ;SAVE IN POLARITY STORAGE
;SAVE THE ERROR MAGNITUDE
   E1A8 22 08 01  SHLD 0108H

;**** CHECK TOO SEE IF ERROR > THRESHOLD ***
  E1AB 3A 02 01   LDA 0102H        ;LOAD THE THRESHOLD
  E1AE 5F         MOV E,A          ;PUT IN DE
  E1AF AF         XORA
  E1B0 57         MOV D,A
  ; [ERROR] - [THRESHOLD]
    E1B1 ED 52    SBC HL,DE        ;(SUBTRACT) ERROR - THRESHOLD
  ;IF THRESHOLD > ERROR THEN OUTPUT 0 CONTROL
    E1B3 DA 02 E2 JC 0E202H
  ;ELSE LOAD ERROR INTO DE
      E1B6 ED 5B 08 01     LD DE,(0108H)

;***** COMPARE ERROR TO LEVEL TABLE TO FIND FLOW-LEVEL ****
;LOAD LEVEL 7
   E1BA 2A 1C 01   LHLD 011CH
   E1BD AF           XORA
   E1BE 3E 07        MVI A,7
   E1C0 ED 52        SBC HL,DE     ;LEVEL7  -  ERROR
   E1C2 DA FC E1   JC 0E1FCH       ;IF ERROR > LEVEL7 THEN FLOW-LEVEL=7
;LOAD LEVEL 6
   E1C5 2A 1A 01   LHLD 011AH
   E1C8 3D           DCR A
   E1C9 ED 52        SBC HL,DE     ;LEVEL6  -  ERROR
   E1CB DA FC E1   JC 0E1FCH       ;IF ERROR > LEVEL6 THEN FLOW-LEVEL=6
;LOAD LEVEL 5
   E1CE 2A 18 01   LHLD 0118H
   E1D1 3D           DCR A
   E1D2 ED 52        SBC HL,DE     ;LEVEL5  -  ERROR
   E1D4 DA FC E1   JC 0E1FCH       ;IF ERROR > LEVEL5 THEN FLOW-LEVEL=5
;LOAD LEVEL 4
   E1D7 2A 16 01   LHLD 0116H
   E1DA 3D           DCR A
   E1DB ED 52        SBC HL,DE     ;LEVEL4  -  ERROR
   E1DD DA FC E1   JC 0E1FCH       ;IF ERROR > LEVEL4 THEN FLOW-LEVEL=4
;LOAD LEVEL 3
   E1E0 2A 14 01   LHLD 0114H
   E1E3 3D           DCR A
   E1E4 ED 52        SBC HL,DE     ;LEVEL3  -  ERROR
   E1E6 DA FC E1   JC 0E1FCH       ;IF ERROR > LEVEL3 THEN FLOW-LEVEL=3
;LOAD LEVEL 2
   E1E9 2A 12 01   LHLD 0112H
   E1EC 3D           DCR A
   E1ED ED 52        SBC HL,DE     ;LEVEL2  -  ERROR
   E1EF DA FC E1   JC 0E1FCH       ;IF ERROR > LEVEL2 THEN FLOW-LEVEL=2
;LOAD LEVEL 1
   E1F2 2A 10 01   LHLD 0110H
   E1F5 3D           DCR A
   E1F6 ED 52        SBC HL,DE     ;LEVEL1  -  ERROR
;IF ERROR > LEVEL1 THEN FLOW-LEVEL=1
   E1F8 DA FC E1   JC 0E1FCH
```

```
;IF ERROR<LEVEL 1 AND > THRESHOLD
    E1FB AF          XORA
;ELSE ERROR > THRESHOLD BUT <LEVEL1 SO ONLY OUTPUT DIRECTION CONTROL

;STORE LEVEL
E1FC 32 06 01      STA 0106H   ;SAVE FLOW-LEVEL
E1FF C3 0D E2      JMP 0E20D   ;GO OUTPUT

;************** OUTPUT 0 FOR CONTROL
E202 AF    XORA              ;CLEAR A
E203 32 06 01      STA 0106H         ;SAVE 0 FOR FLOW-LEVEL
E206 3E 18         MVI A,18H         ;'OFF' DIRECTION CONTROL
E208 32 0A 01      STA 010AH         ;SAVE DIRECTION
E20B 00 00         NOP

;************* OUTPUT ROUTINE ********
E20D 3A 06 01      LDA 0106H         ;LOAD FLOW-LEVEL
E210 6F            MOV L,A           ;SAVE IN L
E211 3A 0A 01      LDA 010AH         ;LOAD DIRECTION
;COMBINE FOR CBYTE (CONTROL BYTE)
  E214 85          ADD L
  E215 32 0C 01    STA 010CH         ;SAVE IT FOR LATER
;SEND TO THE ACCTUATOR
   E218 D3 46      OUT 046H
   E21A 00 00 00 00 00 00          NOP

;********** SECONDARY OUTPUT (D/A CARD) *****
;ADJUST DATA FOR HARDWARE
  E220 AF          XORA              ;CLEAR CARRY
  E221 3A 09 01    LDA 0109H         ;LOAD HIGH BYTE OF ERROR
  E224 1F          RAR               ;ROTATE DOWN INTO CARRY ONCE
  E225 32 09 01    STA 0109H         ;SAVE KNEW HIGH BYTE
  E228 3A 08 01    LDA 0108H         ;LOAD LOW BYTE
  E22B 1F RAR                ;ROTATE THE CARRY BIT INTO LOW BYTE
;OUTPUT THE LOW BYTE TO D/A CARD
  E22C D3 70                 OUT 070H
;MORE ADJUSTMENT FOR HARDWARE
  E22E 3A 0A 01    LDA 010AH         ;LOAD THE DIRECTION INFO
  E231 0F          RRC               ;SHIFT INTO CORRECT POSITION
  E232 6F          MOV L,A           ;SAVE IN L
  E233 3A 09 01    LDA 0109H         ;LOAD THE HIGH BYTE
  E236 B5          ORA L             ;COMBINE
;OUTPUT HIGH BYT TO D/A CARD
  E237 D3 71                 OUT 071H



;RETURN FROM INTERUPT
  E239 ED 45                 RETNMI


;********************** END OF PROGRAM ********************************
```

BIBLIOGRAPHY

SECTION I

Aerospace Fluid Component Designer's Handbook, Volume II, Report FDL-TDR-64-25, TRW Systems Group, Redondo Beach, California, November 1968.

Air Force Rocket Propulsion Laboratory, Research and Technology Division, Air Force Systems Command, Edwards, California, Aerospace Fluid Component Designers' Handbook, Technical Documentary Report No. RPL-TDR-64-25, Volume II, Revision C, November 1968.

Bal-seal Design Manual, Bal Seal Engineering Company, Santa Ana, California.

Dynamic Controls, Inc. Research and Development of Aircraft Control Actuation Systems: The Development of a Direct Drive Fly-By-Wire Flight Control System and Evaluation of a Force Sharing Fly-By-Wire Actuator, AFFDL-TR-77-91, Air Force Flight Dynamics Laboratory, AFWAL-AFSC, Wright-Patterson AFB, Ohio, September 1977.

Jenney, G.D. Theory, Design and Experimental Study of an Eddy-Current/Hydromechanical Stability Augmentor for Aircraft, Ph.D. Dissertation, The Ohio State University, 1979.

Raymond, E.T. Design Guide for Aircraft Hydraulic Systems and Components for Use With the Chlorotrifluoroethylene Nonflammable Hydraulic Fluids, AFWAL-TR-80-2111, Aero Propulsion Laboratory, AFWAL-AFSC, Wright-Patterson AFB, Ohio, March 1982.

SECTION II

Dynamic Controls, Inc. An Investigation of a Digital Electrohydraulic Servovalve, AFWAL-TR-80-3074, Air Force Flight Dynamics Laboratory, AFWAL-AFSC, Wright-Patterson AFB, Ohio, July 1980.

Dynamic Controls, Inc. The Evaluation of A Digital Hardware Voter/Monitor in an Aircraft Control System, AFFDL-TR-77-30, Air Force Flight Dynamics Laboratory, AFWAL-AFSC, Wright- Patterson AFB, Ohio, May 1977.

SECTION III

No citations.

LIST OF ACRONYMS

A/D . . . . . analog-to-digital
AC . . . . . alternating current
AFCS . . . . . automatic flight control system
BHN . . . . . Brinell Hardness Number
C . . . . . capacitance
CAS . . . . . control augmentation system
cis . . . . . cubic inches per second
CTFE . . . . . chlorotrifluoroethelene
DCI . . . . . Dynamic Controls, Incorporated
DDV . . . . . direct drive valve
EMI . . . . . electromagnetic interference
FBW . . . . . fly-by-wire
GD . . . . . General Dynamics
GPATR . . . . general purpose actuator test rig
gpm . . . . . gallons per minute
HUI . . . . . Hydraulic Units, Incorporated
I/O . . . . . input-output
IC . . . . . integrated circuit
ISA . . . . . integrated servoactuator
kg . . . . . kilograms
ksi . . . . . kilograms per square inch
L . . . . . inductance
LED . . . . . light emitting diode
LVDT . . . . linear variable differential transformer
MASTR . . . . Multipurpose Actuation System Test Rig
MAW . . . . . Mission Adaptive Wing
psi . . . . . pounds per square inch
PTFE . . . . . polytrifluoroetheline
PWM . . . . . pulse width modulation
PZ . . . . . piezoelectric
R . . . . . resistance
RS . . . . . reset-set
SCR . . . . . silicon controlled rectifier
VAC . . . . . volts alternating current
VDC . . . . . volts direct current

U.S. GOVERNMENT PRINTING OFFICE: 1989-648-056